Engineering Lipid Nanoparticles for Nucleic Acid Delivery: Effects of Manufacturing, Composition, and Payload on Structure and Performance

Thesis

Caitlin McMillan

Professor Yvonne Perrie's Research Group

Strathclyde Institute of Pharmacy and Biomedical Sciences

University of Strathclyde, Glasgow

DECLARATION OF AUTHENTICITY

‘This thesis is the result of the author’s original research. It has been composed by the author and has not been previously submitted for examination which has led to the award of a degree.

ACKNOWLEDGEMENTS

First and foremost, I would like to thank my supervisor, Professor Yvonne Perrie, for giving me the opportunity to undertake this PhD and for her continued guidance and support throughout my doctoral studies. Her encouragement, trust, and belief in me have been invaluable, and I am deeply grateful for the inspiring research environment she provided.

I would also like to thank my second supervisor, Professor Zahra Rattray, for her advice and support throughout my PhD. I am grateful for the opportunity she gave me to interview in 2022 and for her thoughtful contributions to my research publications.

I gratefully acknowledge Avanti Research for sponsoring my PhD and making this research possible. I would also like to thank Amy Druschitz and Stephen Rumbelow for their time, insight, and valuable discussions throughout the project.

I want to thank the members of the Perrie Lab for creating such a supportive and collaborative research environment. In particular, Jade, Rebecca, Sarah, Catherine, Muattaz, and Ankita, for their help with my research and for their friendship and support beyond the laboratory, which were invaluable throughout my PhD.

I have been extremely lucky to have met my closest friends during my undergraduate studies, who have continued to support me through the past decade of different degrees, jobs, and life stages. I would especially like to thank Amber for providing me with a home in the summer of 2025 when I needed it, as well as Maria, Mary, Meabh, Fiona P., and Fiona E., whose friendship has meant more to me than I can express.

I also want to thank my partner, Jordan, for his love, patience, and unwavering support. I am endlessly grateful for everything you have given me, and I look forward to what lies ahead together.

Finally, I would like to thank my family for their unwavering belief in me. In particular, I am deeply grateful to my mum for always being a phone call away during some of the most challenging times, as well as to my dad, my brother, and my wider family. I would also like to remember my grandmother, Eileen McMillan (1930-2025), and my grandfather, Dr Alastair Cochran (1929-2024), whose kindness and inspiration shaped my path.

ABSTRACT

Lipid nanoparticles (LNPs) are the most clinically advanced delivery systems for nucleic acid therapeutics, with established use in messenger RNA (mRNA) vaccines and growing relevance for RNA- and DNA-based medicines. Despite their success, the relationships among manufacturing conditions, formulation composition, nucleic acid payload, and biological performance are not fully understood. Improved understanding of these relationships is needed to support the development of robust and reproducible LNP formulations.

This thesis examines how manufacturing parameters, lipid composition, and nucleic acid payload influence the physicochemical properties and *in vitro* and *in vivo* performance of LNPs. Reproducible LNPs were first established using a NanoAssemblr-based microfluidic platform, enabling systematic optimisation of key processing variables. Using this foundation, LNP size was controlled by adjusting the aqueous-to-organic phase ratio, demonstrating maintained mRNA expression across a wider size range (60–120 nm) than typically employed, with differing trends observed *in vitro* and *in vivo*.

The role of lipid composition was assessed by comparing clinically used and proprietary ionisable lipids with various sterols. While formulations displayed broadly similar physicochemical characteristics, differences in expression and biodistribution were observed *in vitro* and *in vivo*. Ionisable lipid structure was identified as a primary contributor to LNP performance, whereas sterol choice had more modest effects.

The impact of nucleic acid payload identity was then investigated using LNPs encapsulating mRNA, self-amplifying RNA, plasmid DNA, and defined combinations thereof. Distinct *in vivo* expression profiles were observed, reflecting payload-specific biology, while combined-payload formulations exhibited additive behaviour, enabling modulation of expression kinetics without altering particle composition.

Finally, the scalability of LNP production was briefly evaluated using an alternative microfluidic platform, demonstrating comparable *in vivo* expression across a range of manufacturing flow rates.

Overall, this thesis provides insight into the factors that shape LNP performance and supports the rational design of LNP-based nucleic acid delivery systems.

LIST OF PUBLICATIONS

Included in this thesis:

McMillan, C., Druschitz, A., Rumbelow, S., Borah, A., Binici, B., Rattray, Z., & Perrie, Y. (2024). Tailoring lipid nanoparticle dimensions through manufacturing processes [10.1039/D4PM00128A]. *RSC Pharmaceutics*, *1*(4), 841-853. https://doi.org/10.1039/D4PM00128A

McMillan, C., Druschitz, A., Rumbelow, S., Borah, A., Macfarlane, R., Rattray, Z., & Perrie, Y. (2025). Influence of ionisable lipid and sterol variations on lipid nanoparticle properties and performance. *J Control Release*, *386*, 114056. https://doi.org/10.1016/j.jconrel.2025.114056

McMillan, C., Hussain, M., Punnabhum, P., Varley, A.J., Kong, K.Y.S, Rattray, Z., Druschitz, A., & Perrie, Y. (2025). Comparative and predictive expression kinetics of mRNA, saRNA, and pDNA delivered in a single lipid nanoparticle formulation. *J Control Release (under revision)*.

POSTERS AND ORAL PRESENTATIONS

Impact of formulation composition on efficacy and properties of LNPs for delivery, SCI Young Lipid Scientist Award shortlisted presentations, London, 29th June 2023 (Oral presentation)

Impact of formulation composition on efficacy and properties of LNPs for delivery, CRS 2023, Las Vegas, 24th-27th July 2023 (poster)

Exploring the Implications of Tailoring Lipid Nanoparticle Dimensions Through Manufacturing Processes, Liposome Research Days 2024, Glasgow, 26th-29th June 2024 (Oral presentation and poster)

Influence of ionisable lipid and sterol variations on lipid nanoparticle properties and performance, RNA Vaccines and Therapeutics conference 2025, CPI, London, 23rd-24th September 2025 (Flash oral presentation and poster)

EXTERNAL PROJECTS AND COLLABORATIONS

Laboratory Demonstrator: Assisting Undergraduate and Master 's-level Biomedical, Pharmacy, and Pharmacology laboratory classes, with a particular focus on Pharmacology organ bath practicals (2022–2024).

Imperial College London – helping to test a novel class of PEG-free lipid nanoparticles for RNA delivery, including the *in vivo* evaluation of PEG-free LNP formulations.

Micropore - using the Micropore Pathfinder system to produce LNP formulations at high speed and high throughput to support large-scale manufacturing approaches.

University of British Columbia – testing newly synthesised saRNA, circRNA, and mRNA constructs to assess their efficacy and potency within LNP formulations.

TABLE OF CONTENTS

LIST OF FIGURES

Chapter 1: General Introduction

Chapter 2: Optimisation Experiments

Chapter 5: Assessing Payload Performance Using Controlled Formulations (numbered as published)

LIST OF TABLES

Chapter 2: Optimisation Experiments

Chapter 3: Tailoring Lipid Nanoparticle Dimensions Through Manufacturing Processes (numbered as published)

LIST OF ABBREVIATIONS

AF4	Asymmetrical flow field-flow fractionation
ALC-0159	2-[(polyethylene glycol)-2000]-N,N-ditetradecylacetamide, 1,2-Distearoyl-sn-glycero-3-phosphocholine
ALC-0315	[(4-Hydroxybutyl)azanediyl]di(hexane-6,1-diyl) bis(2-hexyldecanoate)
AUC	Area under the curve
Chol	Cholesterol
COVID-19	Coronavirus disease 2019
Cryo-TEM	Cryogenic transmission electron microscopy
CQA	Critical quality attributes
DiR	1,1'-dioctadecyl-3,3,3',3'-tetramethylindotricarbocyanine iodide
DMEM	Dulbecco's Modified Eagle Medium
DMG-PEG 2000	1,2-dimyristoyl-rac-glycero-3-methoxypolyethylene glycol-2000
DOTAP	1,2-dioleoyl-3-trimethylammoniumpropane
DSPC	1,2-distearoyl-sn-glycero-3-phosphocholine
EE(%)	Encapsulation efficiency (%)
EtOH	Ethanol
FLuc	Firefly luciferase
FRR	Flow rate ratio
IM	Intramuscular (injection)
IPA	Isopropan-2-ol
IV	Intravenous (injection)
LNE	Lipid nanoemulsion
LNP	Lipid nanoparticle
MB(%)	Mass balance (%)
MEM	Minimal Essential Medium
MeOH	Methanol
MPS	Mononuclear phagocyte system

mRNA	Messenger ribonucleic acid
N/P	Nitrogen/phosphate ratio
NCBI	National Centre for Biotechnology Information
NLC	Nanostructured lipid carrier
NTA	Nanoparticle tracking analysis
PBS	Phosphate buffered saline
PDI	Polydispersity index
pDNA	Plasmid deoxyribonucleic acid
PEG	Polyethylene glycol
PolyA	Polyadenylic acid
RES	Reticuloendothelial system
Rg	Radius of gyration
Rh	Hydrodynamic radius
RNA	Ribonucleic acid
saRNA	Self-amplifying ribonucleic acid
SC	Subcutaneous (injection)
SD	Standard deviation
SE/SEM	Standard Error of the Mean
SLN	Solid lipid nanoparticles
SARS-CoV-2	Severe acute respiratory syndrome coronavirus 2
TE buffer	Tris-EDTA buffer
TFR	Total Flow Rate
TFF	Tangential flow filtration
TNS	6-(*p*-Toluidino)-2-naphthalenesulfonic acid

CHAPTER 1: GENERAL INTRODUCTION

Background of lipid-based nanoparticles

Lipid-based nanoparticles, also known as lipidic nanoparticles or lipid-based nanomedicines, are defined as complexes on the nanoscale (i.e., 1-1000nm) primarily composed of lipids [1]. They include liposomes, lipid nanoemulsions (LNEs), lipid nanoparticles (LNPs), solid lipid nanoparticles (SLNs) and nanostructured lipid carriers (NLCs) (the latter two often defined as types of LNPs) [2-5].

Liposomes were the first of this type of structure to be formulated, studied, and clinically approved. First developed by Bangham and his co-workers in the early 1960s, Liposomes are arguably the simplest of these nanoparticles, with the spherical phospholipid bilayer formation leading to the discovery of the cell membrane due to this shared feature [6, 7]. As well as elucidating cell components, liposomes went on to become the first approved lipid-based nanomedicines in the form of Caelyx®/Doxil® for the treatment of various forms of cancer [2, 8], thus progressing the field of chemotherapy and medicine in general. Subsequent decades of research built on these early discoveries, leading to advances in lipid chemistry, formulation strategies, and manufacturing technologies that ultimately enabled the development of lipid nanoparticles (LNPs) optimised for nucleic acid delivery. To provide modern LNP platforms with this broader historical context, a timeline of key milestones in the evolution of lipid-based nanomedicines is shown in Figure 1.

Lipid-based nanoparticles are a significant and valuable advancement in medicine because they can improve the pharmacokinetic properties of certain therapeutics or serve as vaccine adjuvants. They achieve this in various ways. They help protect the drug from degradation and reduce clearance, safeguard RNAs from ribonucleases, control drug release, facilitate transport of the drug to specific target sites, thereby decreasing off-site side effects, and can enhance the bioavailability of the therapeutic. Additionally, they assist non-lipid soluble drugs and RNA in crossing the lipid bilayer of cell membranes [9, 10]. They can aid nucleic acid, peptide, or protein-based vaccines through the above and stimulate immune response from antigen-presenting cells (APCs) and other means, which is necessary for a vaccine to take effect [9].

Among lipid-based nanoparticles, LNPs have emerged as the preferred platform for RNA delivery, including small interfering RNA (siRNA) and messenger RNA (mRNA), as demonstrated by their use in approved therapeutics and vaccines [11-13].

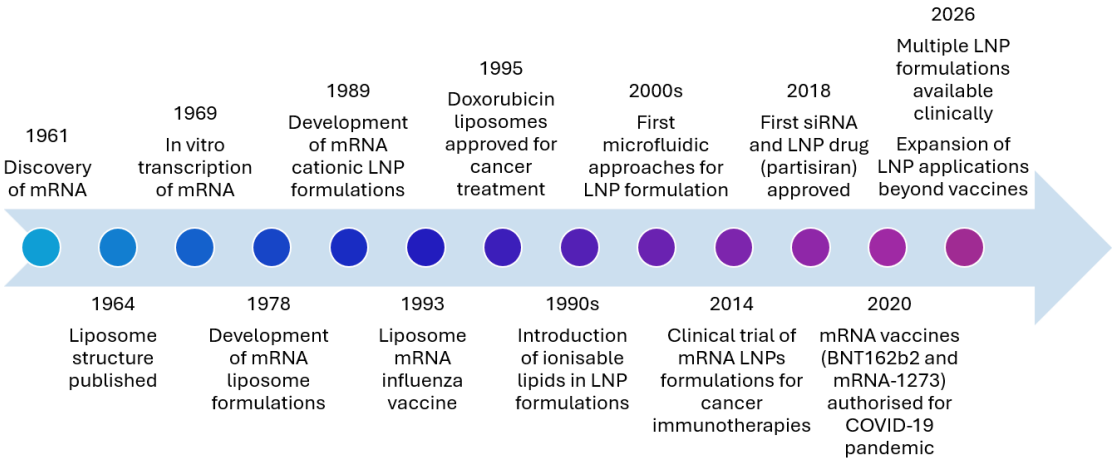

Figure 2.1: Timeline of key events in Lipid nanoparticle development, based on [14-17] .

In addition to lipid-based systems, several other nanoparticle platforms have been investigated for drug delivery, including polymeric nanoparticles, viral vectors, and inorganic materials such as gold or silica nanoparticles [18]. Each of these approaches offers distinct advantages but also has limitations that have influenced their translational success.

Viral vectors, including adenoviral and adeno-associated viral (AAV) systems, are highly efficient gene delivery tools and several viral vector therapies have now been clinically approved [20]. However, they can cause immune responses, have limited cargo capacity, and are difficult and expensive to manufacture at large scale [20, 21]. Repeat dosing can also be challenging because the body may develop immunity against the vector. In addition, concerns around long-term safety and possible insertional mutagenesis have encouraged continued development of non-viral delivery systems [22].

Polymeric nanoparticles, such as polyethyleneimine (PEI), poly(lactic-co-glycolic acid) (PLGA), and chitosan-based systems, have also been explored for nucleic acid delivery [23]. These materials can provide good stability and controlled release, and their chemistry can be easily modified. However, they often show lower transfection efficiency than lipid nanoparticles, and some cationic polymers can cause toxicity through interactions with cell membranes [23].

Inorganic nanoparticles, including gold and silica nanoparticles, have been investigated for drug delivery, imaging, and diagnostic applications because of their unique physical

properties [24, 25]. Despite promising preclinical results, concerns about biodegradability, long-term accumulation, and toxicity have limited their clinical translation [26, 27].

More recently, extracellular vesicles and exosome-based systems have gained interest as naturally derived delivery vehicles with potentially lower immunogenicity and inherent targeting properties [28]. However, challenges in large-scale production, purification, and consistent cargo loading currently restrict their broader clinical use [29, 30].

By comparison, lipid-based nanoparticles are composed of largely biocompatible and biodegradable materials and have an established record of clinical use [15, 18]. These features have supported their regulatory acceptance and contributed to the adoption of lipid nanoparticles, particularly LNPs, as leading platforms in nanomedicine.

Definition and Components of Lipid Nanoparticles

The term “lipid nanoparticle” is often used inconsistently in the literature. In some contexts, LNP is employed as a generic term encompassing all lipid-based nanoparticles [2, 31, 32], whereas other classifications restrict the term to SLNs and NLCs [5, 33]. Representative classes of lipid-based nanoparticles are shown in Figure 1.2A, including liposomes, SLNs, NLCs, and nucleic acid-loaded LNPs.

Although these systems share lipid-based building blocks, they differ substantially in their internal structures, compositions, and intended applications. For instance, liposomes consist of one or more phospholipid bilayers surrounding an aqueous core and are widely used to deliver small-molecule drugs. Liposomes can also be drug-loaded to encapsulate therapeutics either within the aqueous core or within the lipid bilayer, while “stealth” or targeted liposomes incorporate polyethylene glycol (PEG) and/or targeting ligands to extend circulation time and improve tissue specificity.

In contrast, SLNs and NLCs consist of solid or semi-solid lipid matrices rather than bilayer structures. SLNs are formed from solid lipids and provide improved physical stability and controlled release, whereas NLCs incorporate mixtures of solid and liquid lipids to decrease crystallinity and enhance drug-loading capacity [33]. These systems are most commonly applied to topical, transdermal, and oral drug delivery rather than nucleic acid delivery [34, 35].

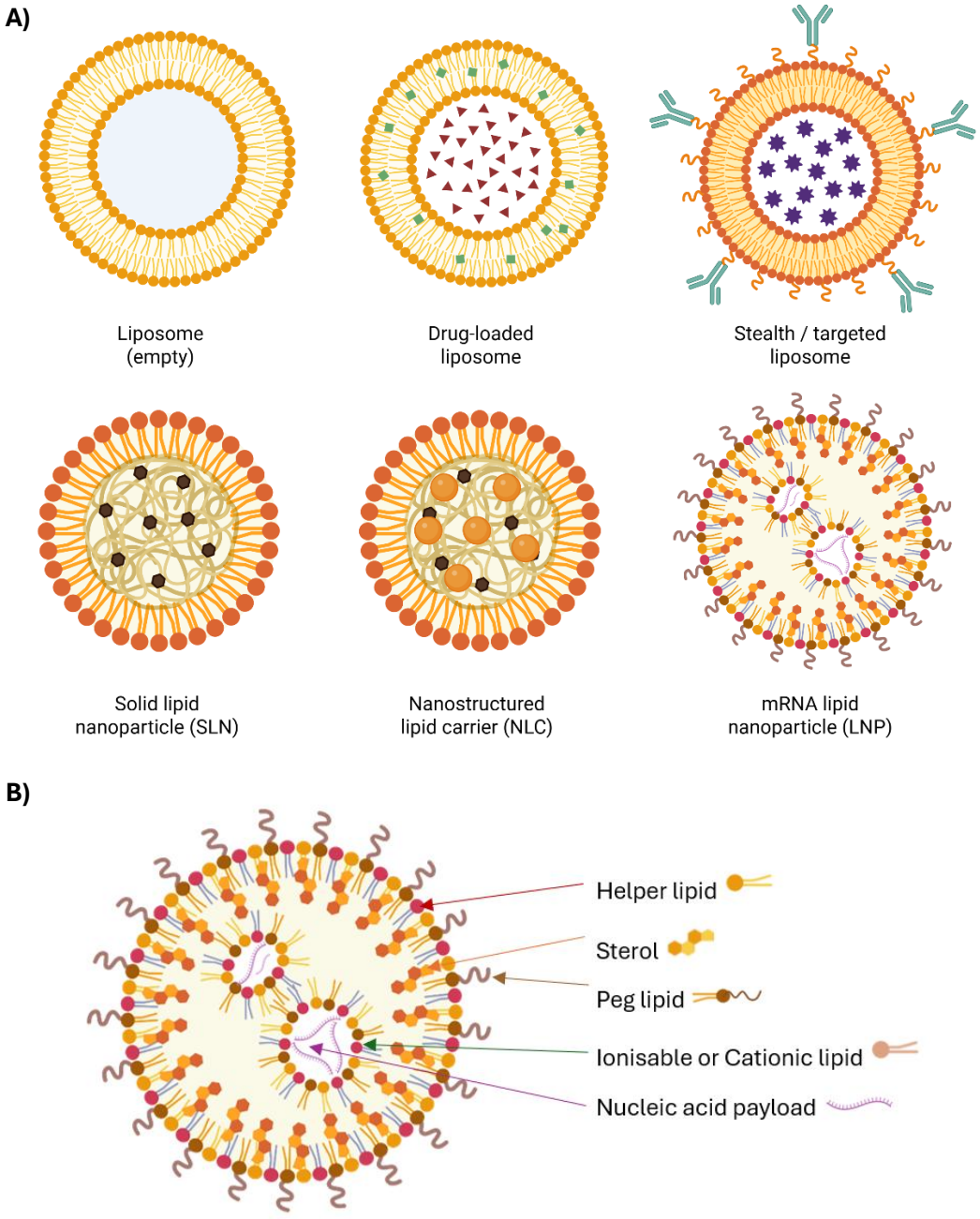

Figure 1.3 A) Types of lipid-based nanoparticles. B) Schematic of an mRNA lipid nanoparticle and its components. Created with BioRender, based on [2].

Lipid nanoparticles designed for nucleic acid delivery (LNPs) fundamentally differ from these systems. Instead of forming bilayers or solid lipid matrices, LNPs contain an ionisable or cationic lipid-rich core that binds nucleic acids through electrostatic interactions. This structure allows for effective encapsulation, protection, and intracellular release of RNA and DNA payloads, setting LNPs apart from other lipid-based nanoparticles in both structure and function.

In this thesis, the entity being described by the term lipid nanoparticle or LNP are those lipid-based nanoparticles with an ionisable/cationic lipid core (positively charged or positively ionisable) in conjunction with other papers published from this research laboratory [36-42], and the majority outwith published since 2020 [12, 15, 43-50]. A schematic diagram of a typical LNP formulation is depicted in Figure 1.2B. LNPs usually consist of four main components: an ionisable (or cationic) lipid, a sterol (most often cholesterol), a helper phospholipid (e.g., DSPC), and a polyethylene glycol (PEG)-conjugated lipid, which surrounds a nucleic acid payload.

The ionisable lipid plays a key role in nucleic acid encapsulation and intracellular delivery. During formulation, LNPs are generally assembled in acidic aqueous buffers at a pH about two units below the pKa of the ionisable lipid, where the lipid is mainly protonated and can electrostatically interact with negatively charged nucleic acids. The ability of ionisable lipids to change their charge in response to the surrounding pH is biologically important. Unlike permanently cationic lipids, ionisable lipids become mostly neutral at physiological pH, reducing systemic toxicity after administration [2]. Upon cellular uptake via endocytosis, endosomal acidification leads to re-protonation of the ionisable lipid, promoting membrane destabilisation and facilitating endosomal escape of the nucleic acid cargo into the cytoplasm, where the mRNA can then be transcribed into proteins [12, 51, 52]. However, reportedly, fewer than 2-3% of nucleic acids escape endosomes to reach the cytosol. Therefore, enhancing cytosolic RNA release is critical to fully realising the potential of LNPs [53, 54].

Aside from the ionisable lipid, LNPs typically contain a sterol (usually cholesterol), a helper phospholipid (most commonly distearoylphosphatidylcholine, DSPC), and a PEGylated lipid, which together form the outer structure of the particle and contribute to its stability and biological performance [9, 37, 55].

Helper phospholipids play an important structural role in LNP formulations. Saturated phospholipids such as DSPC possess high phase transition temperatures and form relatively rigid bilayers, which contribute to particle stability during formulation, storage, and circulation [56, 57]. In addition to providing structural support, helper phospholipids influence membrane packing and can affect interactions with biological membranes following cellular uptake [53]. While DSPC is the most widely used phospholipid in clinically approved LNPs [57], alternative phospholipids with differing acyl chain lengths

and degrees of saturation have been investigated to modulate membrane fluidity and LNP performance [15, 53].

Sterols, most commonly cholesterol, are included in LNP formulations to modulate membrane organisation and mechanical properties. Cholesterol intercalates between lipid molecules, increasing membrane packing density and reducing permeability, which can enhance particle stability and encapsulation efficiency [53]. In LNPs, cholesterol has also been implicated in promoting membrane fusion and facilitating endosomal escape, although its precise mechanistic role remains incompletely understood [57]. Substitution of cholesterol with alternative sterols has been explored as a strategy to alter LNP rigidity, biodistribution, and expression profiles, highlighting the contribution of sterol chemistry to LNP behaviour [15, 58, 59].

The PEGylated lipid consists of polyethylene glycol (PEG) conjugated to a lipid. When formulating LNPs or other lipidic nanoparticles, such as liposomes, this leads to a “hairy” shell around the particle. This shell improves the pharmacokinetic properties of the LNPs by preventing particle aggregation and helping to shield them from antibody opsonisation (i.e., tagging by the immune system) and detection by the mononuclear phagocyte system (MPS/RES) [2]. This, in turn, enhances their tolerability, delivery efficacy, and biodistribution in most individuals [15].

The hydrophobic lipid part of the PEG-lipid acts as an anchor and affects how strongly the PEG remains attached to the surface of the LNP. PEG-lipids with shorter lipid tails, such as DMG-PEG 2000 (C14), detach from the particle surface more quickly after administration, whereas longer-chain PEG-lipids, such as DSG-PEG 2000 (C18), remain associated with the LNP for longer [60]. This process is known as PEG shedding and is important because PEG on the particle surface can reduce interactions with cells by shielding the LNP surface. Faster PEG shedding may therefore improve cellular uptake and intracellular delivery by exposing the underlying lipids after circulation [60]. Recent work from our laboratory showed that LNPs formulated with the shorter-chain PEG-lipid DMG-PEG produced greater *in vitro* and *in vivo* mRNA expression than equivalent formulations containing DSG-PEG, despite having similar particle size and zeta potential [60]. These findings suggest that PEG-lipids play an important role in determining LNP delivery efficiency, in addition to stabilising nanoparticles during formulation and storage.

Despite these benefits, PEG has been associated with rare but severe hypersensitivity reactions, including complement activation-related pseudo-allergy and anaphylaxis [61, 62]. This immunogenicity is thought to arise from pre-existing anti-PEG antibodies due to widespread exposure to PEG in consumer products and pharmaceuticals [61]. Consequently, there is increasing interest in the development of alternative surface-stabilising strategies that retain the favourable pharmacokinetic properties of PEG while reducing immunogenic risk [15].

In addition to their lipid components, LNPs are medically characterised by the nucleic acid payload they carry, which influences therapeutic efficacy and biological response. LNPs have been developed to transport various nucleic acids, including messenger RNA (mRNA), small interfering RNA (siRNA), self-amplifying RNA (saRNA), and plasmid DNA (pDNA), each differing in size, intracellular processing, and expression kinetics [63, 64]. While lipid composition governs particle formation and stability, payload identity determines the expression profile over time and the mechanism of gene expression following delivery [65]. As a result, variations in biological performance can occur even among LNPs with similar physicochemical features. Payload identity, therefore, remains a key consideration alongside lipid composition and manufacturing parameters when developing LNP-based delivery systems.

However, overall, the behaviour of lipid nanoparticles cannot be explained by any single component alone. Instead, LNP performance depends on the combined effects of lipid composition, formulation ratios, manufacturing conditions, and payload identity [38, 66]. Even small changes to one parameter can influence particle formation, stability, and biological behaviour [13, 67, 68]. Understanding how these factors interact is therefore important for the rational design and optimisation of LNP formulations.

Clinical Use and Routes of Administration

Lipid-based nanoparticles facilitate a wide range of therapeutic applications and methods of administration, including topical, oral, intramuscular, and intravenous delivery. Their flexibility stems from the ability to customise lipid composition, particle size, and surface properties to meet specific routes and therapeutic objectives. [69]. While many lipid-based systems remain in the preclinical stage, several have been successfully translated into clinical use, highlighting their potential as versatile drug delivery platforms [14, 15].

Solid lipid nanoparticles (SLNs) and nanostructured lipid carriers (NLCs) are mainly used in topical and transdermal formulations, especially in dermatological and cosmetic applications. Their solid or semi-solid lipid forms can improve drug stability, regulate release, and enhance skin penetration, making them ideal for local delivery [34]. In contrast, liposomes and lipid nanoparticles (LNPs) dominate parenteral clinical applications, especially intravenous and intramuscular delivery, because of their capacity to encase hydrophilic and hydrophobic payloads and their advantageous biocompatibility profiles [70].

Liposomes have a long history of clinical use, particularly for the delivery of small-molecule chemotherapeutics [14, 15]. Encapsulation of cytotoxic drugs within liposomes can reduce systemic toxicity, prolong circulation time, and improve accumulation at tumour sites through altered pharmacokinetics [71]. A prominent example is the liposomal formulation of doxorubicin, which has demonstrated improved tolerability compared with the free drug [71]. As a result, liposomes remain an important and well-established nanomedicine platform.

In contrast, LNPs have emerged as the preferred delivery system for nucleic acid-based therapeutics [14, 45]. Their ability to efficiently encapsulate and protect RNA, facilitate cellular uptake, and promote cytosolic delivery has enabled the clinical translation of therapies that were previously limited by poor stability and low bioavailability [15, 72]. This is exemplified by the approval of siRNA-based therapies delivered via LNPs and the widespread use of LNP-formulated mRNA vaccines against SARS-CoV-2 [45]. The success of these vaccines demonstrated not only the effectiveness of LNP-mediated RNA delivery but also the scalability and robustness of LNP manufacturing at an unprecedented global scale.

Routes of administration play a critical role in determining LNP biodistribution, cellular uptake, and therapeutic outcome. Intravenous delivery is commonly used for systemic applications, often resulting in preferential accumulation in the liver [69], whereas intramuscular administration is particularly effective for vaccination, enabling local antigen expression and immune activation [67]. Therefore, the choice of route of administration is an important design consideration when developing LNP-based therapeutics.

Due to shared structural features and overlapping manufacturing approaches, the extensive body of literature on liposomes provides valuable insight into the formulation, characterisation, and *in vivo* behaviour of LNPs [2, 73]. Lessons learned from decades of liposome research continue to inform the development and optimisation of LNP systems; for example, the comprehensive review published by Allen and Cullis in 2013 describes key advances in liposomal design, stability, surface modification, biodistribution, and clinical translation that remain directly relevant to contemporary LNP formulations [74].

Biological Barriers and Challenges in LNP Delivery

Despite the clinical success of lipid nanoparticles (LNPs), particularly for RNA-based therapeutics, the efficient delivery of nucleic acids *in vivo* remains challenging due to a series of biological barriers encountered following administration. These barriers influence nanoparticle stability, biodistribution, cellular uptake, and intracellular trafficking, and collectively limit the proportion of delivered nucleic acid that ultimately reaches its intracellular site of action [75-77].

Following administration, LNPs rapidly interact with biological fluids such as blood or interstitial fluid, resulting in protein adsorption onto the particle surface and the formation of a protein corona. This corona alters the biological identity of the nanoparticle, influencing interactions with cells, immune recognition, and clearance pathways [77]. The composition of the protein corona depends on LNP physicochemical properties, including size, surface chemistry, and lipid composition, and may differ substantially between *in vitro* and *in vivo* environments [35, 78]. As a result, LNP behaviour observed under simplified *in vitro* conditions typically does not translate directly to *in vivo* outcomes.

Cellular uptake represents a further barrier to effective delivery. LNPs are primarily internalised via endocytic pathways, which can vary depending on cell type, tissue, and physiological context. Even following successful uptake, the majority of internalised LNPs remain trapped within endosomal compartments [75]. Endosomal escape is widely recognised as one of the principal rate-limiting steps in LNP-mediated nucleic acid delivery, with estimates suggesting that only a small fraction of internalised nucleic acid reaches the cytosol [50, 76]. This inefficiency significantly constrains therapeutic

potency and highlights the importance of formulation strategies that promote membrane destabilisation and intracellular release.

The route of administration strongly influences LNP behaviour. After intravenous injection, LNPs commonly accumulate in the liver due to interactions with blood proteins and uptake by liver cells and immune cells [66, 79]. While this is beneficial for liver-targeted therapies, it limits delivery to other tissues. In contrast, intramuscular administration supports local expression and immune activation for vaccination but introduces different challenges, including tissue diffusion, immune cell uptake, and local clearance [80]. These route-specific effects make it difficult to compare or predict LNP performance across different applications directly.

Together, these biological barriers underscore the complexity of LNP delivery *in vivo* and emphasise the need to interpret formulation performance within a biological context. Overcoming these challenges requires not only optimisation of physicochemical properties but also a deeper understanding of how LNPs interact with complex biological systems following administration.

LNPs in COVID-19 Vaccines and Beyond

The COVID-19 pandemic was a key moment in both the development and public awareness of lipid nanoparticle (LNP) technology [10, 14]. The rapid deployment of messenger RNA (mRNA) vaccines by Moderna and Pfizer/BioNTech represented the first widespread clinical use of LNP-mediated RNA delivery and demonstrated the feasibility of this platform at an unprecedented global scale [15]. Importantly, the speed at which these vaccines were developed was not the result of purely innovation, but rather the culmination of decades of prior research into mRNA biology, stabilisation strategies, coronavirus antigen design, and LNP formulation and manufacturing technologies [53, 81]. These foundational advances enabled vaccine development and regulatory approval timelines substantially shorter than the traditional decade-long process associated with conventional vaccine platforms.

The clinical success of LNP-formulated mRNA vaccines had a profound impact on the field of nanomedicine, accelerating both academic and industrial interest in LNP-based delivery systems. This is reflected in the rapid, exponential increase in LNP-related publications in recent years, as illustrated in Figure 1.3.

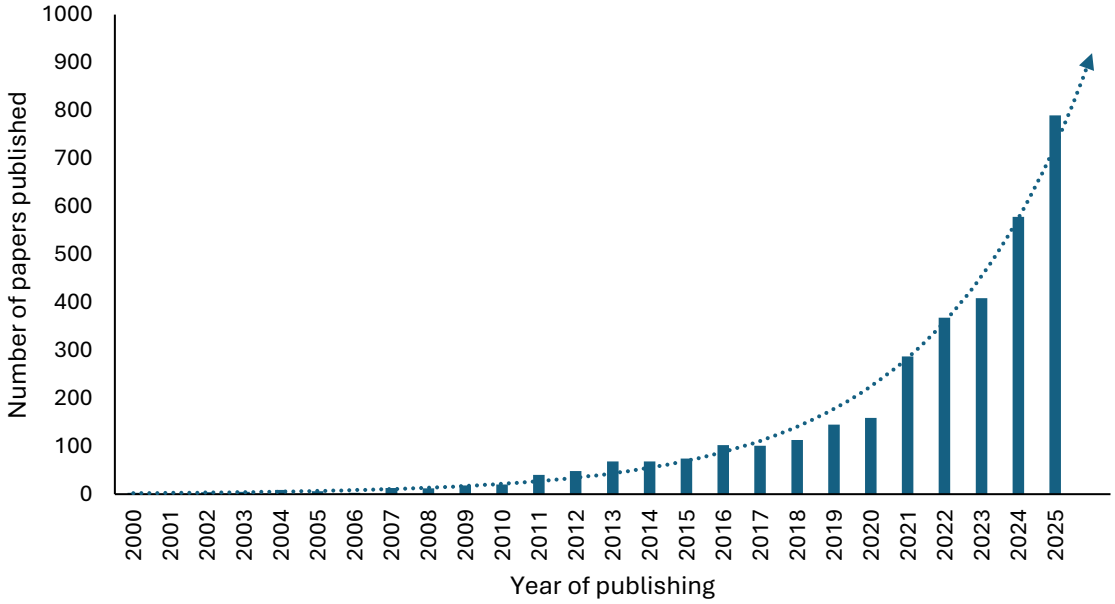

Figure 1.3: Graph showing the number of papers published per year on PubMed containing the search term "Lipid Nanoparticle" from 2000-2025 (data retrieved February 2026) [82].

The pandemic, therefore, served not only as a validation of LNP technology but also as a catalyst for expanded investigation into its broader therapeutic potential.

Beyond prophylactic vaccination, LNPs are increasingly explored for a range of therapeutic applications, particularly in oncology. In cancer therapy, LNPs offer opportunities to improve the therapeutic index of nucleic acid-based drugs by enhancing tumour delivery, reducing off-target exposure, and limiting systemic toxicity [15]. LNP-mediated delivery has enabled the investigation of RNA-based therapeutics, including mRNA, siRNA, and other nucleic acid modalities, that were previously limited by poor stability, rapid degradation, or inefficient cellular uptake [73]. As a result, LNPs are now recognised as a versatile platform with potential applications extending well beyond infectious disease vaccines [10].

In addition to scientific validation, the success of LNP-formulated mRNA vaccines established important regulatory and manufacturing practices. Large-scale production, quality control, and global distribution of LNP-based products were achieved under emergency and subsequently standard regulatory pathways, providing confidence in the scalability and robustness of this technology [15, 44]. This has thus lowered barriers to clinical development for future LNP-based therapeutics and reinforced the concept of LNPs as a versatile platform technology rather than for just for a single use [66, 72].

Formulation and Manufacturing of Lipid Nanoparticles

The methods used to formulate lipid nanoparticles have evolved significantly alongside advances in nanomedicine and process engineering. Early lipid-based nanoparticles, including liposomes and initial LNP formulations, were commonly produced using bulk mixing techniques such as ethanol injection, thin-film hydration, or solvent displacement [83]. While these approaches enabled early proof-of-concept studies, they often suffered from poor reproducibility, broad particle size distributions, and limited scalability [38]. Variability in local mixing conditions and solvent exchange rates made it difficult to precisely control nanoparticle formation, including the encapsulation of nucleic acids.

The introduction of microfluidic technologies represented a major advancement in the manufacturing of lipid nanoparticles. Microfluidic mixing enables controlled, reproducible contact between an organic lipid phase and an aqueous phase containing the nucleic acid payload, thereby enabling consistent self-assembly of LNPs under well-defined flow conditions. Microfluidic systems typically operate at low Reynolds numbers, which describe how smoothly a fluid flows [84]. At low Reynolds numbers, flow is laminar rather than turbulent, meaning that fluids move in smooth, predictable layers rather than mixing chaotically (Figure 1.4). This laminar flow behaviour contrasts with turbulent flow, which exhibits many random fluctuations and eddies. In microfluidic devices, the combination of low Reynolds numbers and small channel sizes ensures that mixing occurs in a controlled and repeatable way, driven by diffusion and the design of the mixer rather than uncontrolled turbulence [84]. This predictable flow behaviour reduces batch-to-batch variability and allows fine control over formulation parameters that influence nanoparticle formation, making microfluidic platforms well-suited to the reproducible production of LNPs [38, 83].

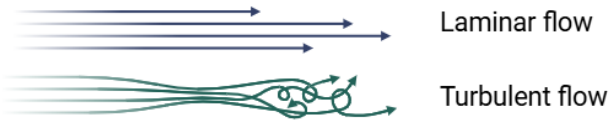

Figure 1.4: Laminar versus Turbulent flow of fluid.

During microfluidic manufacturing, lipid nanoparticles are formed through a rapid self-assembly process driven by controlled solvent exchange between the organic and aqueous phases [85]. Lipids are typically dissolved in an organic solvent, such as ethanol, while the nucleic acid payload is dissolved in an acidic aqueous buffer, such as citrate buffer. Upon contact within the microfluidic mixer, the organic solvent is rapidly diluted by the aqueous phase, thereby reducing lipid solubility and triggering nanoparticle assembly (Figure 1.5).

As solvent exchange proceeds, ionisable lipids become protonated under acidic conditions and electrostatically interact with the negatively charged nucleic acid, thereby forming a complex with the payload. Simultaneously, helper lipids and sterols reorganise around this core, while PEGylated lipids preferentially orient towards the particle surface, stabilising the nanoparticle [55, 86]. This coordinated reorganisation of lipid components results in the formation of a core-shell LNP structure encapsulating the nucleic acid payload [66].

The final structure of the LNP is established early during the mixing process, with downstream processing steps primarily serving to remove solvent and adjust formulation conditions instead of altering particle architecture [2]. As a result, precise control of the initial mixing environment is critical to achieving consistent LNP formation during microfluidic manufacturing.

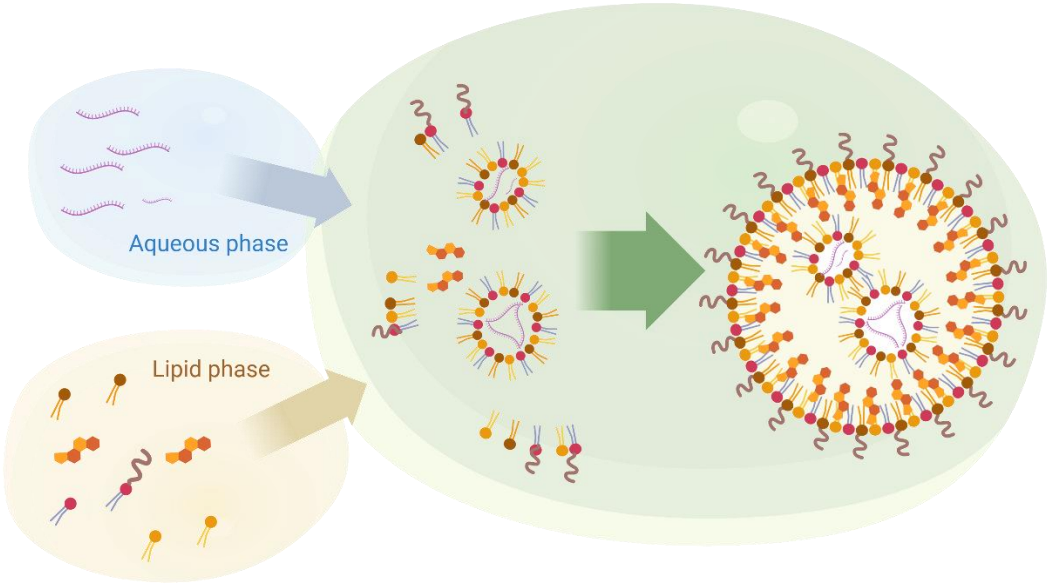

Figure 1.4: LNP formation, based on [87]. Created using BioRender.

In recent years, microfluidic mixing has become the dominant method for LNP production, particularly for RNA-based therapeutics, due to its improved reproducibility, scalability, and compatibility with continuous manufacturing [85]. A range of passive micromixer designs has been developed to enhance mixing efficiency. These include toroidal mixers, which use centrifugal forces generated by curved flow paths, and staggered herringbone mixers, which incorporate embossed chevron structures to induce transverse flows and rapid solvent exchange [9]. Simpler geometries, such as T-junction mixers and hydrodynamic flow-focusing devices, have also been extensively used and remain valuable for controlled nanoparticle assembly under specific flow conditions. Typical micromixer designs frequently employed for LNP production are illustrated in Figure 1.6.

Compared with bulk methods, microfluidic production is generally more time- and resource-efficient, requiring lower energy input, reduced reagent consumption, and smaller working volumes [88]. These advantages make microfluidics especially appealing for early-stage formulation development and for scaling up to larger production. Additionally, microfluidic platforms enable the investigation of formulation parameters, such as flow rate and phase ratio, in a controlled and reproducible manner.

Following formulation, LNP batches typically undergo a purification or buffer exchange step to remove residual organic solvent, unencapsulated nucleic acid, and excess lipids. Several purification approaches are commonly employed during LNP development, including dialysis, centrifugal filtration (spin columns), and tangential flow filtration (TFF) (Figure 1.7). The choice of method is influenced by formulation scale, experimental throughput, and application.

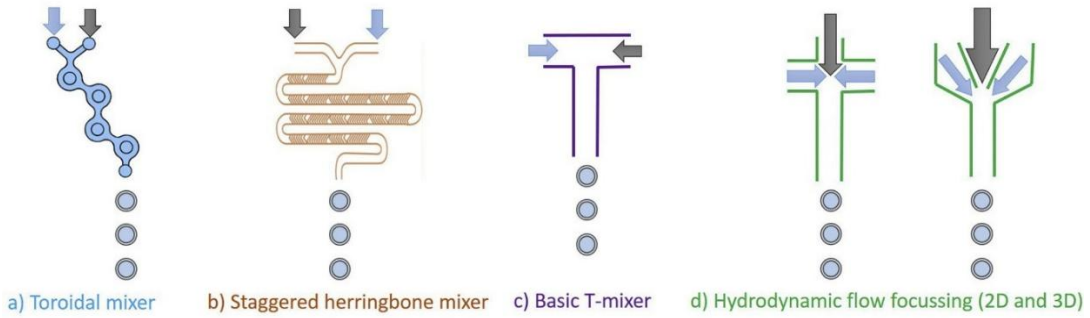

Figure 1.6: Schematic examples of micromixer cartridge designs commonly used in production of lipid nanoparticles: (A) toroidal planar mixer using centrifugal forces, (B) staggered herringbone mixer with embossed chevrons, (C) T-junction mixer with two inlets, and (D) hydrodynamic flow-focusing mixer with three inlets [9].

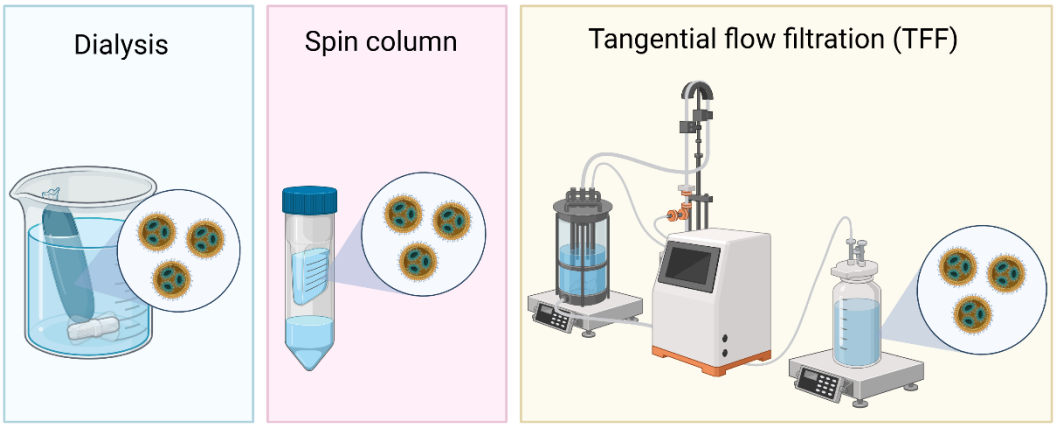

Figure 1.7: Common methods for purifying lipid nanoparticles. Created using BioRender.

Dialysis is one of the simplest purification techniques used in lipid nanoparticle research. In this approach, the LNP suspension is placed within a semi-permeable membrane and immersed in a large volume of exchange buffer, allowing small molecules such as solvent and free nucleic acid to diffuse out over time. Dialysis is well-suited to small-scale laboratory studies due to its simplicity and minimal equipment requirements. However, it is a relatively slow process, offers limited control over buffer exchange kinetics, and is difficult to scale, making it less suitable for high-throughput formulation screening or industrial manufacturing [89].

Centrifugal filtration, often referred to as spin column purification, uses membrane-based filter units and centrifugal force to concentrate and buffer-exchange LNP formulations rapidly. Spin columns enable faster processing than dialysis and are convenient for small volumes, making them widely used in early-stage formulation development and screening studies. Despite these advantages, centrifugal filtration is inherently discontinuous and scale-limited, and it can introduce shear forces that may affect sensitive formulations. As a result, its application is largely restricted to small-scale, preclinical research [89].

Tangential flow filtration (TFF) is a pressure-driven membrane filtration technique in which the formulation flows parallel to the membrane surface, reducing build-up and enabling continuous processing. TFF allows efficient solvent removal, buffer exchange, and concentration of LNPs while maintaining control over processing conditions [90]. Importantly, TFF is readily scalable and compatible with both laboratory and industrial manufacturing [91]. For these reasons, TFF is the most commonly used purification method for LNPs in commercial and clinical production, including large-scale

manufacture of RNA-based therapeutics. Its scalability, reproducibility, and compatibility with good manufacturing practice (GMP) make it the preferred approach for translational and commercial applications [92].

Each purification method therefore contributes a distinct role within LNP development, with dialysis and centrifugal filtration supporting early-stage research and formulation screening, and TFF enabling robust purification at scales relevant to clinical and commercial use.

Together, advances in formulation and manufacturing technologies have enabled the reliable production of LNPs with controlled properties and have been central to the clinical translation of LNP-based therapeutics.

Manufacturing and Translational Challenges in LNP Development

While lipid nanoparticles (LNPs) have demonstrated clear clinical potential, particularly for nucleic acid delivery, their translation from laboratory-scale formulations to clinically and commercially viable products presents several manufacturing and translational challenges [15]. These challenges arise from the need to ensure reproducibility, scalability, robustness, and regulatory compliance, while maintaining consistent physicochemical and biological performance [44].

One key challenge in LNP development is batch-to-batch variability. Small changes in formulation parameters, mixing conditions, or raw material quality can lead to measurable differences in particle size, encapsulation efficiency, and biological performance [80, 93]. This sensitivity places intense demands on manufacturing control and highlights the importance of well-defined and robust operating ranges. While microfluidic platforms offer improved reproducibility compared with bulk mixing approaches, careful optimisation and validation of process parameters remain essential, particularly when transitioning from different scales or manufacturing systems [94].

Scalability is another major challenge when translating LNPs from the laboratory to clinical and commercial use. Most LNP formulations are first developed at small laboratory scales, where material use, processing time, and equipment demands are relatively low. However, producing larger quantities for preclinical studies, clinical trials, or commercial supply requires careful consideration of production speed, process

continuity, and equipment suitability [15]. This can be achieved either by operating multiple microfluidic devices in parallel (scale-out) or by increasing flow rates or switching to alternative manufacturing platforms (scale-up), each of which introduces different technical and regulatory challenges. Maintaining consistent LNP properties across all production scales is essential for successful translation [94].

Manufacturing lipid nanoparticles under good manufacturing practice (GMP) conditions adds further practical challenges. GMP requires tight control over raw materials, manufacturing steps, and final product quality, along with detailed documentation and validation. For LNPs, this includes ensuring consistent lipid quality, effective removal of organic solvents, reliable buffer exchange, and sterility of the final product [44]. Purification and concentration steps must also be compatible with GMP processes and be scalable without altering the formulation's properties. These requirements can restrict formulation flexibility and highlight the importance of developing manufacturing processes that are robust and easily transferable.

Cost and logistics are also important factors in translating LNPs to the clinic. The use of specialised lipids, organic solvents, and tightly controlled manufacturing environments contributes to the high cost of production [95]. In addition, many LNP formulations have limited stability and require frozen storage and cold-chain transport, which increases complexity and expense, particularly for global distribution [44, 96]. Improving formulation stability and manufacturing efficiency is therefore essential to support widespread clinical and commercial use, especially for vaccine applications that require large-scale distribution.

Together, these manufacturing and translational challenges emphasise the need for an integrated approach to LNP development that considers formulation design, manufacturing processes, and scalability from an early stage [97]. Systematic evaluation of formulation robustness and process parameters is key to enabling reliable, scalable, and cost-effective translation of LNP-based therapeutics from the laboratory to the clinic.

Evaluating critical quality attributes of nanoparticles and effectiveness *in vitro* and *in vivo*.

Critical quality attributes (CQAs) are key physical and chemical properties that describe lipid nanoparticle (LNP) formulations and influence their stability, reproducibility, and behaviour in biological systems [15, 80]. Among these, particle size and size distribution are particularly important. LNP size affects how stable the particles are, how efficiently they are taken up by cells, and where they distribute in the body after administration [97]. In microfluidic manufacturing, particle size is closely linked to mixing conditions and formulation parameters, making it a useful indicator of how consistent the manufacturing process is [94].

Polydispersity index (PDI) describes how uniform the particle sizes are within a formulation. Low PDI values indicate a more uniform particle population, which is desirable because particles of very different sizes can behave unpredictably and reduce reproducibility in both *in vitro* and *in vivo* studies [80].

Surface charge, commonly measured as zeta potential, provides information about particle stability and how LNPs interact with their surrounding environment. For ionisable lipid-based LNPs, the surface charge is typically close to neutral at physiological pH, meaning the particles carry very little charge while circulating in the body [66, 98]. This near-neutral charge helps reduce unwanted interactions with blood proteins. It lowers the risk of toxicity while still allowing the particles to become positively charged under acidic conditions during formulation and inside endosomes. Zeta potential, therefore, offers useful insight into how LNPs behave under different biological conditions.

Encapsulation efficiency describes how effectively the nucleic acid payload is packaged inside the LNPs and directly influences dose accuracy and delivery efficiency [66]. High encapsulation efficiency ensures that most of the administered nucleic acid is protected within the particles, reducing degradation and limiting off-target effects from free nucleic acid [94]. Consistent encapsulation is therefore essential when comparing LNP formulations.

After physicochemical characterisation, *in vitro* studies provide an important first step in assessing LNP performance. *In vitro* expression experiments allow different

formulations to be compared under controlled conditions and help identify how CQAs and formulation variables influence transgene expression. In addition to measuring expression [80], *in vitro* toxicity studies are commonly used to assess how well formulations are tolerated by cells, as high levels of cytotoxicity can interfere with expression measurements and limit their translational relevance. However, while *in vitro* assays are valuable for screening and optimisation, they cannot fully replicate the complexity of living systems and often have limited ability to predict *in vivo* behaviour [97].

For this reason, *in vivo* studies are essential for evaluating the functional performance of LNP formulations. Measuring transgene expression after administration provides a direct indication of successful delivery, cellular uptake, and intracellular release of the nucleic acid payload [66]. Long-term *in vivo* expression studies also allow assessment of both the level and duration of expression, which are particularly important for therapeutic and vaccine applications [15].

Although this thesis focuses on expression-based outcomes, it is important to note that vaccine development requires additional evaluation of immune activation, antigen presentation, and protective efficacy [96]. Together, *in vivo* expression studies link formulation characterisation with application-specific outcomes and support the rational development of LNP-based therapeutics and vaccines [99].

In Vitro Models and Their Limitations in Predicting *In Vivo* Performance

In vitro studies play an important role in the development and optimisation of LNP formulations. They provide a controlled and reproducible way to assess delivery efficiency, transgene expression, and cytotoxicity [15, 93]. Immortalised cell lines are commonly used because they are easy to culture, highly reproducible, and well-suited for comparing multiple formulations and manufacturing conditions. These models allow rapid screening of formulation performance and support early-stage optimisation [40, 100].

However, *in vitro* models are a simplified representation of biological systems and have clear limitations in predicting *in vivo* behaviour. Cell lines can differ substantially from primary cells and tissues in receptor expression, uptake pathways, membrane composition, and metabolism. As a result, the cellular uptake and intracellular

processing of LNPs observed *in vitro* may not accurately reflect what occurs *in vivo* [67, 101]. In addition, *in vitro* experiments are typically performed without physiological protein levels, immune components, or dynamic flow conditions, all of which influence LNP behaviour after administration (Figure 1.8). The absence of an *in vivo*-like protein corona can alter uptake and trafficking, while tissue-level processes such as biodistribution, clearance, and off-target interactions cannot be assessed in cell-based assays [93, 102].

Differences between *in vitro* and *in vivo* performance are well documented for LNP systems, with formulations that perform well *in vitro* sometimes showing reduced or altered activity *in vivo* [40, 103]. These discrepancies highlight the need to interpret in vitro expression data as a relative and context-dependent measure rather than a direct predictor of in vivo efficacy. Despite these limitations, *in vitro* models remain valuable for comparative screening and gaining mechanistic insight when their constraints are clearly recognised [103].

For this reason, *in vivo* studies are essential for evaluating LNP performance under physiologically relevant conditions. Combining *in vitro* screening with *in vivo* evaluation provides a more complete understanding of formulation behaviour and supports the rational optimisation and translation of LNP-based delivery systems.

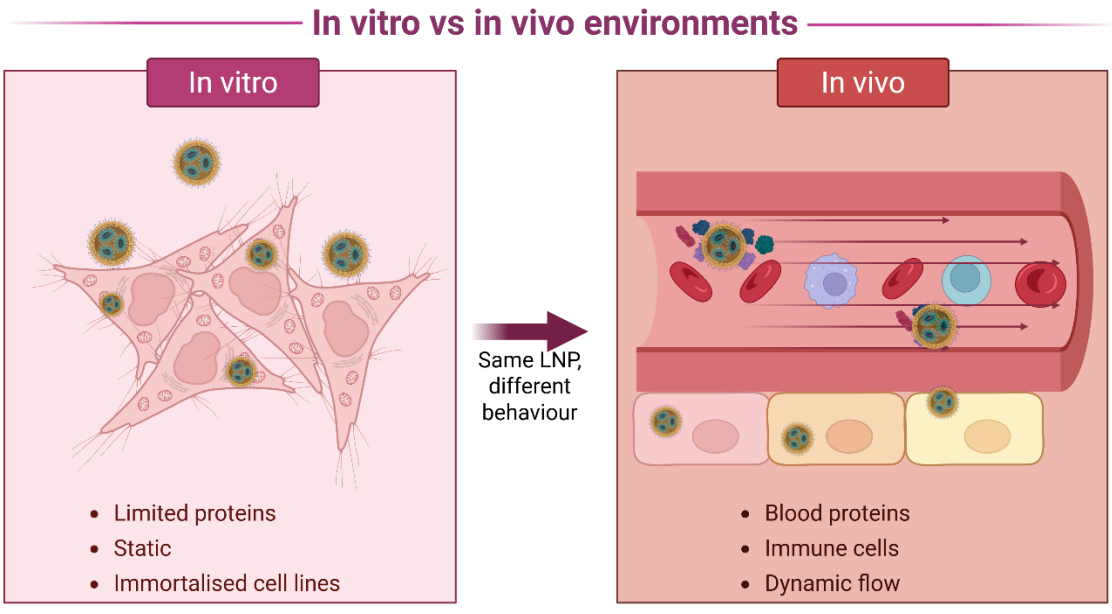

Figure 1.8: Differences between *in vitro* and vivo environments. Created using BioRender.

Scope for improving lipid nanoparticle formulation

Despite the rapid clinical translation of lipid nanoparticles (LNPs), particularly for RNA-based therapeutics, there remains considerable scope for improving their formulation and manufacturing. In the context of microfluidic production, many formulation parameters currently used for LNPs have been adopted directly from optimised methods originally developed for liposomes [9]. This conservative approach has supported reproducibility and accelerated clinical development; however, it has also limited systematic exploration of formulation space. As a result, many LNP formulations rely on established parameter ranges rather than being tailored specifically to the distinct structural and biological requirements of nucleic acid delivery systems.

Current LNP manufacturing approaches are associated with several practical challenges. Production costs remain high, driven by specialised lipids, organic solvents, and controlled manufacturing processes [15, 72]. In addition, many clinically relevant LNP formulations exhibit limited long-term stability at ambient temperatures, necessitating frozen storage and cold-chain distribution [95]. This requirement imposes significant logistical and economic burdens, particularly for large-scale vaccination programmes and global distribution, and highlights the need for improved formulation robustness and stability [96].

Current LNP formulations used in preclinical and clinical settings typically follow a broadly similar compositional framework, consisting of an ionisable lipid, a helper phospholipid, a sterol, and a PEGylated lipid in defined molar ratios [15, 66]. While the specific identities of these components may vary, the relative proportions are often conserved across formulations, reflecting parameter sets that have demonstrated acceptable performance and tolerability in earlier studies. Clinically advanced LNPs commonly employ ionisable lipids at approximately 40–50 mol%, with sterols contributing around 35–45 mol%, helper phospholipids approximately 5–10 mol%, and PEGylated lipids typically present at low levels (around 1–2 mol%) to balance stability and biological performance. These compositions have been widely adopted as reference formulations and form the basis for many experimental and translational studies [67, 104].

Although this compositional framework has proven effective for enabling clinical translation, it has also contributed to a degree of standardisation within the field [15,

66]. As a result, many studies focus on substituting individual lipid components while maintaining similar overall proportions, rather than systematically exploring wider parameters alongside these [67]. This approach supports comparability between studies but may overlook opportunities further to optimise formulation performance, stability, and manufacturability. A more comprehensive understanding of how lipid identity and relative proportions influence LNP behaviour could therefore support the development of formulations that are better tailored to specific payloads, routes of administration, or clinical applications [15, 97].

Extensive optimisation of formulation parameters has been carried out in the field of liposomes, encompassing lipid composition, solvent systems, buffer conditions, and processing variables [9, 105]. For example, the research by Kastner et al. on using microfluidics and varying manufacturing parameters on liposomes directly translates to LNPs manufactured in the same way [106]. Translating this body of knowledge to LNP systems represents a valuable opportunity to enhance formulation performance while using existing understanding of lipid-based nanomedicines. In particular, systematic investigation of formulation parameters such as pH, flow rate ratio (FRR), total flow rate (TFR), N/P ratio, lipid concentration, and solvent composition has the potential to improve reproducibility, stability, and scalability of LNP production [85, 94]. However, while many of these variables have been explored individually, their combined effects and robustness across different formulation conditions have still not been fully studied [55, 107].

The use of high organic solvent content (often 25%), particularly ethanol, during microfluidic formulation is another area where optimisation may be beneficial. Rapid solvent exchange is central to LNP self-assembly, yet excessive solvent concentrations and extreme flow conditions may promote transient intermediate structures or increased heterogeneity, potentially leading to broader size distributions and increased polydispersity [85, 94]. Understanding how such intermediate states arise and how to control or avoid them is important for refining manufacturing strategies.

Beyond optimisation, systematic testing of parameter robustness is essential for defining acceptable operating ranges and identifying formulation limits. Establishing these boundaries can improve manufacturing reliability, facilitate scale-up, and reduce the risk of batch failure [107]. From an engineering perspective, improving cost-

effectiveness through efficient use of materials, simplified processing, and enhanced stability is critical for the long-term viability of LNP-based therapeutics [15].

Collectively, these considerations highlight the need for a structured investigation into the relationships between formulation parameters, manufacturing conditions, and LNP performance. Addressing these gaps provides the foundation for the aims and objectives of this research.

Aim and objectives

The overarching aim of this thesis was to systematically investigate how manufacturing parameters, formulation composition, and nucleic acid payload influence the physicochemical properties and biological performance of lipid nanoparticles (LNPs) for nucleic acid delivery. By examining these factors in a controlled and stepwise manner, this work sought to improve understanding of structure–function relationships within LNP systems and to support the rational design of robust and reproducible LNP formulations for *in vitro* and *in vivo* applications.

To achieve this aim, the following specific objectives were addressed:

1. **To establish reproducible LNP manufacturing conditions using microfluidic formulation approaches.** Initial studies were undertaken to optimise key formulation and processing parameters using a NanoAssemblr-based microfluidic platform. This included evaluating the effects of total flow rate, N/P ratio, lipid concentration, lipid-phase solvent, and aqueous buffer concentration on LNP critical quality attributes (CQAs), including particle size, polydispersity, surface charge, and nucleic acid encapsulation efficiency. In addition, commonly used downstream processing methods, including dialysis, centrifugal filtration, and tangential flow filtration, were compared to assess their impact on LNP CQAs. These studies provided a consistent formulation framework for subsequent investigations.
2. **To investigate size control as a design parameter for LNP performance.** Building on the optimised formulation conditions, the effect of the aqueous-to-organic phase ratio was examined as a strategy to control LNP size while precisely maintaining constant lipid composition. The relationship between controlled size variation and nucleic acid expression was evaluated *in vitro* and *in vivo* to determine the robustness of LNP-mediated expression across a range of particle diameters.

3. **To evaluate the influence of lipid composition on LNP physicochemical properties and biological performance.** A systematic comparison of clinically used and proprietary ionisable lipids was conducted to assess how lipid structure influences LNP characteristics, encapsulation efficiency, expression, and biodistribution. The contribution of sterol identity was also examined to determine its role in modulating LNP properties. Comparisons between *in vitro* and *in vivo* performance were used to assess the predictive value of *in vitro* screening models.
4. **To assess the impact of nucleic acid payload identity on LNP-mediated expression profiles.** LNPs encapsulating messenger RNA (mRNA), self-amplifying RNA (saRNA), plasmid DNA (pDNA), and defined combinations of these payloads were evaluated to determine how payload biology influences expression kinetics *in vitro* and *in vivo*. The behaviour of combined-payload formulations was assessed to establish whether expression profiles could be modulated without altering LNP composition or structure.
5. **To explore the scalability of LNP manufacturing using an alternative microfluidic platform.** Finally, a novel microfluidic manufacturing system was evaluated to assess the effect of increased production flow rates and an alternative manufacturing approach on LNP expression, providing preliminary insight into the scalability and robustness of LNP production.

Together, these objectives were designed to provide a comprehensive and integrated assessment of the key factors governing LNP performance, supporting the development of rational formulation and manufacturing strategies for nucleic acid delivery systems.

CHAPTER 2: OPTIMISATION EXPERIMENTS

Introduction

This chapter describes a systematic optimisation of lipid nanoparticle (LNP) manufacturing using microfluidic formulation, conducted before the main experimental chapters presented in this thesis. The primary aim of this work was to establish robust, reproducible, and cost-effective formulation conditions that could serve as a consistent foundation for subsequent studies. Initial experiments were designed to confirm trends previously established within this research laboratory and reported in the literature [38, 108], before progressing to formulations more closely aligned with clinically advanced systems, including those used in the Pfizer–BioNTech Comirnaty® vaccine.

The general workflow for microfluidic production of LNPs comprises several key stages: (i) nanoparticle manufacture, (ii) purification to remove organic solvent and unencapsulated nucleic acid, (iii) physicochemical characterisation, (iv) sterilisation, and (v) preparation of the final product. Variability introduced at any stage of this process can affect critical quality attributes (CQAs) and complicate the interpretation of downstream experiments. Therefore, careful evaluation of manufacturing and purification parameters is essential before undertaking comparative biological studies.

The CQAs assessed throughout this chapter included particle size, polydispersity index (PDI), zeta potential, encapsulation efficiency (EE%), and mass balance (MB%). Particle size was measured in nanometres, with stable LNP formulations typically ranging from 50–200 nm. The PDI provides a measure of size heterogeneity within a particle population, with values below 0.2 generally considered indicative of uniform formulations [38]. Zeta potential reflects the surface charge of the particles and provides insight into colloidal stability and biological tolerability. This measures the combined surface charge of the whole nanoparticle rather than the charge of one individual lipid [109]. Therefore, the measured charge is influenced by interactions between the cationic or ionisable lipid, the negatively charged nucleic acid cargo, helper lipids, PEG-lipids, and ions present in the surrounding buffer[2]. for LNPs intended for therapeutic applications, near-neutral surface charge (0 ± 10 mV) is generally desirable, as highly charged particles are associated with increased toxicity *in vivo* [2, 15]. As a result, LNPs containing positively charged lipids may still exhibit near-neutral zeta potentials if the lipid charge is balanced by the negatively charged nucleic acid payload.

Encapsulation efficiency was used to assess the proportion of nucleic acid successfully incorporated within LNPs, with values above 90% considered indicative of efficient formulation. Mass balance, defined as the percentage of nucleic acid recovered after formulation and purification, was used to assess material recovery, with values above 80% considered acceptable for experimental and translational workflows.

Three primary LNP formulations were investigated in this chapter, each based on a common lipid framework comprising DSPC, cholesterol, an ionisable or cationic lipid, and a PEGylated lipid at fixed molar ratios. Formulation 1- DSPC:Chol:DOTAP:DMG-PEG, Formulation 2- DSPC:Chol:ALC-0315:DMG-PEG, Formulation 3- DSPC:Chol:ALC-0315:ALC-0159. Individual formulations differed by substitution of the ionisable or PEG-lipid component, allowing assessment of how lipid identity influenced formulation behaviour while maintaining consistent overall composition. The chemical structures of the lipids used are summarised in Table 2.1.

Table 2.1: The structure of each lipid used in the manufacture of LNPs for these experiments.

Lipid type	Name	Structure
Ionisable/ cationic lipid	DOTAP (cationic)	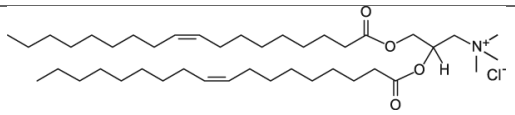
	ALC-0315 (ionisable)	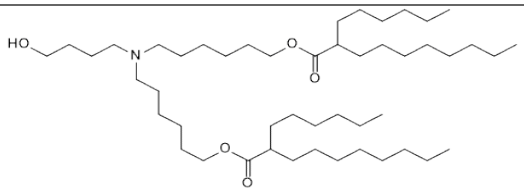
PEG-lipid	DMG-PEG 2000	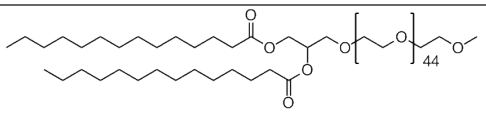
	ALC-0159	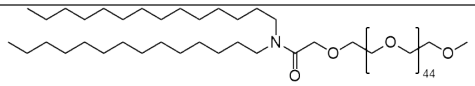
Cholesterol	Cholesterol	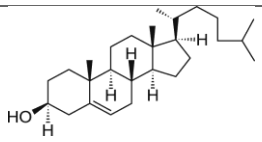
Phospholipid	DSPC	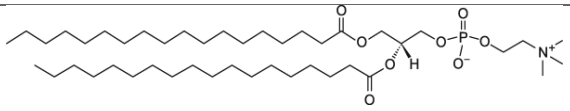

For all formulations, pre-prepared lipid stock solutions (5 mg/mL) and polyadenylic acid (polyA; 1 mg/mL) were used to ensure consistency across experiments. Citrate buffer (50 mM) was used as the aqueous phase for DOTAP-containing LNPs and ionisable lipid formulations, with phosphate-buffered saline (PBS, pH 7.3) used for buffer exchange.

Baseline manufacturing conditions were established using a flow rate ratio (FRR) of 3:1, a total flow rate (TFR) of 20 mL/min, and an N/P ratio of 6, against which the effects of variations in individual parameters were assessed.

Across the three formulations, a variety of microfluidic and formulation parameters were systematically examined, including FRR, TFR, N/P ratio, lipid concentration, choice of solvent for the lipid phase, aqueous buffer concentration and pH, and downstream purification method. Purification techniques evaluated included dialysis, centrifugal filtration (spin columns), and tangential flow filtration (TFF), reflecting methods commonly employed at different stages of LNP development. Selected formulations were also tested for stability over time to assess formulation robustness.

Overall, this optimisation chapter establishes a validated and reproducible microfluidic manufacturing framework for lipid nanoparticle production. The conditions defined here provide a foundation for subsequent investigations, including *in vivo* studies presented in later chapters. By standardising formulation and processing parameters, this work informs the selection of manufacturing conditions used throughout the thesis. It ensures that subsequent experimental chapters can focus on biological and mechanistic questions without confounding effects from manufacturing variability.

Materials and methods

Materials

1,2-distearoyl-sn-glycero-3-phosphocholine (DSPC) was obtained from Lipoid (Ludwigshafen, Germany). 1,2-dioleoyl-3-trimethylammoniumpropane (chloride salt) (DOTAP), and 1,2-dimyristoyl-rac-glycero-3-methoxypolyethylene glycol-2000 (DMG-PEG 2000) were purchased from Avanti Polar Lipids (Alabaster, AL, USA). Cholesterol, citric acid, sodium citrate tribasic dehydrate, polyadenylic acid (PolyA), 6-(*p*-Toluidino)-2-naphthalenesulfonic acid sodium salt, Sodium phosphate monobasic ($NaH_2PO_4 \bullet H_2O$), and Sodium phosphate dibasic (anhydrous)(Na_2HPO_4) were acquired from Sigma-Aldrich (St. Louis, MO, USA). Phosphate-buffered saline tablets (PBS pH 7.4)

were acquired from Oxoid Ltd. (Basingstoke, UK). Tris Base and Ethanol (EtOH) were obtained from Fisher Scientific (Loughborough, UK). Methanol and Propan-2-ol (Isopropanol, IPA) were purchased from VWR Chemicals (Lutterworth, UK). The ionisable lipids [(4-Hydroxybutyl)azanediyl]di(hexane-6,1-diyl) bis(2-hexyldecanoate) (ALC-0315) and 9-Heptadecanyl 8-((2-hydroxyethyl)[6-oxo-6-(undecyloxy)hexyl]amino)octanoate (SM-102) and the PEG-lipid 2-[(polyethylene glycol)-2000]-N,N-ditetradecylacetamide, Methoxypolyethyleneglycoloxy(2000)-N,N-ditetradecylacetamide (ALC-0159) were purchased from BroadPharm (San Diego, CA, USA). Minimum Essential Medium, Trypsin-EDTA (0.05%), PBS, pH 7.4 solution and Quant-it™ RiboGreen RNA Assay Kit and RiboGreen RNA Reagent, RediPlate™ 96 RiboGreen™ RNA Quantitation Kit were purchased from Fisher Scientific UK Limited (Renfrew, UK). EZ Cap™ Firefly Luciferase mRNA was purchased from ApexBio Technology (Houston, TX, USA). The ONE-Glo™ Luciferase Assay System was acquired from Promega UK (Southampton, UK). All solvents and other chemicals were of analytical grade, and an in-house system supplied Milli-Q water.

Aqueous and Lipid Phase Preparation

The aqueous and lipid phases were prepared separately before microfluidic formulation. The aqueous phase contained polyadenylic acid (polyA) as a model nucleic acid payload, while the lipid phase comprised the required lipid components dissolved in organic solvent.

The aqueous phase was prepared by diluting a 1 mg/mL polyA stock solution with a pre-calculated volume of 50 mM citrate buffer to achieve the desired starting polyA concentration. Citrate buffer at pH 6 was used for DOTAP-containing LNPs, while pH 4 citrate buffer was used for ionisable lipid–based LNPs (e.g. ALC-0315 formulations). The required polyA concentration was calculated based on the target nitrogen-to-phosphate (N/P) ratio using Equation (1):

$$PolyA\ starting\ molarity = \frac{Molarity\ ionisable\ lipid}{N/P\ ratio} \times \frac{lipid\ ratio}{aqueous\ ratio} \qquad \textit{Equation (1)}$$

The molarity of the ionisable lipid was determined by multiplying the total lipid molarity of the formulation by the molar fraction of the ionisable lipid. Total lipid molarity was calculated by first determining the average molecular weight of the lipid mixture, obtained by multiplying each lipid component's molar fraction by its molecular weight

and summing the products. The total lipid concentration (mg/mL) was then divided by the calculated average molecular weight to give the total lipid molarity.

Individual lipid stocks were prepared by dissolving each lipid in 100% ethanol at concentrations ranging from 5–20 mg/mL and stored according to manufacturer recommendations. Unless otherwise stated, the lipid phase introduced into the microfluidic device had a total lipid concentration of 5 mg/mL. Variations in lipid concentration were applied only in experiments specifically designed to assess their effect on LNP critical quality attributes.

Detailed lipid- and aqueous-phase calculations for each formulation and experimental condition are provided in Tables 2.2–2.7.

Table 2.2: Lipid phase calculations for Formulation 1

DSPC:Chol:DOTAP:DMG-PEG	Molar fraction (%)	Volume required in 1mL (µL)
DSPC	10	129
Chol	38.5	242
DOTAP	50	568
DMG-PEG	1.5	61

Table 2.3: Aqueous phase calculations for Formulation 1

Flow rate ratio	N/P ratio	PolyA starting concentration (mg/mL)	Volume required for 1mL (µL)
3:1	**6**	**0.074**	**74**
1:1	6	0.222	222
2:1	6	0.111	111
5:1	6	0.044	44
3:1	3	0.148	148
3:1	8	0.056	56

Table 2.4: Lipid phase calculations for formulation 2

DSPC:Chol:ALC-0315:DMG-PEG	Mole fraction (%)	Volume required in 1mL (µL)
DSPC	10	122
Chol	38.5	229
ALC-0315	50	591
DMG-PEG	1.5	58

Table 2.5: Aqueous phase calculations for formulation 2

Flow rate ratio	N/P ratio	PolyA starting concentration (mg/mL)	Volume required for 1mL (µL)
3:1	**6**	**0.070**	**70**
1:1	6	0.211	211
2:1	6	0.105	105
3:1	3	0.141	141
3:1	8	0.053	53

Table 2.6: Lipid phase calculations for formulation 3

DSPC:Chol:ALC-0315: ALC-0159	Mole fraction (%) -a	Volume required for 1mL (µL) -a	Mole fraction (%) -b	Volume required for 1mL (µL) -b
DSPC	10	122	9.4	117
Chol	38.5	230	42.7	261
ALC-0315	50	591	46.3	560
ALC-0159	1.5	57	1.6	62

Table 2.7: Aqueous phase calculations for formulation 3

Flow rate ratio	N/P ratio	PolyA starting concentration (mg/mL)	Volume required for 1mL (µL)-PolyA	mRNA starting concentration (mg/mL)	Volume required for 1mL (µL)-mRNA
3:1	**6**	**0.070**	**70**	**0.073**	**73**
2:1	6	0.105	105	0.109	109
1.5:1	6	0.141	141	0.146	146
1.3:1	6	0.162	162	0.168	168

Manufacture of the LNPs using microfluidics

Lipid nanoparticles were manufactured using the NanoAssemblr® Benchtop system (Precision Nanosystems Inc., now known as Cytiva) for all experiments described in this chapter. The ethanol-based lipid phase and the aqueous phase containing citrate buffer and nucleic acid payload (polyA or firefly luciferase (Fluc) mRNA) were loaded into 1 mL and 3 mL syringes, respectively, and introduced into a reusable microfluidic cartridge incorporating a staggered herringbone mixer design.

Upon controlled mixing of the two phases in the microfluidic chip, lipid nanoparticles formed via rapid self-assembly. The formulation output was collected directly into a 15 mL centrifuge tube. Any material dispensed before and after the formulation run was

collected separately in an additional 15 mL centrifuge tube to ensure accurate recovery of the formulated sample.

The total flow rate (TFR) and flow rate ratio (FRR; aqueous:lipid phase) were controlled using the NanoAssemblr software interface. TFRs ranging from 5–20 mL/min and FRRs between 1:1 and 5:1 were investigated, depending on the experimental condition.

Following each formulation run, the microfluidic cartridge was cleaned for reuse by sequentially flushing the system with 100% ethanol, double-distilled water, and atmospheric air using 3 mL syringes. Cleaning was performed at a flow rate ratio of 1:1 and a total flow rate of 18 mL/min to remove residual material and prepare the cartridge for subsequent formulations.

Purification methods

Dialysis

For dialysis-based purification, 1 mL of LNP formulation in the original ethanol/citrate buffer was transferred into dialysis tubing and sealed using dialysis clips. The sample was dialysed against 200 mL of phosphate-buffered saline (PBS, pH 7.4) for 1 hour at room temperature to remove the organic solvent and exchange the buffer.

Centrifugal Filtration (Spin Columns)

Centrifugal filtration was performed using 100 kDa molecular weight cut-off spin columns. LNP samples were diluted 40-fold in PBS before purification. Samples were centrifuged at 2,000 × g for 5–10 minutes at 4 °C. As the filtrate passed through the membrane, an additional sample was added to the column until a final retentate volume of 1 mL was obtained, matching the original sample volume.

Tangential Flow Filtration (TFF)

Tangential flow filtration was carried out using a KrosFlo® KR2i TFF System (Repligen) equipped with 100-kDa modified polyethersulfone (mPES) hollow-fibre filters, each with a membrane surface area of 20 cm^2. To minimise the system's exposure to high ethanol concentrations, samples were initially diluted fivefold in PBS before concentration. The formulation was then concentrated back to its original volume.

Buffer exchange was performed using 12 diafiltration volumes of PBS (e.g. 24 mL PBS for a 2 mL sample). All TFF steps were conducted at flow rates of 15–20 mL/min, with system pressure kept below 5 psi to protect sample integrity.

Measuring Critical Quality Attributes (CQAs)

Physicochemical Characteristics

Particle size (Z-average diameter), polydispersity index (PDI), and zeta potential were measured using a Zetasizer ZS or Zetasizer Ultra (Malvern Panalytical, UK), with data acquisition performed using Zetasizer software. Particle size and PDI were determined by dynamic light scattering (DLS) using a fixed backscatter detection angle of 173°. Zeta potential measurements were obtained using electrophoretic light scattering within folded capillary cells.

All measurements were performed in triplicate for each experimental repeat (n = 3), yielding 9 measurements per condition. Following purification, samples were diluted to a lipid concentration of 0.1 mg/mL before measurement. Phosphate-buffered saline (PBS) was used as the dispersant for size and PDI measurements. In contrast, double-distilled water (ddH_2O) was used for zeta potential measurements to achieve attenuation values between 7 and 8. Pre-purification size and PDI measurements were performed using citrate buffer as the dispersant.

Disposable ZEN0040 micro-cuvettes were used for size and PDI measurements, with 400 µL of diluted sample added per cuvette. Zeta potential measurements were conducted using DTS1070 folded capillary cells, with 1,000 µL of diluted sample per measurement. The material refractive index and absorption were set to 1.45 and 0.001, respectively. Dispersant refractive indices and viscosities were set as follows: water (1.33, 0.8872 cP), PBS (1.335, 1.02 cP), and citrate buffer (1.47, 1.28 cP).

mRNA content

Encapsulation efficiency (EE%) and mass balance (MB%) were quantified using a RiboGreen™ RNA quantification assay. The supplied 20× TE buffer (10 mM Tris-HCl, 1 mM EDTA, pH 7.5) was diluted to a working concentration (1× TE). A separate 2% (v/v) Triton X-100 solution was prepared in 1× TE buffer.

Two RNA standard curves (0–1,000 ng/mL and 0–200 ng/mL) were prepared in TE buffer. The higher-range standard curve additionally contained 50 µL of 2% Triton-TE buffer per well. LNP samples were plated at a concentration of 3 µg/mL (final RNA concentration of 750 ng/mL in a total well volume of 200 µL). Four wells were allocated per sample: two wells received 50 µL of 2% Triton-TE buffer (to determine total RNA content), and two

wells received 50 µL of TE buffer alone (to determine free, unencapsulated RNA). Control wells without LNPs were included on each plate.

Plates were incubated at 37 °C for 15 minutes before RiboGreen addition to allow complete disruption of LNPs in Triton-containing wells. RiboGreen working solutions were prepared by diluting the reagent in TE buffer at 1:200 for Triton-containing wells and 1:500 for TE-only wells. Under low-light conditions, 100 µL of the appropriate RiboGreen solution was added to each well.

Fluorescence was measured using POLARstar Omega or GloMax plate readers at excitation wavelengths of 475–485 nm and an emission wavelength of 525 nm. Data analysis was performed in Microsoft Excel by generating standard curves and calculating RNA concentrations from fluorescence values after subtracting the background signal. For each sample, values for total RNA (CT) and free RNA (CF) were obtained (n = 2 per condition).

Encapsulation efficiency and mass balance were calculated using the following equations:

$$EE\% = 100 \times \frac{C_T - C_F}{C_T} \qquad \textit{Equation (2)}$$

$$MB\% = 100 \times \frac{C_T}{C_I} \qquad \textit{Equation (3)}$$

where C_T is the total RNA concentration, C_F is the free (unencapsulated) RNA concentration, and C_I is the theoretical RNA input concentration.

In vitro expression

In vitro LNP expression was assessed in HEK293 cells using firefly luciferase as a bioluminescent reporter. Cells were cultured in minimal essential medium (MEM) supplemented with 10% fetal bovine serum (FBS), 1% penicillin/streptomycin, and 1% sodium pyruvate.

Cells were seeded into white, clear-bottom 96-well plates at a density of 10,000 cells per well (100 µL of a 1×10^5 cells/mL suspension) and incubated for 72 hours before treatment. LNPs were formulated as described previously using EZ-Cap™ firefly luciferase mRNA as the payload. Cells were treated with LNPs diluted in complete

medium to final mRNA concentrations of 2, 1, 0.5, and 0.25 µg/mL. Each concentration was tested in triplicate, with untreated wells serving as controls.

Following a 24-hour incubation period, luminescence was measured. Under low-light conditions, 100 µL of luciferase reagent (prepared according to the manufacturer's instructions) was added directly to each well containing 100 µL of medium, resulting in a total volume of 200 µL. Plates were gently mixed and incubated for 3 minutes before luminescence was quantified using a GloMax plate reader (Promega, UK).

Statistical analysis

All data are presented as mean ± standard deviation (SD). Unless otherwise stated, experiments were performed using three independent batches (n = 3), with each batch manufactured on a different day to account for inter-day variability. For hydrodynamic size, polydispersity index (PDI), and zeta potential measurements, three technical replicates were obtained for each batch and purification condition, yielding a total of 9 measurements per group (n = 9) for statistical analysis.

Statistical comparisons were performed using one-way analysis of variance (ANOVA) to assess the effect of a single independent variable, or two-way ANOVA to evaluate the influence of two independent variables. Where appropriate, Tukey's honestly significant difference (HSD) post-hoc test was applied for multiple pairwise comparisons. Unpaired Student's t-tests were used for comparisons between two independent groups, while paired Student's t-tests were applied when comparing matched samples, such as the same batch assessed over time or following different treatments.

Statistical significance is indicated in graphical representations as follows: $p < 0.05$ (*). Results that do not reach statistical significance are denoted as ns.

Results and discussion

Formulation 1- DOTAP LNPs

The preliminary experiments were carried out to identify suitable control parameters for subsequent studies and to confirm findings previously established in this laboratory and reported in the literature. An N/P ratio of 6 and a flow rate ratio (FRR) of 3:1 are optimal for the manufacture of LNPs with respect to their critical quality attributes (CQAs) and *in vivo* performance [110, 111]. These parameters were therefore used as a starting

point, alongside exploration of additional manufacturing conditions. Establishing a reproducible baseline was particularly important to ensure that any changes observed in later optimisation experiments could be attributed to the parameter under investigation rather than uncontrolled variability in the manufacturing process.

For LNPs composed of cholesterol, DSPC, DOTAP, and DMG-PEG 2000 (Formulation 1), no significant effect of total flow rate (TFR) was observed over the range tested (5–20 mL/min), as shown in Figure 2.1. Across all flow rates, the LNPs showed consistent physicochemical properties, with particle sizes around 70 nm, polydispersity indices below 0.2, and near-neutral zeta potentials (−10 mV to +10 mV). Although DOTAP is a permanently positively charged lipid, the LNPs did not show strongly positive zeta potentials. This is because zeta potential measures the overall surface charge of the complete nanoparticle rather than the charge of a single lipid component [109]. During formulation, the positive charge of DOTAP interacts with the negatively charged polyA, which can neutralise much of the overall particle surface charge. In addition, PEG-lipids may further shield the particle surface and reduce the measured zeta potential [112].

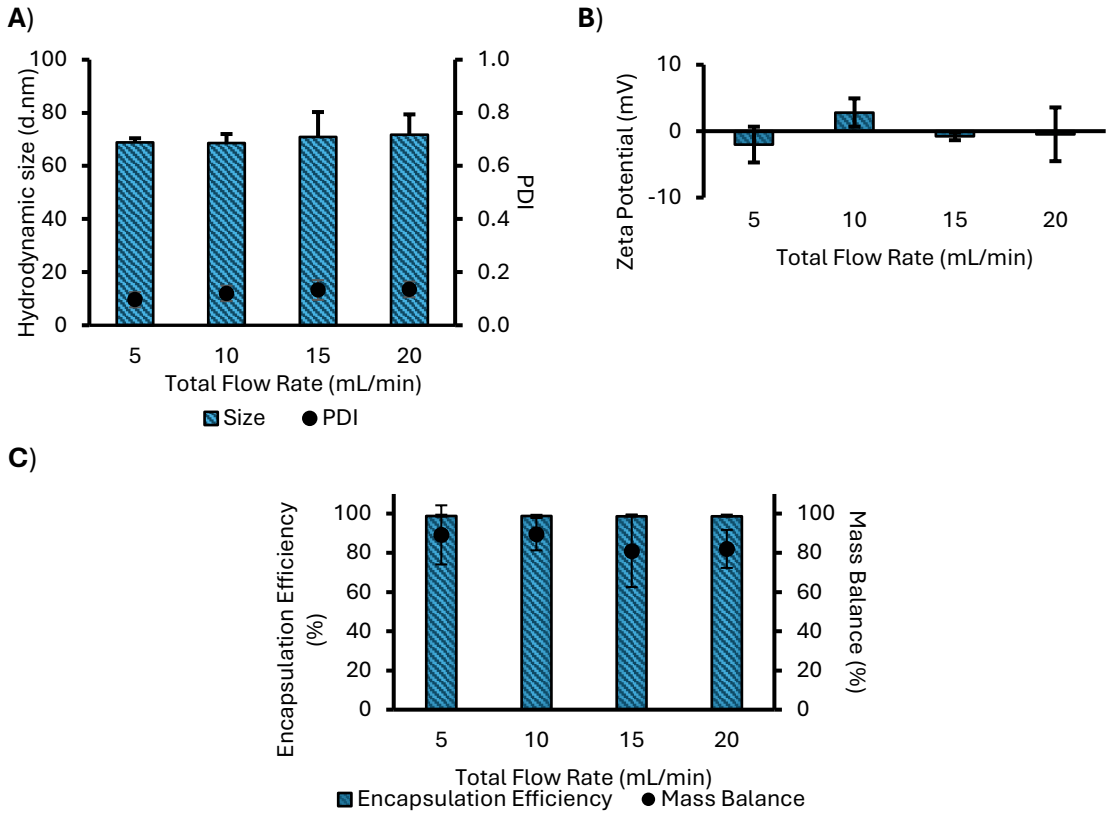

Figure 2.1: Effect of total flow rate (TFR) on hydrodynamic size and PDI (A), zeta potential (B), and encapsulation efficiency and mass balance (C) of DOTAP (Formulation 1) LNPs. LNPs were manufactured at an FRR of 3:1 with an N/P ratio of 6 from 5 mg/mL lipid stocks and purified by 1 h dialysis in PBS (pH 7.4). Data represent mean ± SD of three independent batches (n = 3).

Encapsulation efficiency was nearly 100%, and mass balance values exceeded 80% in all tested conditions. These results demonstrate that this DOTAP formulation can be reliably produced across a variety of total flow rates without affecting LNP CQAs.

This suggests that, within the explored parameter space, TFR does not play a dominant role in determining particle characteristics when FRR and the N/P ratio are held constant. One possible explanation is that, at these moderate flow rates, mixing in the staggered herringbone microfluidic channel remains sufficiently efficient to enable rapid solvent dilution and lipid self-assembly regardless of flow velocity [94, 106]. In contrast to FRR, which directly governs the rate of ethanol dilution and the conditions that drive nanoparticle formation, TFR primarily influences residence time (in the microfluidic mixer) and shear, which may only become influential at more extreme values than those investigated here [107, 113]. The robustness of this formulation to variation in TFR therefore supports its suitability for further optimisation. It suggests a degree of flexibility for potential scale-up, where modest increases in flow rate may be required to increase throughput without compromising particle quality [106].

The next parameter investigated was the flow rate ratio (FRR), defined as the ratio of aqueous phase to lipid phase. Results showed that FRRs of 2:1, 3:1, and 5:1 produced LNPs with comparable CQAs (Figure 2.2), with no significant differences observed between these conditions. Under these ratios, the particles consistently demonstrated the previously described optimal characteristics, including sizes around 70 nm, PDIs below 0.2, near-neutral zeta potentials, high encapsulation efficiency, and acceptable mass balance. These findings are consistent with previous reports demonstrating that, within a suitable operating window, FRR primarily governs the rate of solvent dilution and lipid supersaturation, thereby influencing nucleation and self-assembly kinetics during microfluidic mixing [94, 114]. Once a sufficiently rapid and uniform solvent exchange is achieved, further increases in aqueous phase proportion may have only a limited additional effect on particle size or homogeneity.

In contrast, LNPs manufactured at an FRR of 1:1 displayed markedly different properties. Particle size increased substantially to approximately 300 nm, accompanied by a high PDI of 0.35, indicating a broad size distribution and reduced homogeneity. The zeta potential was also more positive, measuring approximately +17 mV.

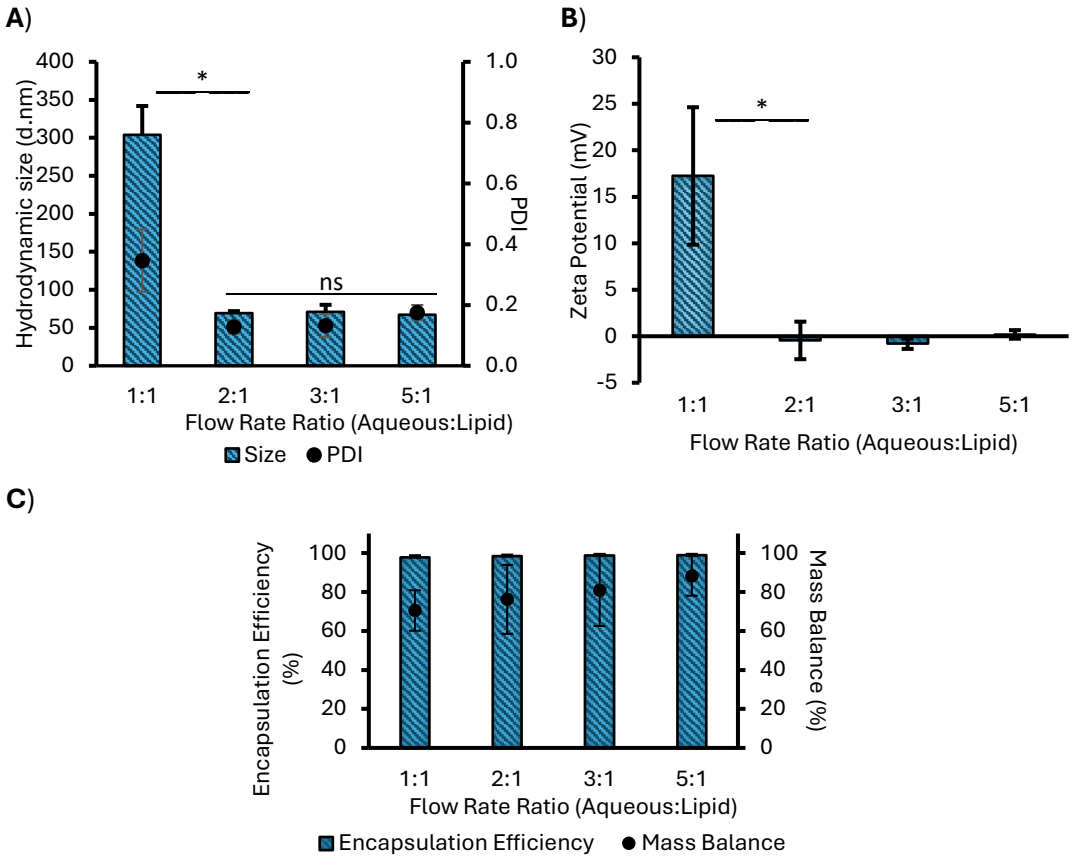

Figure 2.2: Effect of flow rate ratio (FRR) on hydrodynamic size and PDI (A), zeta potential (B), and encapsulation efficiency and mass balance (C) of DOTAP (Formulation 1) LNPs. LNPs were manufactured with an N/P ratio of 6 from 5 mg/mL lipid stocks and purified by 1 h dialysis in PBS (pH 7.4). Data represent mean ± SD of three independent batches (n = 3). Statistical significance is indicated by *p < 0.05; ns denotes no significant difference.

This increase in surface charge may reflect incomplete nucleic acid complexation or altered lipid packing under conditions of slower solvent dilution. At lower FRRs, the relative ethanol content is higher during mixing, which may slow down how quickly the lipids come out of solution and start forming nanoparticles, which may allow larger or less tightly packed particles to form before they fully stabilise [106, 115]. For LNPs, particle formation mainly depends on the attraction between the positively charged lipid and the negatively charged polyA. If there is insufficient aqueous phase, this charge interaction may not occur efficiently, leading to particles that retain excess positive charge and exhibit greater variability in size and structure.

Overall, these findings indicate that FRR is a vital parameter affecting particle formation, with ratios of 2:1 and above ensuring stable and reproducible LNP assembly, while a 1:1 ratio results in greater heterogeneity and less desirable physicochemical properties. The sensitivity observed at low FRR emphasises the importance of rapid, controlled solvent

exchange during microfluidic LNP production and supports choosing FRR values of ≥ 2:1 for further optimisation and biological research.

The final microfluidic parameter investigated for the DOTAP formulation was the N/P ratio, as shown in Figure 2.3. Similar to the results observed for total flow rate, the variation of the N/P ratio within the tested range had no significant impact on the LNP CQAs. Particle size, PDI, zeta potential, encapsulation efficiency, and mass balance remained consistent across all conditions, indicating that this formulation is robust to changes in N/P ratio within the explored parameter space.

The N/P ratio determines the balance between positively charged lipid and negatively charged nucleic acid and therefore influences electrostatic complexation during LNP formation [55, 66]. Within the range tested, sufficient lipid was present to enable effective charge neutralisation and stable particle formation, such that modest changes did not significantly alter physicochemical properties.

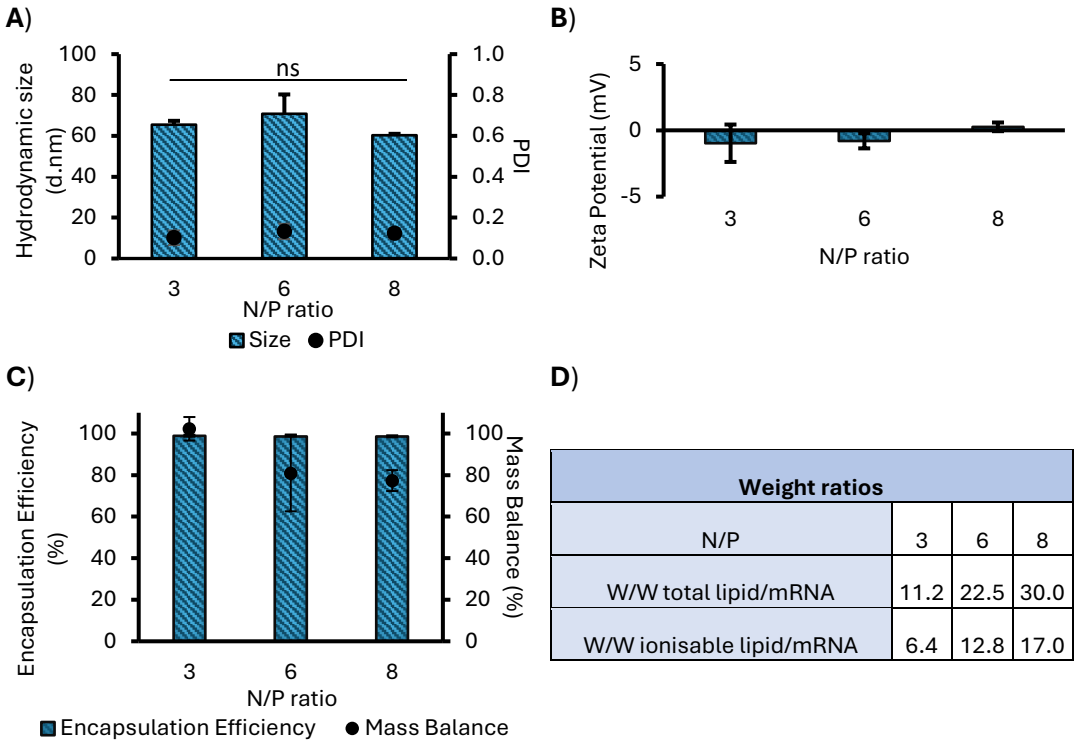

Weight ratios			
N/P	3	6	8
W/W total lipid/mRNA	11.2	22.5	30.0
W/W ionisable lipid/mRNA	6.4	12.8	17.0

Figure 2.3: Effect of N/P ratio on hydrodynamic size and PDI (A), zeta potential (B), and encapsulation efficiency and mass balance (C) of DOTAP (Formulation 1) LNPs. Panel (D) shows conversion of N/P ratios to weight/weight (W/W) ratios for total lipid/mRNA and ionisable lipid/mRNA. LNPs were manufactured at an FRR of 3:1 from 5 mg/mL lipid stocks and purified by 1 h dialysis in PBS (pH 7.4). Data represent mean ± SD of three independent batches (n = 3). ns denotes no statistical significance.

Although encapsulation efficiency remained consistent across the N/P ratios tested, this does not necessarily indicate that the internal distribution of RNA between particles was unchanged. Encapsulation efficiency measures the total proportion of RNA associated with the LNP population but does not distinguish between uniformly loaded particles and mixtures containing differing proportions of RNA-rich, RNA-poor, or empty LNPs. Changes in N/P ratio may therefore influence the amount of RNA packaged per particle or alter the ratio of loaded to unloaded particles without substantially affecting bulk encapsulation measurements. Previous single-particle studies have demonstrated substantial variability in RNA loading between individual LNPs despite similar overall encapsulation efficiencies, highlighting the limitations of ensemble measurements alone [64]. These findings are consistent with reports showing that once a minimum N/P threshold for efficient encapsulation is reached, particle size and homogeneity are more strongly influenced by mixing conditions than by small variations in charge ratio [38, 84].

The effect of buffer exchange was evaluated to determine the impact of 1 hour of dialysis on particle size and PDI for the DOTAP formulation LNPs. Other CQAs could not be measured before buffer exchange due to the presence of ethanol and low pH conditions. As shown in Figure 2.4, dialysis had little to no effect on the size or PDI of LNPs manufactured at FRRs of 2:1 and above, with values remaining within the previously observed optimal range. This suggests that well-formed LNPs generated under appropriate mixing conditions are structurally stable to buffer exchange, consistent with previous reports indicating that mature LNP structures are relatively resistant to moderate environmental changes once assembled [66, 116].

In contrast, a marked change was observed for LNPs manufactured at an FRR of 1:1. Before dialysis, these samples exhibited extremely large apparent particle sizes (>2500 nm) and very high PDIs (~0.7), suggesting that stable nanoparticles had not formed and that large aggregates or unstable intermediates were present. Following dialysis, particle size and PDI decreased substantially to approximately 300 nm and 0.35, respectively. This reduction may reflect partial restructuring or stabilisation as ethanol is removed and the lipid components reorganise in an aqueous environment.

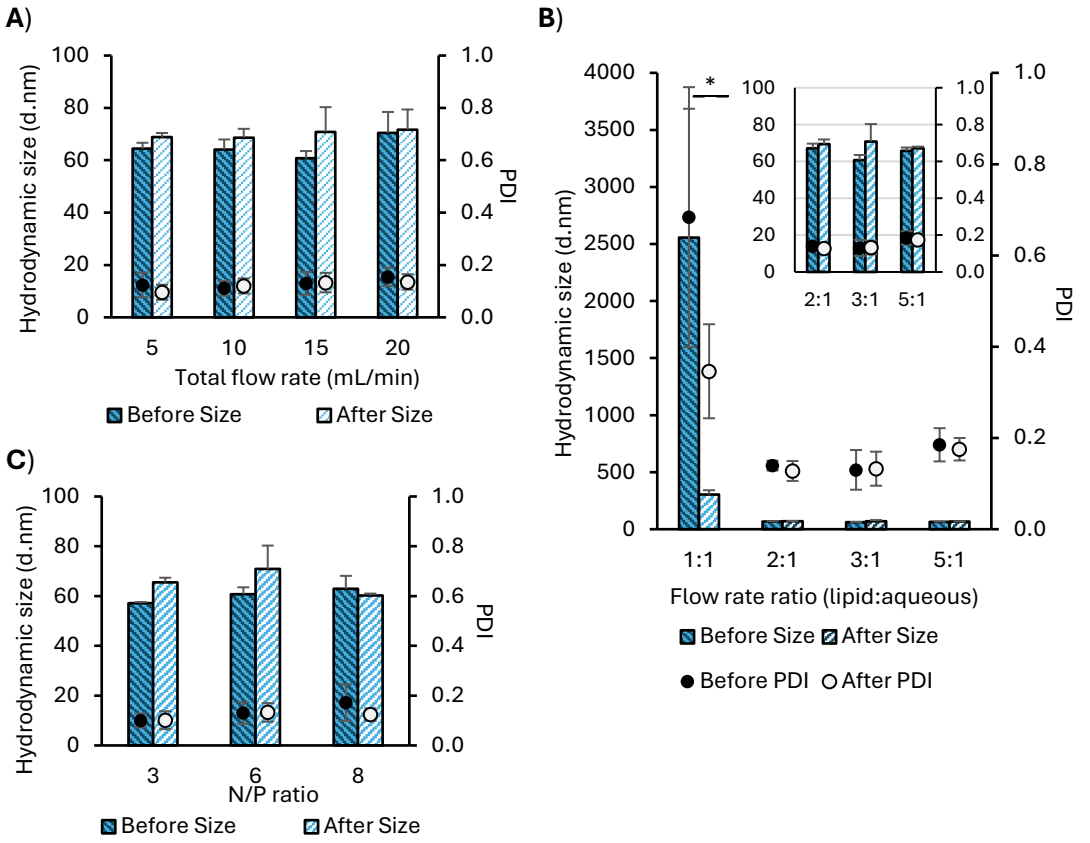

Figure 2.4: Effect of buffer exchange on hydrodynamic size and PDI of DOTAP (Formulation 1) LNPs manufactured at varying total flow rates (A), flow rate ratios (FRRs) (B), and N/P ratios (C). Dark columns indicate size before dialysis and light columns indicate size after 1 h dialysis; closed circles represent PDI before dialysis and open circles represent PDI after dialysis. Control conditions were FRR 3:1, N/P 6, and 5 mg/mL lipid stocks, with dialysis performed in PBS (pH 7.4). Data represent mean ± SD of three independent batches (n = 3). Statistical significance is indicated by *p < 0.05.

However, the resulting particles remained significantly larger and more heterogeneous than those produced at higher FRRs, indicating that dialysis cannot compensate for suboptimal assembly conditions during initial microfluidic mixing.

Overall, the DOTAP Formulation 1 LNPs exhibited robust and reproducible physicochemical characteristics across a range of total flow rates and N/P ratios, with optimal CQAs consistently achieved at FRRs of 2:1 or higher. In contrast, an FRR of 1:1 led to unstable, heterogeneous particles, highlighting the importance of a sufficient aqueous phase during microfluidic assembly. Buffer exchange had minimal impact on well-formed LNPs but partially stabilised those produced under suboptimal conditions. Taken together, these findings confirm that an FRR of 3:1 and an N/P ratio of 6 represent suitable control parameters for this formulation and provide a validated baseline for further optimisation studies in subsequent formulations, as is standard in LNP research [38, 39, 41, 55, 66, 67, 117, 118].

Formulation 2- ALC-0315 (DMG-PEG) LNPs

The next set of LNPs were manufactured using ALC-0315 as the ionisable lipid, while the remaining lipid components (DSPC, cholesterol, and DMG-PEG 2000) were kept the same as in Formulation 1. Transitioning from a permanently cationic lipid (DOTAP) to an ionisable lipid enabled assessment of whether the previously observed trends were maintained in a formulation more closely aligned with clinically advanced LNP systems. Unlike DOTAP, ALC-0315 is predominantly neutral at physiological pH and becomes protonated under acidic conditions during formulation, enabling electrostatic complexation with nucleic acid while reducing surface charge following buffer exchange [15, 66].

Initial experiments investigated the effect of total flow rate (TFR), with LNPs produced at 10 mL/min and 20 mL/min, as shown in Figure 2.5. No significant differences in CQAs were observed between the two flow rates.

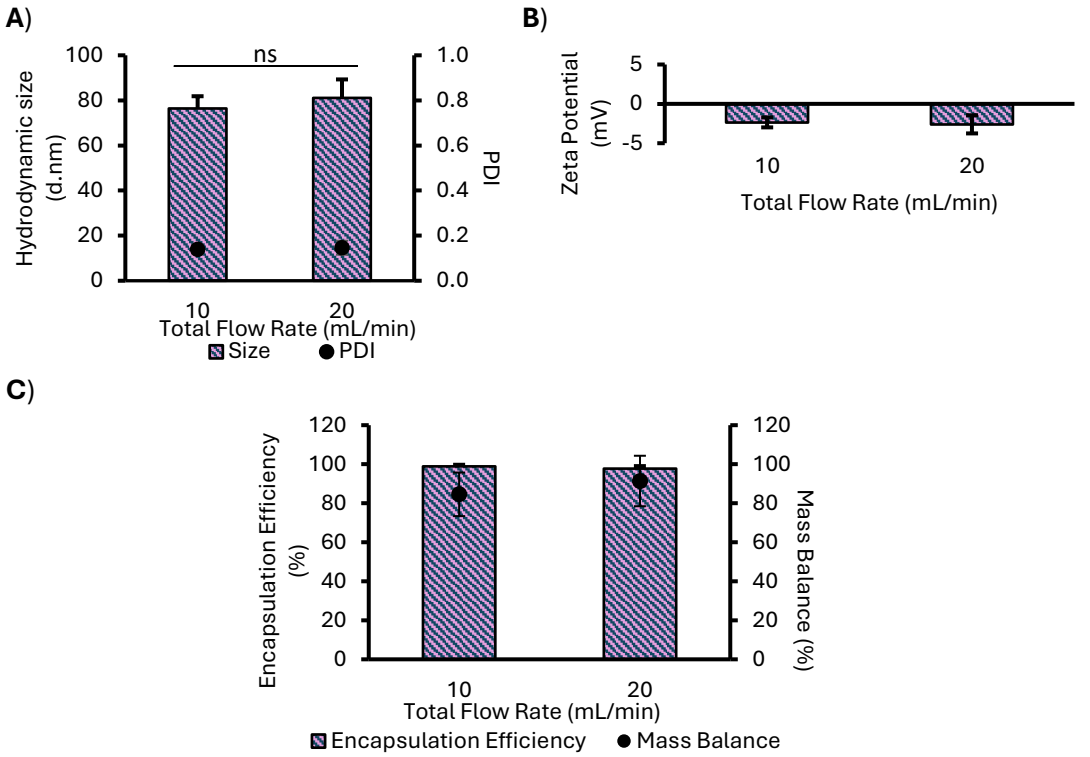

Figure 2.5: Effect of total flow rate (TFR) on hydrodynamic size and PDI (A), zeta potential (B), and encapsulation efficiency and mass balance (C) of ALC-0315 (Formulation 2) LNPs. Columns show size, zeta potential, and encapsulation efficiency (A–C), while closed circles indicate PDI (A) and mass balance (C). LNPs were manufactured at an FRR of 3:1 and N/P 6 using 5 mg/mL lipid stocks and purified by dialysis in PBS (pH 7.4) for 1 h. Data represent mean ± SD of three independent batches (n = 3). (ns) indicates no statistical significance.

In both cases, the LNPs exhibited particle sizes of approximately 80 nm, PDIs below 0.2, near-neutral zeta potentials, and high RNA encapsulation efficiency and mass balance. These results indicate that, similar to Formulation 1, total flow rate does not have a significant impact on the physicochemical properties of ALC-0315 LNPs within the range tested.

This behaviour is consistent with reports that, in microfluidic LNP manufacture, particle formation is primarily governed by the rate of solvent dilution (controlled by FRR) rather than the flow speed, provided efficient mixing is achieved within the device [94, 114]. The comparable performance observed across TFRs suggests that, within this window, mixing conditions were sufficient to promote rapid self-assembly of stable ionisable lipid nanoparticles, supporting flexibility in throughput without compromising formulation quality.

The final microfluidic parameter investigated for ALC-0315 (Formulation 2) LNPs was the N/P ratio, as shown in Figure 2.6. Consistent with the results observed for total flow rate and following the same trend as Formulation 1, variation of the N/P ratio had only a minor effect on particle size. LNPs manufactured at an N/P ratio of 3 were approximately 10-15 nm larger than those produced at higher N/P ratios. At the same time, no significant differences were observed in PDI, zeta potential, encapsulation efficiency, or mass balance across the conditions tested.

The N/P ratio governs the balance between protonatable lipid and nucleic acid charge during assembly [66]. The small increase in size at N/P 3 may reflect slightly less compact complexation at lower charge ratios; however, the consistently high encapsulation efficiencies indicate that effective binding was achieved across all conditions. These findings suggest that, within the range tested, ALC-0315 LNP formation is tolerant to modest variations in charge stoichiometry, with mixing conditions likely playing a more dominant role in determining final particle characteristics [94].

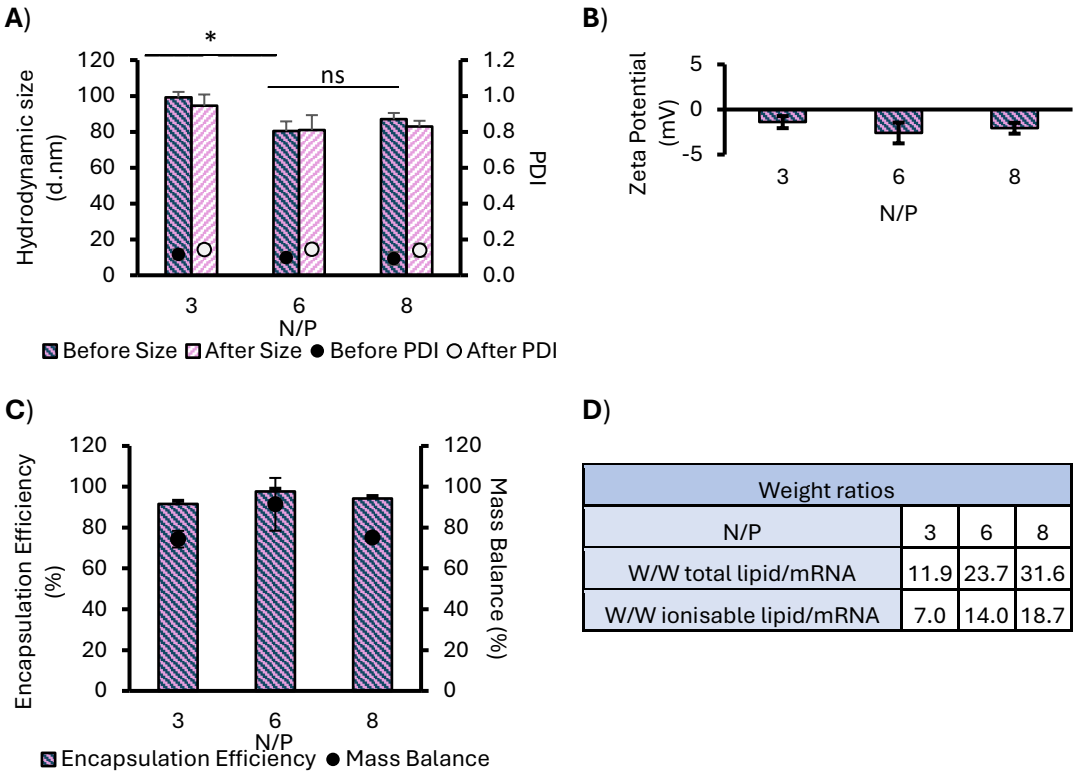

Weight ratios			
N/P	3	6	8
W/W total lipid/mRNA	11.9	23.7	31.6
W/W ionisable lipid/mRNA	7.0	14.0	18.7

Figure 2.6: Effect of N/P ratio on hydrodynamic size and PDI (A), zeta potential (B), and encapsulation efficiency and mass balance (C) of ALC-0315 (Formulation 2) LNPs. Panel (D) shows conversion of N/P ratios to weight/weight (w/w) ratios for total lipid/mRNA and ionisable lipid/mRNA. Columns represent size, zeta potential, and encapsulation efficiency (A–C), while closed circles indicate PDI (A) and mass balance (C). LNPs were manufactured at an FRR of 3:1 using 5 mg/mL lipid stocks and purified by dialysis in PBS (pH 7.4) for 1 h. Data represent mean ± SD of three independent batches (n = 3). Statistical significance is indicated by *p < 0.05; ns denotes no significance.

The effect of buffer exchange was assessed to determine the impact of 1-hour dialysis on particle size and PDI in LNPs produced under various microfluidic conditions. Overall, dialysis had minimal to no influence on particle size or PDI, suggesting that well-formed LNPs remained structurally stable after solvent removal and buffer exchange. Slight variations were observed for LNPs manufactured at lower FRRs, which may indicate reduced intrinsic stability under these assembly conditions; however, these differences were minor and not statistically significant.

To further assess the influence of dialysis duration, selected LNP samples were divided before purification, with half dialysed for 1 hour and the remaining half for 24 hours (Figure 2.7).

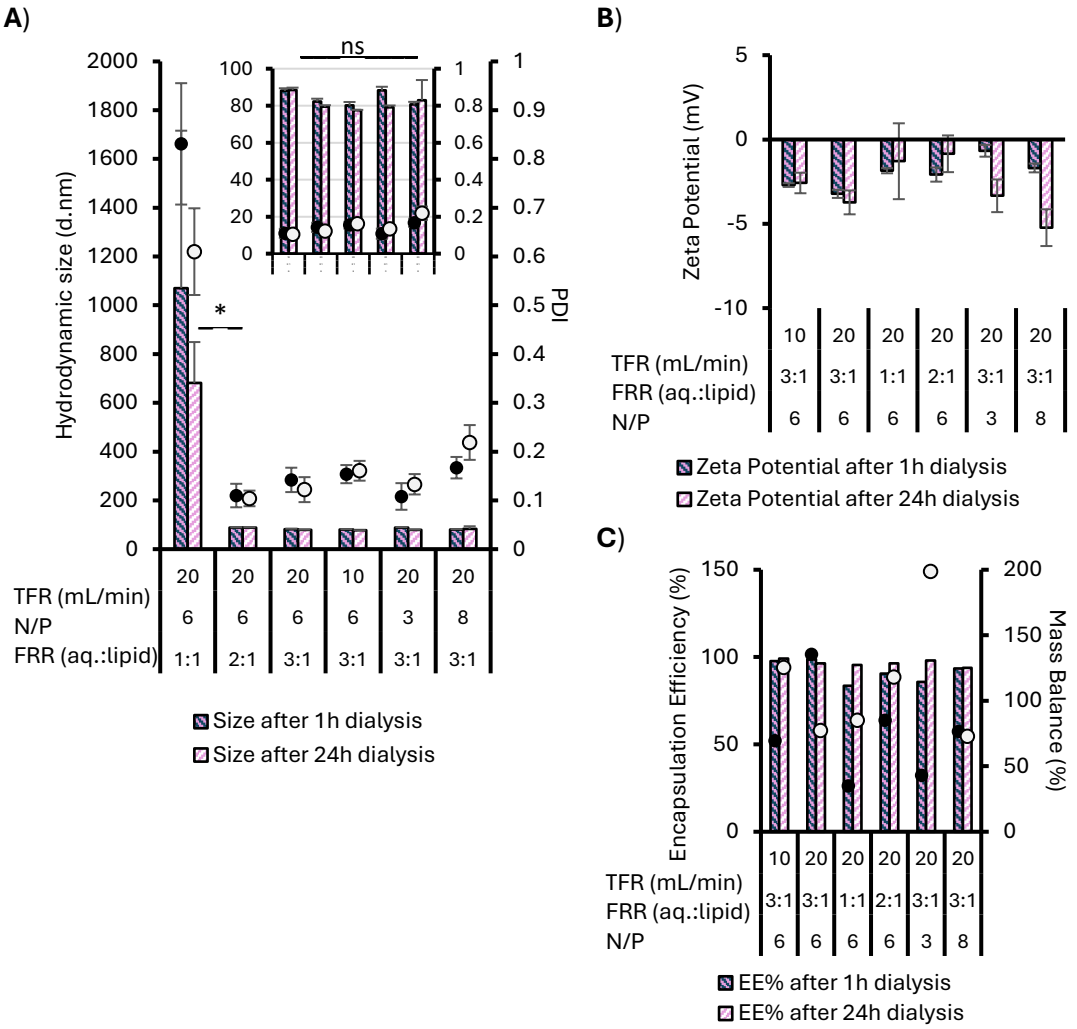

Figure 2.7: Effect of buffer exchange time on hydrodynamic size and PDI (A), zeta potential (B), and encapsulation efficiency and mass balance (C) of ALC-0315 (Formulation 2) LNPs. Darker columns represent size (A), zeta potential (B), and encapsulation efficiency (C) after 1 h dialysis, and lighter columns represent values after 24 h dialysis. Closed circles indicate PDI (A) and mass balance (C) after 1 h dialysis, and open circles indicate values after 24 h. Each dataset represents a single manufactured batch, split equally into 1 h and 24 h dialysis in PBS (pH 7.4). Size, PDI, and zeta potential were measured in triplicate (mean ± SD). Statistical significance is indicated by *p < 0.05; ns denotes no significance.

No differences were observed in particle size, PDI, zeta potential, or encapsulation efficiency between the two durations. A possible variation in mass balance was noted. However, this was not statistically evaluated due to the limited number of replicates and is more likely attributable to sample handling during division than to dialysis time.

Overall, these findings indicate that 1 hour of dialysis is sufficient for routine purification of these LNPs. Extending dialysis to 24 hours did not confer a measurable benefit on the physicochemical properties assessed, suggesting that prolonged buffer exchange is unnecessary under the conditions used in this study. However, this does not confirm that sufficient ethanol has been exchanged for use *in vitro* and *in vivo* studies, which

requires closer to 4h- overnight of dialysis to achieve these negligible amounts of ethanol [119-121].

The next parameter investigated for the ALC-0315 (Formulation 2) LNPs was the effect of the purification method. Up to this point, LNPs had been purified exclusively by dialysis. To determine whether alternative downstream approaches influenced LNP characteristics, centrifugal filtration (spin columns) and tangential flow filtration (TFF), both using 100-kDa molecular-weight cut-off membranes, were evaluated.

Across all purification methods, comparable physicochemical properties were observed (Figure 2.8). LNPs purified by dialysis, spin columns, or TFF exhibited similar particle sizes, PDIs, zeta potentials, encapsulation efficiencies, and mass balance values. Although TFF-purified LNPs were on average slightly larger (~100 nm), this difference was not statistically significant and remained within the typical size range reported for therapeutic LNP systems [55, 66].

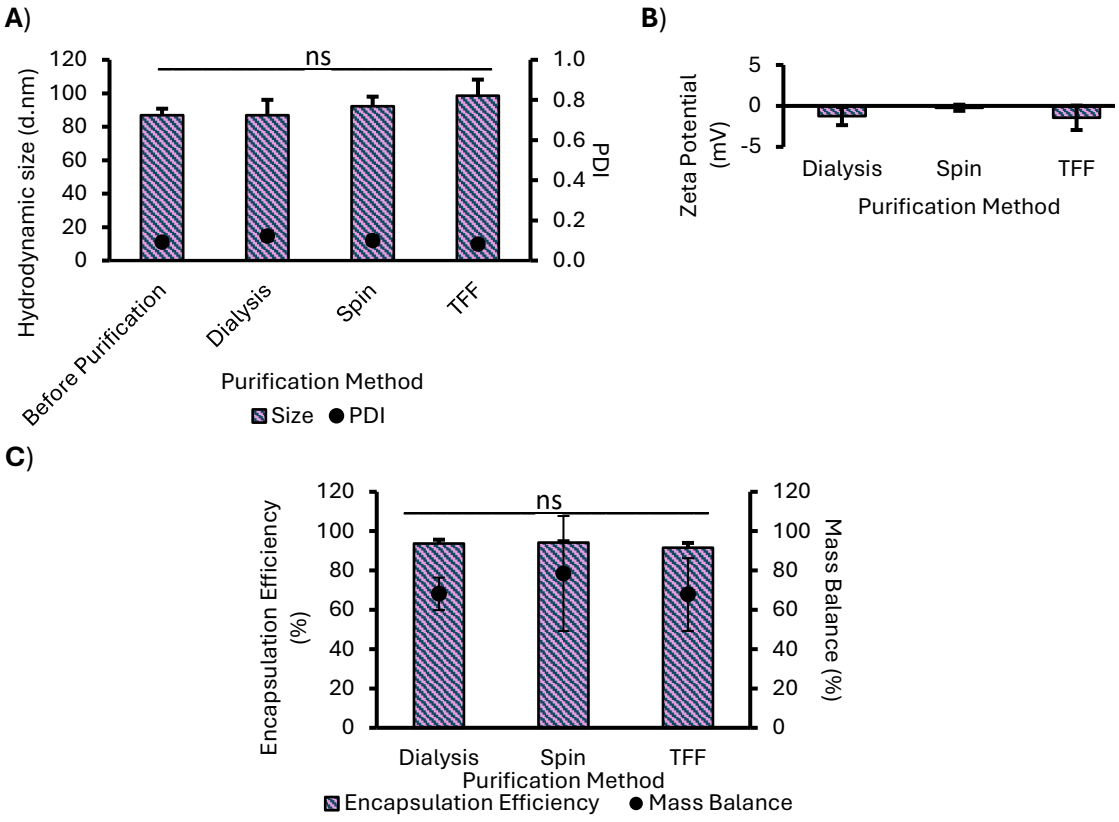

Figure 2.8: Effect of purification method on hydrodynamic size and PDI (A), zeta potential (B), and encapsulation efficiency and mass balance (C) of ALC-0315 (Formulation 2) LNPs. Size, zeta potential, and encapsulation efficiency are shown as columns, with PDI and mass balance shown as closed circles. LNPs were purified by dialysis (1 h), 100 kDa spin columns, or 100 kDa tangential flow filtration (TFF) using PBS (pH 7.4). LNPs were manufactured at an FRR of 3:1 with an N/P of 6 from 5 mg/mL lipid stocks. Data represent mean ± SD (n = 3). ns denotes no statistical significance.

The absence of substantial physicochemical differences suggests that the nanoparticle structure is sufficiently robust to tolerate different purification workflows, including exposure to shear forces during TFF and centrifugal stress during spin filtration, without major disruption of particle integrity [107]. These findings support flexibility in downstream processing, allowing purification strategy to be selected based on scale and manufacturing requirements rather than strict physicochemical constraints.

Dialysis is commonly used at laboratory scale, whereas TFF is widely adopted in scalable and GMP-compliant LNP manufacturing processes [91, 92]. The observed robustness across purification methods is therefore advantageous for translational development and process transfer.

To further investigate the differences observed at lower flow-rate ratios, the effect of the final lipid concentration was examined. All formulations were initially prepared using a 5 mg/mL lipid phase. As altering the FRR changes the aqueous:organic mixing ratio, it also changes the final lipid concentration in the collected suspension. For example, at an FRR of 3:1, the final lipid concentration is one-quarter of the lipid input (1.25 mg/mL). In contrast, at an FRR of 1:1, the final lipid concentration is one-half of the lipid input (2.5 mg/mL), resulting in a more concentrated formulation. It was hypothesised that the altered CQAs observed at 1:1 FRR may be influenced not only by solvent composition but also by differences in final lipid concentration, which can affect particle nucleation and growth during rapid mixing [55, 94].

To test this, 1:1 LNPs were manufactured at a reduced lipid concentration equivalent to that of the 3:1 formulation. Both 3:1 and 1:1 LNPs were produced at final lipid concentrations of 5 mg/mL, 2.5 mg/mL, and 1.25 mg/mL, and their CQAs were assessed.

For 3:1 FRR LNPs, varying lipid concentration had minimal effect. A slight increase in particle size was observed at the highest concentration (~100 nm at 5 mg/mL versus ~80 nm at lower concentrations). At the same time, PDI, zeta potential, encapsulation efficiency, and mass balance remained consistent (Figure 2.9). This behaviour aligns with previous reports indicating that, within moderate concentration ranges, ionisable lipid-based LNP formation is relatively tolerant to lipid concentration when mixing conditions are well controlled [66].

In contrast, 1:1 FRR LNPs showed concentration-dependent behaviour. Particle size and PDI were lower at the highest lipid concentration (5 mg/mL), and mass balance and encapsulation efficiency were also improved under these conditions (Figure 2.9). This may be due to the increased lipid content partially compensating for the destabilising effects associated with the higher relative ethanol concentration present at lower FRRs, thereby promoting improved particle assembly and RNA complexation [118].

Collectively, these findings suggest that the effects attributed to FRR are, at least in part, intertwined with final lipid concentration and solvent environment. This highlights the importance of considering both compositional and mixing-derived variables when interpreting microfluidic LNP optimisation data.

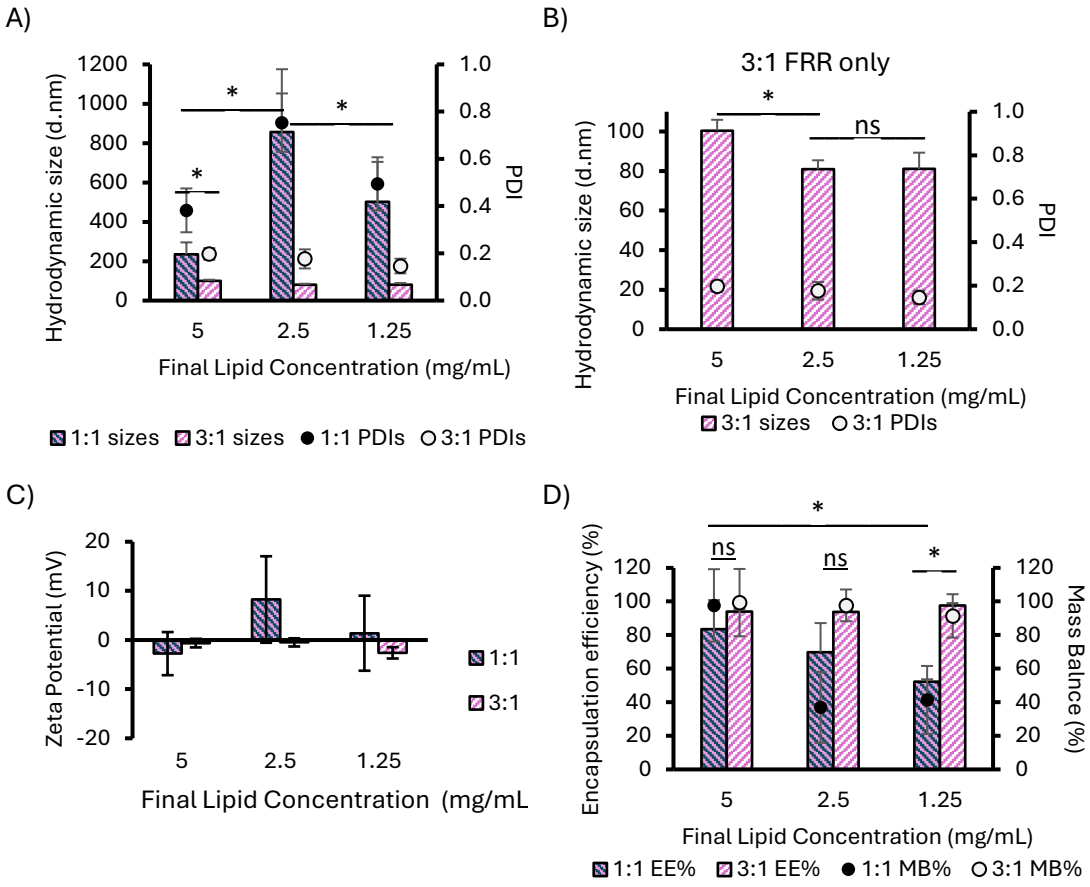

Figure 2.9: Effect of final lipid concentration on hydrodynamic size and PDI for ALC-0315 (Formulation 2) LNPs manufactured at FRRs of 1:1 and 3:1 (A) and 3:1 alone (B), zeta potential (C), and encapsulation efficiency and mass balance (D). Size, zeta potential, and encapsulation efficiency are shown as columns, with PDI and mass balance shown as circles. LNPs were prepared at an N/P of 6 using varying lipid stock concentrations to achieve final lipid concentrations of 1.25, 2.5, or 5 mg/mL, and purified by 1 h dialysis in PBS (pH 7.4). Data represent mean ± SD (n = 3). *p<0.05; ns denotes no statistical significance.

The effect of aqueous buffer concentration was also evaluated for this LNP formulation. The standard formulation using 50 mM citrate buffer at pH 4 was compared with formulations prepared using 10 mM and 100 mM citrate buffer. LNPs formulated with both 10 mM and 100 mM citrate buffer exhibited larger particle sizes than the control, with the 10 mM formulation also showing a higher PDI (Figure 2.10A). In contrast, zeta potential, encapsulation efficiency, and mass balance remained consistent across all buffer concentrations tested (Figure 2.10B–C).

These findings suggest that buffer ionic strength influences particle assembly, even when overall charge balance and encapsulation efficiency are maintained. At lower buffer concentrations (10 mM), reduced ionic strength may lead to less effective electrostatic screening between charged lipid and nucleic acid species during self-assembly, potentially promoting the formation of less compact or more heterogeneous intermediate structures [55].

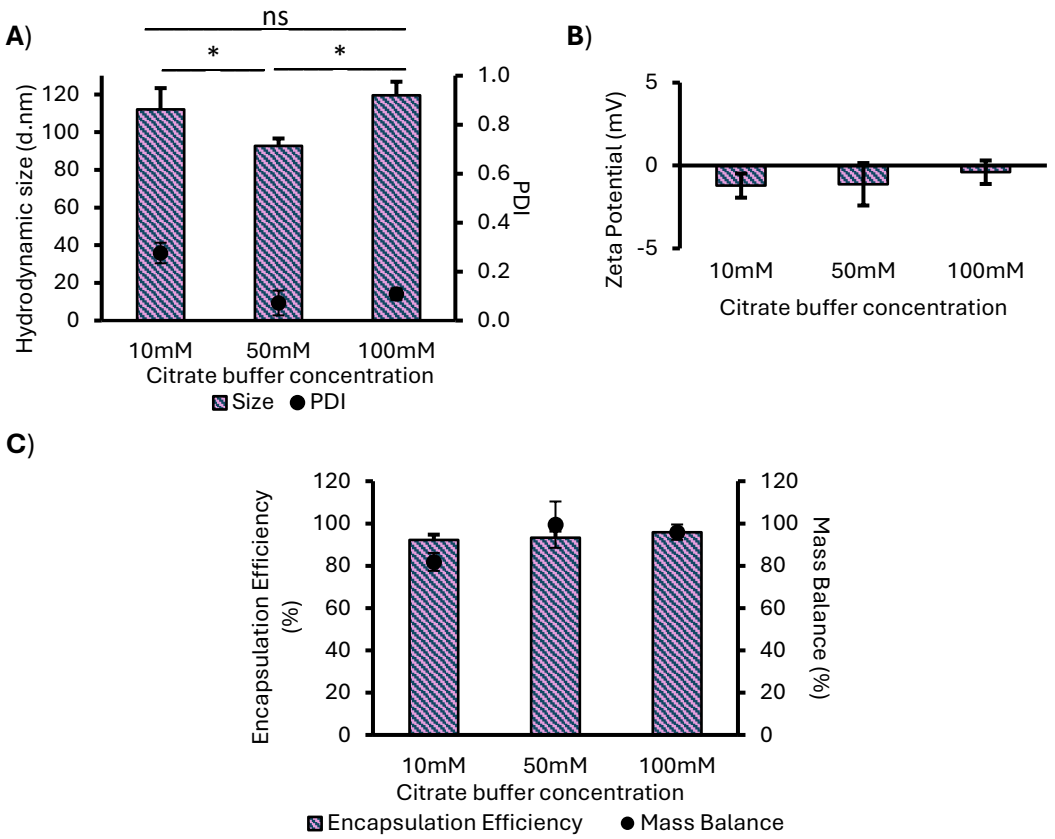

Figure 2.10: Effect of aqueous phase citrate buffer concentration on hydrodynamic size and PDI (A), zeta potential (B), and encapsulation efficiency and mass balance (C) of ALC-0315 (Formulation 2) LNPs. Size, zeta potential, and encapsulation efficiency are shown as columns, with PDI and mass balance shown as circles. LNPs were manufactured at an FRR of 3:1 and N/P of 6 from 5 mg/mL lipid stocks and purified by 1 h dialysis in PBS (pH 7.4). Data represent mean ± SD (n = 3). *p<0.05; ns, not significant.

This may explain the observed increase in size and PDI under these conditions. Conversely, at higher buffer concentrations (100 mM), increased ionic strength can alter lipid packing behaviour and influence the kinetics of nanoparticle nucleation and growth, which may also contribute to modest increases in particle size [94]. The preservation of high encapsulation efficiency across all buffer concentrations indicates that protonation of the ionisable lipid at pH 4 remained sufficient for effective electrostatic complexation with the nucleic acid payload [66]. The observed size differences, therefore, likely reflect subtle effects on particle assembly dynamics rather than disruption of lipid–RNA interactions.

Overall, these results demonstrate that buffer concentration, and therefore ionic strength, can modulate LNP physicochemical characteristics without necessarily affecting encapsulation efficiency. This highlights the importance of controlling buffer composition during formulation, particularly when translating processes between laboratory and larger-scale manufacturing environments.

Following evaluation of the aqueous buffer concentration, the effect of the choice of lipid-phase solvent on LNP CQAs was investigated. In addition to the standard solvent ethanol, methanol and isopropanol (propan-2-ol, IPA) were used to dissolve the lipid phase before microfluidic formulation. A general trend in particle size was observed, with LNPs formulated using methanol producing the largest particles and those formulated with IPA producing the smallest (Figure 2.11A). However, neither solvent showed a statistically significant difference in particle size compared with ethanol.

Differences in solvent properties, including polarity, viscosity, and miscibility with water, can influence the rate of solvent exchange during microfluidic mixing and therefore affect nanoparticle nucleation and growth [94, 122]. When the solvent mixes rapidly with water, the lipids rapidly precipitate from solution and form small particles. If the mixing happens more slowly, the lipids have more time to gather together in larger or less tightly packed structures before stable nanoparticles are formed [55]. The trend observed here may reflect differences in solvent-water mixing kinetics; however, under the conditions tested, these effects were modest.

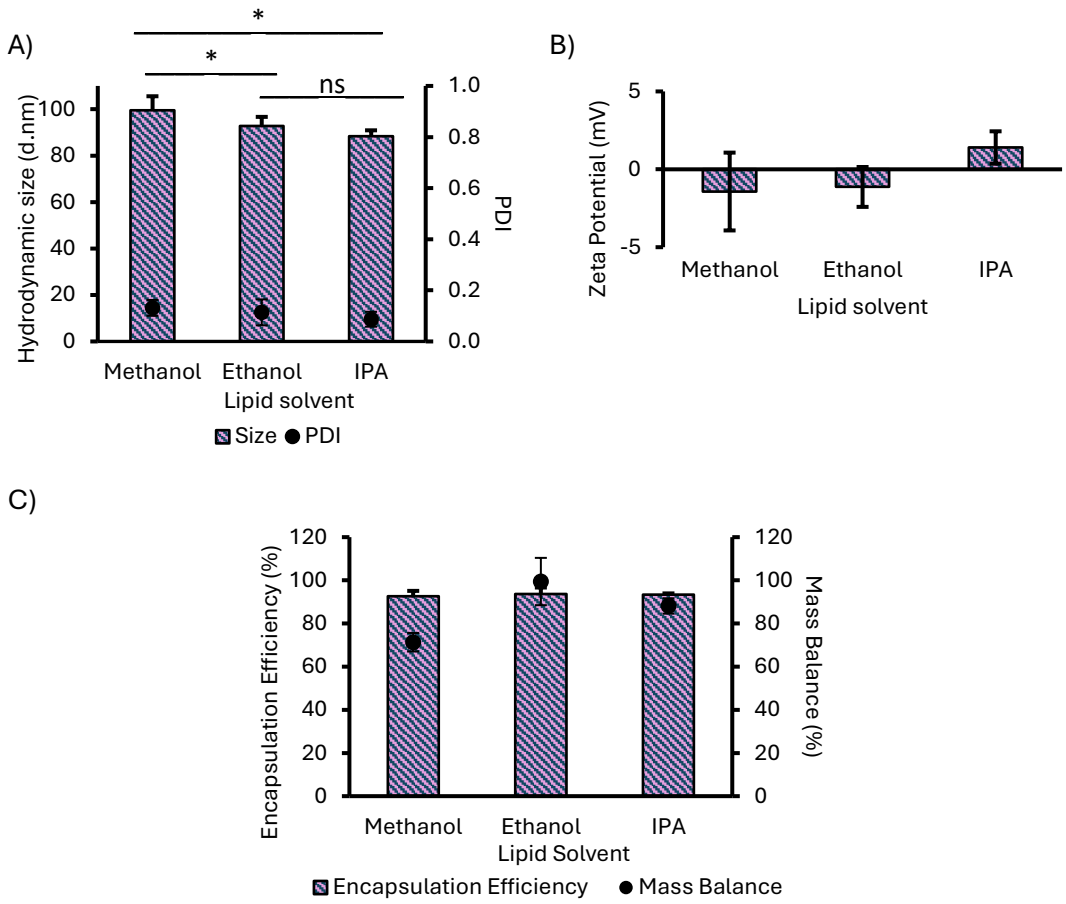

Figure 2.11: Effect of lipid phase solvent choice on hydrodynamic size and PDI (A), zeta potential (B), and encapsulation efficiency and mass balance (C) of ALC-0315 (Formulation 2) LNPs. Size, zeta potential, and encapsulation efficiency are shown as columns, with PDI and mass balance shown as circles. LNPs were manufactured at an FRR of 3:1 and N/P of 6 from 5 mg/mL lipid stocks and purified by 1 h dialysis in PBS (pH 7.4). Data represent mean ± SD (n = 3). *p<0.05; ns, not significant.

Mass balance was reduced for LNPs formulated using methanol relative to the ethanol control (Figure 2.11C), while encapsulation efficiency, PDI, and zeta potential remained comparable across all solvent conditions. The reduced recovery may reflect differences in solvent removal efficiency during dialysis or subtle effects on nanoparticle stability during purification, rather than impaired RNA complexation, given the consistently high encapsulation efficiency [66].

Overall, these findings indicate that within the explored parameter space, solvent choice has only a limited influence on LNP CQAs. Ethanol, therefore, remains a suitable and robust solvent for microfluidic LNP manufacture, consistent with its widespread use in both laboratory-scale and clinically relevant LNP production [15].

The stability of these LNPs was evaluated by measuring CQAs after 4 weeks and comparing them with those obtained at the time of manufacture. A subset of previously

prepared LNPs was used for this analysis because samples manufactured more than 4 weeks earlier were unavailable. The results are presented in Figure 2.12, which shows representative size-intensity distributions, and Table 2.8, which summarises the CQAs of all LNPs assessed at the four-week timepoint.

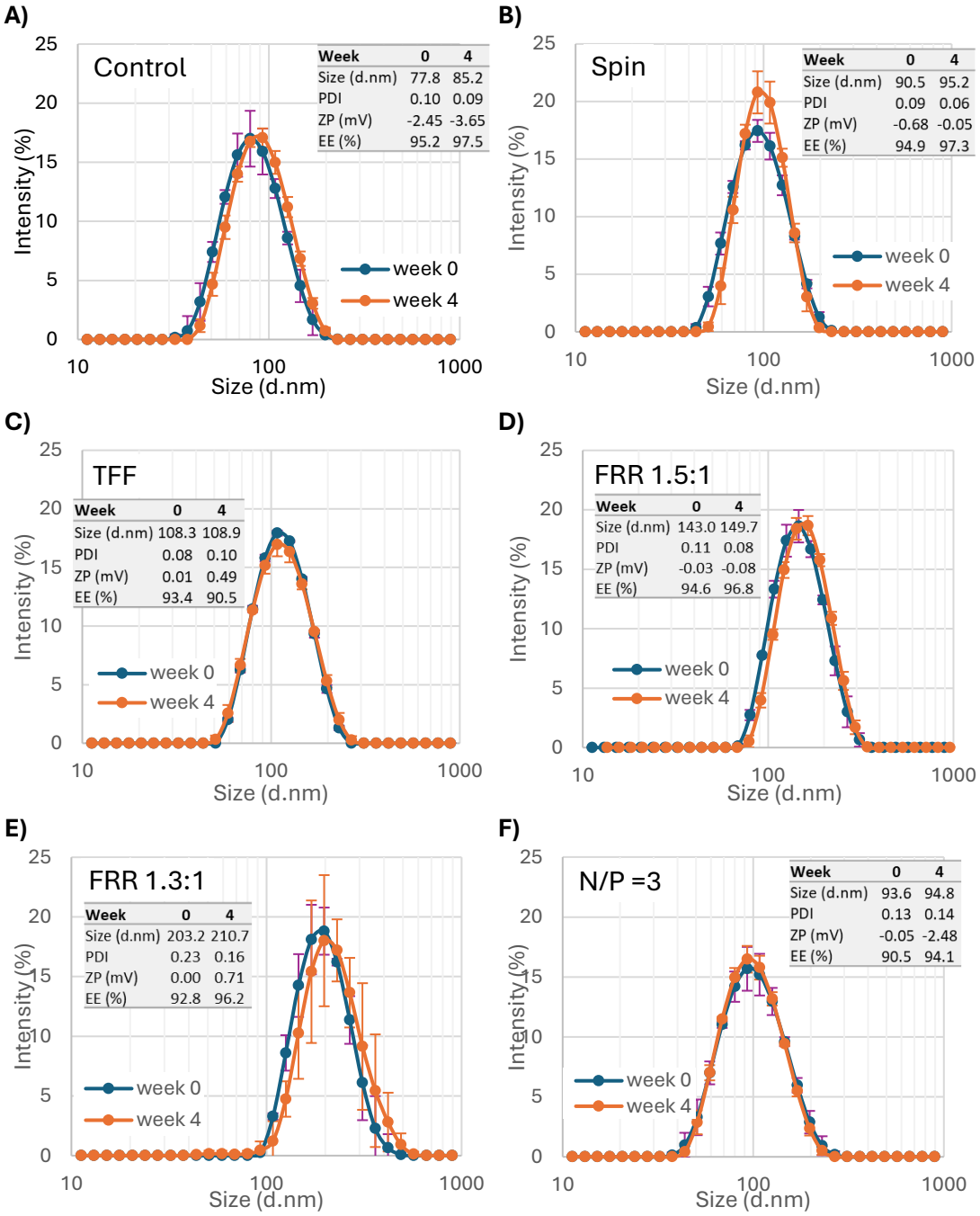

Figure 2.12: Size–intensity plots showing the four-week stability of six ALC-0315 (Formulation 2) LNP samples prepared under varying experimental conditions. Each panel includes an inset table summarising size, PDI, zeta potential (ZP), and encapsulation efficiency (EE%) at 0 and 4 weeks. Unless otherwise stated, LNPs were manufactured at an FRR of 3:1 and N/P of 6 from 5 mg/mL lipid stocks and purified by 1 h dialysis in PBS (pH 7.4). Spin-column (100 kDa, 40× dilution) and TFF (100 kDa, 12× diafiltration) purification conditions are indicated where applicable. Data are representative of a single sample, with measurements performed in triplicate (mean ± SD).

Table 2.8: Stability data for nine pre-made ALC-0315 (Formulation 2) LNP samples manufactured under varying experimental conditions. Each formulation represents a single sample, with repeat measurements indicated as (n = repeat number). Size, PDI, and zeta potential were measured in triplicate and are reported as mean ± SD. Unless otherwise stated, LNPs were manufactured at an FRR of 3:1 and N/P of 6 from 5 mg/mL lipid stocks and purified by 1 h dialysis in PBS (pH 7.4). Spin-purified samples were processed using 100 kDa centrifugal filters (40× dilution), and TFF-purified samples were processed using 100 kDa membranes with 12× diafiltration.

Formulation parameters (that differ from the control)	week 0					week 4				
	Size (d.nm)	PDI	ZP (mV)	EE%	MB%	Size (d.nm)	PDI	ZP (mV)	EE%	MB%
Control	77.8 (±1.3)	0.1 (±0.03)	-2.45 (±0.42)	95.2	76.9	85.2 (±2.5)	0.09 (±0.02)	-3.65 (±0.39)	97.5	93.0
Spin	90.5 (±1.5)	0.09 (±0.03)	-0.68 (±0.37)	94.9	71.0	95.2 (±1.6)	0.06 (±0.02)	-0.05 (±0.64)	97.3	80.6
TFF	108.3 (±1.0)	0.08 (±0.01)	0.01 (±0.07)	93.4	53.7	108.9 (±1.4)	0.10 (±0.01)	0.49 (±0.13)	90.5	63.6
FRR= 1.5 (1)	139.0 (±2.2)	0.07 (±0.02)	-1.18 (±2.09)	96.4	72.5	148.8 (±2.3)	0.05 (±0.04)	5.04 (±2.25)	94.7	72.8
FRR= 1.5 (2)	143.0 (±2.3)	0.11 (±0.03)	-0.03 (±0.15)	94.6	55.2	149.7 (±1.9)	0.08 (±0.02)	-0.09 (±0.16)	96.8	58.6
FRR= 1.5 (3)	134.8 (±2.3)	0.09 (±0.01)	6.53 (±2.87)	96.5	77.4	141.3 (±0.8)	0.06 (±0.02)	3.49 (±1.00)	97.0	78.1
FRR= 1.3 (1)	195.0 (±6.2)	0.21 (±0.08)	2.27 (±0.36)	93	57.2	201.6 (±3.5)	0.14 (±0.04)	0.01 (±0.27)	96.3	82.0
FRR= 1.3 (2)	203.2 (±2.4)	0.23 (±0.05)	0.00 (±0.04)	92.8	79.5	210.7 (±4.1)	0.16 (±0.04)	0.71 (±0.28)	96.2	71.3
N/P= 3	93.6 (±1.6)	0.13 (±0.01)	-0.05 (±0.35)	90.5	74.8	94.8 (±1.0)	0.14 (±0.02)	-2.48 (0.15)	94.1	109.9

Across all formulations tested, particle size remained largely unchanged or increased by less than 10 nm over the four weeks. PDI values remained low, indicating preservation of size homogeneity, and zeta potential values remained near neutral. Encapsulation efficiency and mass balance were also maintained at levels comparable to those measured immediately after manufacture. These findings suggest that no significant aggregation, fusion, or RNA leakage occurred during storage under the conditions used. The minimal change in particle size and PDI indicates good colloidal stability, while sustained encapsulation efficiency implies retention of the nucleic acid payload within the LNP core. Although the LNPs had near-neutral zeta potentials during storage, they still remained physically stable. This suggests that stability was not mainly caused by electrostatic repulsion between particles, which is usually lower in near-neutral systems. Instead, stability was likely maintained by the PEG-lipid coating and the internal structure of the LNPs. PEG-lipids form a protective hydrated layer around the particles, helping to reduce particle aggregation even when surface charge is low [15].

Collectively, these results demonstrate that ALC-0315 (Formulation 2) LNPs are physically stable for at least 4 weeks, supporting their suitability for subsequent biological studies and for short-term storage before *in vivo* evaluation.

Overall, the ALC-0315 with DMG-PEG Formulation 2 LNPs exhibited robust and reproducible physicochemical properties across a wide range of microfluidic and formulation parameters. Total flow rate and N/P ratio had minimal impact on LNP CQAs, while flow rate ratio and final lipid concentration were more influential, particularly at lower FRRs. Buffer exchange conditions, purification method, aqueous buffer concentration, lipid solvent choice, and dialysis duration had limited effects within the ranges tested. Stability studies confirmed that this formulation remained stable for at least four weeks post-manufacture, supporting their suitability for further biological evaluation in subsequent chapters.

Formulation 3- ALC-0315 (ALC-0159 PEG) LNPs

The next set of LNPs were manufactured using ALC-0315 as the ionisable lipid and ALC-0159 as the PEGylated lipid. The remaining lipid components (DSPC and cholesterol) were kept consistent with previous formulations.

This formulation contains the same lipid components as the Pfizer-BioNTech Comirnaty® vaccine. However, the molar ratio of lipids used in the vaccine differs from that employed in the preceding experiments. Therefore, the Pfizer-BioNTech lipid ratio (9.4:42.7:46.3:1.6% DSPC:Chol:ALC-0315:ALC-0159) was compared with the previously used ratio of 10:38.5:50:1.5%. Use of the Pfizer-BioNTech ratio resulted in slightly smaller LNPs, with an average reduction in size of approximately 9 nm; however, this difference was not statistically significant ($P = 0.19$) (Figure 2.13A). Zeta potential remained neutral for both formulations (Figure 2.13B), and no significant differences were observed in RNA encapsulation efficiency.

Although a smaller particle size is often considered advantageous due to potential effects on cellular uptake and biodistribution [66], the modest and statistically non-significant reduction observed here suggests limited practical impact under the conditions tested. The similarity in encapsulation efficiency and surface charge further indicates that both lipid ratios support comparable nanoparticle assembly and RNA complexation.

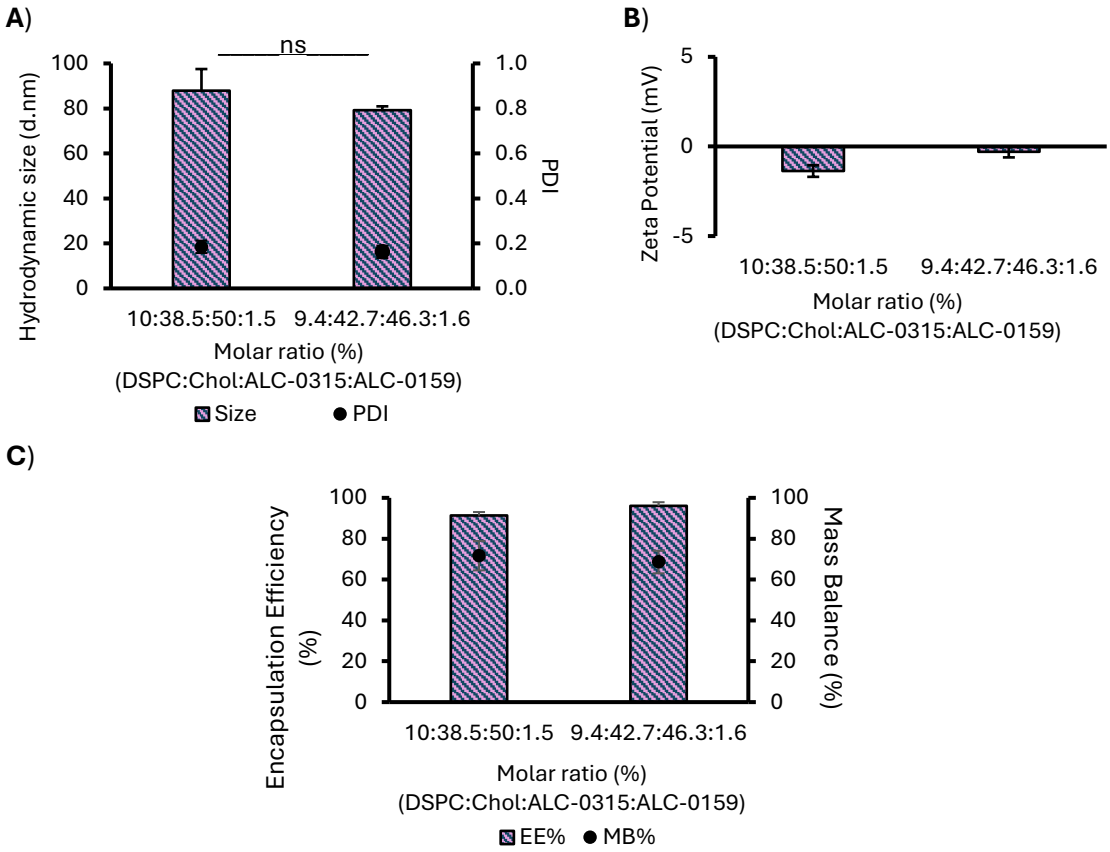

Figure 2.13: Effect of lipid molar ratio on hydrodynamic size and PDI (A) and zeta potential (B) of ALC-0315 (Formulation 3) LNPs. Size and zeta potential are shown as columns, and PDI is shown as closed circles. LNPs were manufactured at an FRR of 3:1 with an N/P of 6 from 5 mg/mL lipid stocks and purified by 1 h dialysis in PBS (pH 7.4). Each measurement represents the mean of three independent batches ± SD. (ns) denotes no statistical significance.

Given the minimal physicochemical differences and the importance of maintaining consistency when investigating additional formulation variables, subsequent experiments were performed using the previously established molar ratio. This approach ensured continuity with earlier optimisation studies while retaining clinical relevance by using identical lipid components.

Stability studies over four weeks were performed on all LNPs of this formulation. Four flow-rate ratios were evaluated, with three independent batches prepared for each condition, yielding a total of 12 LNP samples. Representative size–intensity distribution plots for each FRR are shown in Figure 2.14A-D, illustrating formulation behaviour over the four-week storage period. A summary of all CQAs measured at four weeks is presented in Table 2.9.

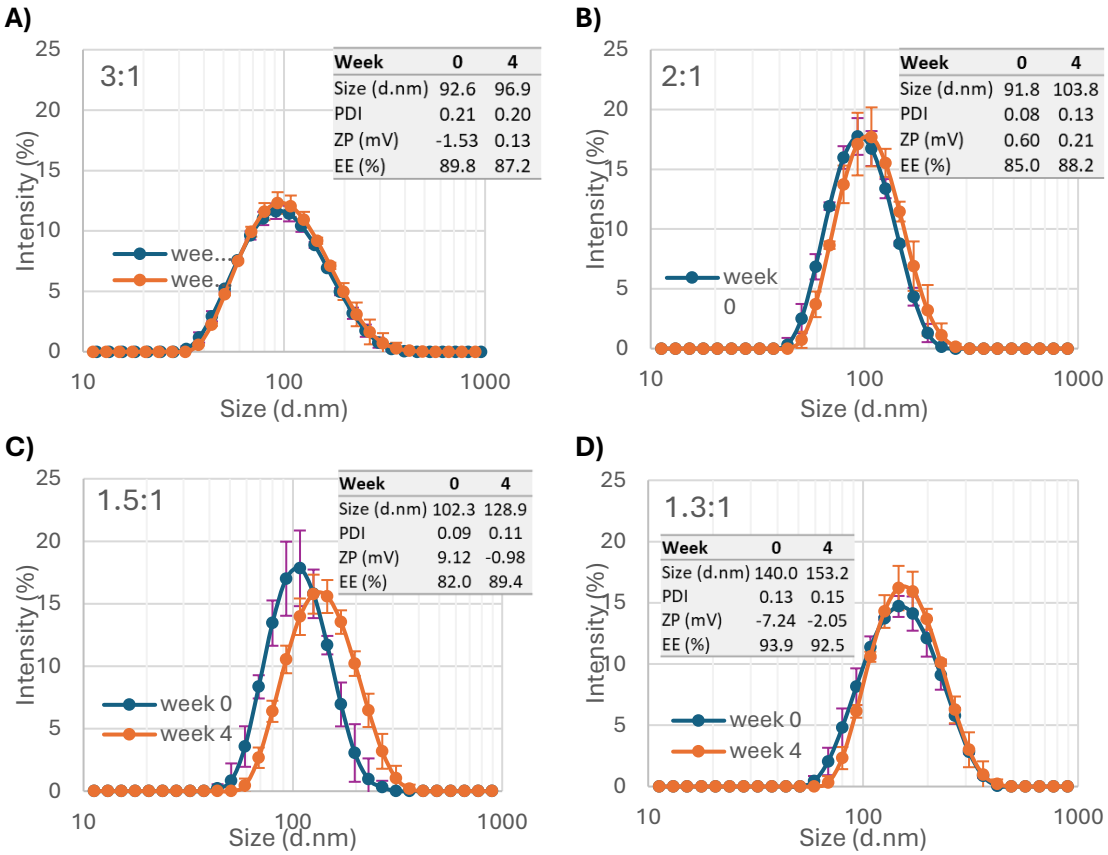

Figure 2.14: Figure 2.14: Stability analysis of ALC-0315 (Formulation 3) LNPs. (A–D) Size–intensity plots showing four pre-made LNP samples manufactured under varying experimental conditions. Each panel includes an overlay table reporting size, PDI, zeta potential (ZP), and encapsulation efficiency (EE%) at 0 and 4 weeks. Data represent measurements performed in triplicate and are shown as mean ± SD. Unless otherwise stated, LNPs were manufactured at an FRR of 3:1 and N/P of 6 from 5 mg/mL lipid stocks and purified by 1 h dialysis in PBS (pH 7.4).

LNPs manufactured at FRRs of 3:1 and 2:1 maintained largely stable physicochemical properties over time, with CQAs remaining consistent and only minor increases in particle size observed. PDIs remained low, and zeta potentials remained near neutral, indicating preservation of colloidal stability and particle homogeneity. In contrast, LNPs produced at lower FRRs exhibited reduced stability. Formulations prepared at an FRR of 1.5:1 showed size increases of at least 20 nm over four weeks, alongside greater variability in zeta potential. The size-intensity distributions for these lower FRRs were also less consistent between samples, suggesting increased heterogeneity and potential structural rearrangement or aggregation during storage. Despite the near-neutral zeta potentials, LNPs manufactured at higher FRRs remained stable over time.

This suggests that particle stability was supported more by PEG-related steric stabilisation and efficient particle assembly than by surface charge alone [15].

Table 2.9: Stability data for twelve ALC-0315 (Formulation 3) LNP samples manufactured at varying flow rate ratios. Each formulation represents a single sample, with repeat measurements indicated as (n = repeat number). Size, PDI, and zeta potential were measured in triplicate and are reported as mean ± SD. All LNPs were manufactured at an N/P of 6 from 5 mg/mL lipid stocks and purified by 1 h dialysis in PBS (pH 7.4).

Experiment FRR (n)	week 0					week 4				
	Size (d.nm)	PDI	ZP (mV)	EE%	MB%	Size (d.nm)	PDI	ZP (mV)	EE%	MB%
3:1 (1)	92.6 (±1.3)	0.21 (±0.11)	-1.53 (±0.14)	89.8	77.8	96.9 (±1.5)	0.19 (±0.01)	0.13 (±0.21)	87.2	98.8
3:1 (2)	95.9 (±1.3)	0.19 (±0.01)	-1.51 (±0.12)	93.2	73.4	99.0 (±0.7)	0.19 (±0.01)	0.16 (±0.23)	81.6	100
3:1 (3)	75.5 (±1.5)	0.15 (±0.01)	-1.07 (±0.43)	91	63.8	79.2 (±0.7)	0.14 (±0.01)	0.23 (0.48)	90.8	95.3
2:1 (1)	92.9 (±1.5)	0.14 (±0.01)	2.37 (±2.30)	88.5	83.3	116.4 (±1.6)	0.16 (±0.02)	-17.68 (±8.58)	89	84.9
2:1 (2)	89.1 (±1.2)	0.11 (±0.01)	1.33 (±1.31)	93.1	66.4	106.2 (±1.2)	0.17 (±0.04)	1.61 (±1.10)	91.4	92.2
2:1 (3)	91.8 (±1.4)	0.08 (±0.02)	0.60 (±1.63)	85	75	103.8 (±1.2)	0.14 (±0.04)	0.21 (±0.76)	88.2	94.9
1.5:1 (1)	108.1 (±2.1)	0.17 (±0.07)	1.60 (±0.87)	95.1	79.2	132.8 (±1.9)	0.15 (±0.02)	-4.81 (0.37)	93.1	82
1.5:1 (2)	98.7 (±2.3)	0.20 (±0.07)	1.36 (±0.41)	93.5	82.8	118.8 (±2.5)	0.19 (±0.03)	-0.49 (±6.69)	90.9	85.8
1.5:1 (3)	102.3 (±2.3)	0.09 (±0.04)	9.12 (±1.02)	82	79.8	128.9 (±3.6)	0.11 (±0.02)	-0.979 (±3.87)	89.4	100.9
1.3:1 (1)	140.0 (±5.5)	0.13 (±0.02)	-7.24 (±1.99)	93.9	92.4	153.2 (±2.1)	0.15 (±0.03)	-2.05 (±0.31)	92.5	58.2
1.3:1 (2)	140.3 (±4.5)	0.22 (±0.05)	7.1 (±1.61)	96.2	99.6	146.8 (±6.3)	0.14 (±0.03)	-8.18 (±1.03)	95.2	76.9
1.3:1 (3)	141.6 (±10.4)	0.26 (±0.02)	1.34 (±0.67)	91.7	98.2	141.3 (±7.2)	0.19 (±0.04)	0.33 (±0.73)	92.6	75.7

In contrast, the lower stability observed at lower FRRs may reflect less optimal lipid packing during particle formation, making these LNPs more prone to aggregation or structural changes during storage.

These findings are consistent with earlier observations that lower FRRs produce particles with less-optimal initial assembly characteristics. Subtle differences in core packing or lipid organisation during formation may predispose these particles to gradual destabilisation. Increased ethanol content during low-FRR mixing and altered nucleation dynamics may also contribute to the formation of less compact or less energetically stable structures, which become more apparent during storage [55].

Overall, these results indicate that higher FRRs support improved long-term stability of the LNPs, whereas lower FRRs may compromise particle robustness during extended storage. Although it should be noted that these assessments reflect physical stability only, and do not address potential chemical degradation of lipids or nucleic acids over time.

The next parameter assessed for these LNPs was the effect of the aqueous buffer pH on LNP CQAs. For this formulation, 50 mM citrate buffer was used as the aqueous phase in which the mRNA was dissolved. The ionisable lipid, ALC-0315, must be positively charged to enable electrostatic complexation with mRNA during LNP formation [66]. As the reported pKa of ALC-0315 is approximately 6.1 [12, 48], the degree of ionisation can be estimated using the Henderson–Hasselbalch equation. At pH 6, where pH ≈ pKa, ALC-0315 is expected to be ~50% protonated; at pH 5, approximately 90% protonated; and at pH 4, approximately 99% protonated.

To investigate the effect of aqueous buffer pH, LNPs were manufactured using citrate buffer at pH 4 (control), 5, 6, and 7.4. Following formulation, samples were purified either by 1-hour dialysis or by 100-kDa spin columns. The results are summarised in Figure 2.15.

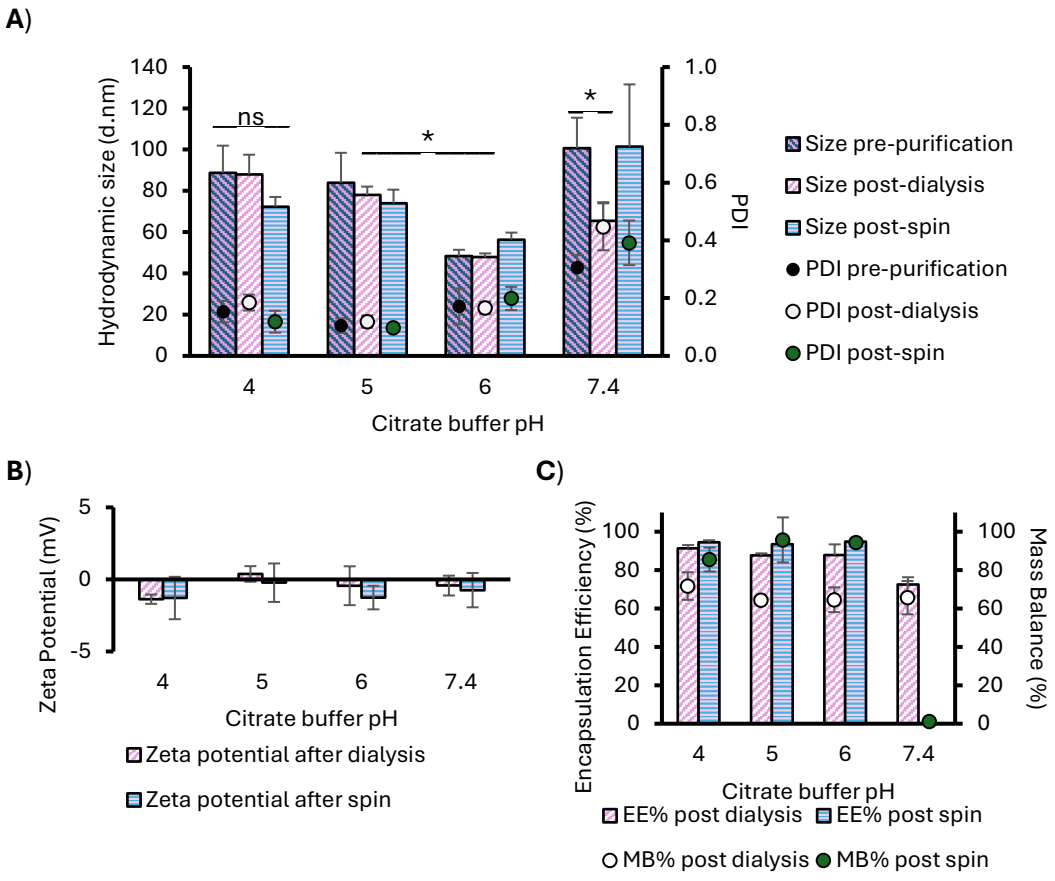

Figure 2.15: Effect of aqueous phase (citrate buffer) pH on hydrodynamic size and PDI before and after purification (A), zeta potential (B), and encapsulation efficiency and mass balance (C) of ALC-0315 (Formulation 3) LNPs. Results are shown for LNPs purified by dialysis or spin columns at each pH. Size, zeta potential, and encapsulation efficiency are shown as columns, while PDI and mass balance are shown as circles. LNPs were manufactured at an FRR of 3:1 with an N/P of 6 from 5 mg/mL lipid stocks and purified into PBS (pH 7.4) by 1 h dialysis or 100 kDa spin columns. Data represent mean ± SD of three independent batches. Statistical significance is indicated by *p < 0.05; ns, not significant.

For hydrodynamic size, LNPs formulated at pH 4 and pH 5 exhibited similar particle sizes, remaining within the range of approximately 70–90 nm both before and after purification, with no significant differences observed between purification methods (Figure 2.15A). LNPs formulated at pH 6 were significantly smaller than the control, with particle sizes of approximately 50 nm both before and after purification. This size reduction may be attributed to decreased electrostatic interaction between the ionisable lipid and mRNA due to reduced protonation, potentially resulting in a more compact ionised core. Interestingly, LNPs formulated at pH 7.4 initially exhibited larger particle sizes of approximately 100 nm. Following purification, these particles decreased in size to approximately 65 nm upon dialysis, whereas no comparable size reduction was observed with spin column purification. Further analysis of pH 7.4-formulated LNPs revealed a complete loss of mRNA (0% encapsulation efficiency and mass balance) following spin column purification. In contrast, pH 7.4 LNPs purified by dialysis retained measurable mRNA, with encapsulation efficiency and mass balance values of approximately 73% and 66%, respectively (Figure 2.15C). For all other pH conditions tested (pH 4–6), encapsulation efficiency remained above 87% regardless of purification method, and mass balance values exceeded 64%. However, slightly lower recoveries were generally observed after dialysis than after spin column purification.

The ability of LNPs formulated at pH 6 to maintain high mRNA recovery may be explained by the robustness of the N/P ratio, as observed previously for Formulations 1 and 2. Earlier results demonstrated that an N/P ratio of 3 encapsulated comparable amounts of mRNA to an N/P ratio of 6. Therefore, if ALC-0315 is approximately 50% protonated at pH 6, an initial N/P ratio of 6 would effectively correspond to a functional N/P ratio of 3, which remains sufficient for complete mRNA encapsulation. This hypothesis could be further explored by repeating experiments at lower initial N/P ratios to define the limits of effective encapsulation.

An alternative explanation is that a shift in dynamic equilibrium occurs during formulation. As protonated ALC-0315 molecules bind mRNA and are removed from solution, additional lipid may become protonated to re-establish equilibrium, thereby enabling continued mRNA complexation. Either or both of these mechanisms may contribute to the efficient encapsulation observed at pH 6 despite partial ionisation.

Polydispersity followed a similar trend, with LNPs formulated at pH 5 and pH 6 maintaining low PDIs (≤0.2), while pH 7.4-formulated LNPs exhibited higher PDIs in the range of 0.3–0.45, indicating increased heterogeneity (Figure 2.15A). Zeta potential remained near neutral across all pH conditions tested (Figure 2.15B).

At pH 7.4, the ionisable lipid ALC-0315 is expected to be only minimally protonated. Based on the Henderson–Hasselbalch relationship, where pH − pKa ≈ 1.3 (and $10^{1.3} \approx 20$), the ratio of unionised to ionised lipid is approximately 20:1, corresponding to ~5% of the lipid being protonated. Under these conditions, LNP formation does not follow the typical mechanism in which positively charged lipids electrostatically interact with negatively charged mRNA to form a stable core. As such, the behaviour observed for pH 7.4-formulated LNPs is atypical compared to conventional LNP assembly.

To further investigate and confirm these findings, the experiment was repeated using a modified approach. Rather than manufacturing separate batches for each purification method, individual LNP batches formulated at pH 7.4 were split equally and then purified by either dialysis or spin column centrifugation. This allowed for direct comparison of purification effects on identical LNP populations (Figure 2.16). Analysis of these data confirmed the trends observed previously. Following dialysis, particle size decreased while mRNA was retained within the LNPs (Figure 2.16A-B).

In contrast, spin column purification resulted in variable particle sizes and complete loss of detectable mRNA. Polydispersity indices remained high across all samples, indicating substantial heterogeneity, while zeta potential remained near neutral. One possible explanation for these observations is that dialysis provides extended contact time under mild conditions, allowing partial reorganisation or stabilisation of otherwise unstable LNP structures, thereby reducing particle size and improving mRNA retention. In contrast, the shear forces generated during centrifugal purification may disrupt the fragile core region of pH 7.4-formulated LNPs, leading to mRNA loss and particle instability.

When the filtrate from one of the spin column samples was analysed using the RiboGreen assay, no detectable mRNA was observed. This suggests that mRNA may have been retained within the filter membrane.

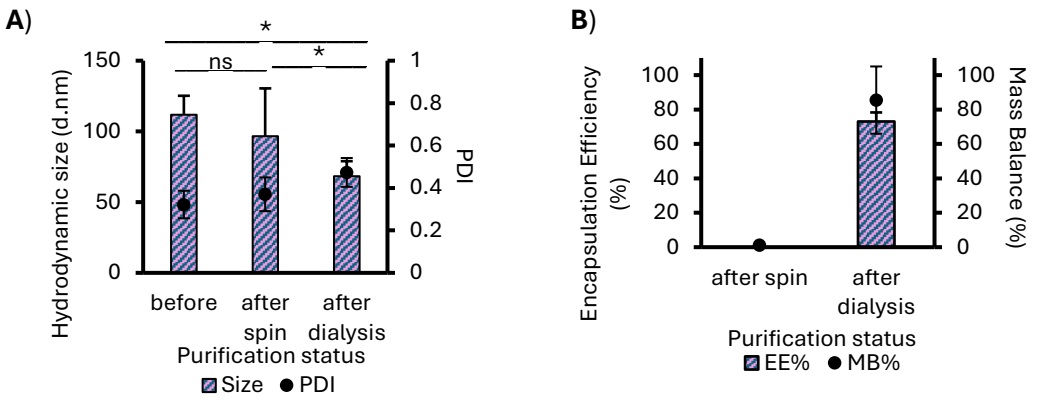

Sizes (d.nm):	Before	Spin	Dialysis
Sample 1	103 ± 5	141 ± 7	82 ± 2
Sample 2	117 ± 2	68 ± 1	63 ± 1
Sample 3	116 ± 23	81 ± 3	60 ± 2
PDIs:	**Before**	**Spin**	**Dialysis**
Sample 1	0.39 ± 0.08	0.43 ± 0.07	0.54 ± 0.09
Sample 2	0.28 ± 0.02	0.29 ± 0.04	0.45 ± 0.01
Sample 3	0.29 ± 0.01	0.39 ± 0.04	0.44 ± 0.01

RNA encapsulation	EE%		MB%	
	Spin	Dialysis	Spin	Dialysis
Sample 1	0	70	1	70
Sample 2	0	71	1	79
Sample 3	0	79	2	108

Figure 2.16: Effect of purification method on hydrodynamic size and PDI (A) and encapsulation efficiency and mass balance (B) of pH 7.4–formulated ALC-0315 (Formulation 3) LNPs. Graphs are paired with tables reporting CQAs for each sample before purification and after dialysis or spin column purification, with each sample split equally between methods. Size and encapsulation efficiency are shown as columns, while PDI and mass balance are shown as circles. LNPs were manufactured at an FRR of 3:1 with an N/P of 6 from 5 mg/mL lipid stocks and purified into PBS (pH 7.4) by 1 h dialysis or 100 kDa spin columns. Data represent mean ± SD of three independent batches. Statistical significance is indicated by *p < 0.05; ns, not significant.

Alternatively, intact LNPs may have been retained by the column, resulting in a recovered sample containing sufficient particles for DLS-based size measurement but insufficient RNA concentration to be detected by RiboGreen at the standard assay volume. Further investigation, such as membrane extraction or recovery analysis, would be required to distinguish between these possibilities.

It was also considered that formulation in citrate buffer at pH 7.4 lies outside the optimal buffering range for citrate and may contribute to particle instability. To determine whether buffer identity influenced the observed behaviour, LNPs were additionally formulated using phosphate-buffered saline (PBS) at pH 7.4 and compared with citrate-buffer-formulated samples (Figure 2.17).

Only a single batch was prepared for this comparison; therefore, further repeats would be required to draw statistically robust conclusions. Nevertheless, the results provided supportive evidence consistent with the trends observed for citrate-buffer-formulated LNPs at pH 7.4.

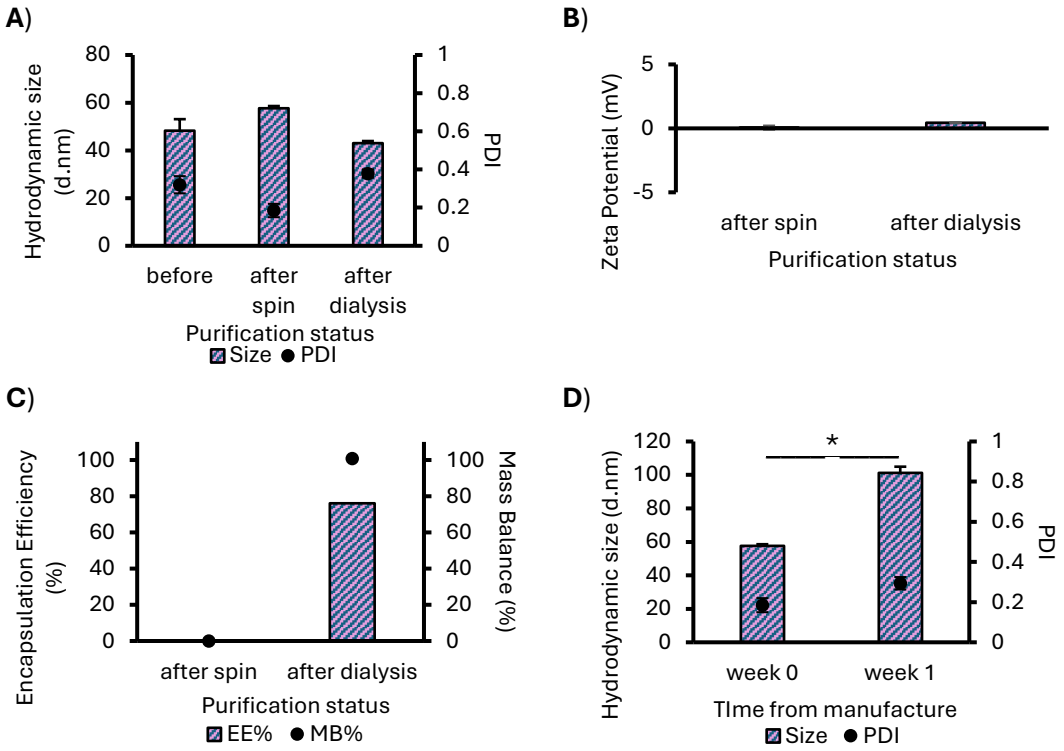

Figure 2.17: Effect of purification method on hydrodynamic size and PDI (A) and encapsulation efficiency and mass balance (B) of ALC-0315 Formulation 3 LNPs manufactured using PBS (pH 7.4) as the aqueous phase. Panel (D) shows the size and PDI of spin-purified LNPs measured immediately after manufacture and after one week. Size and encapsulation efficiency are shown as columns, while PDI and mass balance are shown as circles. LNPs were manufactured at an FRR of 3:1 with an N/P of 6 from 5 mg/mL lipid stocks and purified into PBS (pH 7.4) by 1 h dialysis or 100 kDa spin columns. Data are representative of a single batch; repeat experiments are required to confirm significance. Statistical significance shown (*p < 0.05) applies only within this batch.

Overall, PBS-formulated LNPs exhibited similar behaviour. Upon manufacture, these particles were smaller (~48 nm) than those prepared in citrate buffer. Particle size did not change substantially following purification by either method (Figure 2.17A). Encapsulation efficiency followed the same pattern as previously observed, with complete loss of detectable mRNA following spin column purification and retention of >70% following dialysis. Zeta potential remained near neutral across all conditions.

Interestingly, spin column-purified PBS-formulated LNPs exhibited low PDI values (<0.2), suggesting well-formed, homogeneous particles despite the absence of detectable mRNA. This raised the possibility that “empty” LNPs had formed. To assess structural stability, the same batch was reanalysed after one week of storage.

As shown in Figure 2.17D, both particle size and PDI increased markedly over the one week, from 58 nm and 0.19 at manufacture to 101 nm and 0.29, respectively. These changes indicate poor stability of the spin column–purified PBS-formulated LNPs. This

instability supports the interpretation that, under these conditions, either fragile LNP structures lacking encapsulated mRNA are formed, or that intact LNPs are partially retained within the spin column during purification, leaving an unstable population in the recovered sample.

Overall, the ALC-0315 (ALC-0159 PEG) Formulation 3 LNPs demonstrated the sensitivity of ionisable lipid-based nanoparticle assembly and stability to aqueous buffer pH and purification method when using clinically relevant lipid components. LNPs formulated at pH 4–6 exhibited consistent physicochemical characteristics and high mRNA recovery. In contrast, formulation at pH 7.4 resulted in atypical behaviour, including altered particle size, increased heterogeneity, reduced stability, and purification-dependent loss of encapsulated mRNA.

Dialysis was shown to preserve mRNA encapsulation under destabilising conditions better, whereas spin column purification resulted in complete mRNA loss and the formation of unstable particle populations. In addition, stability studies indicated that higher flow-rate ratios led to improved long-term robustness, reinforcing the importance of controlled mixing conditions not only for initial particle formation but also for downstream stability.

Collectively, these findings emphasise the critical role of formulation pH, mixing parameters, and purification strategy in determining LNP structural integrity and payload retention. The optimisation insights gained here directly informed the selection of formulation and processing conditions for subsequent biological studies, ensuring that downstream experiments were performed with stable and well-characterised LNP systems.

Conclusions and Future Work

This chapter systematically investigated the influence of key microfluidic manufacturing parameters on the physicochemical properties of lipid nanoparticles across multiple formulations. Across all formulations studied, flow rate ratio (FRR) emerged as the most influential parameter affecting LNP critical quality attributes, particularly particle size, polydispersity, stability, and mRNA recovery. Lower FRRs consistently resulted in larger, more heterogeneous, and less stable particles, while FRRs of 2:1 and above supported reproducible formation of LNPs with desirable CQAs. The pH of the aqueous buffer was

also shown to play a critical role, particularly for ionisable lipid-based formulations, where deviation from acidic conditions led to atypical particle behaviour, reduced stability, and purification-dependent loss of encapsulated mRNA.

In contrast, total flow rate (TFR) and N/P ratio had comparatively minor effects on LNP CQAs within the tested parameter ranges, with formulations demonstrating robustness to variation in these parameters. However, encapsulation efficiency measurements alone cannot determine how nucleic acid payload is distributed across the particle population, and it remains possible that changes in N/P ratio altered the proportion of loaded versus empty particles or the amount of RNA packaged per LNP without affecting the overall EE%.

While it is recognised that extreme values of TFR and N/P ratio may significantly affect LNP formation [13, 38, 64], the ranges explored in this chapter were sufficient to establish reliable and reproducible manufacturing conditions for subsequent studies.

Stability assessments demonstrated that well-formed LNPs remained stable for at least four weeks under the storage conditions used. Reduced stability observed for formulations produced at lower FRRs or under non-optimal pH conditions further highlights the importance of carefully controlling early formulation parameters to ensure long-term particle robustness.

Collectively, the results presented in this chapter establish a validated and reproducible microfluidic manufacturing framework for LNP production. This framework provides a solid foundation for the remainder of the thesis by defining robust formulation conditions and identifying parameters most likely to influence downstream biological performance. By characterising and minimising manufacturing-related variability at this stage, subsequent chapters can focus on biological, mechanistic, and translational questions without confounding effects from formulation inconsistency.

Future work arising from this chapter includes further refinement of FRR within the 1:1–2:1 range, where marked changes in CQAs were observed, and expansion of these studies into *in vitro* and *in vivo* models to determine how subtle differences in particle characteristics translate into biological performance. Additional long-term stability studies beyond four weeks may also provide further insight into formulation robustness and storage limitations. Together, these directions build directly on the optimisation

work presented here and support progression toward more advanced biological evaluation of LNP systems.

CHAPTER 3: TAILORING LIPID NANOPARTICLE DIMENSIONS THROUGH MANUFACTURING PROCESSES

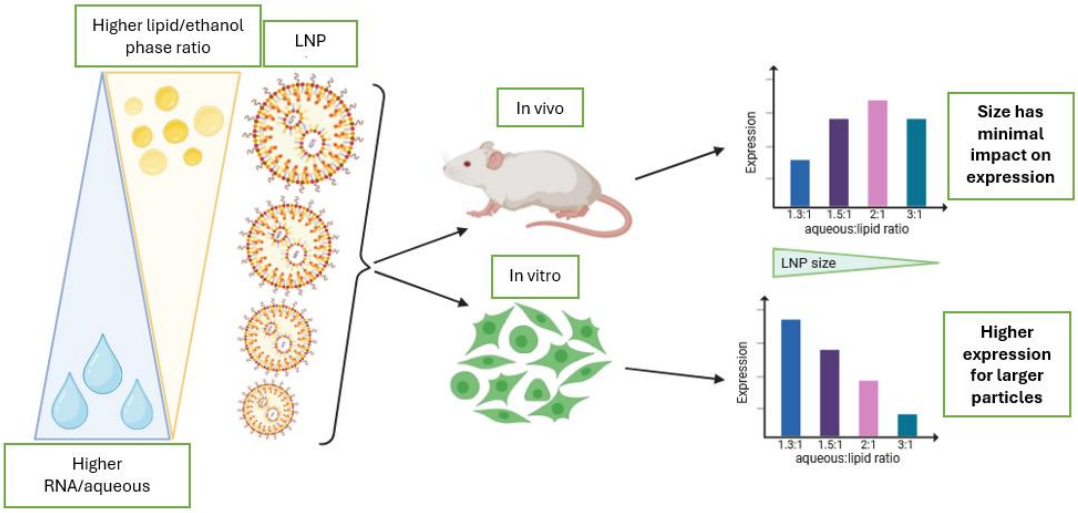

LNP particle size control can be achieved through manufacturing processes. Changes in particle size affect *in vitro* efficacy but not *in vivo* potency. Created with BioRender.com

This Chapter was published as a paper in RSC Pharmaceutics:

McMillan, C., Druschitz, A., Rumbelow, S., Borah, A., Binici, B., Rattray, Z., & Perrie, Y. (2024). Tailoring lipid nanoparticle dimensions through manufacturing processes [10.1039/D4PM00128A]. *RSC Pharmaceutics*, *1*(4), 841-853. https://doi.org/10.1039/D4PM00128A

Abstract

Lipid nanoparticles (LNPs), most commonly recognised for their role in COVID-19 mRNA vaccines, are important delivery vehicles for nucleic acid (mRNA, siRNA) therapies. The physicochemical attributes, such as size, nucleic acid encapsulation and electric charge may have a significant impact on the efficacy of these medicines. In this study, adjustments to aqueous to lipid phase ratios were assessed for their impact on LNP size and other critical quality attributes (CQAs). It was observed that minor adjustments of aqueous to organic lipid phase ratios can be used to precisely control the size of ALC-0315 formulated LNPs. This was then used to evaluate the impact of phase ratio and corresponding size ranges on *in vitro* and *in vivo* expression of these LNPs. In HEK293 cells the larger LNPs led to higher expression of the mRNA cargo within the LNPs, with a linear correlation between size and expression. In THP-1 cells this preference for larger LNPs was observed up to 120 d.nm after which there was a fall in expression. In BALB/c mice however, LNPs at the lowest phase ratio tested, > 120 d.nm showed reduced expression compared to those with the range 60-120 d.nm, within which there was no significant difference between sizes. These results suggest a robustness of LNP expression up to 120 d.nm, larger than those <100 d.nm conventionally used in medicine.

Introduction

Lipid nanoparticles (LNPs) lie within the family of lipid-based nanoparticles, which also include liposomes, and other nanoscale lipid complexes. What differentiates LNPs to other lipid-based nanoparticle formats, is the presence of a solid core created from nucleic acid complexed to a permanent or ionisable cationic lipid. Thus, LNPs are the vector of choice for the delivery of RNA-based therapeutics and vaccines [11-13]. The COVID-19 pandemic placed LNPs in the spotlight, hugely increased interest and recognition of their potential in drug and vaccine delivery, which is evidenced by a doubling of published literature on LNPs in the last 5 years [82].

Optimising LNP manufacture has emerged as valuable research, especially concerning production speeds, scalability, stability and efficacy of the end product [15, 117]. The growth of this field is driven by challenges faced during the rapid mass production of LNP-based mRNA vaccines during the pandemic. One of the biggest challenges was producing formulations rapidly to meet demand. Furthermore, manufacturing formulation parameters have been widely explored in the field of liposomes [9, 105], so

translating this research to LNPs is valuable. In addition to optimisation of the manufacturing process, testing the robustness of parameters used is vital, as this aids in understanding the formulation, as well as defining the limits within formulations and expands the knowledge base in nanomedicine formulation strategy. For example, there is evidence that size impacts LNP immunogenicity and mRNA expression, impacting therapeutic efficacy [13, 123, 124]. However, the impact varies based on the indication and pharmacokinetics, while larger LNPs (>100 d.nm) may have higher mRNA expression[124], there is evidence smaller LNPs (<100 d.nm) are more readily be absorbed from the injection site [123].

Microfluidics is a precise, reproducible, and scalable method for manufacturing LNPs. It has easily adjustable parameters, which can be precisely controlled with relative ease in comparison to other methods of LNP manufacturing [38]. Parameters, such as mixing speed and flow rate ratio, can significantly impact the critical quality attributes of the produced LNPs. The flow rate ratio is equivalent to the ratio of nucleic acid containing aqueous phase to organic phase dissolved in ethanol. Previous work has shown that higher proportions of organic phase and ethanol increase particle size in liposomes and some formulations of LNPs [13, 38, 105, 125]. In this study we assess different formulations of LNPs, and correlate the *in vitro* and *in vivo* response, with a specific focus on the LNP mRNA expression.

To evaluate LNP performance across biologically relevant cellular models, HEK-293, THP-1, and bone marrow-derived macrophage (BMM) cells were used for *in vitro* studies. HEK-293 cells were selected as a highly transfectable epithelial cell line commonly used for assessing nanoparticle-mediated gene delivery [126]. In contrast, THP-1 monocytes and BMMs possess stronger innate immune sensing pathways, including Toll-like receptor and interferon-associated responses, which are highly relevant to nucleic acid delivery systems [127-129]. These immune cell models were included to assess LNP behaviour in cells with greater phagocytic activity and immune responsiveness, which may influence nanoparticle uptake, intracellular processing, and mRNA expression. *In vivo* studies were performed in BALB/c mice, a widely used immunocompetent strain commonly employed in vaccine and nanoparticle research due to their well-characterised immune responses and suitability for evaluating systemic and localised LNP-mediated expression [40, 130].The aim of this study was to assess whether the

phase ratio to size relationship translates to two clinically used LNP formulations- i.e. those formulated with ALC-0315 and SM-102 as the ionisable lipid and evaluate the impact of phase ratio and LNP particle size on *in vitro* and *in vivo* expression.

Materials and methods

Materials

1,2-distearoyl-sn-glycero-3-phosphocholine (DSPC) was obtained from Lipoid (Ludwigshafen, Germany). 1,2-dioleoyl-3-trimethylammoniumpropane (chloride salt) (DOTAP), and 1,2-dimyristoyl-rac-glycero-3-methoxypolyethylene glycol-2000 (DMG-PEG 2000) were purchased from Avanti Polar Lipids (Alabaster, AL, USA). Cholesterol, citric acid, sodium citrate tribasic dehydrate, polyadenylic acid (PolyA), 6-(p-Toluidino)-2-naphthalenesulfonic acid sodium salt, Sodium phosphate monobasic (NaH2PO4•H2O), and Sodium phosphate dibasic (anhydrous)(Na2HPO4) were acquired from Sigma-Aldrich (St. Louis, MO, USA). Phosphate-buffered saline tablets (PBS pH 7.4) were acquired from Oxoid Ltd. (Basingstoke, UK). Tris Base and Ethanol (EtOH) were obtained from Fisher Scientific (Loughborough, UK). Methanol and Propan-2-ol (Isopropanol, IPA) were purchased from VWR Chemicals (Lutterworth, UK). The ionisable lipids [(4-Hydroxybutyl)azanediyl]di(hexane-6,1-diyl) bis(2-hexyldecanoate) (ALC-0315) and 9-Heptadecanyl 8-((2-hydroxyethyl)[6-oxo-6-(undecyloxy)-hexyl]amino)octanoate (SM-102) and the PEG-lipid 2-[(polyethylene glycol)-2000]-N,N-ditetradecylacetamide, 1,2-Distearoyl-sn-glycero-3-phosphocholine (ALC-0159) were purchased from BroadPharm (San Diego, CA, USA). Minimum Essential Medium, Trypsin-EDTA (0.05%), PBS, pH 7.4 solution and Quant-it™ RiboGreen RNA Assay Kit and RiboGreen RNA Reagent, RediPlate™ 96 RiboGreen™ RNA Quantitation Kit were purchased from Fisher Scientific UK Limited (Renfrew, UK). EZ Cap™ Firefly Luciferase mRNA was purchased from ApexBio Technology (Houston, TX, USA). mGreenLantern was provided by CPI by the Intracellular Drug Delivery Centre (IDDC) research programme. ONE-Glo™ Luciferase Assay System was acquired from Promega UK (Southampton, UK). All solvents and other chemicals were of analytical grade, and milliQ-water was provided by an in-house system.

Aqueous and Organic phase preparation

The aqueous phase containing mRNA, and the organic phase were prepared separately before microfluidics. The aqueous phase was prepared using 50mM citrate buffer (pH

4), dissolving PolyA, or Firefly Luciferase (Fluc) mRNA for *in vitro* and *in vivo* experiments, at mRNA concentrations required to maintain a nitrogen to phosphate (N/P) ratio of 6, the molar ratio of ionisable lipid containing positively-charged amines (N) to the mRNA containing negatively-charged phosphates (P). Therefore, the concentrations were adjusted for different aqueous: organic phase ratios and when different lipids or mRNA were used, to maintain this N/P ratio.

The lipid molar ratio of the LNPs was 10:38.5:50:1.5% structural lipid: cholesterol: ionizable lipid: PEGylated lipid. This led to the following combinations utilised in the experiments: (1) DSPC:Chol:ALC-0315:DMG-PEG2000 (2) DSPC:Chol:ALC-0315:ALC-PEG (3) DSPC:Chol:SM-102:DMG-PEG2000. The lipid stocks were prepared and stored at concentrations of 5-20 mg/mL, dissolving each lipid in ethanol. Unless otherwise stated, the organic phase injected into the microfluidic device has a concentration of 5 mg/mL.

Manufacture of the LNPs using microfluidics

The NanoAssemblr benchtop (Precision Nanosystems Inc., Vancouver, Canada) was used in all experiments in this chapter. The ethanol-based organic phase and the citrate buffer-based aqueous phase containing mRNA in the form of PolyA or Fluc mRNA were fed through syringes into a microfluidics chip with a herringbone mixer design. The phase ratio (aqueous: organic phase) was adjusted using the computer interface of the machine, varying between the limits of 1:1-3:1 aqueous: organic phase, respectively.

Purification methods

For purification by dialysis buffer exchange, the LNP sample in the original ethanol/citrate buffer was exchanged into 200 mL PBS (pH 7.4) for every mL of sample. Samples manufactured with PolyA as the internal nucleic acid and mRNA samples for *in vitro* experiments were dialysed for 1 hour at ambient temperature, and for 24 hours at 4°C for *in vivo* studies. Spin columns of 100 kDa MWCO were used for centrifugation and purification of LNPs alongside dialysis in optimisation experiments. LNPs were diluted 40X in PBS. The samples were spun at 2,000 xg at 4°C for 20-40 minutes (time varying with formulation) until the sample reached the original pre-purification volume.

Measuring Critical Quality Attributes (CQAs)

Physicochemical

Size (Z-average diameter), polydispersity index (PDI) and zeta potential were measured using the Malvern Panalytical Zetasizer ZS and Zetasizer Ultra, using the Zetasizer software for data acquisition. Size and PDI were measured *via* dynamic light scattering (DLS), using a measurement angle of 173° backscatter, and zeta potential was measured using voltage measurements in a Folded Capillary cell. Each of these measurements were performed in triplicate for each experimental repeat (nine measurements for each experiment). Post- purification, each sample was prepared for measurement at a lipid concentration of 0.1mg/mL in PBS (for size/PDI) or deionised water (for zeta potential) to achieve attenuation values between 7 and 8. Pre-purification measurements for size and PDI were performed with citrate buffer as the diluent. ZEN0040 disposable micro-cuvettes were used for size and polydispersity, and DTS1070 folded capillary zeta cells were used for zeta potential measurements, adding 400 µL and 1,000 µL of diluted LNPs, respectively. The material refractive index and absorption were 1.45 and 0.001, respectively. The dispersant refractive index and absorption were 1.33 and 0.8872 cP, respectively for water, 1.335 and 1.02 cP, respectively for PBS, and 1.47 and 1.28 cP for citrate buffer.

Nanoparticle tracking analysis was performed on samples post-purification using the Malvern Panalytical NanoSight Pro (Malvern Panalytical, Malvern, Worcestershire) and the NS Xplorer software was used for data analysis. Nanoparticle size distribution and estimated particle concentration was measured using a 488 nm laser block and videos were captured using a high sensitivity sCMOS camera with the light scatter filter. Samples were diluted to 0.05-0.1 µg/mL and analysed under constant flow (1-1.5 µL/min) using a syringe driver, with temperature (20°C). Five 11.5 second videos were captured for each sample and optimised using the automated optimal settings employed by the software. Between 2700 and 5100 particle trajectories (valid tracks) were analysed depending on the sample to gather the NTA data. These values were 2774, 3623, 4976 and 5056 for the aqueous: organic phase ratios of 1.3:1, 1.5:1, 2:1 and 3:1 respectively, which equates to the total number of particles measured per sample (Table S1).

mRNA content

Encapsulation efficiency and mRNA recovery were measured using the RiboGreen™ mRNA quantification assay kit according to manufacturer recommendations. Tris-EDTA (TE) buffer was used as the diluent in all steps of this assay. The fluorescent dye was used to quantify mRNA in the presence and absence of 1% Triton, for lysis of the LNPs. Two RNA standard curves were used to quantify mRNA. The fluorescence signal was read using the POLARstar Omega and GloMax plate readers using 475-485 nm excitation and 525 nm emission wavelengths.

When analysing the results, the total RNA for each sample from the Triton wells and free (unentrapped) RNA from the TE-only wells were obtained. The following equations were used to calculate encapsulation efficiency (EE%) and mRNA recovery as follows:

$$EE\% = 100 \times (CT - CF)/CT \qquad \textit{Equation (1)}$$

$$mRNA\ recovery(\%) = 100 \times CT/CI \qquad \textit{Equation (2)}$$

Where:

CT = Total RNA concentration (based on results from the wells prepared with Triton-TE buffer)

CF = Free, unentrapped RNA concentration (based on results from the wells prepared with TE buffer)

CI= RNA inputted into the experiment, the theoretical concentration of RNA

Cryogenic Transmission Electron Microscopy (Cryo-TEM)

Lipid nanoparticle samples were prepared as previously stated and kept at manufacturing concentrations in pH 7.4 PBS. 3 µL of samples were blotted using FEI Vitrobot (Thermo Fisher Scientific, UK) for 3 seconds and 5 force onto a 300-mesh lacey carbon-coated copper grid, then immediately vitrified in liquid ethane, cooled by liquid nitrogen, and held in a cryo-specimen holder (Gatan Elsa) before transfer to the TEM. LNP morphology was observed and captured under liquid nitrogen temperature using a Jeol JEM-F-200 microscope (Jeol, Japan) at 200kV.

In vitro expression

LNP FLuc mRNA expression was analysed in HEK293, THP-1 and BMM (bone marrow-derived macrophages) cells using firefly luciferase as a bioluminescent reporter. Cells were cultured in minimal essential medium (MEM) (for HEK-293 cells) or RPMI 1640 (for THP-1 and BMM cells), supplemented with 10% foetal bovine serum (FBS), 1% penicillin/streptomycin and 1% sodium pyruvate. Cells were added to a 96-well white/clear bottom plate, at a concentration of 10,000 cells/well in media and cultured for 72 hours, after which LNPs were added. LNPs were formulated as above, with EZ Cap™ Firefly Luciferase mRNA as the internal RNA. LNP formulations were added to the cells, replacing growth media, and diluted in media at total mRNA concentrations of 2 µg/mL, 1 µg/mL, 0.5 µg/mL and 0.25 µg/mL, using three wells per concentration and leaving three wells free from LNPs (control wells). Cells were incubated with LNPs for 24 hours prior to addition of the luciferase reagent. Luciferase reagent, prepared as per the manufacturer's instructions, was added to each well of the 100 µL of media and cells containing LNPs from the previous day, creating a total volume of 200 µL, mixed thoroughly and left to incubate for 3 minutes. The luminescence of the plates was read using the GloMax plate reader (Promega, UK).

LNP FLuc mGreenLantern expression was analysed in HEK293, THP-1 and BMM (bone marrow-derived macrophages) cells using Green Lantern mRNA for taking fluorescence images of LNP expression. Cells were cultured as above in 6-well plates and transfection with LNPs at a total mRNA concentration of 2 µg/mL. Cells were incubated with LNPs for 24 hours prior to imaging using the GFP filter on the EVOS M5000 microscope (Thermo Fisher Scientific, UK). The total fluorescence of these images was quantified using ImageJ, using 5 images per sample.

In vivo expression

LNP expression was analysed in BALB/c mice using firefly luciferase as a bioluminescent reporter. These LNPs were manufactured incorporating 1% DiR dye in the organic phase, to confirm successful administration of the LNPs at the injection site and with EZ Cap™ Firefly Luciferase mRNA as the internal RNA. Three BALB/c mice were injected with each formulation in each study (N=3 per formulation, 9 mice per formulation). Each mouse was injected intramuscularly (I.M.) with (50 µL in each quadricep) 0.1 mg/mL of mRNA LNPs prior to anaesthetic and imaging. Imaging was performed at four time points after LNP injection: 0, 6, 24 and 48 hours. The mice were

anaesthetised and maintained under anaesthesia using isoflurane before imaging using the IVIS® Spectrum and the associated Living Image® software (PerkinElmer, Buckinghamshire, UK). For confirming successful I.M. injection of the LNPs, the presence of DiR was detected using the fluorescence setting, at wavelengths of 710 nm excitation and 780 nm emission. For the Fluc mRNA expression the mice were firstly injected subcutaneously with 30 mg/mL D-luciferin solution (5 µL per gram of body weight, corresponding to 150 mg/kg). This SC injection was repeated at each of the four time points, and these mice were imaged 10 minutes after injection using the luminescence setting. After the 48-hour time point the mice were terminated whilst still under anaesthetic using a schedule 1 method. The images were collated and normalised, and the fluorescence and bioluminescence signals were quantified by selecting regions of interest on the software.

pKa determination

The effective pKa of the ionisable lipid ALC-0315 within the formulation was determined using 6-(*p*-Toluidino)-2-naphthalenesulfonic acid (TNS) as a fluorescent marker for positively-charged particles, adapted from Tanaka *et al* method [131]. The LNPs were titrated in buffers from pH3-9 and the pH at which 50% of the maximum fluorescence signal was taken as the pKa. ALC-0315 (formulation 3) and DOTAP (formulation 1) LNPs were manufactured and diluted to a concentration of 0.5 mM. Buffers of pH 3, 4, 4.5, 5, 5.5, 6, 6.5, 7, 7.5, 8, 8.5 and 9 were prepared at a concentration of 20 mM. Citrate buffer was used for pHs 3-6, sodium dihydrogen phosphate buffer was used for pHs 6.5-8, and tris buffer was used for pHs 8.5 and 9. TNS was prepared by dissolving 6-(*p*-Toluidino)-2-naphthalenesulfonic acid sodium salt in water, to a concentration of 0.6 mM. 186 µL of each buffer was added to the appropriate wells, followed by the addition of 12 µL of LNP solutions, and subsequent addition of TNS solution (2µL). The fluorescence of TNS was measured using a POLARstar Omega plate reader at 355 excitation and 460 emission wavelengths.

Statistical analysis

The mean and standard deviation were calculated for all experiments, performed in independent triplicate batches unless otherwise stated, each batch was manufactured on a different day, to account for inter-day variation. For hydrodynamic size, polydispersity, and zeta potential, three measurements were taken for each batch and purification status, therefore these groups for statistical analysis were n=9. For

statistical comparison of groups, one way (for one independent variable) or two/three-way (for two-three independent variables respectively) analysis of variance (ANOVA) was performed with Tukey's HSD post-hoc for pairwise comparisons. Unpaired t-tests were used when comparing just two groups, and paired t-tests were used for comparing the same group/batch over time or treatment. On graphs, the statistical significance is indicated by individual p values for $p<0.05$, whereas (ns) denotes no statistical significance.

RESULTS AND DISCUSSION

The effect of altering manufacturing parameters on the physicochemical attributes of lipid nanoparticles (LNPs)

To confirm one hour of dialysis was sufficient for LNP sample purification, samples manufactured at an aqueous to organic phase ratio of 3:1 were purified by both dialysis and spin columns (Table 1). This showed that although spin columns slightly reduced the size of these LNPs, the other CQAs were unaffected by the differing purification methods. It was necessary to use dialysis for the purification of LNPs in the upper size range. Based on these results, dialysis was used as the purification method for all subsequent samples and extended to 24 hours for samples *in vivo* to optimise buffer exchange.

The impact of aqueous: organic phase ratio across different LNP formulations

The impact of the proportion of aqueous to organic phase on the LNP physicochemical attributes, i.e. size, polydispersity, zeta potential and nucleic acid recovery, was evaluated across three different LNP formulations.

Table 1: Comparison of different purification methods. Dialysis was performed for 1 hour. 100kDa spin columns were used for centrifugation of LNPs diluted 40X in PBS back to the original sample volume. Each measurement is a mean of three independent batches with error bars showing ±SD. The Significance is indicated by (*) $p<0.05$.

Purification status	Size (nm)	PDI	Zeta potential (mV)	EE (%)	mRNA recovery (%)
Before purification	89 ± 13	0.15 ± 0.04	n/a	n/a	n/a
Dialysis	88 ± 10	0.18 ± 0.03	-1.4 ± 0.3	91 ± 2	72 ± 7
Spin column	72 ± 5*	0.12 ± 0.04	-0.4 ± 1.3	95 ± 1	86 ± 6

These were (1) DSPC:Chol:ALC-0315:DMG-PEG2000, (2) DSPC:Chol:ALC-0315:ALC-0159 and (3) DSPC:Chol:SM-102:DMG-PEG2000, each at a molar ratio of 10:38.5:50:1.5 for each of the lipids respectively. LNPs composed of ALC-0315 as the ionisable lipid and DMG-PEG2000 as the PEGylated lipid, were initially used. Seven different aqueous to organic phase ratios were tested and the results showed a trend of decreasing LNP size as the proportion of aqueous phase to organic phase increased (Figure 1B). For samples manufactured at ratios of 1:1 and 1.2:1, the polydispersity was high, with values of 0.58 and 0.76, suggesting a highly heterogeneous population. These more heterogeneous LNP batches also tended to show more variability in terms of zeta potential, encapsulation efficiency (EE%) and mRNA recovery (%) (Table 2). Due to this, the mixing ratios of 1:1 and 1.2:1 were not further investigated. 1.8:1 was also not included in future experiments for simplification purposes.

The second LNP formulation tested used ALC-0315 in combination with ALC-0159 as the pegylated lipid, similar to the Pfizer/BioNTech Comirnaty® mRNA vaccine lipid composition. The aqueous: organic phase ratios tested were 1.3:1, 1.5:1, 2:1 and 3:1. The same trend of size decreasing as the aqueous phase increased was observed (Figure 1A). The PDI remained low through all phase ratios of approximately <0.2, and the zeta potential remained neutral (-5 to 5 mV) (Table 2).

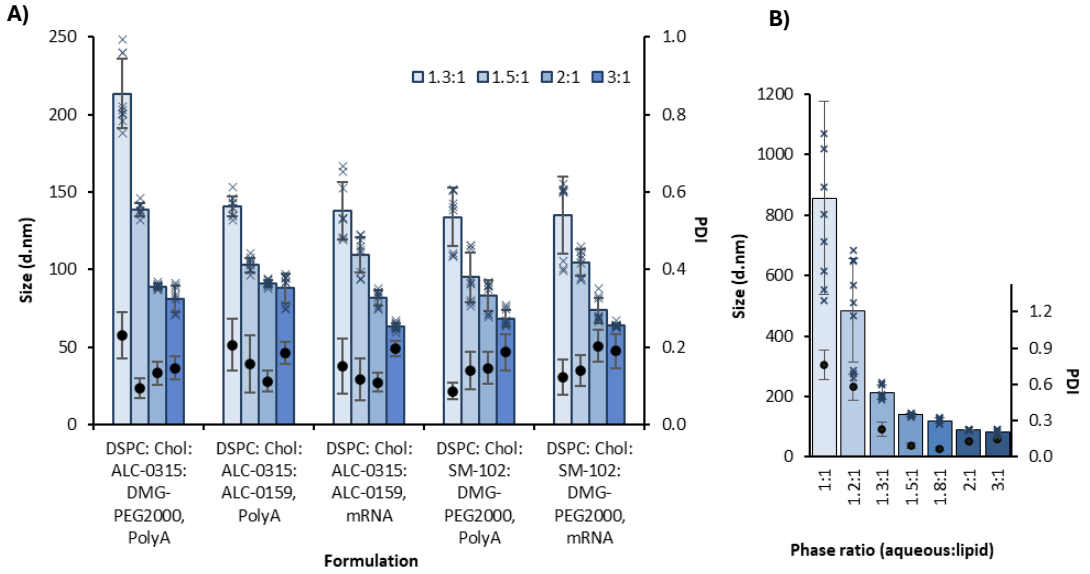

Figure 1: The effect of aqueous: organic phase ratio on LNP size across different lipid combinations and nucleic acid cargos. (A) Comparing phase ratios of 1.3, 1.5, 2 and 3 (:1) in five LNP formulations. (B) Looking at a wider range of phase ratios in the first formulation (ALC-0315:DMG-PEG2000). The sizes are shown as columns, with individual measurements shown as crosses and the polydispersity indices (PDI) are shown as closed circles. The LNPs were manufactured with an N/P of 6 from 5mg/mL lipid stocks and purified by dialysis in pH 7.4 PBS for 1 hour. Each measurement is a mean of three

independent batches with error bars showing ±SD. The significance is indicated by (*) between each of the phase ratios analysed by two-way ANOVA with Tukey's pairwise comparison.

Table 2: Physicochemical attributes of each of the tested LNP formulations. The LNPs were manufactured with an N/P of 6 from 5mg/mL lipid stocks and purified by dialysis in pH 7.4 PBS for 1 hour. Each measurement is a mean of three independent batches ± standard deviation. EE%= encapsulation efficiency.

DSPC: Chol:	Aqueous: organic phase ratio	Zeta potential (mV)	EE%	mRNA recovery (%)
ALC-0315: DMG-PEG2000, PolyA	1:1	8.3 ± 8.3	70 ± 14	37 ± 17
	1.2:1	6.0 ± 6.8	61 ± 19	68 ± 4
	1.3:1	4.6 ± 5.0	75 ± 23	65 ± 10
	1.5:1	1.8 ± 3.8	96 ± 1	68 ± 10
	1.8:1	2.8 ± 3.0	96 ± 1	79 ± 10
	2:1	-1.7 ± 1.3	94 ± 1	93 ± 6
	3:1	-2.6 ± 1.2	98 ± 1	91 ± 13
ALC-0315: ALC-0159, PolyA	1.3:1	0.4 ± 6.4	94 ± 2	97 ± 4
	1.5:1	4.0 ± 3.9	90 ± 7	81 ± 2
	2:1	1.4 ± 1.7	89 ± 4	75 ± 8
	3:1	-1.4 ± 0.3	91 ± 2	72 ± 7
ALC-0315: ALC-0159, mRNA	1.3:1	-1.3 ± 2.2	61 ± 18	82 ± 4
	1.5:1	-0.2 ± 2.1	79 ± 7	86 ± 7
	2:1	-1.5 ± 1.0	89 ± 2	83 ± 12
	3:1	-0.9 ± 1.4	91 ± 2	94 ± 13
SM-102: DMG-PEG2000, PolyA	1.3:1	5.6 ± 0.8	97 ± 2	78 ± 5
	1.5:1	3.7 ± 3.0	98 ± 1	89 ± 5
	2:1	4.6 ± 1.5	99 ± 1	95 ± 8
	3:1	3.4 ± 1.2	99 ± 1	87 ± 0
SM-102: DMG-PEG2000, mRNA	1.3:1	-0.9 ± 12	95 ± 4	93 ± 11
	1.5:1	5.2 ± 1.2	94 ± 5	82 ± 11
	2:1	4.8 ± 1.4	96 ± 3	84 ± 11
	3:1	3.4 ± 1.5	96 ± 3	100 ± 20

This pattern was repeated with LNPs prepared using SM-102 and DMG-PEG2000 (a mimic to the Moderna Spikevax® lipid composition). These formulations were measured using both PolyA and mRNA as the nucleic acid cargo, both of which gave the same phase ratio-size relationship.

A two-way ANOVA with Tukey's post hoc analysis found a significant difference in size output for all of these phase ratios, with average sizes being approximately 3:1= 70 d.nm, 2:1= 80 d.nm, 1.5:1= 110 d.nm and 1.3:1 = 145 d.nm (aqueous: organic phase) (Figure 1A). Within these phase ratios tested, PDI remained low (<0.2), zeta potential was near neutral and EE% and mRNA recovery% was > 60% (Table 2). This correlation between phase ratio and LNP particle size results from the rate of polarity change induced by

ethanol dilution with the aqueous phase. Because lipids are amphiphilic, as the ethanol is diluted (and the polarity increases), the lipids will self-assemble to form LNPs. In higher proportions of aqueous phase to ethanol concentrations, the ethanol is diluted faster, the lipids have less opportunity to aggregate, and hence, this drives the formation of smaller LNPs [132].

The size of different phase ratios was also measured using nanoparticle tracking analysis (Figure 2). This technique allowed for the number of particles to be estimated in each sample (Fig. 2A), showing per 1 mg/mL lipid concentration there were more particles for smaller LNPs and fewer particles of the larger LNPs, which makes sense, due to the same amount of material being present in each sample. All of the samples tested had a similar span of between 0.9-1.1, indicating the same particle size distribution in the formulations tested.

Interestingly, the same number of particles were found in the 1.5:1 and 1.3:1 samples, despite a 20 nm difference in their z-average size, suggesting that this difference in particle size is not solely dependent on the number of lipid molecules within each LNP. Comparing the intensity to frequency plots (Fig. 2B-E) showed a similar size distribution given by both techniques. The smaller particles (2:1 and 3:1, 90 d.nm and 70 d.nm) map (Fig 2. D-E), whereas the larger particles (1.3:1 and 1.5:1, 140 d.nm and 120 d.nm) show a shift in the DLS intensity readings towards higher particle size. This is likely due to larger particles contributing more to the overall intensity in scattered light for DLS measurements, 15,16 resulting in a greater intensity value in the intensity distributions shown. Overall, these data confirm the ability to precisely control LNP size through adjustments in the aqueous to organic phase ratio for both ALC-0315 and SM-102 lipid-containing LNPs, as previously seen with liposomes and LNPs [13, 105, 123, 124, 133].

To further investigate LNPs made at different sizes, the corresponding pKa for these LNPs were measured using the TNS assay (Fig. 3), using a method adapted from [38, 131]. The pKa of LNPs generally fall within the range of 6-7 [48, 134]. Using the Henderson-Hasselbalch equation, this signifies that at pH conditions equal to the pKa the ionisable lipid is 50% protonated, at one pH unit below the pKa 90% protonated, and at two units 99% protonated. This indicates that at a manufacturing pH of 4, the ionisable lipid is almost entirely cationic, and therefore has been used as a reliable manufacturing pH for LNPs in research and commercially [2, 55].

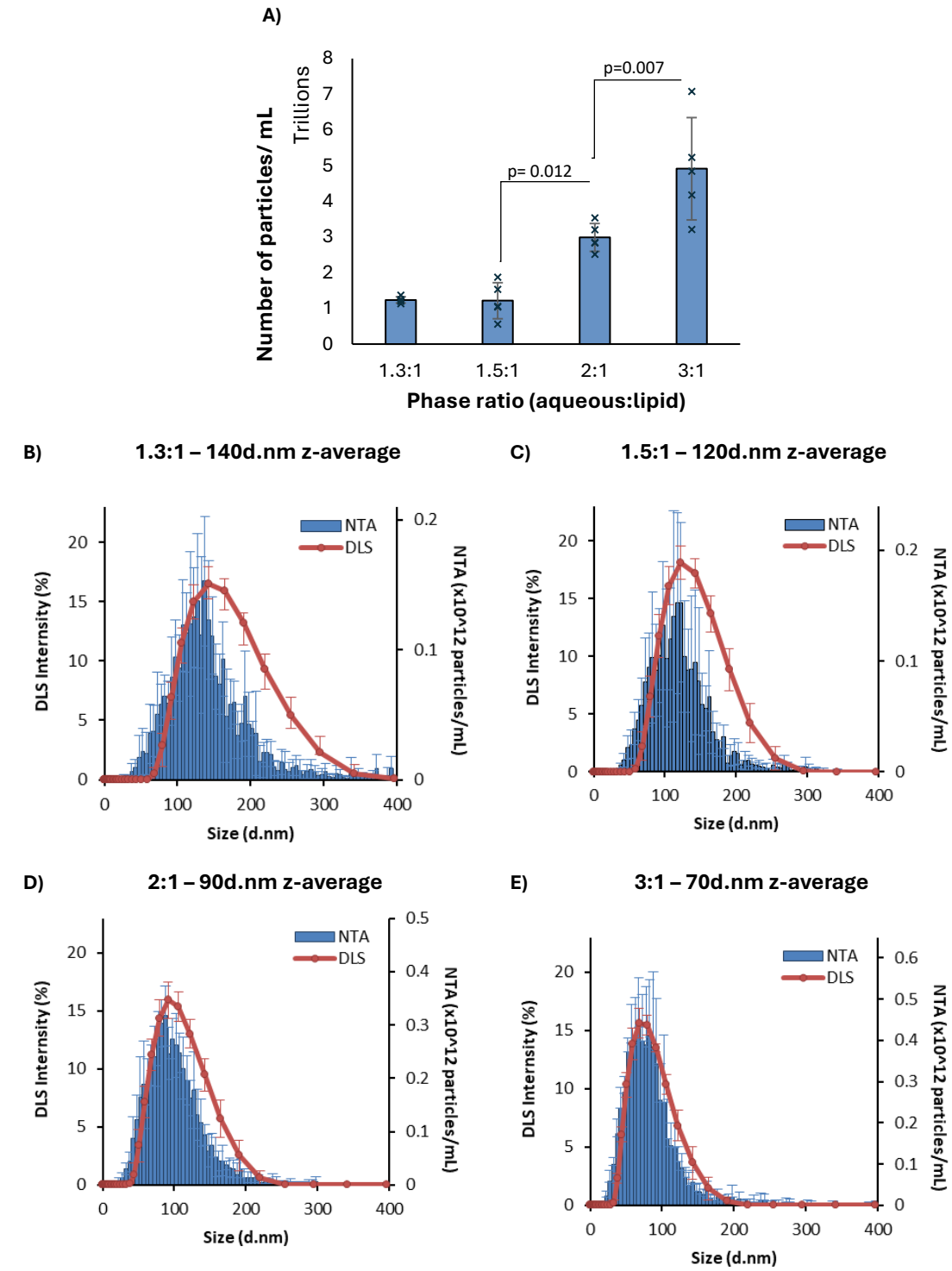

Figure 2: NTA vs DLS data. (A) Number of particles per mL in 1mg/mL LNP formulation. (B-E) NTA Concentration vs DLS Intensity plots at four different aqueous: organic phase ratios. NTA data (blue) and DLS traces (orange). The z-average is the intensity mean given by the DLS for each sample. The LNPs were manufactured with an N/P of 6 from 5 mg/mL lipid stocks and purified by dialysis in pH 7.4 PBS for 1 hour. Each measurement is a mean of three independent batches with error bars showing ±SD. The significance is indicated by (*) between each of the phase ratios analysed by one-way ANOVA with Tukey's pairwise comparisons. NTA= nanoparticle tracking analysis, DLS= dynamic light scattering.

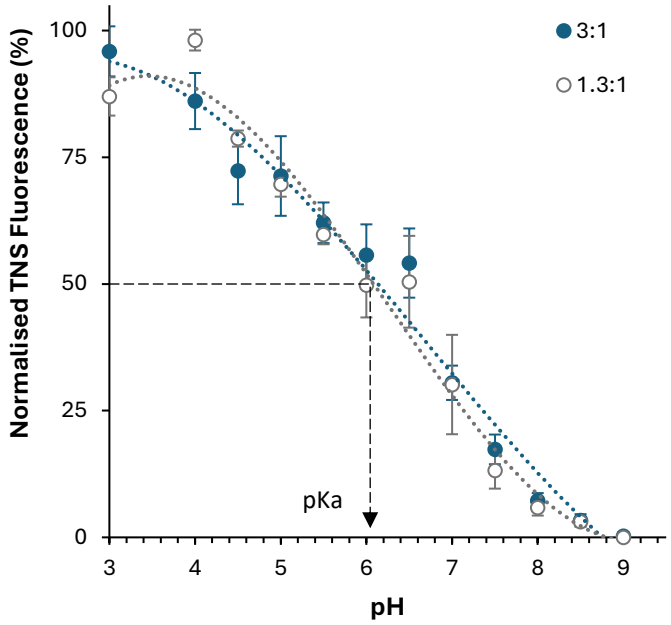

Figure 3: Measuring the pKa of ALC-0315 ionisable lipid LNPs. The normalised fluorescence values of TNS when incubated with ALC-0315 LNPs titrated in buffers over a pH range of 3-9. Citrate buffer was used for pHs 3-6, sodium phosphate buffer was used for pHs 6.5-8, and Tris buffer was used for pH 8.5-9. The readings were normalised per each maximum given for each LNP batch. Each data set is representative of 3 batches of LNPs manufactured at an aqueous:lipid phase ratio of 3:1 (blue closed circles) or 1.3:1 (grey open circles). pKa was found by taking the pH value at 50% of the maximum fluorescence. To fit a sigmoidal curve to the data, polynomial lines of best fit to the order of 3 were used. The LNPs were manufactured at an FRR of 3:1 with an N/P of 6 from 5mg/mL lipid stocks, pH 7.4 PBS was used as the exchange buffer.

The TNS fluorescence is a direct indicator of the % protonation of the ionizable lipid. By taking the pH at which the TNS emits 50% of the maximum fluorescence in the presence of the ALC-0315 LNPs, the pKa can be estimated. For both small (phase ratio= 3:1) and large (phase ratio= 1.3:1) LNPs, the pKa was approximately 6.1, in agreement with prior literature [48, 134] and confirms that the lipid is sufficiently protonated under manufacturing conditions (pH 4) for full mRNA encapsulation.

We also observe that the manufacturing phase ratio and size of the LNP has no impact on the pKa and so this variable should not impact the mRNA encapsulation and expressing potential of the LNPs To examine any potential physical differences between the different-sized LNPs, cryo-TEM was performed to image each phase ratio of LNPs (Figure 4), this presented a similar filled-circular structure for the first three smaller ratios, however at the 1.3:1 double-lamellar LNP were found to be the most-commonly presenting structure.

Cryo-TEM of ALC-0315 LNPs

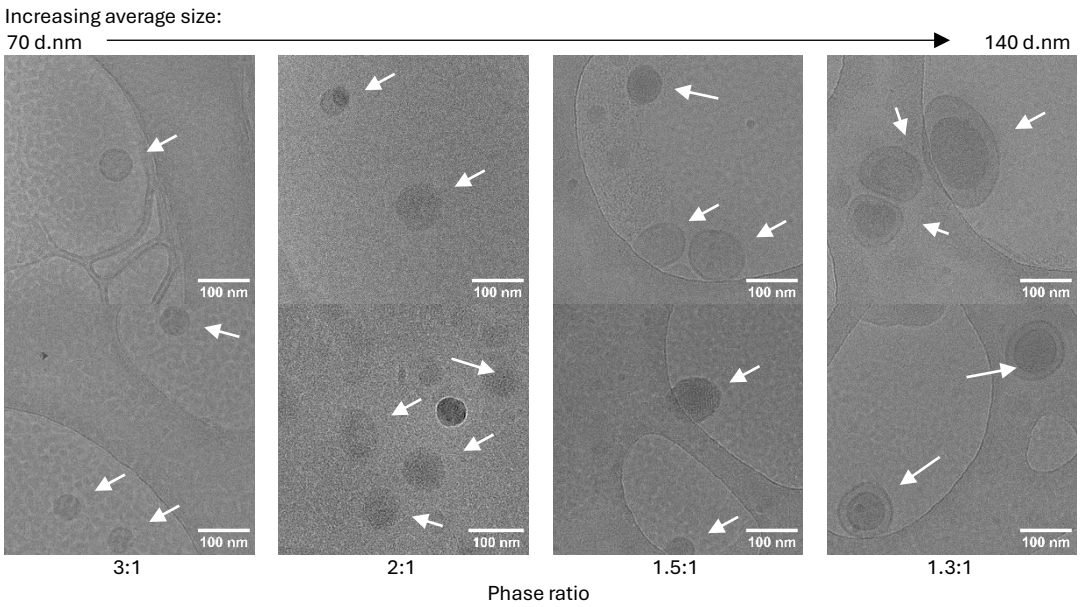

Figure 4: Cryogenic Transmission Electron Microscopy of LNPs with ALC-0315 as the ionisable lipids, manufactured at four different aqueous:lipid phase ratios. There are two images at 30,000 x magnification for each manufacturing phase ratios, LNPs are shown by white arrows. The LNPs were manufactured with an N/P of 6 from 5mg/mL lipid stocks, pH 7.4 PBS was used as the exchange buffer, they were maintained in this buffer at manufacturing concentrations when cryogenically frozen in liquid ethane and imaged in liquid nitrogen using the Jeol JEM-F-200 microscope at 200kV.

This shows that there are structural differences between this size of LNP and smaller LNPs, which are perhaps necessary to form a stable lipid nanoparticle of this size.

Furthermore, as stated, during the formation of these LNPs where the ethanol concentration is higher, there is more opportunity for lipids to aggregate and form larger LNPs. This may result in different morphological structures with the potential for phase separation of the dense mRNA and ionisable lipid core, leaving the other lipids to form extra layers, similar to what has been observed in the formation of bleb-rich LNPs [135]. Furthermore, this double-layer morphology has previously been observed in larger LNPs and liposomes [13, 108].

The impact of aqueous: organic phase ratio and LNP size on *in vitro* and *in vivo* expression

As aqueous: organic phase ratio reliably and reproducibility enabled the control on LNP size, this was then used to infer impact of LNP size on expression, both *in vitro* and *in vivo*. LNPs encapsulating firefly luciferase mRNA were prepared, which when expressed catalyse luciferin into a bioluminescent product. The LNPs were added to HEK293, THP-1 and BMM cells, as three distinct cell lines at four standard concentrations in the 0.25-2 µg/mL test concentration range [136-138].

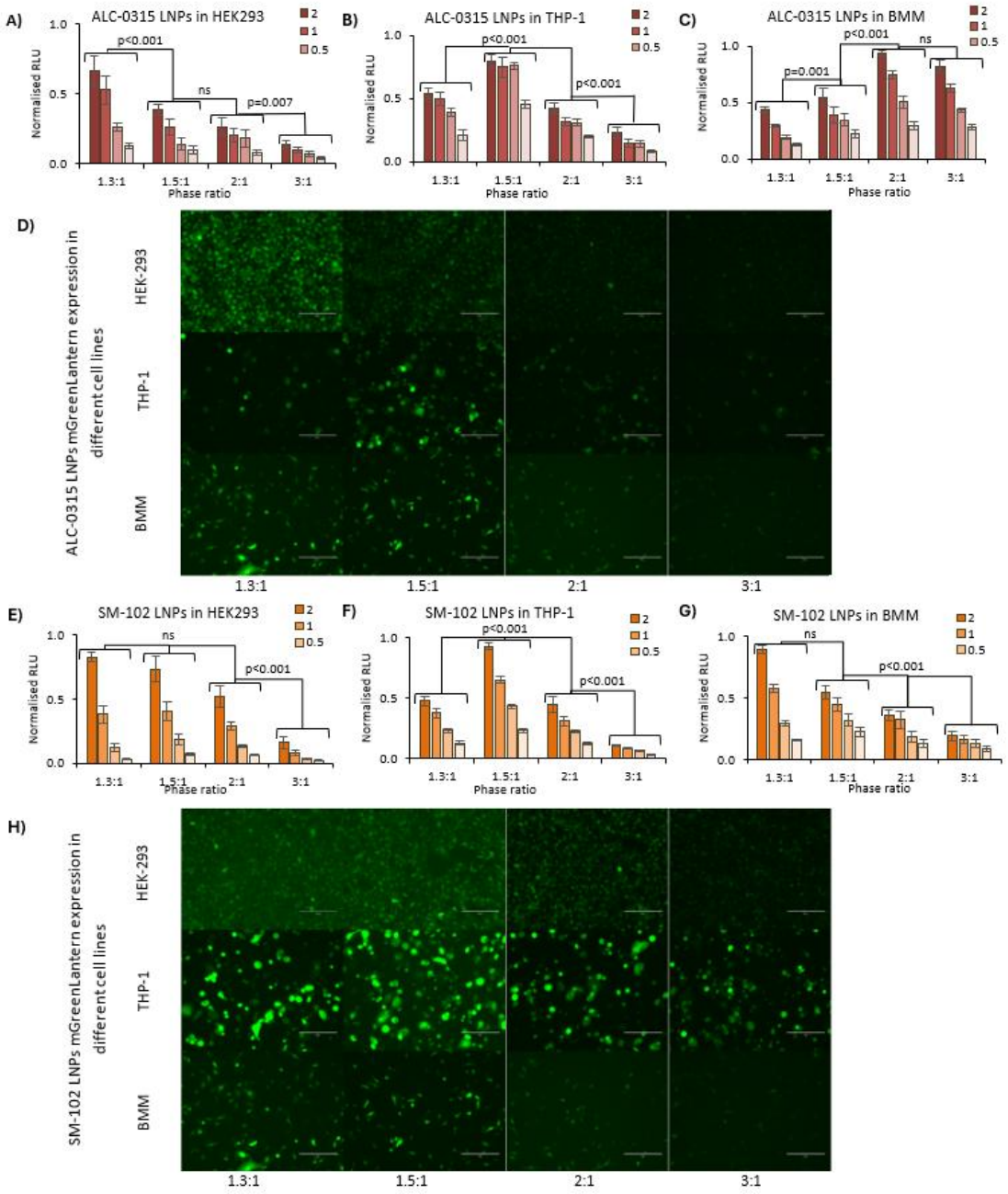

Figure 5: *In vitro* expression of LNPs in HEK-293, THP-1 and BMM (bone marrow-derived macrophages) cells. A-C) FLuc mRNA expression of ALC-0315 LNPs in HEK-293 (A), THP-1 (B) and BMM (C) cells. D) Images showing mGreenLantern expression of ALC-0315 LNPs in HEK-293, THP-1 and BMM cells. E-G) FLuc mRNA expression of SM-102 LNPs in HEK-293 (E), THP-1 (F) and BMM (G) cells. H) Images showing mGreenLantern expression of SM-102 LNPs in HEK-293, THP-1 and BMM cells. For the luciferase expression (A-C, E-F), each formulation was added to the cells at four concentrations of mRNA shown as dark-light coloured bars as the concentration decreases from 2 µg/mL, 1 µg/mL, 0.5 µg/mL to 0.25 µg/mL. The expression is shown as normalised relative light units (RLU), taking the maximum measurement from each plate reading and dividing all the values by this. For the mGreenLantern expression, LNPs were added to the cells at a concentration of 2 µg/mL .The LNPs were manufactured with an N/P of 6 with either Fluc mRNA (A-C, E-G) or mGreenLantern mRNA (D, H) from 5mg/mL lipid stocks and purified by dialysis in pH 7.4 PBS for 1 hour. For the graphs, each measurement is a mean of three independent batches with error bars showing ± SEM. The significance is indicated by p values obtained by two-way ANOVA for individual treatment group comparisons.

We observed that in HEK-293 cells the largest LNPs resulted in a 4 times higher expression than the smallest LNPs (Figure 5A, E), with a pattern of gradually decreasing comparative expression as the phase ratio increases (and size decreases). This was true for both ALC-0315 and SM-102 LNPs adjusted to four different concentrations of mRNA. This same trend of higher expression for larger LNPs versus standard-size LNPs has previously been observed in LNPs manufactured with Dlin-MC3-DMA as the ionizable lipid in NCI-H358 cells [124]. Larger LNPs were more likely to be internalised by cells via macropinocytosis instead of receptor-dependent endocytosis. In addition, larger LNPs are likely to encapsulate a great amount of mRNA per particle, which is supported by our findings (figure 2A), showing fewer particles with larger-sized LNPs, whilst containing the same amount of mRNA within the sample. A reason why fewer particles with higher mRNA content may be more efficient for mRNA delivery and expression than more small particles containing less mRNA may be due to limited cell uptake. Though the uptake of labelled mRNA was found to be the same for each LNP size, expression differences were found to be independent of internalization, perhaps owing to the differing effects of LNP composition and internalisation mechanism on downstream intracellular processes.

In THP-1 cells, a similar pattern was observed, except with slightly lower expression in the 1.3:1 phase ratio samples (Fig. 5B, F), this may be due to less uptake of these larger LNPs into this cell type. For BMM cells, a differing trend was seen between ALC-0315 and SM-102 manufactured LNPs (Fig. 5C, G), the SM-102 samples exhibiting the same preference for larger particles as shown in the other cell lines, but the ALC-0315 data showing an opposite trend. It is unknown as to why the expression pattern is different in this cell line, specifically for one ionisable lipid, where the LNPs manufactured with different ionisable lipids have previously shown the same pattern. This shows that the trend of larger LNPs expressing more is true for most, but not all formulations of LNPs in the tested cell lines.

To visually observe differences in mRNA expression in these three cell lines, LNPs were manufactured with mGreenLantern mRNA for capturing images of this green fluorescent protein when expressed in cells (Fig. 5 D, H), these showed the same expression patterns as the Fluc mRNA LNPs, with the exception being the ALC-0315 LNPs in BMM again (quantified in Figure S1). This is observed in Figure 6E, showing a CT scan and 3D biodistribution and expression of ALC-0315 and SM-102 LNPs. Furthermore, contrary to

most of the *in vitro* results, the largest LNPs had the lowest expression *in vivo* (Figure 6), and the other sizes showed no significant difference in expression, which was found to be variable. These largest LNPs manufactured at a phase ratio of 1.3:1 have a notable different morphology with potentially phase separation of the lipids and this, combined with their larger size could be impacting on *in vivo* performance as a result of different biological interactions and/or stability.

This lack of correlation between *in vitro* and *in vivo* results in respect to LNPs and other nanomedicines is not uncommon [103, 139-141], as there are many different impacting factors *in vivo*, such as the biological milieu interactions[142], immune system interactions[143], circulation and movement to target site amongst others. This presents major challenges in the screening of LNPs and the down-selection from *in vitro* to *in vivo* studies. Furthermore, homogenous cell cultures do not represent the heterogeneity complexity of a living organism, and the different pharmacokinetic barriers, which could impact the stability and potency of different formulations. This indicates major limitations in relying on these *in vitro* models to predict *in vivo* outcomes and highlights the importance *in vivo* testing. However, there is also potential for discrepancies between preclinical trials in murine mammals and clinical outcomes, and therefore additional models are required to better predict clinical outcomes. Typically the optimal size for LNPs is in 50- 100 nm size range depending on the formulation [13, 144], and previous studies have suggested that smaller LNPs may be better indicated for siRNA-based therapies, and larger for those mRNA-based, in conjunction with the molecular sizes of the nucleic acid cargo [124], so it may be that larger sizes can more efficiently pack mRNA, but smaller LNPs are more stable, creating an optimal range for LNP expression.

Our data suggests that LNPs between approx. 60 to 120 d.nm have equivalent mRNA expression after intramuscular injection. This suggests that particle size is a key Critical Quality Attribute and is sensitive to small changes in the microfluidic mixing processes; however, is less influential on potency in small animal studies. Indeed, this has also been shown in mRNA vaccine studies as Hassett et al [13] looked at immune responses in mice and non-human primates, where all tested sizes of SM-102 ionisable lipid LNPs from 60-150 d.nm gave consistent results.

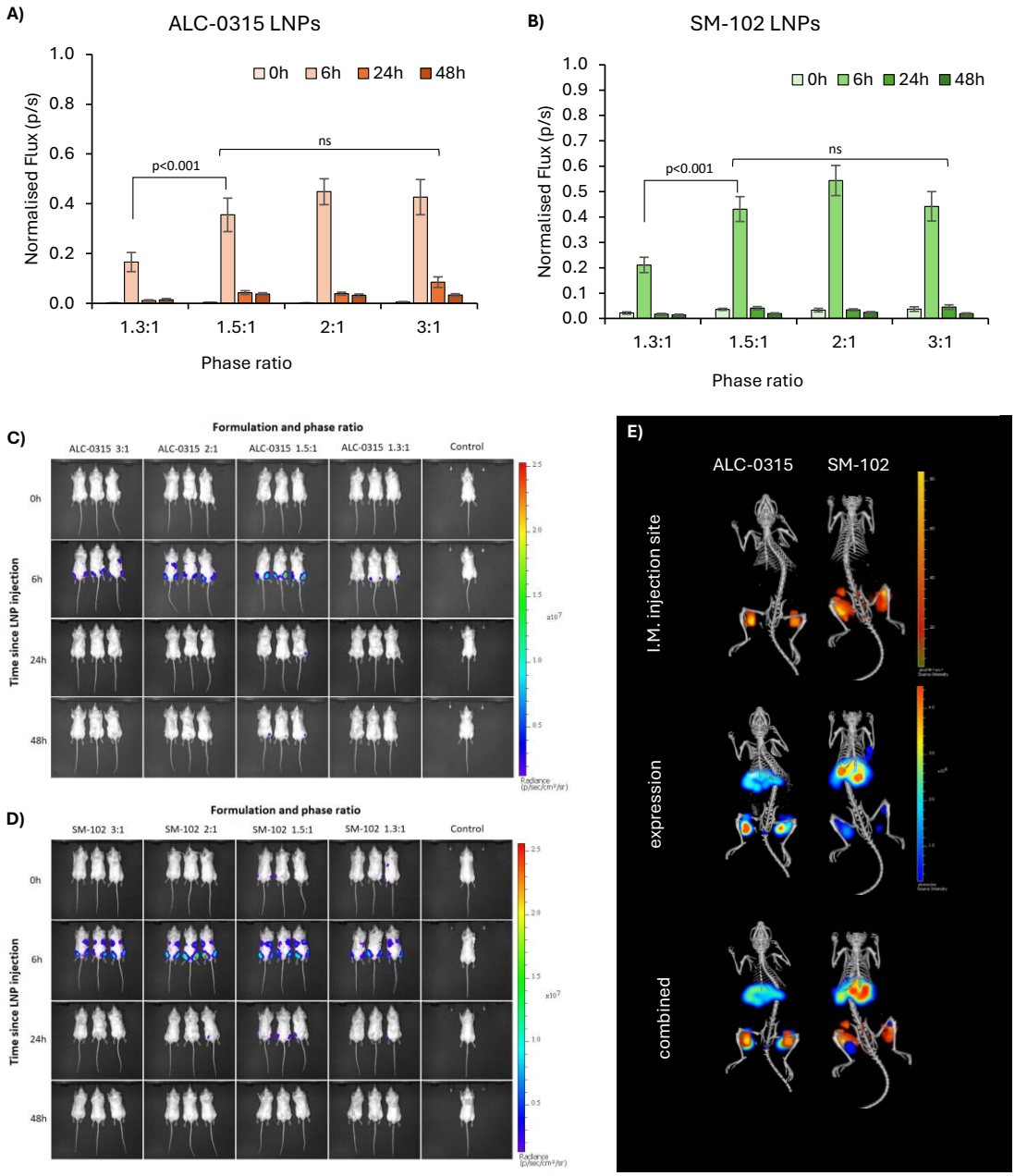

Figure 6: Biodistribution and expression of ALC-0315 and SM-102 LNPs following I.M. injection in BALB/C mice. A-B) Expression is shown as normalised bioluminescence at four time points after injection- 0 (10 minutes), 6, 12 and 24 hours (light to dark bars) in ALC-0315 LNPs (A) and SM-102 LNPs (B). Error bars are representative of SEM. The significance is indicated by (*) between each of the phase ratios analysed by three-way ANOVA with Tukey's pairwise comparisons, and two-way ANOVA for individual treatment group comparisons C) bioluminescence- mRNA expression images in mice injected with ALC-0315 LNPs D) bioluminescence- mRNA expression images in mice injected with SM-102 LNPs E) CT scans of one mouse from each group, showing the 3D expression and intramuscular (injection site) biodistribution of the LNPs. Images C-D are one of 3 repeats, representative of the overall results.

This study supports and further investigates this work, by specifically looking at mRNA expression in *in vitro* and *in vivo* across the same size range in both SM-102 and ALC-0315 LNPs.

Conclusions

In this study, the impact of aqueous: organic buffer phase ratio was evaluated for its ability to alter ALC-0315 and SM-102 formulated LNP critical quality attributes. We observed that the phase ratio correlated with LNP size leading to the manufacture of LNPs with differing sizes ranging from 60-140 nm in diameter to be further evaluated. LNPs over the size of 120 d.nm showed a different morphology to smaller LNPs observed using CryoTEM, with a double lamellar structure being the most common. Particle size is a well-recognised critical quality attribute for LNPs and critical to the quality and efficacy of an LNP product. Generally, LNPs used in the clinic are in the 50-100 nm size range and manufactured at a phase ratio of 3:1. Manufacture of smaller size ranges and larger LNPs can be used to infer a more detailed view on the impact of LNP particle size on expression. Our *in vitro* experiments in three distinct cell lines revealed that larger LNPs usually resulted in higher mRNA expression than smaller sized LNPs. This has been attributed to different uptake mechanisms and the impact of this downstream intracellular processes. However, when tested *in vivo*, this was no longer the case. *In vivo*, we saw the largest LNPs give the lowest expression, and the other sizes were not significantly different from each other.

Here we show that small changes in manufacture will impact LNP particle size, but this does not necessarily translate to changes in their efficacy. Furthermore, the issue regarding the lack of correlation between *in vitro* and *in vivo* results elucidates that although *in vitro* studies are fundamental for assessing toxicity and baseline expression of formulations, *in vivo* studies are crucial when evaluating the efficacy of formulations.

CHAPTER 4: INFLUENCE OF IONISABLE LIPID AND STEROL VARIATIONS ON LIPID NANOPARTICLE PROPERTIES AND PERFORMANCE

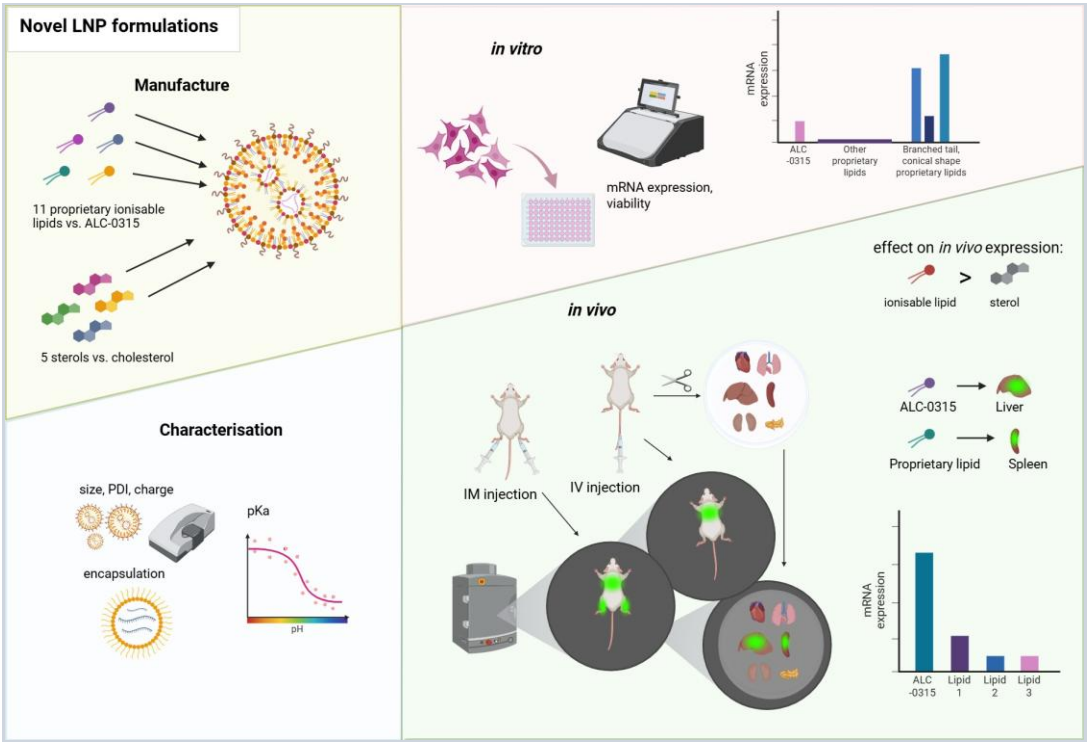

Created with BioRender.com

This Chapter was published as a paper in the Journal of Controlled Release:

McMillan, C., Druschitz, A., Rumbelow, S., Borah, A., Macfarlane, R., Rattray, Z., & Perrie, Y. (2025). Influence of ionisable lipid and sterol variations on lipid nanoparticle properties and performance. *J Control Release*, *386*, 114056. https://doi.org/10.1016/j.jconrel.2025.114056

Abstract

Lipid nanoparticles (LNPs) have emerged as a vital delivery system for nucleic acids, particularly in the context of mRNA vaccines and therapeutics. This study evaluates the impact of various proprietary ionisable lipids on the physicochemical characteristics, encapsulation efficiency, and expression of mRNA within LNP formulations. We compared 11 novel ionisable lipids against the clinically used ALC-0315 in both in vitro and *in vivo* models. Alongside comprehensive physicochemical characterization (including size, zeta potential, and polydispersity index), we uncovered significant variations *in vitro* in formulation performance influenced by lipid structure, where LNPs formulated with cone-shaped ionisable lipids exhibited markedly higher mRNA expression in HeLa cells compared to the control. *In vivo* assessments revealed distinct biodistribution patterns, with ALC-0315 formulations demonstrating preferential delivery to the liver and an alternative ionisable lipid to the spleen, emphasising the role of lipid composition in therapeutic efficacy. Notably, some proprietary LNPs performed well *in vitro* but showed poor *in vivo* expression, especially via IV administration, underscoring the importance of delivery context and offering novel insight into route-independent formulation performance trends. However, the overall performance ranking was consistent across both *in vivo* administration routes, with the best and worst performing formulations maintaining their relative expression profiles. Our findings also indicate that while differences in sterol choice modulate LNP properties, the choice of ionisable lipids is crucial for optimizing mRNA delivery. Furthermore, the study highlights the discrepancies between *in vitro* and *in vivo* results, emphasizing the need for further research into the biological complexities of LNP behaviour. Collectively, this work offers new insight into structure–function relationships within LNP systems and provides valuable formulation strategies for next-generation RNA therapies.

Key words: lipid nanoparticles, LNPs, nanoparticle formulation, ionisable lipids, cationic lipids, sterol substitution, mRNA delivery, biodistribution, *in vitro- in vivo* correlation

Introduction

Lipid nanoparticles (LNPs) are commonly used delivery vehicles for therapeutics and vaccines, with several medically approved formulations and many in clinical development. Specifically, ionisable lipid nanoparticles allow for the delivery of different types of nucleic acid, such as mRNA and siRNA, to their target site *in vivo* to enable the

therapeutic effect. Without such protection, the charged and exposed molecule cannot pass through lipophilic cell membranes and is quickly degraded before it can be expressed at the target site.

LNPs consist of five key structural components. These are a phospholipid, a sterol, a pegylated lipid, a cationic lipid and the nucleic acid payload (e.g. mRNA). In brief, the phospholipids are the key helper lipids, forming the outer membrane of the lipid nanoparticle, helping with cellular uptake and encapsulating the inner content of the LNP. The sterols integrate with phospholipids to improve the structural stability and rigidity of the LNP outer shell. Pegylated lipids help to prevent particle aggregation and improve circulation time *in vivo*. As nucleic acids are anionic and hydrophilic molecules, in order to encapsulate them within a lipophilic LNP, cationic lipids are used to bind to the nucleic acid payload and incorporate within the other lipids in LNP formation. These are often ionisable, such that they are positively charged at a lower pH and neutral at physiological pH. Therefore, the performance of LNPs is highly dependent on these structural components, particularly ionisable lipids and sterols, which are investigated in this study.

Ionisable lipids are the most important component of the LNP in regard to encapsulating the nucleic acid payload. This is due to the electrochemical ability of the positive charges on this lipid to attract the negatively charged phosphate backbone of nucleic acids. Therefore, changing the chemistry of this lipid can have a dramatic impact on the resulting LNP formulation. Cationic lipids have three main structural components: an ionisable head group, aliphatic tail regions, usually consisting of between two and four hydrocarbon chains, and a chemical linker [101]. These structural components are illustrated in Figure 1.

The ionisable lipid headgroup holds a positive charge, either permanently (cationic) or when in an acidic environment (ionisable). Ionisable lipids have triple-bonded amine groups, where the free electron pair on the nitrogen is susceptible to accepting hydrogen ions in more acidic environments, making them positively charged. Cationic lipids contain quaternary amines, which carry a permanent positive charge, therefore these lipids are positively charged in any pH environment.

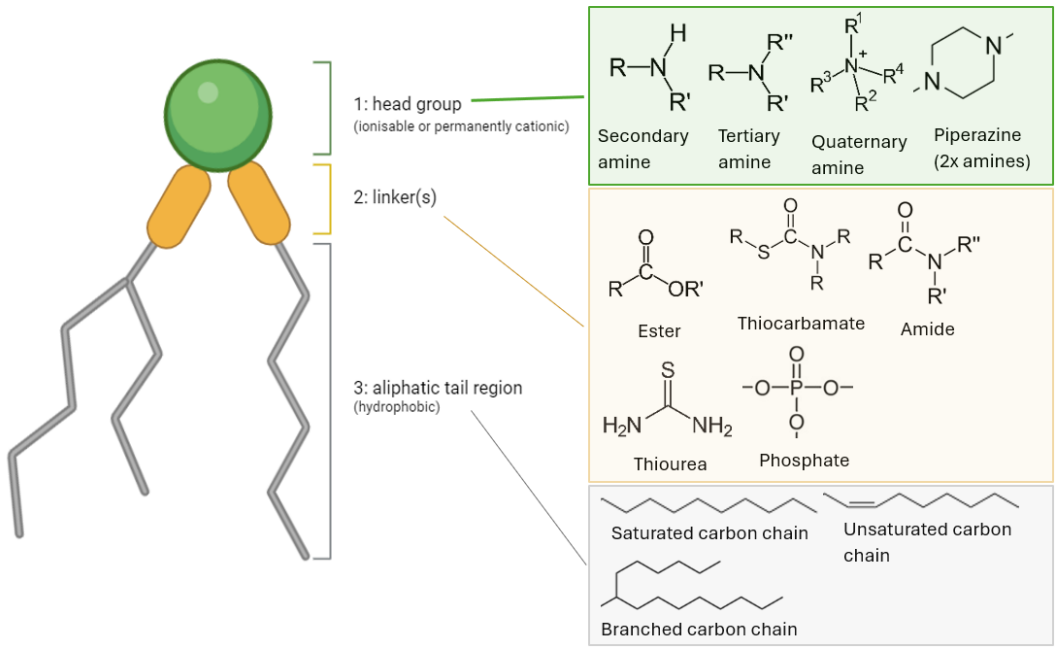

Figure 1: The structural components of ionisable/ cationic lipids utilised to make lipid nanoparticles in this chapter. Based on the diagram from [101], created using Biorender.

The linker structure connects the hydrophilic head group to the hydrophobic tail region and is key in the synthesis of the ionisable lipid in joining these two regions together [145]. This has many important properties in terms of the lipid function *in vivo*, including reducing cytotoxicity [146]. These linkers also need to be chemically stable for storage and circulation stability, whilst being capable of being broken down at target sites for release of nucleic acid cargo [147]. The tail region is important as the lipophilic moiety of the molecule; it allows the lipid to complex with the other lipids within the LNP and therefore affects the stability and the formation ability of the LNP [101]. These can be saturated, unsaturated, and branched aliphatic chains. Unsaturated chains have been shown to increase membrane destabilisation and payload release; similarly branched chains create a cone-shaped structure to the ionisable lipid, which increases membrane disrupting properties due to the non-bilayer conformity of the shape [146, 148].

In addition to ionisable lipids, sterols also affect LNP structure and function. Cholesterol is traditionally used in LNPs; however, it has also been shown that using different sterols in place of cholesterol can create functional LNPs with varying impacts, both in morphology and mRNA delivery [59]. Alternative sterols such as β-Sitosterol, Campesterol and Stigmasterol have been shown to modify LNP morphology and gene expression efficiency [58, 59]. While previous studies have demonstrated enhanced

efficacy with certain sterol modifications [149, 150], the extent to which these alternatives influence LNP performance *in vivo* remains unclear, with β-Sitosterol being the only alternative sterol tested *in vivo*, where it increased mRNA expression in comparison to the cholesterol LNPs [151, 152].

This study aimed to evaluate whether altering the lipid composition of LNPs, specifically the ionisable lipid and sterol, impacts their *in vitro* and *in vivo* performance. By examining physicochemical attributes such as particle size and mRNA encapsulation in novel LNP formulations, we sought to understand how differing proprietary ionisable lipids and sterol alternatives influence LNP structure and expression, with the goal of optimizing LNP-based drug delivery systems.

Materials and Methods

Materials

The following were provided by Avanti Polar Lipids (Alabaster, AL, USA): 1,2-distearoyl-sn-glycero-3-phosphocholine (DSPC), 1,2-dimyristoyl-rac-glycero-3-methoxypolyethylene glycol-2000 (DMG-PEG 2000), 2-[(polyethylene glycol)-2000]-N,N-ditetradecylacetamide, 1,2-Distearoyl-sn-glycero-3-phosphocholine (ALC-0159), Cholesterol, β-Sitosterol, Campesterol, Lanosterol, Stigmasterol, Delta 5-avenasterol, [(4-Hydroxybutyl)azanediyl]di(hexane-6,1-diyl) bis(2-hexyldecanoate) (ALC-0315) and all of the other proprietary ionisable lipids.

EZ Cap™ Firefly Luciferase mRNA was purchased from ApexBio Technology (Houston, TX, USA). Citric acid, sodium citrate tribasic dehydrate, polyadenylic acid (PolyA), 6-(p-Toluidino)-2-naphthalenesulfonic acid sodium salt, Sodium phosphate monobasic (NaH2PO4•H2O), Sodium phosphate dibasic (anhydrous)(Na2HPO4) and 25 mm dialysis membrane (MWCO 12,000–14,000 Da) were acquired from Sigma-Aldrich (St. Louis, MO, USA). Phosphate-buffered saline tablets (PBS pH 7.4) were acquired from Oxoid Ltd. (Basingstoke, UK). Tris Base and Ethanol (EtOH) were obtained from Fisher Scientific (Loughborough, UK). Minimum Essential Medium, Trypsin-EDTA (0.05%), PBS, pH 7.4 solution and Quant-it™ RiboGreen RNA Assay Kit and RiboGreen RNA Reagent, RediPlate™ 96 RiboGreen™ RNA Quantitation Kit were purchased from Fisher Scientific UK Limited (Renfrew, UK). ONE-Glo™ Luciferase Assay System and VivoGlo™ Luciferin (*In Vivo* Grade) were acquired from Promega UK (Southampton, UK). BD Insulin Syringes

were purchased from Scientific Laboratory Supplies Limited (Nottingham, UK) All solvents and other chemicals were of analytical grade, and milliQ-water was provided by an in-house system.

Aqueous and Organic phase preparation

The aqueous phase containing mRNA and the organic (lipid) phase were prepared separately before microfluidics. The aqueous phase was prepared using 50 mM citrate buffer (pH 4), dissolving PolyA as an mRNA surrogate, or Firefly Luciferase (Fluc) mRNA for *in vitro* and *in vivo* experiments, at mRNA concentrations required to maintain a nitrogen to phosphate (N/P) ratio of 6, the molar ratio of ionisable lipid containing positively-charged amines (N) to the mRNA containing negatively-charged phosphates (P). Therefore, the concentrations were adjusted for different aqueous: organic phase ratios and when different lipids or mRNA were used, to maintain this N/P ratio.

The lipid molar ratio of the LNPs was 10:38.5:50:1.5% structural lipid: sterol: cationic lipid: PEGylated lipid. This led to the following lipid combinations utilised in the experiments: DSPC as the structural lipid; one of six different sterols- cholesterol, β-sitosterol, campesterol, lanosterol, stigmasterol or delta-5-avenasterol; one of twelve different cationic lipids- ALC-0315 or a proprietary lipid; and DMG-PEG 2000 or ALC-0159 as the PEGylated lipid. The lipid stocks were prepared and stored at concentrations of 5-100 mg/mL, dissolving each lipid in ethanol. The organic phase injected into the microfluidic device had a concentration of 5 mg/mL.

Manufacture of the LNPs using microfluidics

The NanoAssemblr benchtop (Precision Nanosystems Inc., Vancouver, Canada, now under Cytiva, Massachusetts, USA) was used in all experiments in this chapter. The ethanol-based organic phase and the citrate buffer-based aqueous phase containing mRNA in the form of PolyA or Fluc mRNA were fed through syringes into a microfluidics chip with a herringbone mixer design. The phase ratio or flow rate ratio (aqueous: organic phase) was set to 3:1 and total flow rate at 20mL/min.

Purification

Due to a mix of permanently cationic and ionisable lipid cargos and previous observations that permanently cationic particles can get caught in filtration membranes, the LNPs were purified by dialysis buffer exchange, the LNP sample in the

original ethanol/citrate buffer was exchanged into 200 mL PBS (pH 7.4) for every mL of sample. Samples were dialysed for 4 hours, after which the pH becomes neutral and ethanol content is negligible (<1%).

Measuring Critical Quality Attributes (CQAs)

Physicochemical properties

Size (Z-average diameter), polydispersity index (PDI) and zeta potential were measured using the Malvern Panalytical Zetasizer ZS and Zetasizer Ultra, using the Zetasizer software for data acquisition. Size and PDI were measured *via* dynamic light scattering (DLS), using a measurement angle of 173° backscatter, and zeta potential was measured using voltage measurements in a Folded Capillary cell. Each of these measurements were performed in triplicate for each experimental repeat (nine measurements for each experiment). Post-purification, each sample was prepared for measurement at a lipid concentration of 0.1mg/mL in PBS (for size/PDI) or deionised water (for zeta potential) to achieve attenuation values between 7 and 8. Pre-purification measurements for size and PDI were performed with citrate buffer as the diluent. ZEN0040 disposable micro-cuvettes were used for size and polydispersity, and DTS1070 folded capillary zeta cells were used for zeta potential measurements, adding 400 µL and 1,000 µL of diluted LNPs, respectively. The material refractive index and absorption were 1.45 and 0.001, respectively. The dispersant refractive index and absorption were 1.33 and 0.8872 cP, respectively, for water, 1.335 and 1.02 cP, respectively for PBS, and 1.47 and 1.28 cP for citrate buffer.

mRNA content

Encapsulation efficiency and mRNA recovery were measured using the RiboGreen™ mRNA quantification assay kit according to manufacturer recommendations. Tris-EDTA (TE) buffer was used as the diluent in all steps of this assay. The fluorescent dye was used to quantify mRNA in the presence and absence of 2% Triton, for lysis of the LNPs. Two RNA standard curves were used to quantify mRNA. The fluorescence signal was read using the POLARstar Omega (BMG Labtech, UK) and GloMax (Promega, UK) plate readers using 475-485 nm excitation and 525 nm emission wavelengths. The total RNA for each sample from the Triton wells and free (unentrapped) RNA from the TE-only wells were obtained when analysing the results. The mRNA encapsulation efficiency (EE%) and recovery were calculated as previously described [153].

In vitro expression and viability

LNP FLuc mRNA expression was analysed in HeLa cells using firefly luciferase as a bioluminescent reporter. Cells were cultured in Dulbecco's Modified Eagle Medium (DMEM) with sodium pyruvate, supplemented with 10% foetal bovine serum (FBS), 1% penicillin/streptomycin and L-glutamine. Cells were added to a 96-well white/clear bottom plate, at a concentration of 10,000 cells/ 100µL in media and cultured for 48 hours, after which LNPs were added. LNPs were formulated as previously stated in this methods section, with EZ Cap™ Firefly Luciferase mRNA as the internal RNA. LNP formulations were added to the cells, replacing growth media, and diluted in media at total mRNA concentrations of 1 µg/mL and 0.5 µg/mL, in triplicate and control wells with cells only. Cells were incubated with LNPs for 24 hours prior to addition of the luciferase reagent. Luciferase reagent, prepared as per the manufacturer's instructions, was added to each well of the 100 µL of media and cells containing LNPs from the previous day, creating a total volume of 200 µL, mixed thoroughly and left to incubate for 3 minutes. The luminescence of the plates was read using the GloMax plate reader (Promega, UK). To assess cell viability independently of mRNA expression, LNP-treated wells were incubated for 24 hours alongside two control groups: healthy cell-only control wells and toxic control wells, the latter prepared by adding 100 µL of 1% Triton X-100 prior to incubation. After the 24-hour incubation period, 10 µL of Alamar Blue was added to each well, followed by a 4-hour incubation. Fluorescence intensity was then measured using a GloMax plate reader with an excitation wavelength of 520 nm and an emission range of 580–640 nm. Viability was calculated by subtracting the average fluorescence of the toxic control from each LNP-treated well and expressing the result as a percentage of the average signal from the healthy control wells.

In vivo expression

LNP expression was analysed in BALB/c mice using firefly luciferase as a bioluminescent reporter. Three BALB/c mice per formulation were injected intramuscularly (IM) and intravenously (IV) with each formulation with 50 µL in each quadricep (x2 =100 µL total) or lateral tail vein. respectively of 40 µg/mL LNPs (mRNA concentration), resulting in a 2 µg IV dose and 4 µg total IM dose (2 µg per leg). The mice were anaesthetised and maintained under anaesthesia using isoflurane before imaging using the IVIS® Spectrum and the associated Living Image® software (PerkinElmer, Buckinghamshire, UK). For the Fluc mRNA expression, the mice were firstly injected

subcutaneously (SC) with 30 mg/mL D-luciferin solution (5 µL per gram of body weight, corresponding to 150 mg/kg). This SC injection was repeated at each imaging time point, and these mice were imaged 10 minutes after injection using the luminescence setting on the software. For the I.M. study, the whole mice were imaged 6h and 24h after injection, taking and quantifying bioluminescence from the injection site (legs) and the upper abdomen (liver). For the I.V. study, the mice were imaged whole at 6h and immediately culled using a schedule 1 method, then dissected where the following individual organs were imaged on a petri dish: the heart, lungs, liver, spleen, kidneys and pancreas, taking bioluminescence readings from each of these sites.

pKa determination

The effective pKa of the ionisable lipid ALC-0315 within the formulation was determined using 6-(*p*-Toluidino)-2-naphthalenesulfonic acid (TNS) as a fluorescent marker for positively-charged particles, adapted from Tanaka *et al* method [131]. LNPs were titrated in buffers from pH 3-10, and the pH at which 50% of the maximum fluorescence signal was determined as the pKa. LNPs were manufactured as previously and diluted to a concentration of 0.5 mM total lipid. Buffers of pH 3-10 were prepared at a concentration of 20 mM. Citrate buffer was used for pH 3-6, sodium dihydrogen phosphate buffer was used for pH 6.5-8, and tris buffer was used for pH 8.5-10. TNS was prepared by dissolving 6-(*p*-Toluidino)-2-naphthalenesulfonic acid sodium salt in water, to a concentration of 0.6 mM. 186 µL of each pH buffer, 12 µL of LNP solutions and 2µL TNS solution were added to the appropriate wells. The fluorescence of TNS was measured using a POLARstar Omega plate reader at 355 excitation and 460 emission wavelengths.

Statistical analysis

The mean and standard deviation were calculated for all experiments, performed in independent triplicate batches unless otherwise stated, each batch was manufactured on a different day, to account for inter-day variation. For hydrodynamic size, polydispersity, zeta potential and pKa, three measurements were taken for each batch, therefore these groups for statistical analysis were n=9. For statistical comparison of groups, Kruskal-Wallis with Dunn's post hoc test was performed for the non-parametric data sets. On graphs, the statistical significance is indicated by individual p values for $p<0.05$, whereas (ns) denotes no statistical significance.

Results and Discussion

This study involved assessing 11 proprietary cationic/ionisable lipids used to manufacture LNPs in comparison to ALC-0315 as a clinically used positive control. This was reduced from an original set of 13 proprietary lipids, from which lipids 8 and 9 were eliminated due to dissolution difficulties. Therefore, the lipids were labelled 1-14, excluding 8 and 9, and ALC-0315 was referred to as lipid 1. The structures and the structural components of these ionisable lipids are shown in Table S1.

The headgroup structures included secondary and tertiary amines, as well as quaternary amines (lipids with these are permanently cationic) and piperazine moieties, which have two ionisable nitrogen atoms. The ionisable lipids in LNPs used clinically- ALC-0315, SM-102 and DLin-MC3-DMA, all have tertiary amine headgroups, which positively ionise at low pHs. As secondary and tertiary amines are both triple-bonded nitrogen atoms, the key differences are likely to arise from the functional groups to which they are bonded. For quaternary amines, due to being permanently cationic, these may be better at encapsulating and storing the mRNA, potentially increasing the expression of LNPs and slowing mRNA degradation in storage and *in vivo*, however, these are likely to have a higher toxicity due to this permanent charge [2]. Piperazine-based ionisable lipids in LNPs have been shown to preferentially deliver mRNA to immune cells without targeting off-target ligands such as antibodies, peptides and aptamers [154], and also prolong stability when stored at refrigerated temperatures [155].

The linker groups include esters, thiocarbamate, amides, thiourea and phosphate groups. Similar to the head group, all the clinically used formulations containing ALC-0315, SM-102 and DLin-MC3-DMA have ester linker groups, as do most of the proprietary lipid formulations here. The ester linker has shown to be effective in the synthesis and *in vivo* performance of LNPs, and is also biodegradable, which leads to fewer toxic effects as the ionisable lipids can be quickly metabolised [145, 156]. Similarly, amides and phosphates are readily cleaved by endogenous enzymes and so are a viable option [156]. Thiocarbamates (and carbamates) are stable molecules at neutral pH, such as within the bloodstream and susceptible to cleavage at lower pHs, such as in late-stage endosomes, where the LNP has released its payload [145]. The thiourea group can act as a secondary head group, and has been previously used instead of a cationic/ionisable head group in non-cationic LNPs, as it can bond to the phosphate backbone of nucleic

acids through hydrogen bonds [157]. Furthermore, the thiourea group can be used in conjunction to the ionisable tertiary amine in an ionisable lipid, such as in lipid 4, where this addition has previously been shown to boost the mRNA expression of these LNPs [158]. Additionally, this shares the same pH sensitive aspect to thiocarbamates, so this may boost the LNP *in vivo* activity further [159]. The tail groups are aliphatic carbon tails, which were in multiple numbers, branched and saturated or unsaturated as previously described.

Five sterol alternatives were also tested and compared to cholesterol as a standard; these are β-Sitosterol, Campesterol, Lanosterol, Stigmasterol and Delta-5-avenasterol (Table S2). All of these, except Lanosterol, are derived from plants and are steroids that differ from cholesterol by alkyl substitution at C24 in the tail region of the molecule. Lanosterol is found in animals and fungi, where it serves as a key precursor in the biosynthesis of cholesterol and other sterols, with extra methyl groups attached to the hydrocarbon rings. It has been found previously that substituting in these derivatives leads to LNP structural differences, where standard LNPs are spherical with one outer lipid layer, to instead be polyhedral shape for β-Sitosterol and Stigmasterol, and induces multilamellar structures particularly with Campesterol [58, 59]. These have also been shown to enhance gene expression in various cell lines [58, 59, 150, 160]. With β-Sitosterol, which has been the most researched alternative to cholesterol, many more studies have supported the higher efficacy of LNPs manufactured with β-Sitosterol in cells [161-163] and a number of studies *in vivo* in BALB/c mice administered by intramuscular injection and inhalation, again showing the higher expression in these LNPs [151, 152]. These observations have been suggested to occur due to LNPs being better able to escape endosomal entrapment when in the cytosol [149], however, when this was directly assessed it was found that endosomal escape did not differ between formulations [161]. At the time of this manuscript, neither lanosterol nor delta-5-avenasterol had been incorporated in ionisable lipid nanoparticles, and Campesterol and stigmasterol had not yet been assessed *in vivo*.

Despite being able to characterise and predict the behaviour of individual lipid moieties, it is challenging in practice to predict how these lipids will behave in differing combinations as molecules and within LNPs. Therefore, the experiments in this chapter

provide insight of these molecular combinations and function in practice within LNP formulations.

Prior to any functionality studies, the physicochemical attributes of the LNPs made with each of the different ionisable lipids were measured and compared at the time of manufacture and after five weeks to assess stability (Figure 2).

Aside from changing the ionisable lipid, these formulations were identical, with the same molar ratio of lipids as previously described (10:38.5:50:1.5% of DSPC: Chol: ionisable: DMG-PEG). Whilst the zeta potential remained approximately neutral for each formulation, with a range of means from -3 mV to +5 mV, there was a large observed variation in LNP size (Figure 2A). The polydispersities of a few of these LNP formulations were also slightly higher than the traditionally accepted value of 0.2, indicating mild heterogeneity of particle sizes [41, 164]. The largest LNPs were consistently those manufactured with Lipid 10 (9:1 HPPPG), at ~ 173 d.nm. Lipids 5, 6, 7 and 14 were both consistently the smallest in size and had the lowest mRNA encapsulation (Fig. 2B).

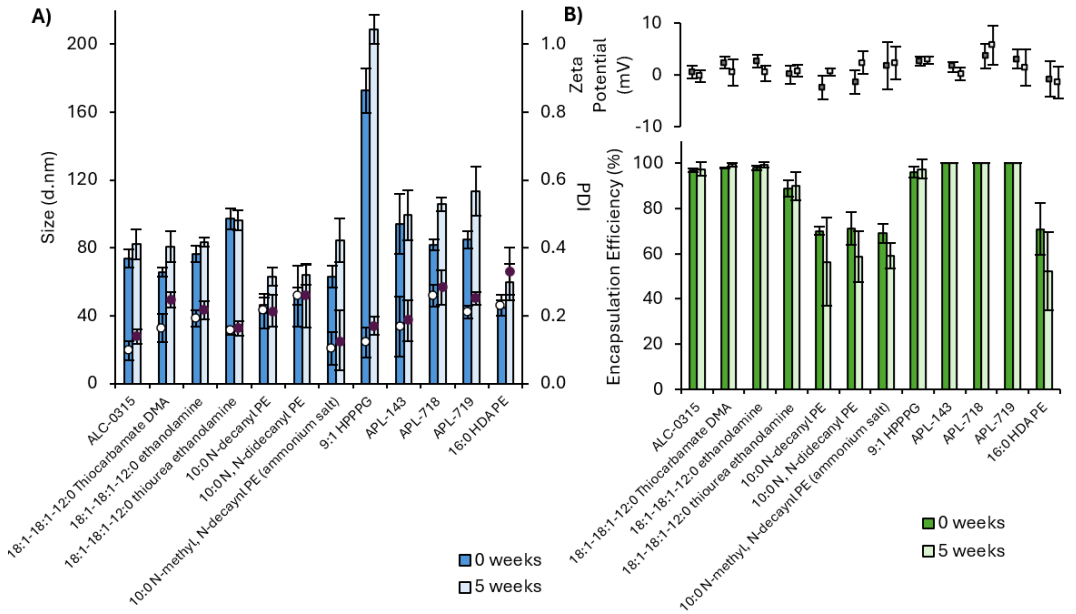

Figure 2: The effect of proprietary ionisable lipid composition on physicochemical attributes of lipid nanoparticles at 0 weeks and 5 weeks after manufacture. A) The size and polydispersity (PDI) of 12 lipid nanoparticle batches, each with a different ionisable lipid, immediately and 5 weeks after manufacture. (B) The zeta potentials of the 12 batches. The mRNA encapsulation efficiency (EE%) of the lipid nanoparticles batches. The sizes and EE% are shown as columns, and the polydispersity indices (PDI) and zeta potentials are shown as points. The LNPs were manufactured with an N/P of 6 from 5mg/mL lipid stocks and purified by dialysis in pH 7.4 PBS. Each measurement is a mean of three independent batches with error bars showing ±SD.

This is undoubtedly related, potentially due to the lack of ionisable lipid within the centre of the LNP to encapsulate the mRNA, or simply due to the lack of mRNA itself reducing the mass of the LNP [93, 94]. Otherwise, the formulations had similar physicochemical critical quality attributes to the control LNPs made with ALC-0315, with sizes from 70-100 d.nm and high mRNA recovery (>90%). After 5 weeks, there were only minor changes in a few of the formulations. The zeta potentials remained the same, and the size only increased slightly in some of the larger formulations (Figure 2A). As for the mRNA recovery, this reduced slightly for the smaller-sized LNP formulations, which had lower encapsulation and mass balance (Figure 2B). Additionally, the variation in samples also increased over time for these measurements, suggesting that for some formulations, some of the batches were more stable than others.

A unique property of the ionisable lipids is that, as weak bases, they can accept protons in acidic environments to attain a positive charge and complex with and therefore encapsulate the mRNA within the LNP. The pH values at which these lipids become positively charged can be obtained by measuring the surface pKa of the LNPs made with each ionisable lipid. The TNS assay was used as previously [153] to measure ionisation of the LNPs, as TNS fluorescence intensity is directly proportional to the amount of positive charge (Figure 3). For ionisable lipids in a range of pH solutions, this forms a sigmoid curve, from which the pKa is found to be the pH value which gives 50% of the maximum fluorescence and is therefore 50% protonated. LNPs used clinically have a pKa between 6 and 7 [43], which allows for >99% protonation in a manufacturing buffer of pH 4. The proprietary lipid LNPs were measured against previously assessed ALC-0315 LNPs, with a given pKa of 6.09. The proprietary lipid LNPs pKa values ranged from 5.75 to 7.43. For the permanently cationic lipids APL-718 and APL-719, pKa was unable to be obtained as the LNPs stay mostly protonated in all pH solutions. Lipid 14- 16:0 HDA PE had both positive and negative charge (zwitterionic) and subsequently gave a curve that levelled out at 25% of the maximum fluorescence; this profile hindered accurate determination of its pKa using the TNS assay, as the standard sigmoidal fluorescence-pH relationship was not observed.

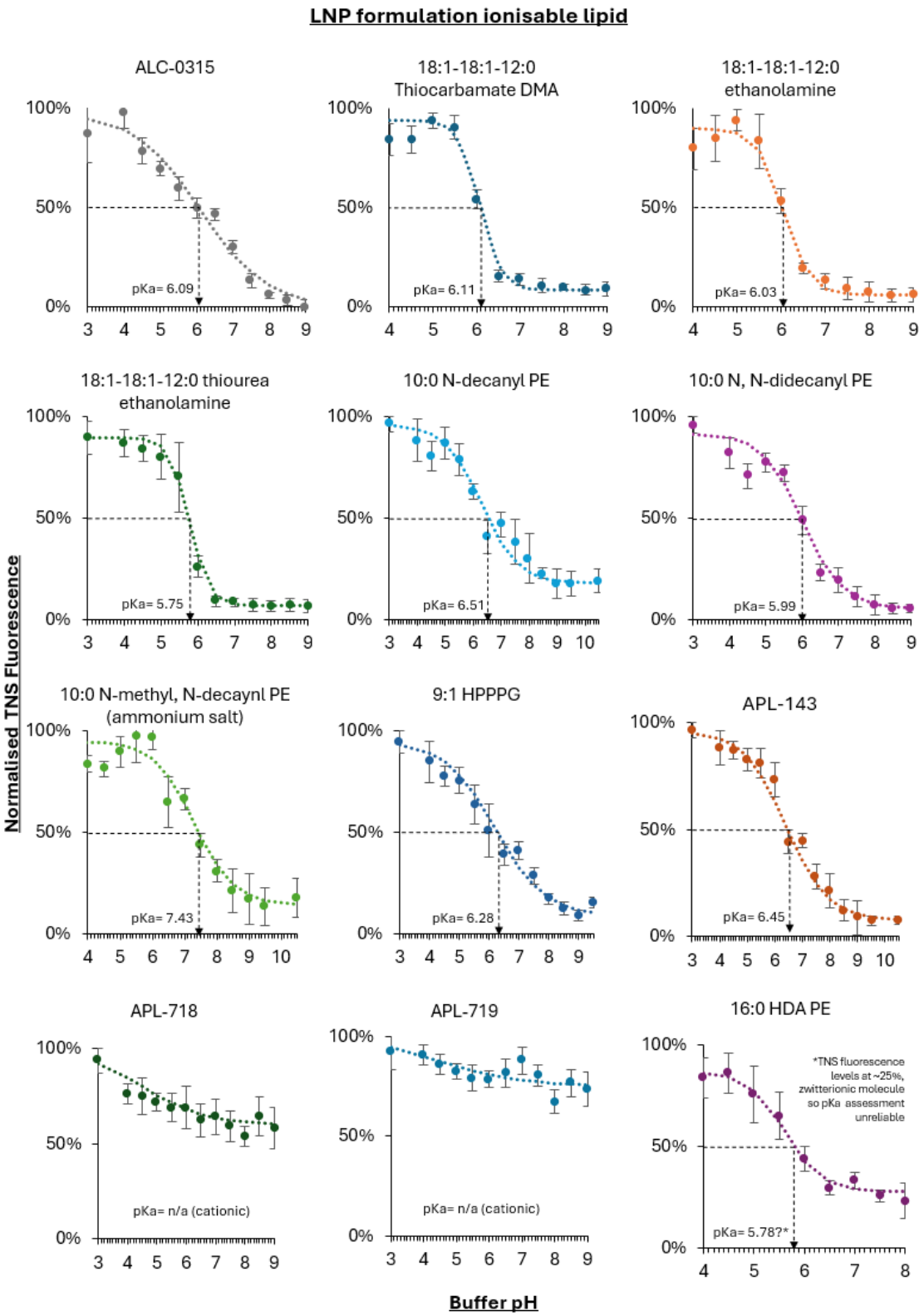

Figure 3: Measuring the pK_a of the proprietary ionisable lipid LNPs. The normalised fluorescence values of TNS when incubated with LNPs titrated in the following buffers over a pH range of 3–10.5 Citrate buffer (pH 3–6) sodium phosphate buffer (pH 6.5–8) and Tris buffer (≥ pH 8.5). The readings were normalised per each maximum value for each LNP batch. Each data set is representative of 3-4 batches of LNPs. The pK_a value was found by fitting a sigmoidal curve to the data and taking the pH value at 50% of the maximum fluorescence.

These variations in pKa could impact LNP behaviour, namely mRNA encapsulation, endosomal escape efficiency, and so potentially mRNA expression *in vitro* and *in vivo* [43, 134].

To test the implications of these different CQAs on the *in vitro* performance of the LNPs, mRNA expression was measured in HeLa cells (Figure 4). These were formulated with the two PEG lipids in clinical use- DMG-PEG and ALC-0159 and confirmed that changing the PEG lipid had little to no impact on the LNP CQAs (Table S3). As these proprietary lipids had not been tested for cell viability previously, this was also measured using resazurin to evaluate the change in cell viability after the addition of LNPs (Figure S1). This showed that none of the LNP formulations impacted cell viability across the concentration range tested. As for the LNP expression, those formulated with lipids 11-13 expressed the most, and significantly higher than the ALC-0315 control, which exhibited low expression, as previously seen with these formulation parameters (aqueous to lipid phase ratio of 3:1 and size of ~70 d.nm) [153]. Out of the three highest performing proprietary lipids, APL-143 (lipid 11) and APL-719 (lipid 13) expressed the highest compared to APL-718 (lipid 12) and ALC-0315.

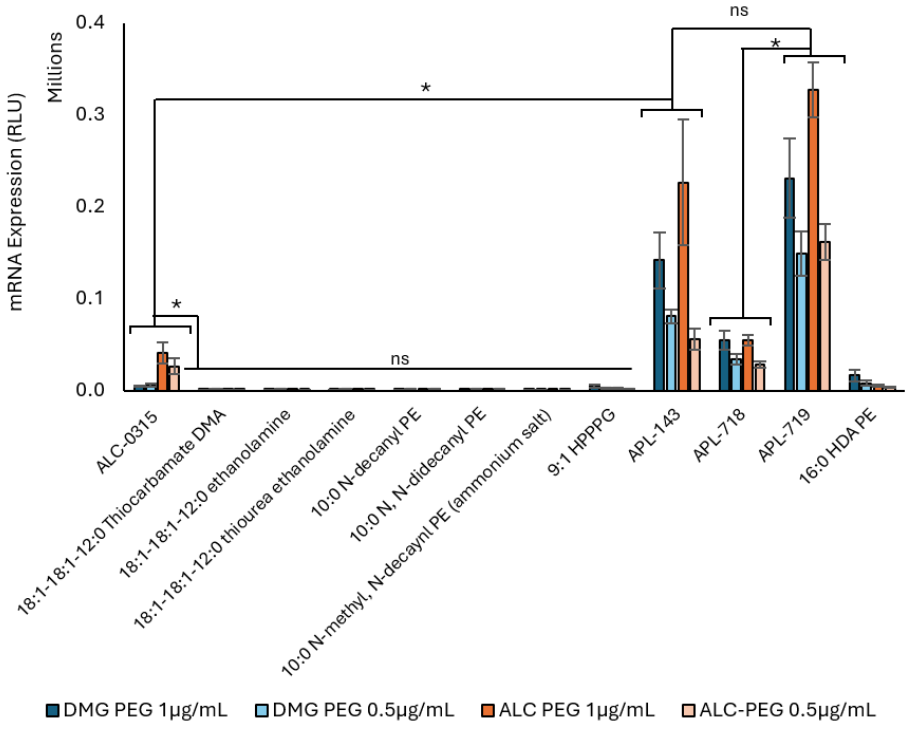

Figure 4: The Fluc mRNA expression of proprietary ionisable lipid LNPs in HeLa cells dosed with either 1µg/mL or 0.5 µg/mL total mRNA. The LNPs were manufactured with an N/P of 6 from 5mg/mL lipid stocks and purified by dialysis in pH 7.4 PBS. Each measurement is a mean of three independent batches with error bars showing ±SD.

Each of the structures of the lipids which performed well *in vitro* had multiple tails and branching, making the lipids more cone-shaped compared to others, which has previously been shown to aid the expression of LNPs through enhanced membrane disruption when inside the cell [41, 43]. Lipids 12 and 13 were also permanently cationic and so may have better electrostatic attraction in enhancing the stability of the LNP *in vitro*, or potentially more disruptive properties in the endosome (where the pH is low) of the cell due to this more positive charge. These also have a phosphate group, which is more likely to carry a negative charge at physiological pH and so may act in reducing the toxicity of the lipid through neutralising the overall charge. Lipid 11 has a piperazine moiety as its head region, which may be more effective than the tertiary amines seen in other lipids for expression, due to its efficient targeting properties [154, 155]. Additionally, each of these lipids have multiple ester linkers which have shown to be very effective linkers, particularly in their biodegradability [145]. These are just speculations as to why these LNPs have performed the best out of those tested, however, it may also be due to other properties of these lipids.

To investigate whether substituting cholesterol for a different sterol increased the cellular expression of any of these LNPs, in line with our previous observations with β-sitosterol in ALC-0315 LNPs (Hussain et al., unpublished data), LNP samples were formulated once with each of the ionisable lipids and each of the sterol alternatives- β-sitosterol, campesterol, lanosterol, stigmasterol and delta 5-avenasterol, and evaluated in cells (Figure S2). This showed no drastic increase for any ionisable lipid-formulated LNP and therefore warranted no further testing. They also confirmed that the four ionisable lipids chosen- ALC-0315 (control), APL-143 (Lipid 11), APL-718 (Lipid 12), APL-719 (Lipid 13) exhibited significantly higher expression profiles than the other proprietary lipid LNP formulations and were selected for further evaluation. Other CQAs for these 60 LNPs were compared to the cholesterol formulations using heat maps (Figure S3), where variation was observed in size and PDI, however the mRNA encapsulation remained consistent with changing the sterols, as this is primarily dictated by the ionisable lipid, and none of the samples were toxic *in vitro*.

ALC-0315 and the proprietary ionisable lipids- APL-143, APL-718, and APL-719 were then formulated with the six sterols in triplicate and evaluated for expression and viability in HeLa cells (Figure 5). This showed continued expression for all of these LNP

formulations in combination with each of these sterol alternatives. For ALC-0315 LNPs, each of these sterols increased the expression of mRNA relative to cholesterol. Aside from this, the overall expression of proprietary ionisable lipids was still highest in lipids APL-143 and APL-719, performing significantly better than APL-718 (Figure 4). Comparing all ionisable lipids, β-sitosterol, Campesterol, stigmasterol and Delta 5-avenasterol LNPs had the highest expression, with Cholesterol and Lanosterol LNP mRNA being slightly lower. However, the results fluctuated depending on the formulation, for the cationic lipids (APL-718, APL-719), there were no significant changes in mRNA expression when incorporating the different sterols, suggesting ionisable lipids are more sensitive to changes in LNP sterol composition. This may be due to differences in endosomal escape, ionisable lipids depend on pH-dependent transition to a cationic state in order to facilitate mRNA endosomal escape [50].

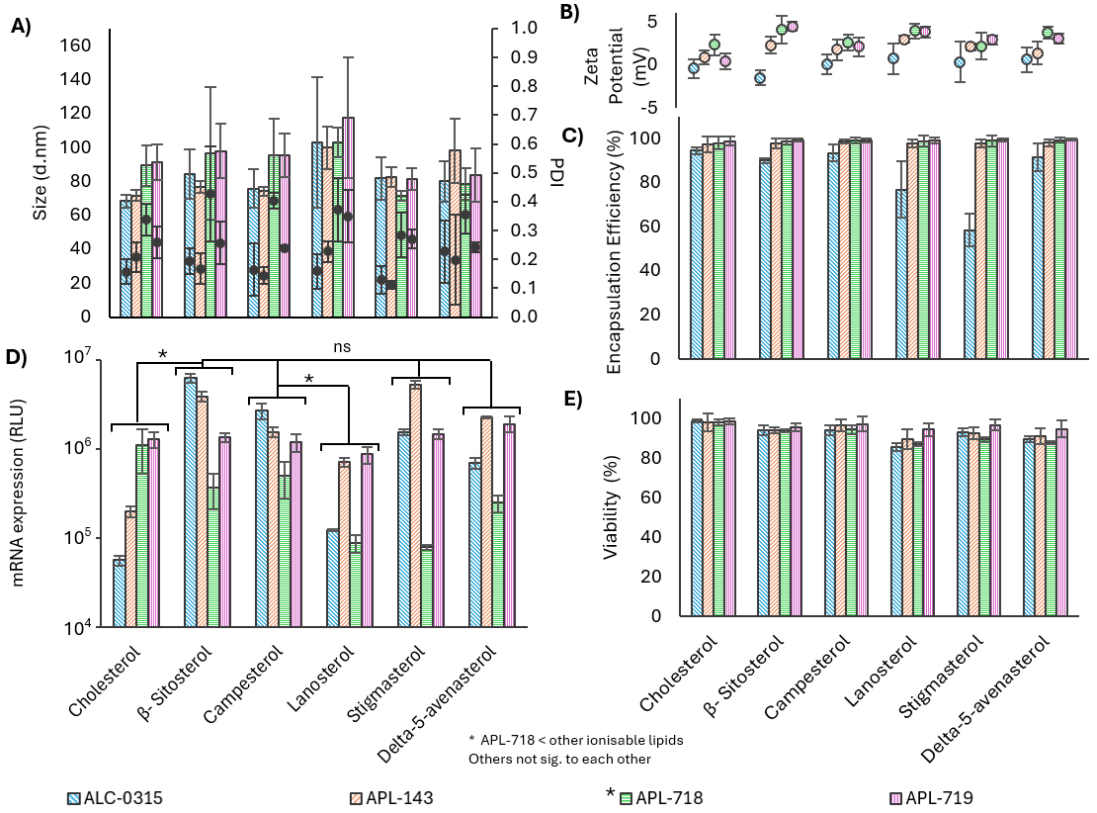

Figure 5: Properties of mRNA LNPs manufactured with varying combinations of ionisable lipids and sterols. A) Size (bars) and PDI (closed circles) of the LNP formulations, B) Zeta potential, C) mRNA encapsulation , D) HeLa cell expression of FLuc mRNA from the LNP formulations, E) HeLa cell viability of the LNP formulations. The LNPs were manufactured with an N/P of 6 from 5mg/mL lipid stocks and purified by dialysis in pH 7.4 PBS. Each measurement is a mean of three independent batches with error bars showing ± SD.

This transition could depend on LNP structure and packing, which changes depending on sterol choice; for example, β-sitosterol and stigmasterol have a multi-faceted polyhedral surface as opposed to the smooth spherical LNPs manufactured with cholesterol [59]. For these samples, there were some variations in size with the latter two ionisable lipids producing LNPs with higher PDIs (Figure 5A); however, the mRNA encapsulation remained high, except for the ALC-0315 + lanosterol and stigmasterol samples (Figure 5C), and these factors did not appear to have any significant impact on the mRNA expression. The measured zeta potentials also remained around neutral for all samples, which was marginally more positive for the cationic ionisable lipid samples (APL-718, APL-719; Figure 5B), and cell viability remained high (Figure 5E), indicating no impact on cell viability.

While *in vitro* studies can provide valuable insights into cellular uptake, mRNA expression, and toxicity, they fail to fully capture the complexities of a living system, including biodistribution, clearance, immune response, and tissue-specific delivery [165, 166]. Therefore, *in vivo* testing of lipid nanoparticles (LNPs) is essential for translating promising *in vitro* results into effective therapeutic applications [40, 103]. In this study BALB/c mice were used to evaluate the mRNA expression of these LNPs *in vivo*. This was first assessed through intramuscular administration (Figure 6), followed by intravenous administration, looking at whole body bioluminescence (Figure 7) and organ biodistribution (Figure 8).

ALC-0315 LNPs were first assessed in order to down-select ionisable-sterol LNP combinations for progressing to *in vivo* studies for the proprietary ionisable lipids. The ALC-0315 LNPs gave high mRNA expression, indicated by higher bioluminescence across all sterol formulations (Figures 6-8), where cholesterol, β-sitosterol, campesterol and delta 5-avenasterol gave higher mRNA expression than lanosterol and stigmasterol (Figure 6A, 6B, 7, 8A). Cholesterol, β-sitosterol, campesterol and delta 5-avenasterol also had higher liver expression compared to the intramuscular injection site (the legs) 6 hours post administration. However, after 24 hours, the proportional liver expression had decreased more rapidly than expression in the legs (Figure 6C). ALC-0315 lanosterol and stigmasterol LNPs also exhibited higher expression at the injection site and the legs relative to the liver.

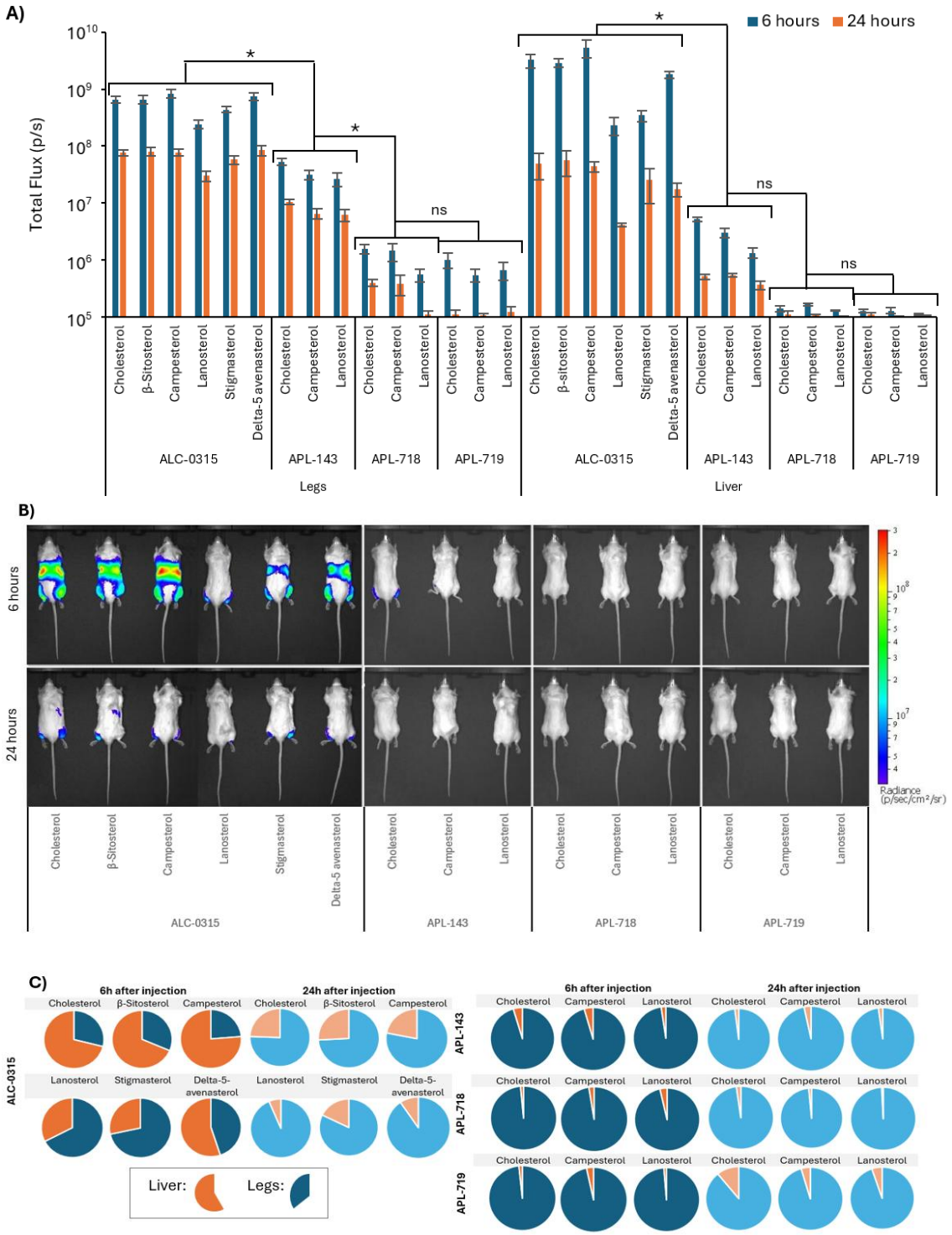

Figure 6: Intramuscular *in vivo* expression of LNPs in BALB/c mice manufactured with ALC-0315 or proprietary ionisable lipids in combination with sterol variations. Mice were imaged at 6 hours and 24 hours after IM injection of the 2µg mRNA per leg. ALC-0315 was tested with 6 sterols, before down-selecting for the proprietary ionisable lipids. A) Graph showing FLuc mRNA expression for the different formulations in the injection site (quadriceps/legs) and the liver. B) Representative images of the Fluc expression in mice. C) Pie charts showing the proportion of expression in the liver vs the legs (injection site) at 6 hours and 24 hours after injection.

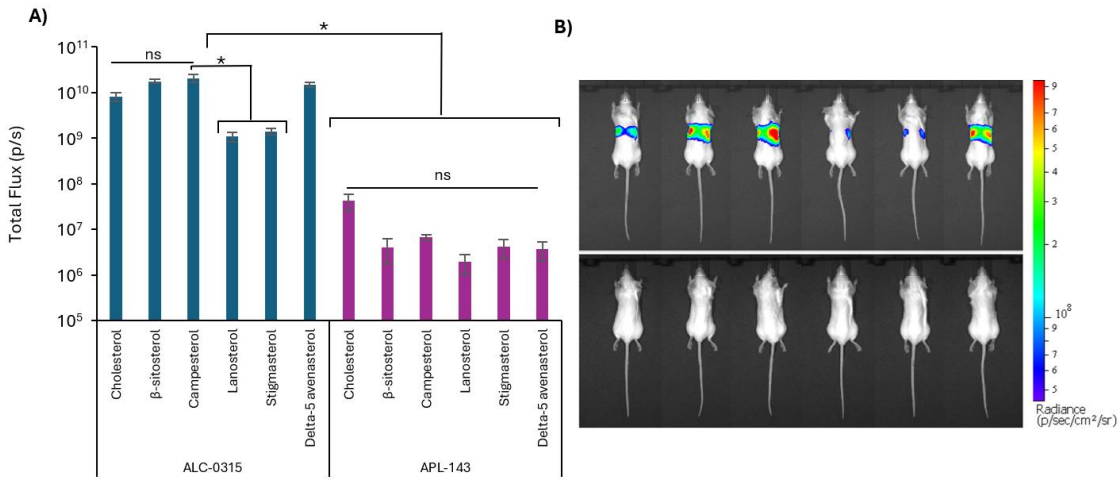

Figure 7: Intravenous *in vivo* expression of LNPs in BALB/c mice manufactured with ALC-0315 or proprietary ionisable lipid APL-143 in combination with sterol variations. Mice were imaged at 6 hours IV injection of the 2µg mRNA in a bilateral tail vein. A) Graph showing FLuc mRNA expression for the different formulations. B) Representative images of the Fluc expression in mice.

When looking at the organ biodistribution (Figure 8), it was observed that the ALC-0315 lanosterol LNPs expression was highest in the spleen, in contrast to other formulations, where the expression was highest in the liver, furthermore, these LNPs expressed highest in the spleen compared to the other formulations (Figure S4) despite having the lowest expression overall. A slight proportional increase in spleen expression was also seen in ALC-0315 stigmasterol formulation, however not to the same extent (Figure 8B, S4). Based on this data, it was decided for the proprietary ionisable lipids that the sterols used would be cholesterol (the control sterol), campesterol (the joint highest expressing in ALC-0315 and not previously having been taken *in vivo*) and lanosterol (seemingly different expression profile to others).

These LNPs were firstly administered intramuscularly, where all proprietary lipid LNP formulations gave significantly lower mRNA expression than the ALC-0315 clinical standard (Figure 6). It was also observed that these LNPs primarily expressed in the injection site (leg) as opposed to the liver (Figure 6A, 6C). This was particularly apparent with APL-718 and APL-719, where there was negligible liver expression, indicating these LNPs may have degraded in the systemic circulation. Notably, these proprietary formulations are cationic lipids, which may perform poorly *in vivo* compared to *in vitro* due to increased immune interaction and toxicity [2, 15].

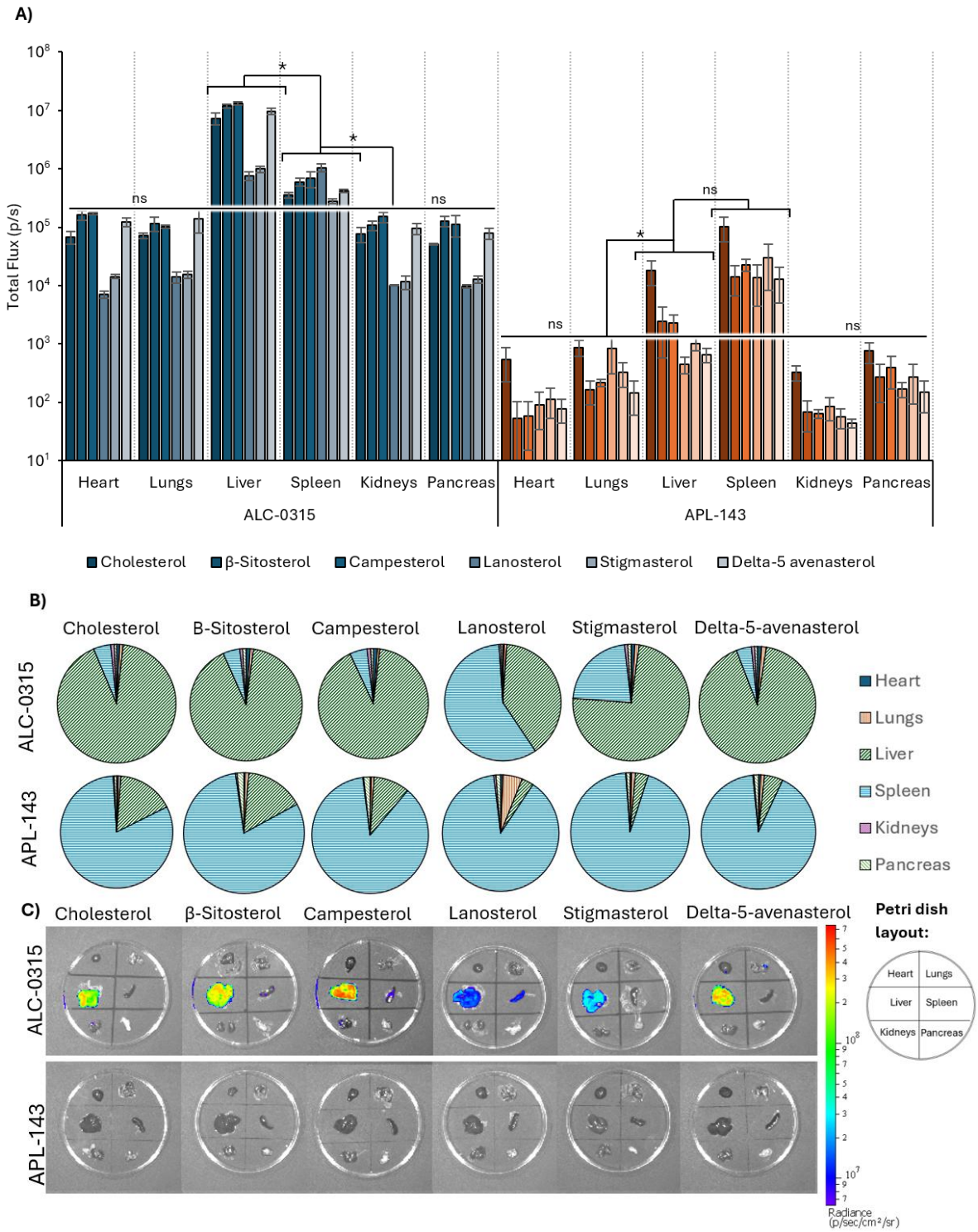

Figure 8: Intravenous *In vivo* expression of LNPs in BALB/c mice manufactured with ALC-0315 or proprietary ionisable lipid APL-143 in combination with sterol variations. Mice were dissected at 6 hours IV injection of the 2µg mRNA in a bilateral tail vein. The heart, lungs, liver, spleen, kidneys and pancreas were imaged for Fluc mRNA expression. A) Graph showing FLuc mRNA expression in each organ for the different formulations. B) Pie charts showing the proportion of expression in each organ for each formulation. C) Representative images of the petri dishes with the organs from each mouse showing FLuc mRNA expression.

Although absolute expression levels varied between intramuscular and intravenous routes, the relative performance ranking of formulations remained consistent, highlighting an important consideration for formulation screening.

Out of the proprietary lipid LNPs, APL-143 gave the highest expression after intramuscular administration. Based on these results, only the APL-143 LNPs were taken intravenously for biodistribution assessment. As with the intramuscular administration, overall, the APL-143 LNP expression was significantly lower than the ALC-0315 LNPs across all sterol combinations. While sterol substitutions such as β-sitosterol and campesterol subtly influenced LNP properties and improved expression in some cases, their impact was secondary to that of the ionisable lipid. These findings reinforce the importance of ionisable lipid chemistry as the primary driver of LNP efficacy, with sterols acting as useful modifiers for fine-tuning performance.

In terms of organ biodistribution, APL-143 LNPs had a preference for the spleen and liver (Figure 8A, 8B); the other organs showed little to no expression above background luminescence (estimated ~10^2 flux (p/s) per mg). These findings emphasise the critical role of the ionisable lipid in determining LNP efficacy and biodistribution. While sterols modulate LNP properties, their impact on mRNA expression is significantly lower *in vivo* than that of the ionisable lipid. The spleen accumulation observed with ALC-0315-lanosterol containing LNPs may indicate altered clearance mechanisms, potentially due to differences in LNP stability or interactions with immune cells [58, 167].

While further validation is needed, this finding supports the idea that adjusting sterol composition could help redirect LNP biodistribution and expand therapeutic applications beyond the liver. This may also be the reason for less liver preference in the lower-expressing APL-143 LNPs. It is also apparent that there is no relationship between the *in vitro* and *in vivo* results in terms of the better performing formulations, an issue that is frequently encountered in LNP research and is yet to be resolved [40, 103, 153, 168]. While the divergence between *in vitro* and in *vivo* performance is a known challenge in the field, our findings provide insight into how the route of administration influences LNP behaviour.

In addition to performance data, our results begin to uncover structure-function relationships that may guide future LNP design. Variations in lipid pKa, degree of branching, and lipid geometry (e.g. cone-shaped structures) were associated with

differences in mRNA encapsulation and expression, suggesting that structural features may play a more significant role than previously appreciated [58, 98]. Interestingly, the permanently cationic lipids APL-718 and APL-719 demonstrated high expression *in vitro* but poor performance *in vivo*, potentially due to enhanced immune clearance, offering further mechanistic insight into how lipid charge affects biodistribution and stability. Moreover, lanosterol-containing LNPs consistently showed a shift in expression toward the spleen, particularly in the ALC-0315 formulation, indicating potential for tissue-specific targeting through sterol selection.

Conclusions

Overall, this study presents a comprehensive comparison of proprietary cationic and ionisable lipids and sterol alternatives, evaluating 11 novel lipids and five sterol substitutions across a wide range of formulations of lipid nanoparticles (LNPs) for effective mRNA delivery. Our investigations into various proprietary cationic/ionisable lipids, compared to the clinically relevant control of ALC-0315, revealed significant variations in mRNA encapsulation efficiency and expression levels *in vitro*. While sterols influenced some physicochemical properties and biodistribution patterns, their impact on mRNA expression was secondary to that of the ionisable lipids. Moreover, we observed notable discrepancies between *in vitro* and *in vivo* results, not uncommon in LNP evaluation, emphasising the complexities in LNP performance that require further investigation. Collectively, these findings add to the understanding of LNP formulations for RNA therapeutics by identifying key structure-function relationships, highlighting the dominant role of cationic/ionisable lipid chemistry, and demonstrating that sterol composition can modulate biodistribution profiles, including potential spleen-targeting, thereby informing future design strategies for tissue-specific and administration route-appropriate RNA delivery systems.

CHAPTER 5: COMPARATIVE EXPRESSION KINETICS OF MRNA, SARNA, AND PDNA DELIVERED USING A SINGLE LIPID NANOPARTICLE FORMULATION

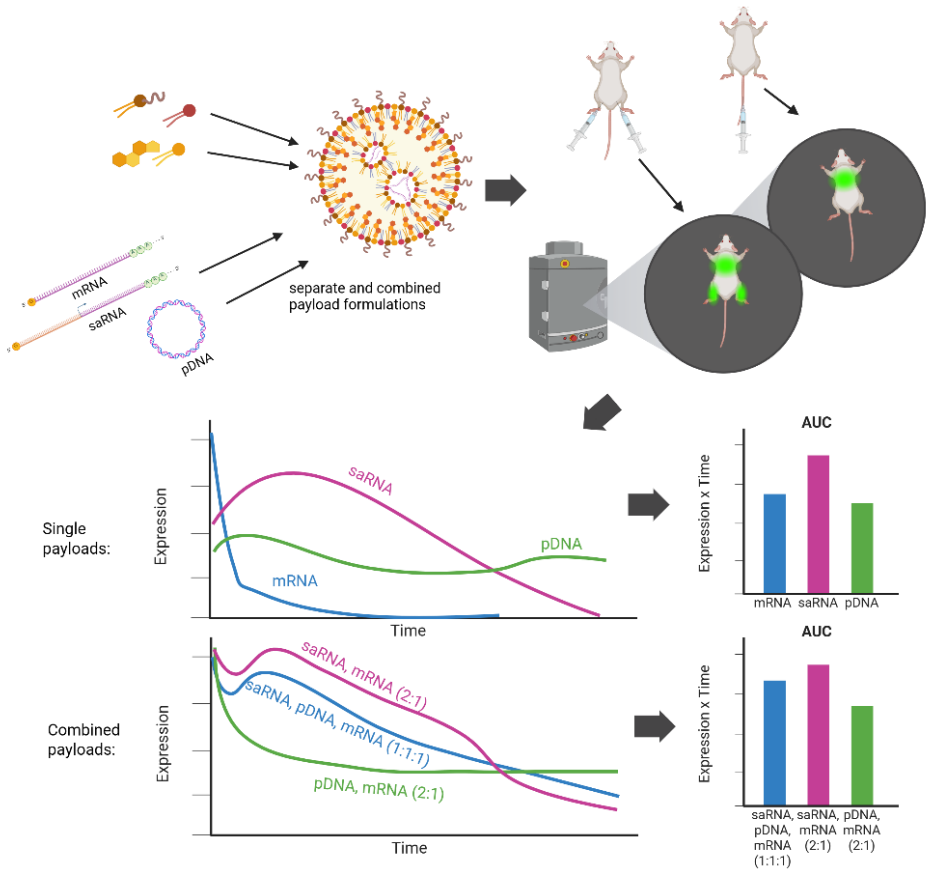

Created with BioRender.com

This Chapter has been accepted and under revision in the Journal of Controlled Release.

Author Credits:

Caitlin McMillan, Muattaz Hussain, Panida Punnabhum , Kirsten Kong, Andrew Varley, Zahra Rattray, Amy Druschitz and Yvonne Perrie.

Abstract

Lipid nanoparticles (LNPs) are clinically established carriers for nucleic acid therapeutics, most notably messenger RNA (mRNA). However, LNPs can be used to encapsulate alternative nucleic acids with distinct expression patterns, offering opportunities to modulate the magnitude and duration of gene expression compared to mRNA alone. Here, we systematically compared LNPs formulated with firefly luciferase (FLuc)-encoding mRNA, self-amplifying RNA (saRNA), and plasmid DNA (pDNA), as well as defined combinations of these payloads, to assess how payload identity and composition influence expression *in vitro* and *in vivo*.

Using an identical ALC-0315-based lipid composition and microfluidic formulation process, single-payload LNPs displayed distinct expression profiles following intramuscular and intravenous administration in mice: mRNA drove potent, yet transient expression, saRNA produced delayed and sustained expression, and pDNA enabled prolonged low-level expression. Combined-payload formulations, prepared either by co-encapsulation or by post-formulation mixing, exhibited expression profiles consistent with the proportional contributions of their constituent payloads, with no evidence of synergistic or antagonistic interactions. The combination of mRNA with saRNA achieved the highest cumulative expression over the study period.

Comprehensive physicochemical and structural characterisation showed minimal differences between formulations, indicating that expression kinetics are driven primarily by payload-specific biology rather than particle structure under the conditions tested. Together, these results indicate that gene expression magnitude and duration can be modulated through nucleic acid payload composition without altering the carrier system, providing a flexible strategy for the design of LNP-based therapeutics.

Introduction

Lipid nanoparticles (LNPs) are clinically validated delivery systems for nucleic acid therapeutics and are used in several approved medicines, most notably the COVID-19 mRNA vaccines. LNPs typically comprise an ionisable lipid, structural lipid, cholesterol, and a PEGylated lipid, which together enable encapsulation, stability, and controlled intracellular delivery of nucleic acids. LNPs protect nucleic acids from degradation, facilitate cellular uptake, and enable cytosolic release, thereby overcoming key barriers associated with naked nucleic acid delivery [1]. While current clinically approved LNP

formulations predominantly encapsulate mRNA or small interfering RNA (siRNA), LNPs are capable of delivering a wide range of nucleic acid payloads with distinct structural and biological properties.

Beyond mRNA and siRNA, alternative protein-coding nucleic acids offer the potential for altered expression (or inhibitory) kinetics, improved stability, or reduced immunogenicity. Analysis of the recent literature suggests that approximately 23% of LNP-focused research explores other nucleic acid payloads (Figure 1), highlighting growing interest in expanding the functional scope of LNP platforms. Broadly, nucleic acid therapeutics can be categorised into those that drive gene expression, such as mRNA, and those that silence or regulate gene expression, such as siRNA. While

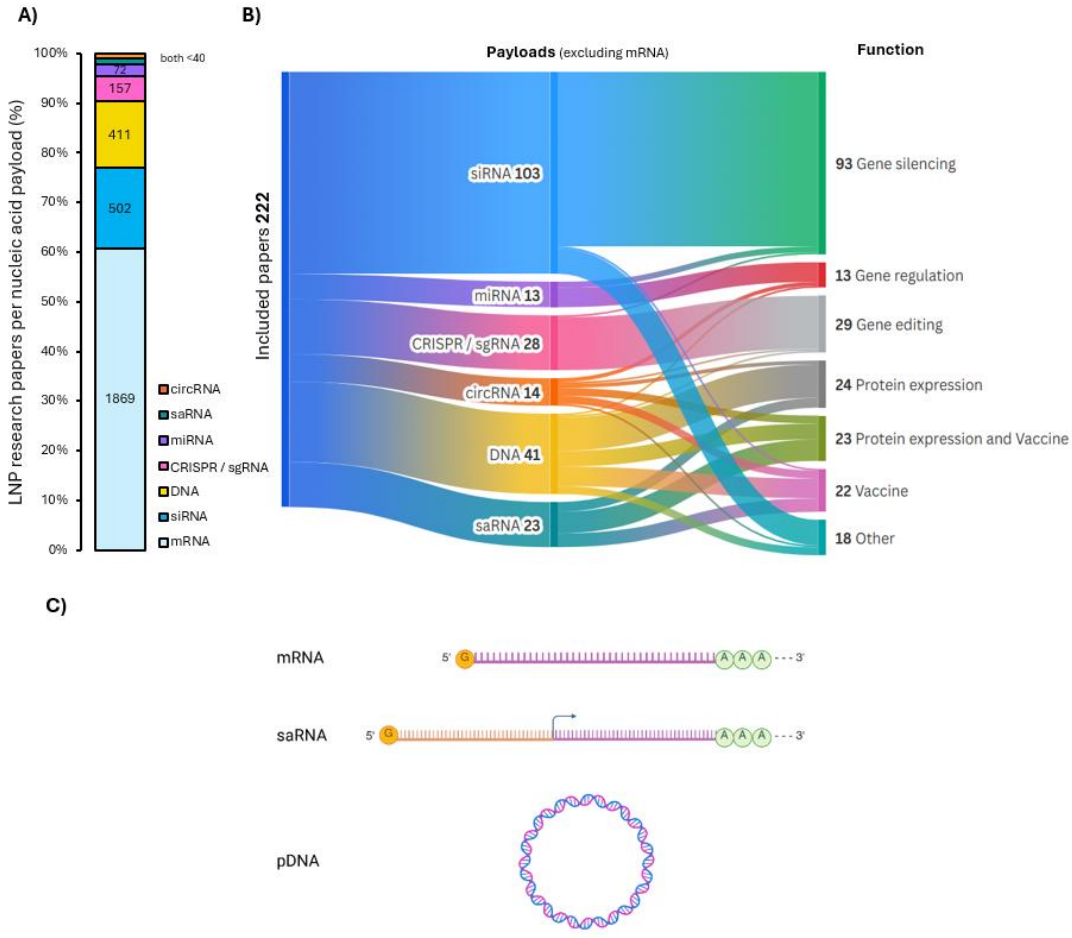

Figure 5 : A survey of the literature on payloads used in LNPs. A) Number of publications retrieved for each LNP payload on PubMed B) Sankey diagram showing functional categorisation of non-mRNA nucleic acid payloads following application of inclusion and exclusion criteria (222 of 265 articles included). Search strategy and screening criteria are described in the Methods section. C) Nucleic acids to be investigated in this chapter (Created with BioRender).

mRNA can elicit robust protein expression following successful intracellular delivery, this expression is often transient due to mRNA instability. In addition, mRNA, as well as by-products that can arise during *in vitro* transcription (IVT), including double-stranded RNA and uncapped 5'-triphosphate species, can be highly immunogenic [2]. This immunostimulatory property is advantageous for vaccine applications but may be undesirable in other therapeutic contexts, including gene replacement strategies or certain cancer treatments. Several gene-expressing alternatives to mRNA have therefore been explored for use in LNPs, including self-amplifying RNA (saRNA), circular RNA (circRNA), and plasmid DNA (pDNA).

Self-amplifying RNA (saRNA) retains the core structural features of mRNA but incorporates alphavirus-derived replication machinery, enabling intracellular RNA replication and leading to prolonged protein expression from a lower initial RNA dose [3, 4]. As a result of this additional machinery, saRNA is substantially larger than conventional mRNA (typically ~9-12 kb compared to 1-2 kb for mRNA), encoding four viral non-structural proteins and a subgenomic promoter that drives transgene expression.

This increased size may present challenges for LNP encapsulation and formulation but also enables effective protein expression at significantly lower doses than mRNA. As such, reduced dosing requirements have the potential to lower manufacturing costs and improve global accessibility of RNA-based vaccines [5]. Clinical studies further suggest that the unique biology of self-amplifying RNA can influence downstream immune outcomes in humans. For example, vaccination regimens incorporating saRNA have been associated with enhanced antibody breadth and $CD8^+$ T cell responses compared with mRNA vaccination alone, consistent with altered antigen exposure dynamics, although expression kinetics were not directly measured [6]. In line with this, preclinical studies have shown that LNP-formulated saRNA can drive robust *in vivo* antigen expression and immune activation following intramuscular administration, supporting the translational potential of saRNA delivery systems. However, in many such studies, expression is inferred from immunogenicity endpoints rather than being directly quantified over time [7]. Recently, self-amplifying RNA vaccines have been approved for clinical use, delivered either with lipid nanoparticles (e.g., ARCT-154/Zapomeran) or other lipid-based systems [8, 9]. As these platforms advance, there is an increasing need

to understand how intrinsic payload biology contributes to expression behaviour independently of delivery particle design.

Plasmid DNA represents another alternative gene-expressing payload with distinct advantages and limitations. DNA vaccines have been under development since the 1990s, initially for HIV, and the first DNA vaccine for SARS-CoV-2 was approved during the COVID-19 pandemic [10]. Hundreds of DNA-based vaccines are now in clinical trials for infectious diseases and cancer indications. Most DNA vaccines rely on naked plasmid DNA or viral vectors, as plasmids are often considered sufficient for delivery without a carrier. However, pDNA administration without advanced delivery methods such as electroporation has demonstrated limited uptake and efficacy [10, 11], motivating the exploration of non-viral delivery systems such as LNPs.

Compared to RNA, pDNA has much higher structural stability and does not require ultra-low-temperature storage, offering practical advantages for distribution and long-term storage [11]. However, pDNA must reach the nucleus to be transcribed, introducing additional intracellular barriers relative to mRNA, which is translated directly in the cytoplasm. This requirement generally results in lower expression levels compared to mRNA [12]. Furthermore, although LNPs facilitate cellular uptake and cytosolic release, they do not support nuclear delivery. As a result, LNP-mediated pDNA delivery is expected to be most effective in dividing cells, where temporary nuclear envelope breakdown allows nuclear entry [13]. To improve transcriptional efficiency and nuclear access, therapeutic pDNA constructs are often engineered with specific regulatory elements, such as strong promoters and sequence features that minimise non-specific recombination or unintended genomic integration. Importantly, pDNA remains episomal and does not integrate into the host genome, enabling sustained expression with minimal risk of insertional mutagenesis [11]. In the context of vaccination, excessively prolonged antigen expression may not always be advantageous, as sustained antigen exposure has been suggested to influence immune regulation and T-cell responses in certain settings [14]. This highlights the importance of tailoring expression kinetics to the intended therapeutic application.

Despite growing interest in alternative nucleic acid payloads, direct experimental comparisons of mRNA, saRNA, and pDNA formulated within the same LNP system are limited. Moreover, to our knowledge, the impact of co-encapsulating multiple gene-

expressing nucleic acids within a single LNP has not been systematically investigated, despite its potential relevance for combination therapies and gene delivery strategies. In many existing studies, comparisons between payload types are confounded by differences in delivery systems, formulation parameters, or experimental conditions, making it difficult to disentangle the contribution of payload identity from that of the carrier. As a result, a systematic evaluation under controlled formulation conditions is needed to directly assess how intrinsic payload properties influence expression behaviour.

In this study, we employ a controlled formulation approach to compare the physicochemical properties and biological performance of ALC-0315-based LNPs encapsulating firefly luciferase-encoding mRNA, saRNA, or pDNA. By maintaining a constant LNP composition and manufacturing process, we aim to isolate the effect of payload identity on expression kinetics, rather than to optimise delivery performance for each individual nucleic acid modality. Expression profiles are evaluated *in vitro* and through extended *in vivo* studies in mice, enabling assessment of both expression magnitude and duration. In addition, we investigate LNPs co-encapsulating multiple nucleic acid payloads to explore how combined delivery influences particle characteristics and expression behaviour. Together, this work provides a systematic comparison of gene-expressing nucleic acid payloads within a unified LNP platform and offers insights into how payload identity and combination affect LNP performance.

Materials and Methods

Materials

The following were provided by Avanti Research, a Croda Brand (Alabaster, AL, USA): 1,2-distearoyl-*sn*-glycero-3-phosphocholine (DSPC), 1,2-dimyristoyl-*rac*-glycero-3-methoxypolyethylene glycol-2000 (DMG-PEG 2000), 2-[(polyethylene glycol)-2000]-*N,N*-ditetradecylacetamide, Methoxypolyethyleneglycoloxy(2000)-*N,N*-ditetradecylacetamide (ALC-0159), [(4-Hydroxybutyl)azanediyl]di(hexane-6,1-diyl) bis(2-hexyldecanoate) (ALC-0315).

Firefly Luciferase mRNA and saRNA were purchased from UBC RNA and Formulation Core (Vancouver, BC, Canada). Plasmid DNA (pDNA) was purchased from Aldevron (Fargo, ND, USA). All RNA materials were supplied by the manufacturer with

accompanying quality control data, including confirmation of identity and integrity. Where applicable, RNA constructs incorporated standard modifications to enhance stability and reduce immunogenicity. Plasmid DNA encoding firefly luciferase was obtained in purified form and handled according to standard protocols. Citric acid, sodium citrate tribasic dehydrate, and 25 mm dialysis membrane (MWCO 12,000–14,000 Da) were acquired from Sigma-Aldrich (St. Louis, MO, USA). Phosphate-buffered saline tablets (PBS pH 7.4) were acquired from Oxoid Ltd. (Basingstoke, UK). Tris Base and Ethanol (EtOH) were obtained from Fisher Scientific (Loughborough, UK). Dulbecco's Modified Eagle's Medium, Trypsin-EDTA (0.05%), PBS, pH 7.4 solution and Quant-it RiboGreen RNA Assay Kit and Quant-iT PicoGreen dsDNA Reagent were purchased from Fisher Scientific UK Limited (Renfrew, UK). ONE-Glo™ Luciferase Assay System and VivoGlo Luciferin (*In Vivo* Grade) were acquired from Promega UK (Southampton, UK). BD Insulin Syringes were purchased from Scientific Laboratory Supplies Limited (Nottingham, UK). All solvents and other chemicals were of analytical grade, and milliQ-water was provided by an in-house system.

Aqueous and Organic Phase Preparation

The aqueous phase containing mRNA and the organic (lipid) phase were prepared separately before microfluidics. The aqueous phase was prepared using 50 mM citrate buffer (pH 4), diluting Firefly Luciferase (Fluc) mRNA, saRNA or pDNA, as well as defined combinations of these payloads (1:1:1 mRNA:saRNA:pDNA and 2:1 mRNA:saRNA or pDNA), at concentrations required to maintain a nitrogen to phosphate (N/P) ratio of 6, the molar ratio of ionisable lipid containing positively-charged amines (N) to the mRNA containing negatively-charged phosphates (P).

The lipid molar ratio of the LNPs was 10:38.5:50:1.5% structural lipid: sterol: cationic lipid: PEGylated lipid, these were DSPC, cholesterol, ALC-0315 and DMG-PEG 2000, respectively. The lipid stocks were prepared and stored at concentrations of 5-100 mg/mL, dissolving each lipid in ethanol. The organic phase injected into the microfluidic device had a concentration of 5 mg/mL.

Manufacture of LNP formulations using microfluidics

The NanoAssemblr benchtop (Precision Nanosystems Inc., Vancouver, Canada, now under Cytiva, Massachusetts, USA) was used in all experiments in this chapter. The ethanol-based organic phase and the citrate buffer-based aqueous phase containing

mRNA, saRNA and/or pDNA were fed through syringes into a microfluidics chip with a herringbone mixer design. The phase ratio or flow rate ratio (aqueous: organic phase) was set to 3:1, and the total flow rate was at 20mL/min.

Purification

The LNP suspension was purified by dialysis buffer exchange; the LNP sample in the original ethanol/citrate buffer was exchanged into 200 mL PBS (pH 7.4) for every mL of sample. Samples were dialysed for 4 hours, after which the pH becomes neutral and the ethanol content is negligible (<1%).

Measuring LNP Formulation Critical Quality Attributes (CQAs)

Physicochemical properties

Size (Z-average diameter), polydispersity index (PDI) and zeta potential were measured using the Malvern Panalytical Zetasizer ZS and Zetasizer Ultra, using the Zetasizer software for data acquisition. Size and PDI were measured *via* dynamic light scattering (DLS), using a backscatter measurement angle of 173°, and zeta potential was measured by electrophoretic light scattering using voltage measurements in a Folded Capillary cell. Each of these measurements were performed in triplicate for each experimental repeat (nine measurements for each experiment). Post-purification, each sample was prepared for measurement at a lipid concentration of 0.1 mg/mL in PBS (for size/PDI) or deionised water (for zeta potential) to achieve attenuation values between 7 and 8. Pre-purification measurements for size and PDI were performed with citrate buffer as the diluent. ZEN0040 disposable micro-cuvettes were used for size and polydispersity, and DTS1070 folded capillary zeta cells were used for zeta potential measurements, adding 400 µL and 1,000 µL of diluted LNPs, respectively. The material refractive index and absorption were 1.45 and 0.001, respectively. The dispersant refractive index and absorption were 1.33 and 0.8872 cP, respectively, for water, 1.335 and 1.02 cP, respectively for PBS, and 1.47 and 1.28 cP for citrate buffer.

Nanoparticle tracking analysis was performed on samples post-purification using the Malvern Panalytical NanoSight Pro (Malvern Panalytical, Malvern, Worcestershire, UK) and the NS Xplorer software was used for data analysis. Nanoparticle size distribution and estimated particle concentration were measured using a 488 nm laser block and videos were captured using a high sensitivity sCMOS camera with a light-scatter filter.

Samples were diluted to 0.05 µg /mL and analysed under constant flow (1 µL/min) using a syringe pump, with the temperature set at 20 °C. Five 11.5 s videos were captured for each sample and optimised using the automated optimal settings employed by the software.

Asymmetric flow field-flow fractionation (AF4) was used to further characterise the samples. The AF4 system (AF2000, Postnova Analytics, Malvern, UK) was coupled to an inline multidetector (MD) setup comprising a multiangle light scattering detector (MALS-PN3621, Postnova Analytics), a UV detector (PN3242, 260 nm, 0.5 sensitivity, Postnova Analytics), and a dynamic light scattering detector (Zetasizer Nano ZS, Malvern Panalytical, Worcestershire, UK). Separation was performed using a frit-inlet channel (300 mm × 60 mm × 40 mm) with a 350 µm spacer, a 10 kDa MWCO amphiphilic regenerated cellulose membrane, and 10 mM Tris buffer (pH 7.5) as the carrier liquid at 25 °C. The FI-AF4-MD procedure was adapted from [169] with an initial cross-flow (XF) hold of 0.75 mL/min for 15 min, followed by a 60 min exponential XF decay from 0.75 mL/min to 0 mL/min, and a final 5 min hold at 0 mL/min. A constant detector flow (DF) of 0.3 mL/min was maintained throughout the separation.

Quantification of the mRNA content

Encapsulation efficiency was measured using the RiboGreen™ nucleic acid quantification assay according to the manufacturer's instructions. This assay was used for RNA-only LNPs and for formulations containing RNA in combination with pDNA, as RiboGreen™ detects both single- and double-stranded nucleic acids as shown in Figure S1. For LNPs loaded exclusively with pDNA, encapsulation efficiency was instead quantified using the PicoGreen™ assay, which is selective for double-stranded DNA (Figure S1). Tris-EDTA (TE) buffer was used as the diluent in all steps of this assay. The fluorescent dye was used to quantify mRNA in the presence and absence of 2% Triton, for lysis of the LNPs. Two RNA standard curves were used to quantify mRNA. The fluorescence signal was read using the POLARstar Omega (BMG Labtech, UK) and GloMax (Promega, UK) plate readers using 475-485 nm excitation and 525 nm emission wavelengths. The total RNA for each sample from the Triton wells and free (unentrapped) RNA from the TE-only wells were obtained when analysing the results. The mRNA encapsulation efficiency (EE%) was calculated as previously described [153].

Cryogenic transmission electron microscopy (cryo-TEM)

Lipid nanoparticle samples were prepared as previously stated and maintained at manufacturing concentrations in pH 7.4 PBS. 3 µL of each sample was blotted using an FEI Vitrobot (Thermo Fisher Scientific, UK) for 3 seconds and 5 force onto a 300-mesh lacey carbon-coated copper grid, then immediately vitrified in liquid ethane, cooled by liquid nitrogen, and held in a cryo-specimen holder (Gatan Elsa) before transfer to the TEM. LNP morphology was observed and captured at liquid nitrogen temperature using a Jeol JEM-F-200 microscope (Jeol, Japan) at 200 kV.

In vitro expression

LNP FLuc mRNA expression was analysed in HeLa cells using firefly luciferase as a bioluminescent reporter. Cells were cultured in Dulbecco's Modified Eagle Medium (DMEM) with sodium pyruvate, supplemented with 10% foetal bovine serum (FBS), 1% penicillin/streptomycin and L-glutamine. Cells were seeded in a 96-well white/clear bottom plate, at a concentration of 10,000 cells/ 100 µL in media and cultured for 48 hours, after which LNPs were added. LNPs were formulated as above with payloads comprising Firefly Luciferase- encoding mRNA, saRNA and/or pDNA. LNP formulations were added to the cells, replacing growth media, and diluted in media at total mRNA concentrations of 1 µg/mL and 0.5 µg/mL, in triplicate and control wells with cells only. Cells were incubated with LNPs for 24 hours prior to addition of the luciferase reagent. Luciferase reagent, prepared as per manufacturer's instructions, was added to each well of the 100 µL of media and cells containing LNPs from the previous day, creating a total volume of 200 µL, mixed thoroughly and left to incubate for 3 minutes. The luminescence of the plates was read using the GloMax plate reader (Promega, UK).

In vivo expression

LNP expression was analysed in female BALB/c mice (8-10 weeks old at the start of the study, supplied in-house) using firefly luciferase as a bioluminescent reporter. Three BALB/c mice per formulation were dosed intramuscular (IM) and intravenous (IV) injection with each formulation with 50 µL in each quadricep (x2 =100 µL total) or lateral tail vein. respectively of 40 µg/mL LNPs (mRNA concentration), resulting in a 2 µg (0.1 mg/kg) IV dose and 4 µg (0.2 mg/kg) total IM dose (2 µg per leg). The mice were anaesthetised and maintained under anaesthesia using isoflurane before imaging using the IVIS® Spectrum and the associated Living Image® software (PerkinElmer,

Buckinghamshire, UK). For the Fluc mRNA expression, the mice were firstly injected subcutaneously (SC) with 30 mg/mL D-luciferin solution (5 µL per gram of body weight, corresponding to 150 mg/kg). This SC injection was repeated at each imaging time point, and these mice were imaged 10 minutes after injection using the luminescence setting on the software. For both intramuscular (IM) and intravenous (IV) studies, mice were imaged at 6 h and 24 h post-injection, with an additional 1 h time point included for IV administration. Imaging was then performed on subsequent days up to 9 days post-injection (excluding the day 4 time point), followed by weekly imaging up to week 10-12. Thereafter, imaging intervals were gradually extended to every 2–4 weeks until study termination. Bioluminescence was quantified from the injection site (hind limbs) and upper abdominal region (liver) for IM studies, and from the whole body for IV studies. A longitudinal imaging approach was employed to enable repeated, non-invasive monitoring of expression kinetics in the same animals, thereby reducing the total number of animals required.

Statistical analysis

The mean and standard deviation were calculated for all experiments, performed in independent triplicate batches unless otherwise stated. Each batch was manufactured on a different day, to account for inter-day variation. For hydrodynamic size, polydispersity, zeta potential and pKa, three measurements were taken for each batch, therefore these groups for statistical analysis were n=9. For statistical comparison of groups, One- or Two- way ANOVA was performed on parametric data sets, whereas Kruskal-Wallis with Dunn's post hoc test was performed for the non-parametric data sets. Statistically significant differences are annotated in each figure by individual p values for $p<0.05$, whereas (ns) denotes no statistical significance.

Literature search

A structured literature search was performed in PubMed to identify primary research articles reporting experimental use of non-mRNA nucleic acid payloads in lipid nanoparticles (LNPs). Searches were conducted using the terms ("lipid nanoparticle" OR "LNP") AND ("siRNA" OR "saRNA" OR "circRNA" OR "DNA" OR "pDNA" OR "microRNA" OR "miRNA"), excluding review articles, and restricted to publications between 2011 and 2025 (search performed 14 April 2025). Results were ranked using the "Best Match" option to prioritise relevance. Articles were manually screened to exclude

studies focused on mRNA payloads, protocol-only papers, review articles, or studies not reporting experimental nucleic acid delivery using LNPs.

Results and Discussion

Comparing mRNA, saRNA and pDNA singly- encapsulating LNPs

Nucleic acid-loaded LNPs were manufactured by microfluidic mixing using ALC-0315 as the ionisable lipid and encapsulating either mRNA, saRNA, or plasmid DNA (pDNA). A fixed N/P ratio of 6 and identical lipid compositions were used across all formulations, ensuring that any observed differences in physicochemical properties or biological performance could be attributed to the nucleic acid payload rather than formulation variables.

The LNP formulations were first compared based on their physicochemical properties at the time of manufacture, post-purification (Table 1). No statistically significant differences were observed between the mRNA-, saRNA-, and pDNA-loaded LNPs, with all formulations exhibiting particle sizes below 100 nm, low polydispersity indices (PDI), near-neutral zeta potentials, and comparable payload encapsulation efficiencies.

The LNP formulations were next compared for their *in vitro* performance by measuring firefly luciferase expression in HeLa cells after incubation with the LNPs for 24 hours (Figure 2). This timepoint was selected as it captures robust transgene expression across nucleic acid modalities while minimizing confounding effects associated with rapid cell proliferation and signal dilution in dividing cell lines such as HeLa. LNPs encapsulating mRNA produced the highest levels of expression, whereas saRNA- and pDNA-loaded LNPs showed expression only marginally above background. The limited *in vitro* signal may reflect differences in intracellular processing and expression kinetics between payload types.

Table 8 Physico-chemical attributes of ALC-0315 LNPs with different nucleic acid payloads. The LNPs were manufactured with an N/P of 6 from 5mg/mL lipid stocks and purified by dialysis in pH 7.4 PBS for 4 hours. Each measurement is a mean of three independent batches ± standard deviation.

Payload	Size (d.nm)	PDI	Zeta Potential (mV)	Encapsulation Efficiency
mRNA	77 ± 6	0.10 ± 0.04	-4.5 ± 1.5	89 ± 4
saRNA	83 ± 7	0.11 ± 0.05	-7.2 ± 2.0	84 ± 10
pDNA	76 ± 2	0.07 ± 0.03	-5.4 ± 1.3	92 ± 2

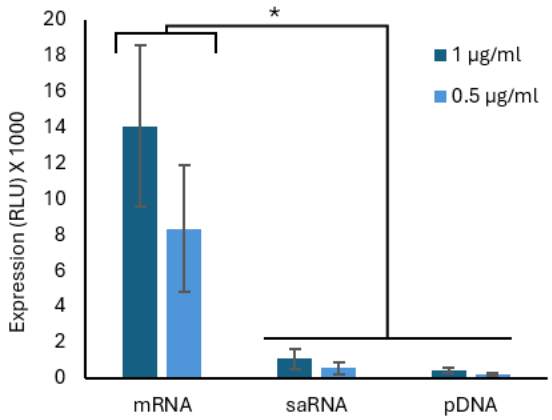

Figure 6: *In vitro* Fluc expression in HeLa cells dosed with either 1 µg/mL or 0.5 µg/mL total either mRNA, saRNA or pDNA for 24 h. The LNPs were manufactured with an N/P of 6 from 5 mg/mL lipid stocks and purified by dialysis in pH 7.4 PBS. Each measurement represents the mean of three independent batches, with error bars indicating ± SEM.

In vivo, saRNA-LNPs exhibited delayed peak expression, occurring several days post-administration rather than within hours (Figure 3), while pDNA-LNPs displayed substantially lower early expression levels, approximately 100–250-fold lower than mRNA during the first 24 h.These delayed and attenuated expression profiles likely contribute to the limited signal observed in short-term *in vitro* assays. Expression outcomes may also be influenced by formulation, cell type and dosing conditions, as previous studies have reported improved saRNA performance in alternative LNP formulations, different cell lines, such as HEK293, or at higher inoculation concentrations [170].

Although extended *in vitro* studies across multiple cell passages could provide further insight into longer-term expression kinetics [171], such analyses are inherently constrained in rapidly dividing cell systems. The *in vivo* data presented here more comprehensively captures the expression profiles of each payload and provides greater relevance to therapeutic performance.

For the *in vivo* studies, LNPs were first evaluated following intramuscular administration and imaged at increasing time intervals for up to 24 weeks (168 days) (Figure 3A, 3C). Within the first 6 h post-injection, mRNA-LNPs produced the highest levels of luciferase expression and exhibited the greatest overall peak among the payloads. Expression declined rapidly in the first few days (approximately fivefold in the first 24h), followed by a more gradual decrease, reaching background levels by approximately 5 weeks post-injection.

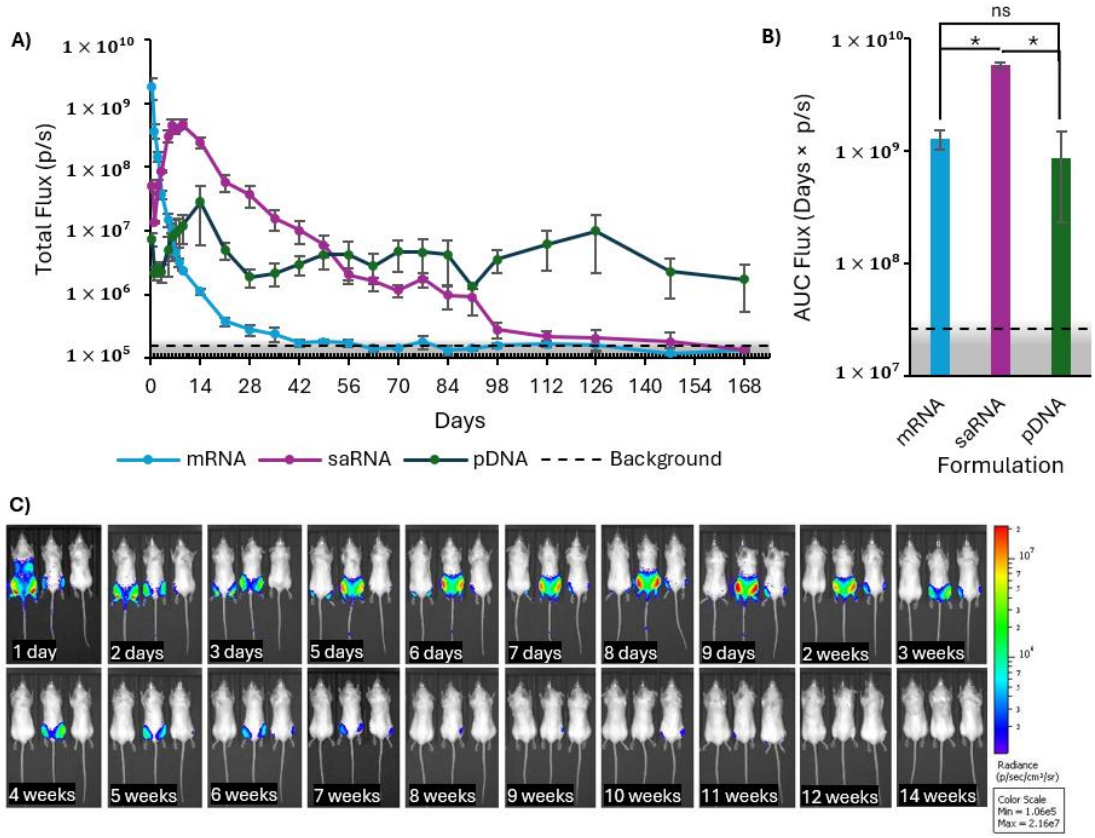

Figure 7: Intramuscular *in vivo* expression of mRNA-, saRNA-, and pDNA-loaded ALC-0315 lipid nanoparticles (LNPs) in BALB/c mice. Mice received 2 µg total nucleic acid per intramuscular dose and were imaged beginning 6 h post-injection and periodically up to 168 days (24 weeks). Bioluminescent signal is reported as total photon flux (photons per second, p/s). A) Individual average readings of each formulation at each timepoint. B) Area under the curve (AUC) of each formulation readings over time as luminescence x time, for the 24 weeks measurement period. C) Representative IVIS image of mice from 1 day to 14 weeks (after which expression is not visible on the same scale). Mice left to right: mRNA, saRNA, pDNA. Each measurement represents the mean of three independent repeats, with error bars indicating ± SE.

In contrast, saRNA-LNPs displayed delayed expression kinetics, with peak expression occurring around one week post-injection, at levels comparable to mRNA-LNP expression at 24 h. saRNA-mediated expression was sustained for substantially longer than that of mRNA, consistent with its self-amplifying mechanism, and as seen in previous studies [49, 171, 172]. Expression decreased gradually over time, remaining detectable for approximately 14-16 weeks (over 100 days) before returning to background levels.

pDNA-LNPs exhibited both the lowest overall expression and the most prolonged expression profile. No clear peak was observed, and low-level expression persisted throughout the 24-week study period. This behaviour is likely attributable to the

additional intracellular processing steps required for pDNA expression, including nuclear entry and transcription prior to translation, which may limit expression magnitude [173]. Conversely, the inherent structural stability of pDNA and its protection from cytosolic enzymes within the nucleus likely contribute to the extended expression duration observed. Consistent with this, pDNA has previously been shown to support transgene expression for several months following successful transfection in the liver [174], suggesting that similarly prolonged expression may occur in other tissues.

More recently, pDNA-LNP delivery has been shown to engage cGAS-STING-mediated innate immune sensing, which may further limit expression magnitude while still permitting extended transgene expression when appropriately managed [175]. Together, these observations support the conclusion that the prolonged but low-level expression observed for pDNA-LNPs is primarily dictated by payload-specific intracellular processing rather than formulation differences

To capture the overall expression output from each payload across the 24-week study, the area under the bioluminescence-time curve was calculated for individual mice and compared between groups (Figure 3B). This analysis showed that saRNA-LNPs produced the greatest cumulative expression over the study duration. Although mRNA-LNPs achieved peak expression levels approximately 100-fold higher than pDNA-LNPs, their rapid signal decline resulted in a cumulative expression that was not significantly different from that of pDNA after 24 weeks. The sustained, low-level expression observed with pDNA-LNPs therefore compensated for its lower peak signal over time. While early timepoints contribute substantially to the total AUC, particularly for mRNA-LNPs, the temporal expression profiles shown in Figure 3A provide a complete time-resolved comparison of each formulation. These data clearly demonstrate the delayed peak expression of saRNA and the distinct, sustained profile of pDNA, independent of early mRNA-driven signal.

We next examined how intravenous (IV) administration influenced LNP biodistribution and expression kinetics, as the route of administration substantially affects pharmacokinetics and IV delivery is commonly used for LNP-based therapeutics. As expected, IV injection resulted in high liver expression; however, the duration of expression following IV delivery was considerably longer than anticipated (Figure 4A,C).

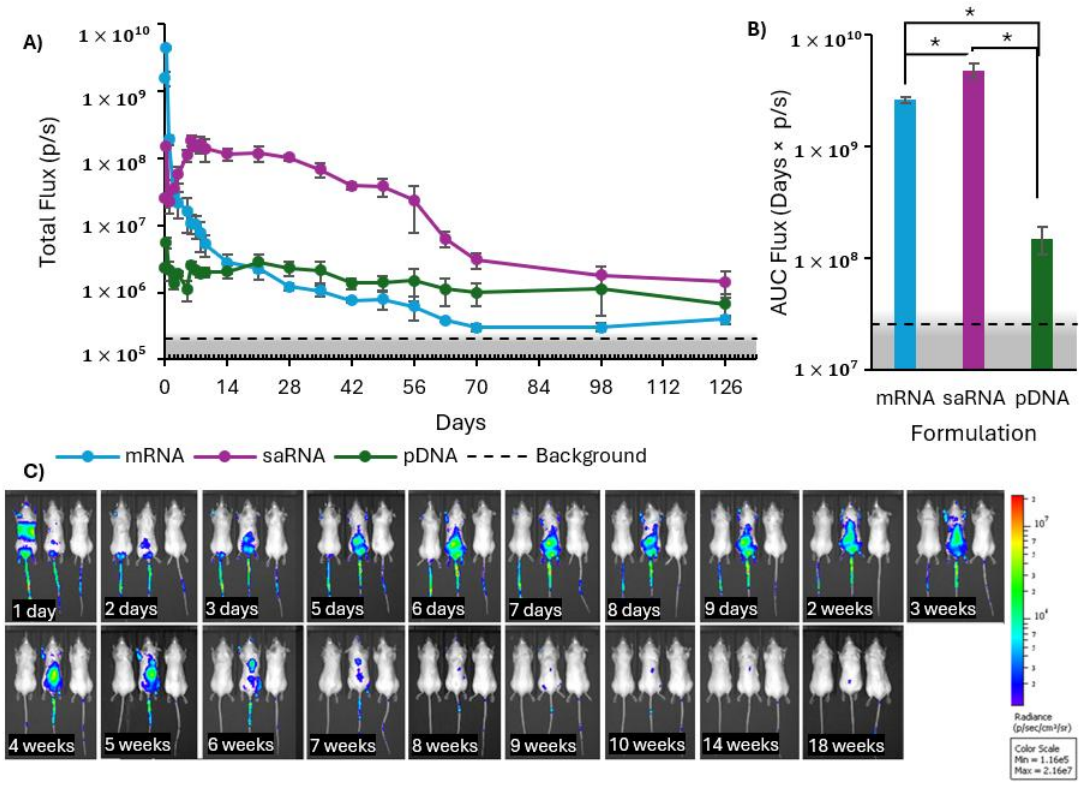

Figure 8: Intravenous *in vivo* expression of mRNA-, saRNA-, and pDNA-loaded ALC-0315 lipid nanoparticles (LNPs) in BALB/c mice. Mice received 2 µg total nucleic acid by tail vein injection and were imaged beginning 1 h and 6 h post-injection and periodically up to 126 days (18 weeks). Bioluminescent signal is reported as total photon flux (photons per second, p/s). A) Individual average readings of each formulation at each timepoint. B) Area under the curve (AUC) of each of the formulations readings over time as luminescence x time, for the 28 weeks measurement period. C) Representative IVIS image of mice from 1 day to 14 weeks (after which expression is not visible on the same scale). Mice left to right: mRNA, saRNA, pDNA. Each measurement represents the mean of three independent repeats, with error bars indicating ± SE.

Following IV injection, mRNA-LNPs showed a rapid decrease in expression during the first few days, similar to the IM profile, but this was followed by a more gradual decline, with the signal not approaching background levels until approximately 10 weeks, around twice the duration observed after IM administration. For saRNA-LNPs, peak expression was lower and less pronounced than after IM injection; however, expression declined more slowly and remained above background for over 18 weeks (126 days). Here, unlike in IM administration, there was no indication of when expression would reach background levels.

In contrast, pDNA-LNPs exhibited a profile comparable to IM administration, characterised by the absence of a clear peak and sustained low-level expression throughout the study period, with no evident decline by the endpoint. Area under the curve (AUC) analysis revealed a larger difference between mRNA- and pDNA-LNPs

following IV administration (Figure 4B), with mRNA-LNPs showing higher cumulative expression due to both an increased peak magnitude of expression and a prolonged signal. This also reduced the difference in cumulative expression between mRNA- and saRNA-LNPs, resulting in similar overall expression despite their distinct expression profiles. Comparison of the AUCs over the first 18 weeks (corresponding to the duration of the IV study) showed that mRNA-LNPs generated greater cumulative expression following IV administration compared to IM administration. In contrast, pDNA-LNPs exhibited higher cumulative expression after IM delivery, while saRNA-LNPs showed broadly similar cumulative expression across both administration routes despite differing expression kinetics (Figure S2).

Additionally, liver expression from saRNA-loaded LNPs could not be reliably assessed in this study, as tissue-level biodistribution analysis was not performed. A longitudinal, non-invasive imaging approach was intentionally employed to enable repeated measurements in the same animals over extended time periods, which precludes terminal sampling required for detailed biodistribution analysis. This limitation may be particularly relevant for saRNA, which exhibits delayed expression kinetics compared with mRNA. Whereas mRNA-LNP–mediated liver expression typically peaks within 6- 24 h post-administration, saRNA expression often increases more gradually and reaches maximal levels several days after delivery. As a result, early hepatic expression may have been missed. In addition, previous studies suggest that saRNA replication in hepatocytes may be limited by rapid intracellular clearance or post-transcriptional regulatory mechanisms [49]. Together, these factors may explain the absence of a clear liver signal in this study.

To investigate the prolonged expression observed after IV administration, saRNA-treated mice were imaged in multiple orientations (Figure S3). Persistent signal coincided with known adipose depots [176, 177], suggesting that some LNPs redistribute to adipose tissue, where slow metabolic turnover may contribute to extended FLuc expression. Although adipose accumulation was not directly measured, the spatial overlap supports it as a plausible site contributing to prolonged signal.

Our findings show that saRNA-LNP expression profiles depend on both the payload and the route of administration. Previous studies reported strong, long-lasting expression after intramuscular dosing, while intravenous delivery produced weaker or altered

patterns, as well as a peak for saRNA expression around 5-7 days [49, 178]. In addition, saRNA-driven expression is strongly influenced by innate immune sensing, where type I interferon responses can suppress translation and introduce nonlinear dose-response behaviour, effects that may be partially mitigated through payload-level modulation rather than delivery reformulation [179]. Together, these observations are consistent with our delayed peak expression signal and highlight that expression outcomes arise from the combined effects of RNA biology, LNP formulation, and administration route.

In vivo studies revealed clearly distinct expression magnitudes and expression time profiles for each nucleic acid payload. mRNA-LNPs produced the highest initial expression that declined rapidly whereas, saRNA-LNPs showed delayed onset with sustained expression over several weeks. pDNA-LNPs showed the lowest overall expression levels but maintained persistent, low-level expression throughout the study. These differences highlight complimentary advantages in potency and durability. Based on these observations, we next investigated whether mixing nucleic acid payloads within a single LNP formulation could combine these complementary properties to achieve robust expression with extended duration.

Comparing mRNA, saRNA and pDNA co-encapsulation and mixed LNPs

To explore whether combining nucleic acid payloads could modulate expression kinetics, mixed LNP formulations were generated using two distinct strategies. In the first approach, payloads were mixed prior to LNP manufacture to enable co-encapsulation within the same particles. In the second approach, LNPs were formulated separately with single payloads, and subsequently combined post-formulation to generate mixed-payload LNP preparations (Figure 5). All mixed formulations were prepared in defined proportions. Each formulation contained 33% mRNA to preserve the rapid, high initial expression characteristic of mRNA-LNPs, supplemented with either 33% saRNA and 33% pDNA (mixture 1), 67% saRNA (mixture 2), or 67% pDNA (mixture 3). This resulted in a total of six distinct formulations, reflecting both payload composition and formulation strategy. We hypothesised that combining payloads prior to or after LNP formulation would not substantially alter overall expression outcomes.

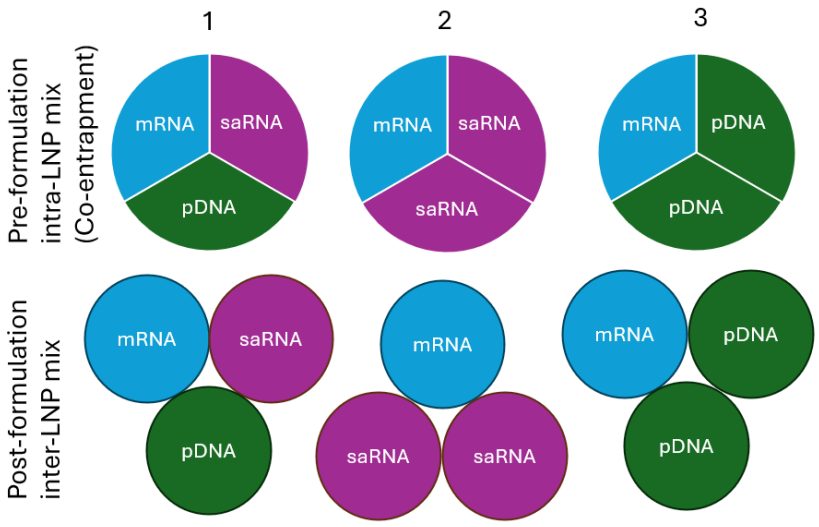

Figure 9: Schematic representation of LNP payload combinations, including three defined payload ratios and two mixing strategies: co-encapsulation prior to formulation and post-formulation mixing of single-payload LNPs.

When assessing the physicochemical properties of the mixed-payload LNPs, compared with single-payload LNPs (Table 1), the mixed-payload LNPs showed no significant differences across the formulation compositions (Table 2). All formulations consistently exhibited particle sizes below 100 nm, low polydispersity indices (PDI), near-neutral zeta potentials, and similar payload encapsulation efficiencies.

When FLuc expression was assessed *in vitro*, no significant differences were observed between the mixed-payload formulations, and pre- versus post-formulation mixing had no overall impact (Figure 6). Because all combined-payload formulations contained a fixed amount of mRNA, while only the saRNA and pDNA content was varied, the observed reporter expression- together with the single-payload *in vitro* data (Figure 2)- suggests that mRNA is the dominant contributor to luciferase expression under these experimental conditions.

Table 9 Physicochemical attributes of ALC-0315 LNPs with different combinations of nucleic acid payloads. The LNPs were manufactured with an N/P of 6 from 5mg/mL lipid stocks and purified by dialysis in pH 7.4 PBS for 4 hours. Each measurement is a mean of three independent batches ± standard deviation.

Payload	Size (d.nm)	PDI	Zeta Potential (mV)	Encapsulation Efficiency
mRNA, saRNA + pDNA	80± 5	0.11 ± 0.06	-6.3 ± 1.2	89 ± 6
mRNA + saRNA	83 ± 4	0.10 ± 0.04	-6.3 ± 3.0	85 ± 7
mRNA + pDNA	81 ± 4	0.08 ± 0.03	-5.3 ± 2.7	91 ± 5

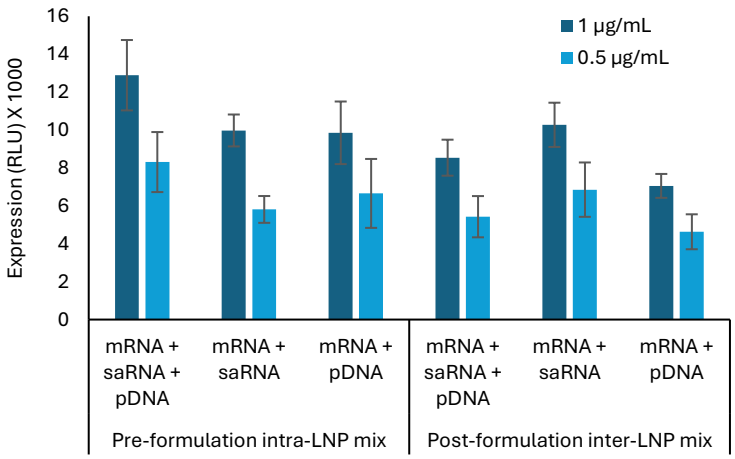

Figure 10: *In vitro* Fluc expression in HeLa cells dosed with either 1 µg/mL or 0.5 µg/mL total of varying combinations of mRNA, saRNA and pDNA. Each sample is 33.3% mRNA. Pre-formulation (left) and post-formulation (right) mixing conditions are indicated. The LNPs were manufactured with an N/P of 6 from 5 mg/mL lipid stocks and purified by dialysis in pH 7.4 PBS. Each measurement represents the mean of three independent batches, with error bars indicating ± SD.

However, the relative encapsulation efficiency and distribution of each nucleic acid species within the LNPs were not directly measured. As in the single-payload studies, combined-payload LNPs were subsequently evaluated *in vivo* following intramuscular (IM) and intravenous (IV) administration, with expression monitored over a 14-week period.

To help interpret the expression profiles, expected expression curves were first estimated using the single-payload data. For each combined formulation, expression at each time point was calculated by adding together the contributions from each payload in proportion to how much of that payload was present, (e.g. for the mRNA/saRNA/pDNA formulation, one-third of each single-payload signal was totalled).

This then produced predicted expression-time profiles and corresponding AUC values for both IM and IV administration (Figures 7 and 8). Following IM administration, the experimentally measured expression profiles closely matched the predicted values (Figure 7A-C), indicating that payload co-delivery resulted in largely additive expression behaviour, with no evidence of synergistic or antagonistic interactions between the different nucleic acids.

These results do not distinguish between co-encapsulation within individual LNPs and uptake of multiple distinct LNPs by the same cell, both of which are plausible.

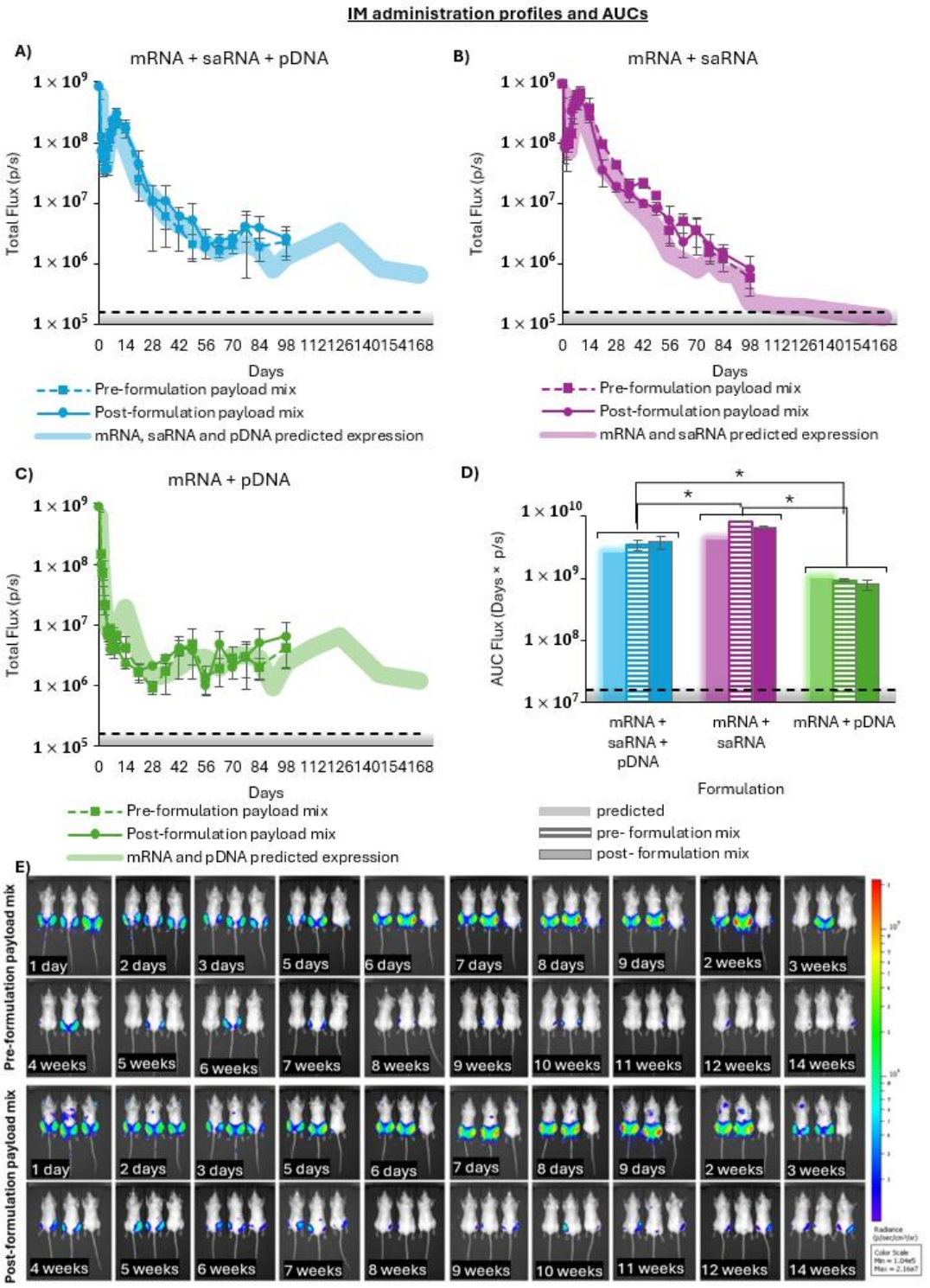

Figure 11: Predicted and measured intramuscular *in vivo* expression of combined-payload ALC-0315 lipid nanoparticles (LNPs) in BALB/c mice. Mice received a 2 µg total nucleic acid dose by intramuscular injection and were imaged starting 6 h post-injection and at intervals up to 168 days (24 weeks). Bioluminescent signal is reported as total photon flux (photons s^{-1}). (A–C) Predicted and experimentally measured expression profiles for LNPs co-encapsulating (A) mRNA + saRNA + pDNA, (B) mRNA + saRNA, and (C) mRNA + pDNA, shown as mean luminescence over time. (D) Comparison of predicted and measured area under the curve (AUC; luminescence × time) for each combined-payload formulation. (E) Representative IVIS images from 1 day to 14 weeks post-injection (left to right: mRNA + saRNA + pDNA, mRNA + saRNA, mRNA + pDNA). Data represent the mean ± SE of three independent experiments.

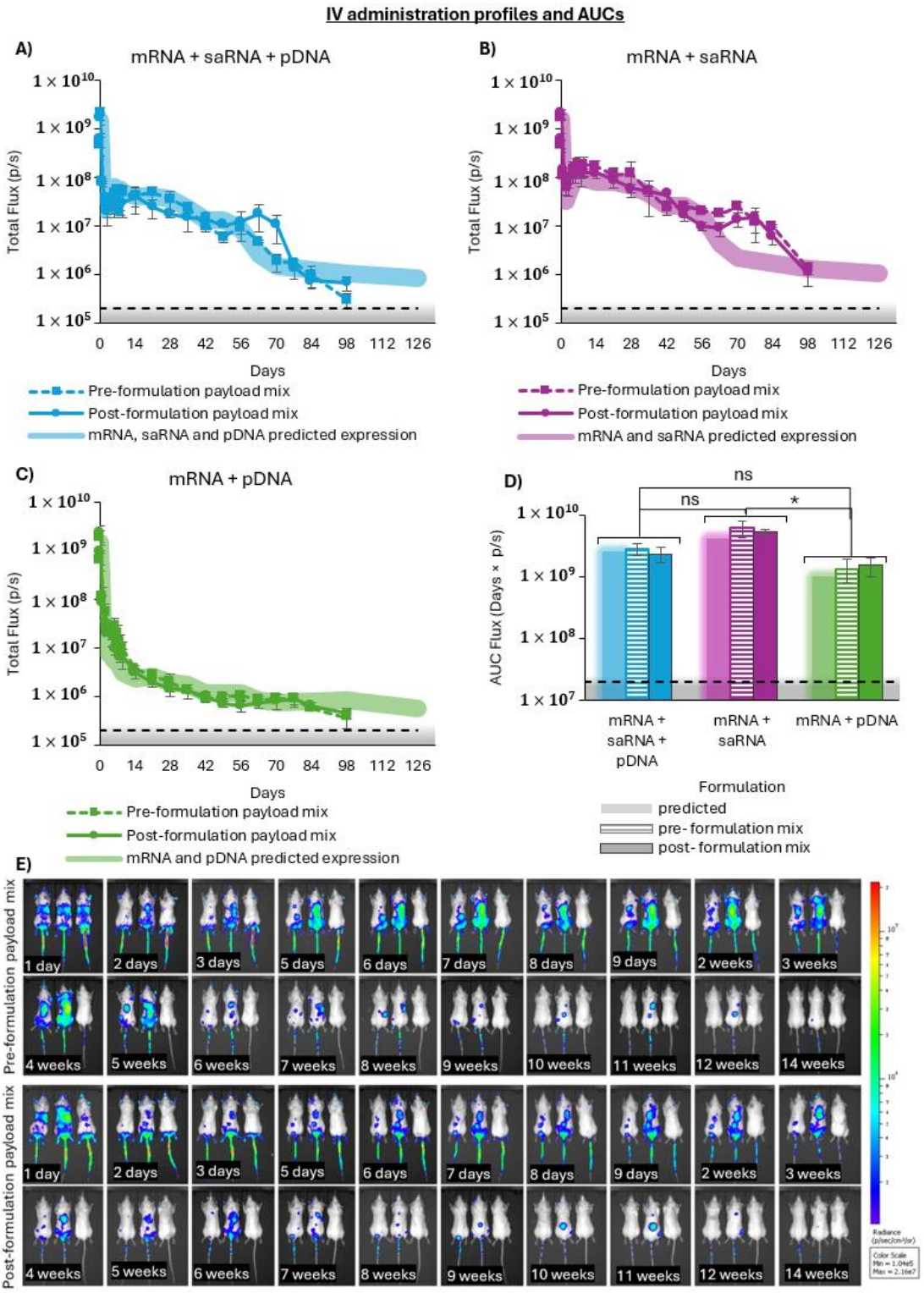

Figure 12: Predicted and measured intravenous *in vivo* expression of combined-payload ALC-0315 lipid nanoparticles (LNPs) in BALB/c mice. Mice received a 2 µg total nucleic acid dose via intravenous administration and were imaged starting 6 h post-injection and at intervals up to 168 days (24 weeks). Bioluminescent signal is reported as total photon flux (photons s^{-1}). (A–C) Predicted and experimentally measured expression profiles for LNPs co-encapsulating (A) mRNA + saRNA + pDNA, (B) mRNA + saRNA, and (C) mRNA + pDNA, shown as mean luminescence over time. (D) Comparison of predicted and measured area under the curve (AUC; luminescence × time) for each combined-payload formulation. (E) Representative IVIS images from 1 day to 14 weeks post-injection (left to right: mRNA + saRNA + pDNA, mRNA + saRNA, mRNA + pDNA). Data represent the mean ± SE of three independent experiments.

However, the close agreement between predicted and observed expression suggests that competitive encapsulation effects are minimal under the conditions tested.

All combined formulations exhibited comparable expression within the first 48 h, after which there was divergence depending on saRNA and pDNA content.

The mRNA/saRNA formulation produced the highest expression for approximately the first ~50 days, after which expression levels across formulations converged and were not significantly different until day 98. This corresponds with the overlap observed between saRNA and pDNA expression profiles in the single-payload IM study (Figure 3A). At later time points, as saRNA expression declined toward background, formulations containing pDNA exhibited relatively higher expression.

Consistent with these trends, AUC analysis showed that the mRNA (33%)/ saRNA (66%) formulation produced the highest cumulative expression, followed closely by the equally proportioned mRNA/saRNA/pDNA formulation, with the mRNA/pDNA formulation ranking next. As observed in the *in vitro* studies, no differences were detected between pre- and post-formulation mixing, with each combination showing comparable cumulative expression regardless of whether payloads were co-encapsulated or mixed post-formulation (Figure 7C-D).

As this study concluded at 14 weeks, the continued expression observed for pDNA-containing formulations suggests that longer study durations would likely further reduce these differences and may result in pDNA-containing combinations surpassing the mRNA/saRNA formulation, particularly for the triple-payload LNPs.

Following intravenous (IV) administration, the combined-payload LNPs again showed expression profiles that closely aligned with the predicted values derived from the single-payload datasets (Figure 8A-C), indicating predominantly additive behaviour between payloads.

Furthermore, no significant differences were observed between pre-formulation co-encapsulation and post-formulation mixing approaches, with matched formulations showing alike expression profiles and AUCs (Figure 8A-D). This consistency suggests that the method of payload combination does not substantially influence *in vivo* expression following IV administration.

Across formulations, distinct expression profiles for IV administration were observed until approximately day 98. The mRNA (33%)/ saRNA (66%) formulation again generally produced the highest expression, followed by the mRNA/saRNA/pDNA formulation, although increased variability was observed for this formulation during days 56-70. As expression declined over time, the profiles of all combined formulations converged, with no significant differences detected beyond approximately day 98, matching the convergence observed in the single-payload IV studies.

Consistent with these trends, AUC analysis showed slightly increased overall expression for the mRNA/pDNA formulations, such that their cumulative expression was not significantly different from the triple-payload formulation (Figure 8D). This is likely due to the higher initial mRNA-driven expression observed following IV administration compared to IM delivery, which reduces the relative contribution of longer-term expression differences beyond 48 h. In contrast, lower overall expression was observed for the mRNA/saRNA formulation, reflecting the reduced peak magnitude and overall expression profile observed for saRNA following IV administration compared with IM. Together, these data indicate that, following IV administration, combined-payload LNPs behave predictably with respect to their constituent payloads, with early expression driven largely by mRNA and longer-term expression becoming increasingly similar across formulations.

In this study, firefly luciferase was used as a model reporter to enable quantitative comparison of expression kinetics across payload types. While luciferase expression does not directly reflect therapeutic efficacy or immunogenicity, it provides a sensitive and well-established system for assessing relative expression magnitude and duration. The present work therefore focuses on comparative delivery behaviour rather than application-specific outcomes, which may vary depending on the therapeutic context and transgene of interest.

Together, these findings demonstrate that both single- and combined-payload LNP expression profiles are primarily governed by the intrinsic biological properties of the nucleic acid payloads, rather than by differences in LNP structure or formulation strategy. mRNA consistently drove rapid, high-level early expression, saRNA produced sustained intermediate expression through self-amplification, and pDNA enabled

prolonged low-level expression consistent with its requirement for nuclear localisation and transcription.

While prior studies have demonstrated that saRNA delivery often requires extensive optimisation of formulation composition and process parameters to preserve particle quality and biological activity [100], our data show that tuneable and predictable expression profiles can also be achieved by modulating payload composition within a single, clinically relevant LNP system. This suggests that payload mixing may offer a complementary strategy to formulation redesign when tuning expression magnitude and duration.

When combined within a single formulation, these behaviours were retained and integrated in a largely additive manner, allowing expression magnitude and duration to be predictably tuned through payload composition despite substantial differences in nucleic acid size (saRNA > mRNA and pDNA) and intracellular processing. Among the formulations tested, the mRNA/saRNA combination achieved the highest overall expression within the 14-week study period. To assess whether these expression differences were associated with changes in particle structure or population characteristics, further physicochemical and structural characterisation was undertaken.

Analysis of LNP Formulation Microarchitecture

To determine whether differences in payload composition or combination strategy influenced LNP structure beyond basic physicochemical properties, further characterisation was performed using complementary analytical techniques. Cryogenic transmission electron microscopy (cryo-TEM) was used to directly visualise particle morphology and internal structure, nanoparticle tracking analysis (NTA) was used to assess particle size distributions on a number-weighted basis, and asymmetrical flow field-flow fractionation (AF4) was used to separate any LNP populations and assess heterogeneity. Measurements of radius of gyration (Rg) and hydrodynamic radius (Rh) enabled calculation of shape factors and further evaluation of particle morphology.

The six LNP formulations were imaged using cryo-TEM to assess whether differing payloads, on their own or in the above mixtures, induced observable morphological differences (Figure 9).

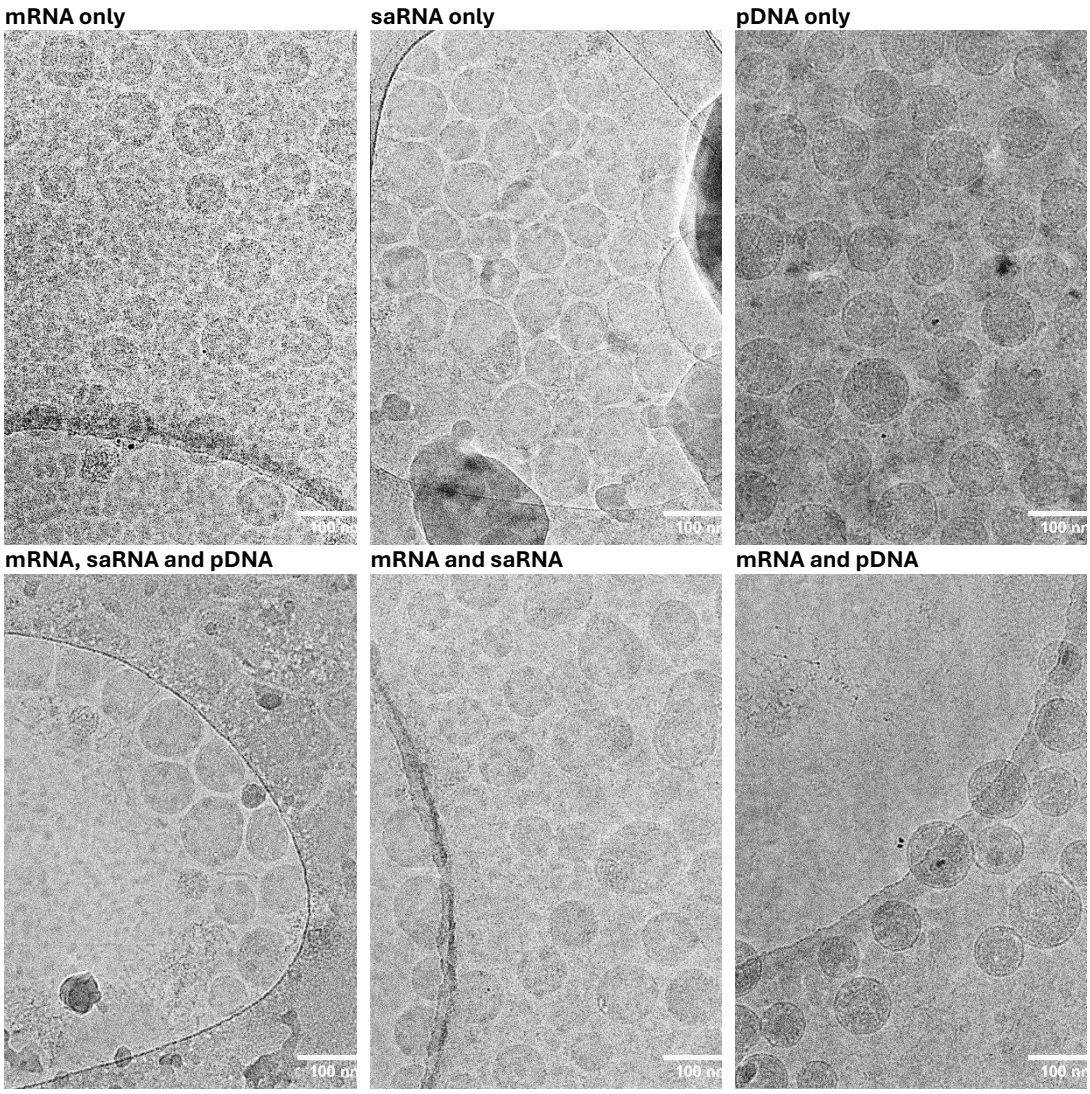

Figure 13: Cryogenic transmission electron microscopy (cryo-TEM) images of ALC-0315 lipid nanoparticles (LNPs) formulated with different single-payload or combination nucleic acids. Samples were vitrified in liquid ethane and imaged under liquid nitrogen using a Jeol JEM-F200 microscope operating at 200 kV and 30,000× magnification.

Across all formulations, particles were predominantly spherical with similar overall morphology, and no substantial structural differences were observed between single- and combined-payload LNPs. saRNA-containing formulations appeared to exhibit a slightly higher prevalence of surface irregularities or blebs; however, the majority of particles remained spherical, consistent with previous cryo-TEM observations of saRNA-loaded LNPs [170].

Overall, payload composition does not substantially alter LNP morphology, and NTA and AF4 analyses show minimal differences between formulations, indicating that divergent expression profiles are driven primarily by payload-specific biological processing rather than structural variation in the LNPs.

NTA measurements showed highly comparable mean and mode particle sizes, and percentile diameters (D10, D50, and D90) across all formulations, indicating similar size distributions (Table 3). Consistent with this, particle size by concentration distributions exhibited largely overlapping distributions for all LNPs (Figure 10A, Figure S4). Individual particle size distributions for each formulation are shown in Figure S4.

Notably, pDNA-loaded LNPs displayed an approximately 25% higher particle concentration, evident from both the elevated distribution curve and the increased number of particles quantified per milligram of formulation (Figure 10A-B). As these particles were not significantly smaller than the other formulations, this increase in particle number is unlikely to be driven by size differences. It may instead reflect differences in packing density associated with pDNA.

AF4 analysis further supported these findings, with all formulations exhibiting highly similar multi-angle light scattering (MALS) fractogram traces and comparable hydrodynamic (Rh) and radius of gyration (Rg) distributions (Figure 10C-H). Recoveries across formulations ranged from approximately 80% to 91% (Table S1), consistent with acceptable AF4 performance and in line with ISO recommendations. Shape factor analysis (Rg/Rh) yielded values between 0.6 and 0.85 (Figure S5), consistent with predominantly spherical particles, where 0.775 is considered to be a perfect sphere [180], and in agreement with cryo-TEM observations. No pronounced sub-populations or aggregation were observed in the AF4 traces.

Table 10: Nanoparticle tracking analysis (NTA) size distributions for ALC-0315 lipid nanoparticles (LNPs) formulated with different single-payload or combination nucleic acids.

LNP payload	Size values (d.nm)					Span	Valid Tracks
	Mean	Mode	D10	D50	D90		
mRNA	86.8 ± 0.6	86.8 ± 0.7	53.3 ± 0.5	80.1 ± 0.4	125.7 ± 1.4	0.90	4668 - 6397
saRNA	88.7 ± 0.5	88.7 ± 0.6	53.5 ± 0.3	82.2 ± 0.3	128.7 ± 0.8	0.91	5530 - 6523
pDNA	83.6 ± 0.3	72.1 ± 1.6	49.4 ± 0.7	78.0 ± 0.4	122.8 ± 0.8	0.94	6621 - 8037
mRNA, saRNA and pDNA	93.6 ± 0.5	79.3 ± 1.2	56.8 ± 0.3	87.1 ± 0.3	135.4 ± 0.9	0.90	5897 - 6825
mRNA and saRNA	90.4 ± 0.3	71.9 ± 1.9	41.4 ± 0.7	83.1 ± 0.3	140.1 ± 0.4	1.11	6368 - 7017
mRNA and pDNA	86.9 ± 0.4	70.1 ± 1.4	51.3 ± 0.4	80.4 ± 0.2	127.8 ± 1.4	0.95	6329 - 6978

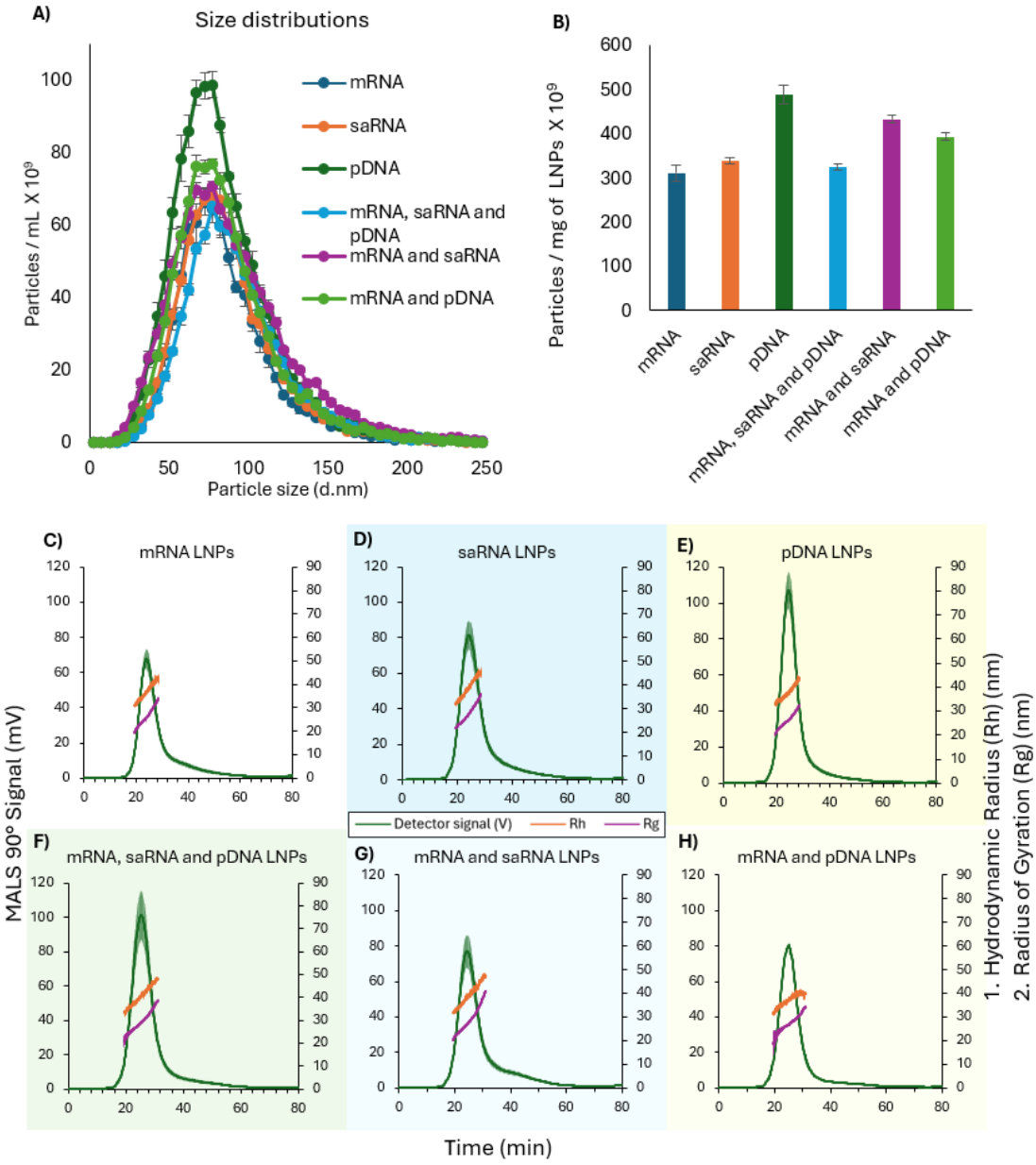

Figure 14: NTA and AF4–MALS–DLS characterisation of ALC-0315 lipid nanoparticles (LNPs) formulated with different nucleic acid payloads. A) Nanoparticle Tracking Analysis (NTA) size distributions. B) Particle count per milligram of formulation. C) Asymmetric Flow Field-Flow Fractionation (AF4) coupled with multi-angle light scattering (MALS) and dynamic light scattering (DLS), showing elution profiles with corresponding radius of gyration (Rg, determined by MALS) and hydrodynamic radius (Rh, determined by the on-line DLS detector). Data represent the mean of three independent measurements ± standard deviation.

Together, NTA and AF4 show that payload composition minimally affects LNP size, morphology, or heterogeneity, indicating that divergent *in vivo* expression arises primarily from payload-specific biological processing rather than particle structure.

Conclusions

This study systematically compared mRNA, saRNA, and plasmid DNA as lipid nanoparticle (LNP) payloads and evaluated whether combining these nucleic acids could rationally tune expression magnitude and duration *in vivo*. Using a consistent ALC-0315 LNP formulation, we show that differences in expression profiles are driven primarily by the intrinsic biological properties of the payloads rather than by changes in particle size or morphology.

mRNA produced rapid and high peak expression that declined quickly, saRNA exhibited delayed but sustained expression consistent with intracellular self-amplification, and pDNA enabled prolonged low-level expression over several months, likely reflecting nuclear localisation and transcriptional control. These distinct expression profiles highlight complementary advantages in expression magnitude and duration across payload types.

Importantly, when payloads were combined within a single formulation, either by co-encapsulation or post-formulation mixing, their expression behaviours were retained and combined in a largely additive manner. This predictability enabled rational modulation of expression kinetics through payload composition alone. Among the combinations tested, mRNA/saRNA formulations achieved the highest cumulative expression over the study timeframe, whereas pDNA-containing formulations sustained expression at later time points.

Physicochemical and structural characterisation using cryo-TEM, NTA, and AF4 confirmed that neither payload identity nor combination strategy substantially altered LNP morphology, size distributions, or population heterogeneity, thereby reinforcing that biological processing of nucleic acids determines expression outcomes.

Together, these findings indicate that payload composition represents an important and tuneable design parameter for LNP-mediated gene delivery, allowing expression profiles to be modulated without altering the underlying carrier formulation.

CHAPTER 6: INVESTIGATING OTHER MANUFACTURING PROCESSES AND UPSCALING LNP PRODUCTION USING THE MICROPORE PATHFINDER.

Abstract

Microfluidic mixing is widely used in LNP manufacturing because it offers tight control over critical process parameters and reproducibly generates mRNA-loaded particles with strong biological performance. However, commonly used development platforms (e.g., NanoAssemblr staggered herringbone mixers) are limited in throughput, hindering translation to manufacturing-relevant scales. This chapter investigated high-throughput LNP production using the Micropore Pathfinder™ crossflow membrane micromixer, systematically varying total flow rate (TFR) from 20 to 200 mL/min (3:1 aqueous:organic flow-rate ratio; N/P 6; ALC-0315/DSPC/cholesterol/DMG-PEG2000 at 50/10/38.5/1.5 mol%). LNPs were purified by dialysis into PBS and assessed for physicochemical critical quality attributes, *in vitro* transfection in HeLa cells, and *in vivo* luciferase expression following intramuscular dosing in BALB/c mice.

Across 20 -180 mL/min, LNPs maintained low polydispersity (PDI < 0.2) and near-neutral zeta potential (approximately -1 to -8 mV). Particle size decreased with increasing TFR and plateaued at ~95-100 nm between 60 and 160 mL/min, consistent with a size limit where assembly becomes less sensitive to further increases in mixing intensity. At 200 mL/min, particle size and heterogeneity increased, and mRNA encapsulation efficiency decreased, indicating an upper operational boundary for this formulation-device combination. Functionally, *in vitro* luciferase expression was broadly comparable across most conditions, with reduced expression observed only for 200 mL/min, aligning with lower encapsulation. Importantly, *in vivo* imaging showed robust expression kinetics for representative formulations (20, 60, 100, 140, 180 mL/min) with no significant differences in time-point signals or area under the curve. Overall, these data demonstrate that crossflow micromixing can increase LNP manufacturing rate to ≥180 mL/min without compromising *in vivo* efficacy, supporting its suitability for scalable production of functional mRNA-LNPs.

Introduction

Microfluidic mixing has become the most widely used approach for manufacturing lipid nanoparticles (LNPs) due to its ability to tightly control critical process parameters (CPPs) and generate reproducible particles with high nucleic acid encapsulation and robust biological performance [45, 85]. Throughout the preceding chapters of this thesis, LNPs were manufactured using a staggered herringbone microfluidic mixer

operated on the NanoAssemblr platform. Such systems are well established for LNP development; however, their limited throughput (up to 20 mL/min) restricts translation to manufacturing-relevant scales. The NanoAssemblr platform relies on staggered herringbone microfluidic mixing, utilizing herringbone-shaped grooves within microchannels to induce chaotic advection. This mechanism enhances mixing efficiency and enables controlled lipid nanoparticle (LNP) formation at relatively low flow rates. Conversely, the Micropore Pathfinder™ system employs cross-flow membrane micromixing (Figure 6.1), where the aqueous and organic phases are forced through micron-sized membrane pores at high velocities to achieve rapid precipitation at significantly higher flow rates [39].

While the NanoAssemblr is primarily used for bench-scale formulation development, the Pathfinder system is engineered for continuous, scalable manufacturing; a detailed comparison of their specifications is provided in Table 6.1. Ultimately, these distinct mixing geometries and hydrodynamic conditions govern the self-assembly pathways, potentially altering the physicochemical properties and biological performance of the resulting LNPs. Studies indicate that LNPs with CQAs can be produced using a range of controlled mixing technologies, as long as essential factors, such as solvent polarity shifts, mixing duration, and flow-rate ratio, are properly managed [181]. For instance, Forrester et al. reported that alternative mixing approaches, including non-herringbone microfluidic systems and impingement-based mixers, can generate LNPs with comparable size, polydispersity, and encapsulation efficiency, despite differences in mixer design and hydrodynamic conditions [42].

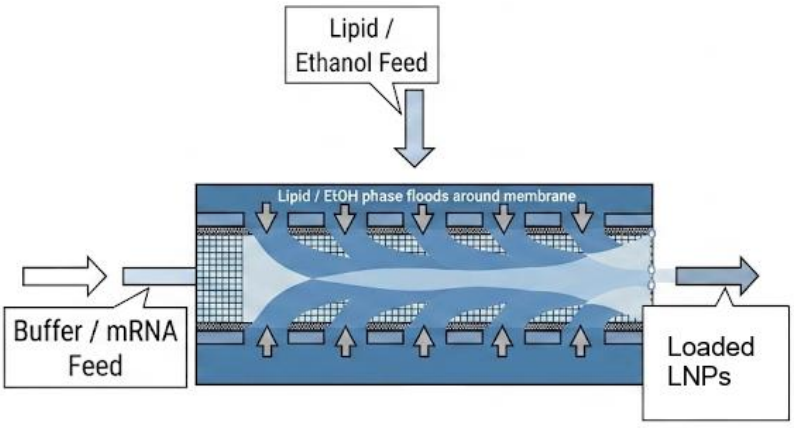

Figure 6.1: Schematic of the Micropore Crossflow micromixer.

Table 6.1: A comparison the Micropore Pathfinder mixer to the NanoAssemblr microfluidic mixer used in the previous chapters of this thesis.

NanoAssemblr (PNI)	Micropore Pathfinder
Staggered herringbone micromixer	Crossflow membrane micromixer
Mixing inside microchannels with herringbone grooves	Mixing across a membrane/crossflow interface
Lower throughput (~up to 20 mL/min)	High throughput (20–200+ mL/min)
Commonly used for lab-scale formulation	Designed for scalable/manufacturing-scale production
Chaotic advection-driven mixing	Crossflow/continuous high-speed mixing
Disposable cartridge system	Stainless steel scalable system

These findings suggest that LNP assembly depends primarily on nanoprecipitation kinetics rather than on mixer design, thereby supporting the use of other high-throughput microfluidic platforms.

As LNP production scales from laboratory to clinical and commercial settings, interest is growing in microfluidic systems capable of operating at much higher flow rates (greater than 100 mL/min) while preserving control over particle CQAs. Scaling these systems is challenging, however, because increasing total flow rate changes mixing time, shear forces, and mixing behaviour, all of which can influence nanoparticle formation and structure. [117]. Consequently, changes in manufacturing speed can affect not only physicochemical attributes such as particle size, polydispersity, and encapsulation efficiency, but also downstream biological performance, including cellular uptake and *in vivo* protein expression.

Recent work by Hussain et al. has provided important validation of crossflow membrane micromixing as a scalable and manufacturing-relevant approach for mRNA–LNP production [39]. Using stainless-steel crossflow micromixing platforms, these authors demonstrated reproducible production of mRNA–LNPs across a wide range of flow rates (10–500 mL/min), while maintaining consistent particle size, low polydispersity, and high encapsulation efficiency from discovery scale through to GMP-relevant production speeds. Importantly, comparable *in vitro* and *in vivo* performance was observed across platforms and scales, highlighting the potential of crossflow micromixing as a robust alternative to conventional microfluidic and jet-based mixers for LNP manufacture.

This final chapter explores the use of the Micropore Pathfinder system to produce mRNA-loaded LNPs at total flow rates ranging from 20 to 200 mL/min, representing a substantial increase in throughput relative to the NanoAssemblr studies reported earlier in this thesis. These experiments represent the first assessment in this work of high-speed, high-throughput LNP manufacturing. LNPs made across this range were evaluated using key physicochemical, *in vitro*, and *in vivo* assays to see whether faster manufacturing affects their properties or performance. By comparing LNPs produced under conditions closer to real manufacturing, this chapter examines whether production speed can be increased without reducing LNP quality or function.

Materials and Methods

Materials

The following were provided by Avanti Research(TM), a Croda brand (Alabaster, AL, USA): 1,2-distearoyl-sn-glycero-3-phosphocholine (DSPC), 1,2-dimyristoyl-rac-glycero-3-methoxypolyethylene glycol-2000 (DMG-PEG 2000), 2-[(polyethylene glycol)-2000]-N,N-ditetradecylacetamide,), [(4-Hydroxybutyl)azanediyl]di(hexane-6,1-diyl) bis(2-hexyldecanoate) (ALC-0315).

EZ Cap™ Firefly Luciferase mRNA was purchased from ApexBio Technology (Houston, TX, USA). Citric acid, sodium citrate tribasic dehydrate, and 25 mm dialysis membrane (MWCO 12,000–14,000 Da) were acquired from Sigma-Aldrich (St. Louis, MO, USA). Phosphate-buffered saline tablets (PBS pH 7.4) were acquired from Oxoid Ltd. (Basingstoke, UK). Tris Base and Ethanol (EtOH) were obtained from Fisher Scientific (Loughborough, UK). Dulbecco's Modified Eagle's Medium, Trypsin-EDTA (0.05%), PBS, pH 7.4 solution and Quant-it™ RiboGreen RNA Assay Kit and Quant-iT™ PicoGreen™ dsDNA Reagent, were purchased from Fisher Scientific UK Limited (Renfrew, UK). ONE-Glo™ Luciferase Assay System and VivoGlo™ Luciferin (*In Vivo* Grade) were acquired from Promega UK (Southampton, UK). BD Insulin Syringes were purchased from Scientific Laboratory Supplies Limited (Nottingham, UK). All solvents and other chemicals were of analytical grade, and an in-house system provided Milli-Q water.

Aqueous and Organic Phase Preparation

The aqueous phase containing mRNA and the organic (lipid) phase were prepared separately before microfluidics. The aqueous phase was prepared using 50 mM citrate

buffer (pH 4), dissolving Firefly Luciferase (Fluc) mRNA, saRNA or pDNA, as well as combinations of these, at concentrations required to maintain a nitrogen to phosphate (N/P) ratio of 6, the molar ratio of ionisable lipid containing positively-charged amines (N) to the mRNA containing negatively-charged phosphates (P).

The lipid molar ratio of the LNPs was 10:38.5:50:1.5% (structural lipid: sterol: cationic lipid: PEGylated lipid), with DSPC, cholesterol, ALC-0315, and DMG-PEG 2000, respectively. The lipid stocks were prepared and stored at concentrations of 5-100 mg/mL, dissolving each lipid in ethanol. The organic phase injected into the microfluidic device had a concentration of 5 mg/mL.

Manufacture of the LNPs using the Micropore Pathfinder™

Lipid nanoparticles (LNPs) were manufactured using the Micropore Pathfinder™20 system (Micropore Technologies Ltd., Redcar, UK), which was used for all experiments in this chapter. The organic phase, containing lipids dissolved in ethanol, and the aqueous phase, consisting of citrate buffer with Firefly Luciferase (FLuc) mRNA, were loaded into stainless steel syringes. The two phases were delivered through separate tubing into the Micropore Pathfinder™ crossflow membrane micromixer, where controlled mixing and LNP self-assembly occurred before the formulations were collected into a 24-well deep-well plate.

A constant aqueous-to-organic flow-rate ratio of 3:1 was used for all formulations. LNPs were produced at total flow rates ranging from 20 to 200 mL/min, in increments of 20 mL/min, yielding 10 distinct flow-rate conditions. All other formulation and processing parameters were held constant to ensure that any differences in LNP physicochemical or biological properties were attributable solely to changes in total flow rate.

Purification

The LNPs were purified by dialysis buffer exchange; the LNP sample in the original ethanol/citrate buffer was exchanged into 200 mL PBS (pH 7.4) for every mL of sample. Samples were dialysed for 4 hours, after which the pH became neutral and the ethanol content was negligible (<1%).

Measuring Critical Quality Attributes (CQAs)

Physicochemical properties

Size (Z-average diameter), polydispersity index (PDI), and zeta potential were measured with the Malvern Panalytical Zetasizer ZS and Zetasizer Ultra, with the Zetasizer software for data acquisition. Size and PDI were measured *via* dynamic light scattering (DLS), using a measurement angle of 173 ° backscatter, and zeta potential was measured using voltage measurements in a Folded Capillary cell. Each of these measurements was performed in triplicate for each experimental repeat (nine measurements per experiment). Post-purification, each sample was prepared for measurement at a lipid concentration of 0.1mg/mL in PBS (for size/PDI) or deionised water (for zeta potential) to achieve attenuation values between 7 and 8. Pre-purification measurements for size and PDI were performed with citrate buffer as the diluent. ZEN0040 disposable micro-cuvettes were used to measure size and polydispersity, and DTS1070 folded capillary zeta cells were used for zeta potential measurements, with 400 µL and 1,000 µL of diluted LNPs added, respectively. The material refractive index and absorption were 1.45 and 0.001, respectively. The dispersant refractive index and absorption were 1.33 and 0.8872 cP, respectively, for water; 1.335 and 1.02 cP, respectively, for PBS; and 1.47 and 1.28 cP for citrate buffer.

mRNA content

Encapsulation efficiency and mRNA recovery were measured using the RiboGreen™ mRNA quantification assay kit according to manufacturer recommendations. Tris-EDTA (TE) buffer was used as the diluent throughout this assay. The fluorescent dye was used to quantify mRNA in the presence and absence of 2% Triton to lyse the LNPs. Two RNA standard curves were used to quantify mRNA. The fluorescence signal was read using the POLARstar Omega (BMG Labtech, UK) and GloMax (Promega, UK) plate readers using 475-485 nm excitation and 525 nm emission wavelengths. The total RNA for each sample from the Triton wells and the free (unentrapped) RNA from the TE-only wells were obtained during analysis. The mRNA encapsulation efficiency (EE%) and recovery were calculated as previously described [153].

In vitro expression

LNP FLuc mRNA expression was analysed in HeLa cells using firefly luciferase as a bioluminescent reporter. Cells were cultured in Dulbecco's Modified Eagle Medium

(DMEM) with sodium pyruvate, supplemented with 10% foetal bovine serum (FBS), 1% penicillin/streptomycin and L-glutamine. Cells were added to a 96-well white/clear bottom plate, at a concentration of 10,000 cells/ 100µL in media and cultured for 48 hours, after which LNPs were added. LNPs were formulated as above with payloads comprising Firefly Luciferase- encoding mRNA, saRNA and/or pDNA. LNP formulations were added to the cells, replacing the growth medium, and diluted in medium to total mRNA concentrations of 1 µg/mL and 0.5 µg/mL, in triplicate, with control wells containing cells only. Cells were incubated with LNPs for 24 hours prior to the addition of the luciferase reagent. Luciferase reagent, prepared as per the manufacturer's instructions, was added to each well containing 100 µL of media and cells from the previous day, bringing the total volume to 200 µL. The mixture was mixed thoroughly and left to incubate for 3 minutes. The luminescence of the plates was read using the GloMax plate reader (Promega, UK).

In vivo expression

LNP expression in BALB/c mice was assessed using firefly luciferase as a bioluminescent reporter. Three mice per formulation received intramuscular injections of 50 µL into each quadriceps (100 µL total) containing 40 µg/mL LNPs, yielding a total dose of 4 µg mRNA (2 µg per leg). Mice were anaesthetised and imaged using the IVIS® Spectrum system and Living Image® software (PerkinElmer, UK). For luciferase measurements, each mouse was injected subcutaneously with a 30 mg/mL D-luciferin solution (5 µL per gram of body weight, 150 mg/kg). This was repeated at every imaging time point, with images collected 10 minutes after injection using the luminescence setting. Mice were imaged at 6 h, 24 h, 48 h, and on days 5 and 8. Bioluminescence was quantified at the injection sites (hind limbs) and in the upper abdominal region (liver) from both supine and prone positions.

Statistical analysis

The mean and standard deviation were calculated for all experiments, performed in independent triplicate batches unless otherwise stated. Each batch was manufactured on a different day to account for inter-day variation. For hydrodynamic size, polydispersity, zeta potential, mRNA encapsulation, and mass balance, three measurements were taken for each batch; therefore, the statistical analysis groups were n=9. For statistical comparison of groups, one- or two-way ANOVA was performed

on parametric data sets, and the Kruskal-Wallis test with Dunn's post hoc test was performed on non-parametric data sets. On graphs, statistical significance is indicated by individual p-values <0.05, whereas (ns) denotes no statistical significance.

Results and Discussion

LNPs manufactured across a range of total flow rates were first characterised to determine how increases in process speed influenced key physicochemical critical quality attributes (CQAs). Particle size showed a dependence on total flow rate, spanning mean hydrodynamic diameters of approximately 95-122 nm (Figure 6.2B). Increasing the total flow rate from 20 mL/min resulted in a progressive reduction in particle size, consistent with faster solvent exchange and enhanced micromixing, leading to more rapid lipid nanoprecipitation and restricted particle growth [38]. A plateau in particle size was observed across intermediate flow rates (60–160 mL/min), with LNPs consistently measuring approximately 95–100 nm, suggesting that above a threshold mixing intensity, further increases in flow rate do not substantially alter nanoparticle assembly under these formulation conditions. At the highest flow rate tested (200 mL/min), a modest increase in particle size was observed, with average diameters increasing to approximately 122 nm, potentially indicating a transition to a different hydrodynamic or mixing regime or the onset of less-controlled assembly at extreme processing speeds.

Polydispersity indices (PDI) remained low (<0.2) across all flow-rate conditions (Figure 6.2B), indicating that narrow size distributions were maintained even under intensified manufacturing conditions. However, the slightly elevated PDI observed at 200 mL/min suggests increased heterogeneity in particle formation at the upper limit of the system's operating range. Zeta potential measurements were close to neutral for all samples, with average values ranging from approximately -1 to -8 mV (Figure 6.2A), indicating that variation in total flow rate did not substantially affect LNP surface charge and suggesting consistent lipid ionisation and surface composition across conditions.

Compared with size and zeta potential, mRNA encapsulation efficiency was more strongly affected by the manufacturing speed of the LNPs. At total flow rates between 20 and 180 mL/min, encapsulation efficiency remained at around 74-86%, even though these values were lower than those often reported for other microfluidic systems [153, 182].

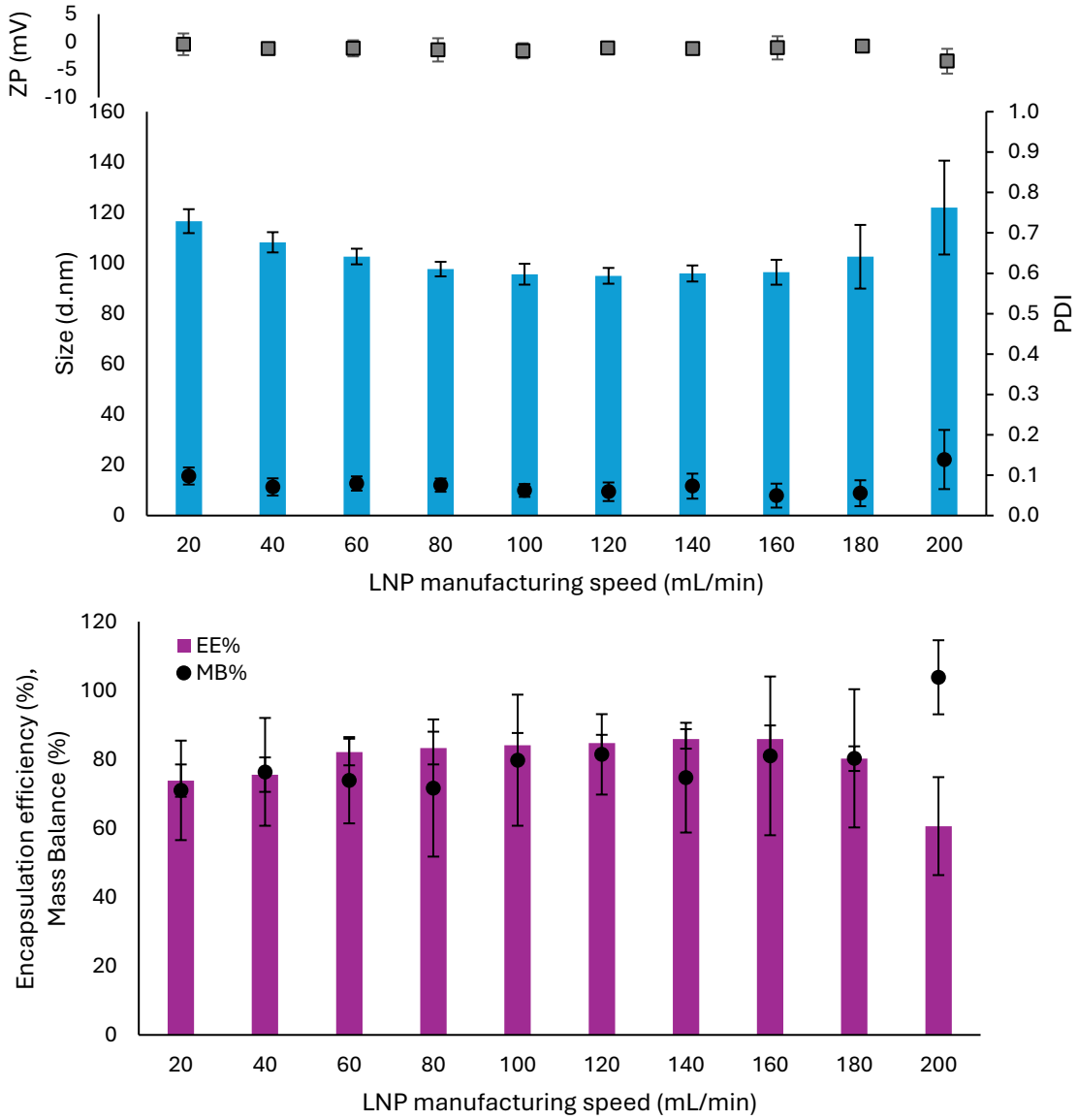

Figure 6.2: Physico-chemical attributes of ALC-0315 LNPs with different manufacturing speeds on the Pathfinder. The LNPs were manufactured with an N/P of 6 from 5mg/mL lipid stocks and purified by dialysis in pH 7.4 PBS for 4 hours. Each measurement is a mean of three independent batches ± standard deviation.

At 200 mL/min, however, encapsulation efficiency decreased to approximately 61% and became more variable. This suggests that at very high flow rates, the timing of lipid assembly and mRNA loading may no longer be well aligned. Despite this, mRNA mass balance remained above 70% across all samples, indicating that little mRNA was lost during processing and that the drop in encapsulation at 200 mL/min was likely due to changes in particle formation rather than degradation or system loss.

Overall, these results show that the Micropore Pathfinder™ platform supports reproducible LNP manufacture across a wide range of manufacturing-relevant flow rates, with key physicochemical CQAs largely maintained up to 180 mL/min. This behaviour is consistent with the concept of "limit-size" LNP formation, in which sufficiently rapid microfluidic mixing results in particle sizes that become largely insensitive to further increases in flow rate, with LNP dimensions instead governed by formulation composition and self-assembly kinetics [94].

To understand these dynamics, it is useful to contrast the mixing mechanics of this system with traditional microfluidics. The NanoAssemblr platform uses staggered herringbone microchannels to cause chaotic advection, enabling controlled LNP self-assembly at relatively low flow rates. Conversely, the Micropore Pathfinder™ system uses cross-flow membrane micromixing, forcing fluid phases through micron-scale pores at high speeds to drive rapid nanoprecipitation [39]. While herringbone mixers are optimised for lab-scale development, the Pathfinder system is engineered for continuous, high-throughput manufacturing.

These different geometries and fluid dynamics alter assembly kinetics, which can modify the properties and biological performance of the resulting LNPs. This difference in mixing intensity explains why although deviations in particle size and encapsulation efficiency were observed at 200 mL/min, physicochemical characterisation alone is insufficient to predict functional performance. Therefore, LNPs produced across the tested flow-rate range were next evaluated in *in vitro* and *in vivo* models to determine whether flow-rate-dependent differences influence mRNA delivery and expression.

The functional performance of LNPs manufactured at different total flow rates was evaluated *in vitro* using HeLa cells. Luciferase expression was assessed 24 hours post-transfection and showed variability across flow-rate speeds (Figure 6.3).

LNPs produced at 200 mL/min resulted in the lowest luciferase expression levels. They were significantly less effective than LNPs manufactured at intermediate flow rates of 80, 100, 120, and 160 mL/min, which produced the highest mean expression levels. However, variability in expression limited the statistical significance of differences between most flow rates, with the 200 mL/min condition being the only group consistently distinguishable from the higher-performing samples.

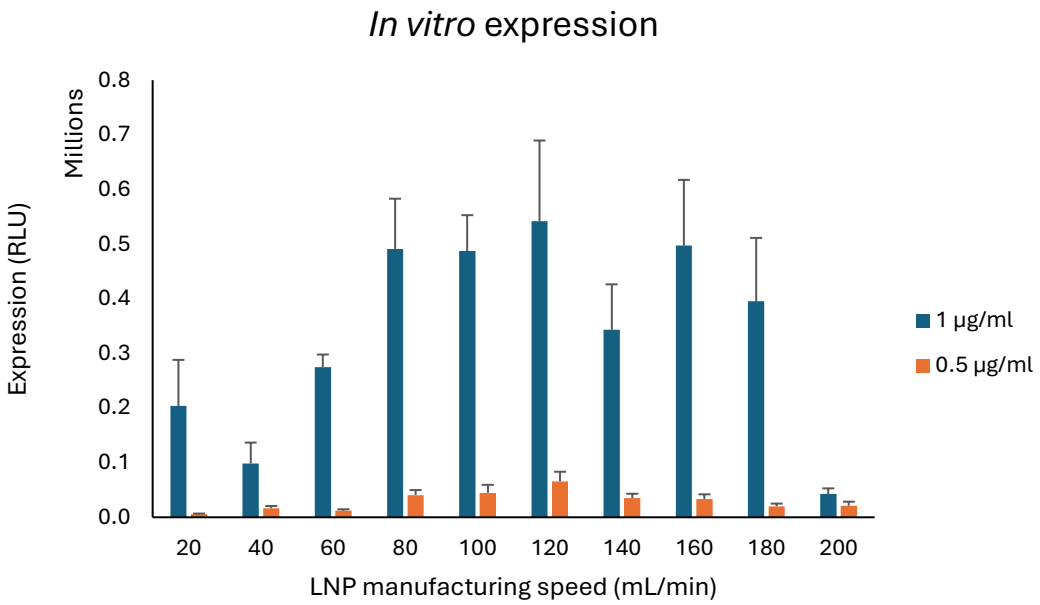

Figure 6.3: *In vitro* Fluc expression in HeLa cells dosed with either 1 µg/mL or 0.5 µg/mL total mRNA. The LNPs were manufactured at different speeds on the Pathfinder, with an N/P of 6 from 5 mg/mL lipid stocks and purified by dialysis in pH 7.4 PBS. Each measurement represents the mean of three independent batches, with error bars indicating ± SEM.

The lower *in vitro* expression observed for LNP samples produced at 200 mL/min is consistent with their reduced mRNA encapsulation efficiency, suggesting that lower nucleic-acid loading contributes to weaker transfection. In contrast, LNPs manufactured at flow rates between 20 and 180 mL/min showed similar levels of luciferase expression, indicating that moderate increases in manufacturing speed do not meaningfully affect functional delivery in this assay. Overall, these findings show that LNPs made across most of the tested flow-rate range maintain comparable *in vitro* performance. Consistent with observations by Shkodra et al. (2025), who reported no flow-rate-dependent differences in LNP activity using a jet-impingement mixer [118], the present study also demonstrates that *in vitro* performance remains stable across a wide range of manufacturing speeds when using a crossflow micromixing platform.

In vivo performance of LNPs manufactured at different total flow rates was assessed by measuring luciferase expression over time using bioluminescence imaging (Figure 6.4). Signal intensity was quantified at multiple post-dosing time points for each formulation, enabling comparison of expression profiles across manufacturing conditions.

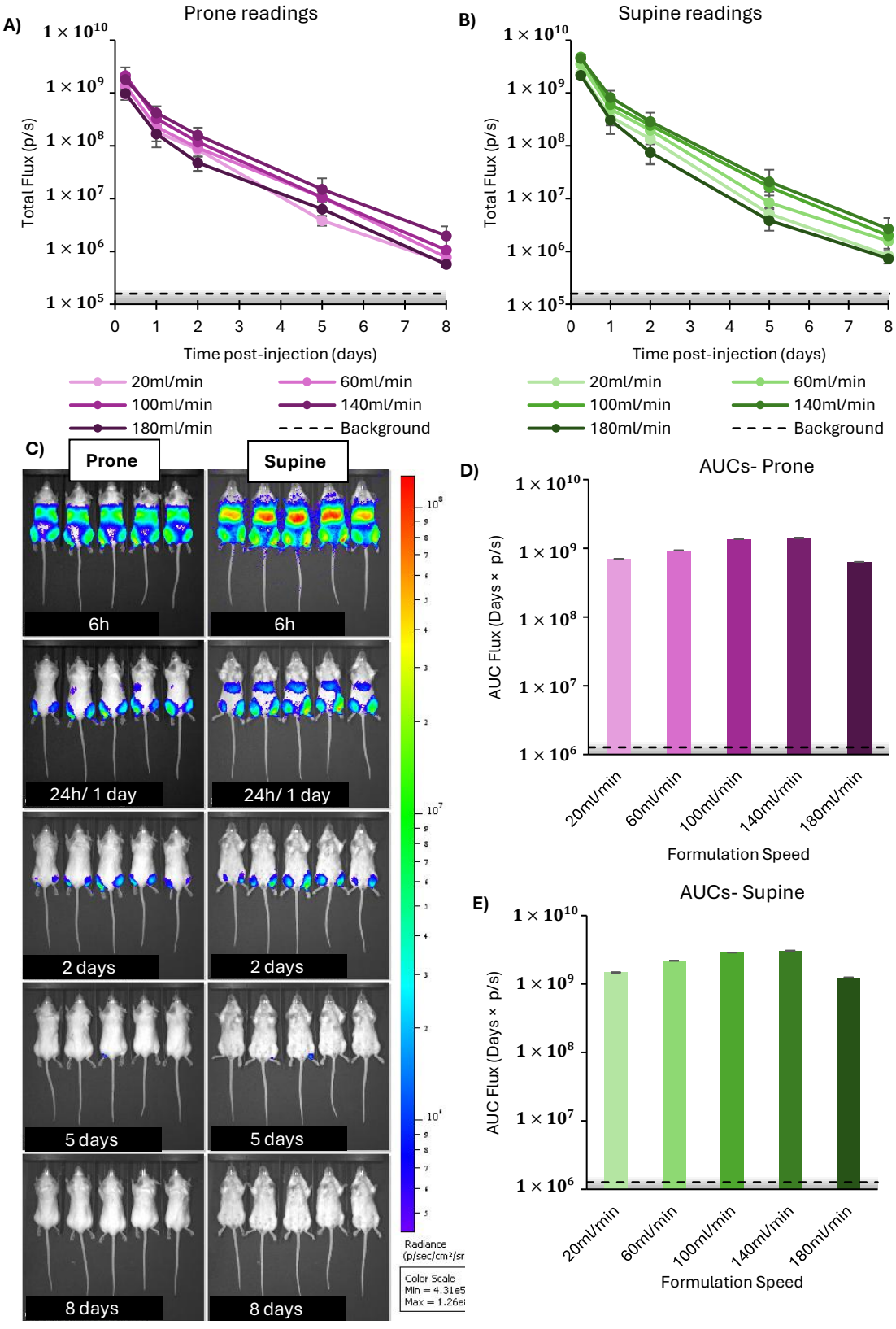

Figure 6.4: Intramuscular *in vivo* expression of ALC-0315 LNPs produced at different total flow rates in BALB/c mice. Mice received 2 µg of total nucleic acid per intramuscular injection and were imaged starting 6 hours after injection, then periodically up to 168 days (24 weeks). A-B) Average luminescence values for each formulation at each time point, measured with mice in the prone (A) or

supine (B) position. C) Representative IVIS images showing expression from 6 hours to 8 days after injection. D-E) Area under the curve (AUC) of luminescence over time for prone (D) and supine (E) measurements.Mice left to right = 20, 60, 100, 140, and 180 mL/min. Each data point represents the mean of three independent repeats, with error bars showing ± SE.

To enable a representative yet practical comparison across the full flow-rate range, five formulations were selected for *in vivo* evaluation at flow rates of 20, 60, 100, 140, and 180 mL/min, spanning low, intermediate, and high manufacturing speeds.All formulations produced robust luciferase expression *in vivo*, with signal intensity decreasing over time as expected for transient mRNA expression. No statistically significant differences in bioluminescence were observed between LNPs manufactured at different flow rates at any individual time point. To account for potential differences in overall expression kinetics, the area under the bioluminescence–time curve (AUC) was calculated for each formulation (Figure 6.4D-E). Consistent with the time-point analysis, AUC values did not differ significantly between samples, indicating comparable total protein expression throughout the study.This outcome was observed for measurements acquired from mice imaged in both supine and prone orientations, supporting the robustness of the equivalence observed across formulations.

Collectively, these *in vivo* data demonstrate that LNP formulations manufactured using the Micropore Pathfinder™ platform across a wide range of total flow rates exhibit comparable functional performance. Importantly, despite modest flow-rate-dependent differences observed during physicochemical characterisation and *in vitro* transfection, these variations did not translate into measurable differences in *in vivo* protein expression within the tested operating window. To date, few studies have directly examined how LNP manufacturing speed affects *in vivo* performance. In line with our finding that changing flow rate did not meaningfully alter *in vivo* expression, Shepherd et al. reported that luciferase mRNA-LNP potency in mice remained unchanged when production throughput was scaled across microfluidic devices [107, 117]. Although previous work has shown that LNPs produced under fast, efficient mixing conditions can retain strong *in vivo* activity, systematic comparisons across a broad range of total flow rates are still limited [39, 42, 118].

The *in vivo* findings in this study support the conclusion that high-throughput microfluidic manufacture can be achieved without compromising *in vivo* efficacy, provided that flow rates remain within an appropriate operational range.

Conclusions

This chapter evaluated the impact of manufacturing speed on the physicochemical and biological performance of mRNA-loaded lipid nanoparticles produced using the Micropore Pathfinder™ crossflow mixing platform. By systematically varying total flow rate across a manufacturing-relevant range (20–200 mL/min), this work aimed to determine whether process intensification alters LNP critical quality attributes or functional efficacy.

Physicochemical characterisation demonstrated that LNP size, polydispersity, and surface charge were largely preserved across a broad flow-rate window, with consistent particle formation observed up to 180 mL/min. While particle size plateaued at intermediate flow rates, modest deviations in the size distribution and a reduction in mRNA encapsulation efficiency were observed at the highest flow rate tested (200 mL/min), suggesting an upper operational boundary for this formulation and system configuration.

Functional assessment revealed that flow-rate-dependent differences observed at the physicochemical level had a limited impact on biological performance. *In vitro* luciferase expression in HeLa cells was broadly comparable across most manufacturing conditions, with reduced expression only evident for LNPs produced at 200 mL/min, consistent with their lower encapsulation efficiency. Importantly, *in vivo* evaluation demonstrated robust and comparable protein expression for LNPs manufactured across representative low, intermediate, and high flow rates, with no significant differences in expression kinetics or total protein output observed over the study period.

Overall, these findings demonstrate that high-throughput microfluidic manufacture of mRNA–LNPs using the Micropore Pathfinder™ platform can be achieved without compromising *in vivo* efficacy across a wide range of operating conditions. This work supports the translational relevance of crossflow membrane mixing as a scalable manufacturing strategy for LNP-based therapeutics. It highlights the importance of defining operational flow-rate windows to balance throughput with formulation robustness. Together, the results presented in this chapter reinforce the feasibility of accelerating microfluidic processes for the scalable production of functional mRNA-LNPs.

CHAPTER 7: FINAL CONCLUSIONS AND FUTURE WORKS

Overview and Scope of the Thesis

The overarching aim of this thesis was to investigate how manufacturing parameters, lipid composition, and nucleic acid payload influence the physicochemical properties and biological performance of lipid nanoparticles (LNPs) formulated using microfluidic technologies. Through a combination of systematic optimisation studies and targeted *in vitro* and *in vivo* evaluations, this work sought to improve understanding of structure–function relationships within LNP systems and to support the rational design of robust and reproducible formulations for nucleic acid delivery.

The thesis was organised to progress from basic manufacturing optimisation, through controlled examination of particle size and lipid composition, to assessment of alternative nucleic acid payloads and scalable manufacturing methods. Together, these chapters provide a thorough evaluation of how formulation and process variables interact to influence LNP performance across various experimental settings.

Establishment of Robust Microfluidic Manufacturing Conditions (Chapter 2)

The initial optimisation results chapter established a reproducible microfluidic manufacturing framework that supported all subsequent experimental work. Systematic evaluation of key process parameters, including flow rate ratio (FRR), total flow rate (TFR), N/P ratio, lipid concentration, solvent choice, buffer composition, and purification method, showed that small changes in manufacturing conditions can greatly affect critical quality attributes (CQAs), such as particle size, polydispersity, surface charge, encapsulation efficiency, and mass balance.

This work emphasised the FRR/lipid: aqueous phase ratio as a key factor influencing particle size and uniformity, while downstream processing steps, especially the purification method, were shown to impact formulation recovery and stability. These studies facilitated the identification of parameter ranges that produced stable, reproducible LNPs suitable for subsequent biological evaluation. By establishing and standardising manufacturing conditions, this chapter ensured that variability from formulation processes did not interfere with the interpretation of results in later chapters.

Size Control as a Design Parameter for LNP Performance (Chapter 3)

Building on the optimised manufacturing framework from the previous chapter, this chapter demonstrated that controlled modulation of LNP size could be achieved by adjusting the aqueous-to-organic phase ratio during microfluidic formulation. This method allowed precise size adjustment without altering lipid composition, offering a useful strategy for investigating the role of particle size independently of other formulation variables.

In vitro studies showed a size-dependent relationship between LNP transgene expression and particle size, with larger particles generally exhibiting higher expression in certain cell lines, up to a clear threshold. Conversely, *in vivo* studies displayed a broader tolerance to size variation, with strong expression observed across a specific size range and decreased performance at larger diameters. These findings imply that although size is a key design factor, *in vivo* expression is relatively tolerant to moderate size variations compared to *in vitro* systems. This emphasises the importance of assessing LNP performance in different biological contexts.

Influence of Lipid Composition on Physicochemical Properties and Biodistribution (Chapter 4)

A systematic comparison of clinically relevant and proprietary ionisable lipids showed that lipid identity critically influences the physicochemical properties of LNPs, *in vitro* expression, and *in vivo* biodistribution. Although some formulations exhibited strong *in vitro* performance, this did not always correspond to similar *in vivo* expression, especially after intravenous administration.

These results reinforce the idea that lipid structure–function relationships are highly context-dependent and that *in vitro* screening alone is inadequate to forecast *in vivo* performance. Variations in biodistribution patterns, including preferential liver or spleen expression, further highlight the importance of lipid chemistry in shaping biological fate. Although sterol substitution influenced LNP properties, the choice of ionisable lipid proved to be the main factor affecting overall formulation performance.

Modulation of Expression Kinetics Through Payload Identity (Chapter 5)

A key contribution of this chapter was the systematic comparison of LNPs encapsulating different nucleic acid payloads, including messenger RNA (mRNA), self-amplifying RNA (saRNA), plasmid DNA (pDNA), and specific combinations of these. Using identical lipid compositions and manufacturing conditions, distinct expression profiles were observed for each payload type in both *in vitro* and *in vivo* models.

mRNA produced rapid, high early expression; saRNA generated delayed but sustained expression; and pDNA enabled prolonged, low-level expression. Importantly, combined-payload formulations behaved predictably according to the proportional contributions of each payload, with no evidence of synergistic or antagonistic interactions. These findings demonstrate that expression kinetics can be modulated through payload selection without altering the LNP carrier system, providing a flexible strategy for tailoring therapeutic profiles.

Assessment of Alternative Manufacturing Platforms (Chapter 6)

The final experimental chapter evaluated an alternative microfluidic manufacturing platform to assess the robustness and scalability of LNP production. Across the range of flow rates tested, no significant differences in *in vivo* expression were observed, indicating that LNP performance was maintained despite increased manufacturing throughput. These findings provide preliminary support for the scalability of microfluidic LNP manufacturing and suggest that alternative platforms may be suitable for higher-throughput production without compromising biological performance.

Future Directions and Outlook

While this thesis helps advance understanding of LNP formulation and performance, several challenges remain. A recurring limitation identified throughout the work was the weak correlation between *in vitro* and *in vivo* expression outcomes. This is a common problem in LNP and other pharmaceutical research. Formulations that performed well *in vitro* did not always exhibit comparable *in vivo* behaviour, and vice versa. This lack of predictability complicates formulation screening, increases development costs, and raises ethical considerations related to animal use, such as we don't know if what we're injecting in animals is worthwhile.

Future efforts should aim to enhance the predictive power of *in vitro* models, possibly by employing three-dimensional cell cultures, co-culture systems, and organ-on-chip technologies that more accurately simulate physiological environments. Incorporating initial *in vivo* pilot studies early on may also help lessen false-negative and false-positive outcomes during formulation selection.

Further investigation into the mechanistic basis of payload-specific expression kinetics, endosomal escape efficiency, and protein corona formation would improve understanding of LNP behaviour *in vivo*. Additionally, expanded exploration of formulation robustness and long-term stability, especially under non-frozen storage conditions, would support better manufacturability and global distribution of LNP-based therapeutics.

Concluding Remarks

In summary, this thesis offers a detailed investigation into the formulation, manufacturing, and biological performance of lipid nanoparticles for nucleic acid delivery. By combining optimisation of microfluidic processes with systematic assessment of size, lipid composition, payload identity, and scalability, this work advances the rational design of durable LNP systems and supports their ongoing development for therapeutic and vaccine applications.

REFERENCES

1. Jeevanandam, J., et al., *Review on nanoparticles and nanostructured materials: history, sources, toxicity and regulations.* Beilstein J Nanotechnol, 2018. **9**: p. 1050-1074.
2. Tenchov, R., et al., *Lipid Nanoparticles–From Liposomes to mRNA Vaccine Delivery, a Landscape of Research Diversity and Advancement.* ACS Nano, 2021. **15**(11): p. 16982-17015.
3. Wahlich, J., et al., *Nanomedicines for the Delivery of Biologics.* Pharmaceutics, 2019. **11**(5).
4. Stewart, M.P., et al., *Challenges in carrier-mediated intracellular delivery: moving beyond endosomal barriers.* Wiley Interdiscip Rev Nanomed Nanobiotechnol, 2016. **8**(3): p. 465-78.
5. Mahmoud, K., et al., *Lipid based nanoparticles as a novel treatment modality for hepatocellular carcinoma: a comprehensive review on targeting and recent advances.* J Nanobiotechnology, 2022. **20**(1): p. 109.
6. Bangham, A.D., M.M. Standish, and J.C. Watkins, *Diffusion of univalent ions across the lamellae of swollen phospholipids.* J Mol Biol, 1965. **13**(1): p. 238-52.
7. Bangham, A.D. and R.W. Horne, *Negative Staining of Phospholipids and Their Structural Modification by Surface-Active Agents as Observed in the Electron Microscope.* J Mol Biol, 1964. **8**: p. 660-8.
8. Chang, H.I. and M.K. Yeh, *Clinical development of liposome-based drugs: formulation, characterization, and therapeutic efficacy.* Int J Nanomedicine, 2012. **7**: p. 49-60.
9. Shah, S., et al., *Liposomes: Advancements and innovation in the manufacturing process.* Adv Drug Deliv Rev, 2020. **154-155**: p. 102-122.
10. Parvin, N., T.K. Mandal, and S.W. Joo, *The Impact of COVID-19 on RNA Therapeutics: A Surge in Lipid Nanoparticles and Alternative Delivery Systems.* Pharmaceutics, 2024. **16**(11).
11. Kiaie, S.H., et al., *Recent advances in mRNA-LNP therapeutics: immunological and pharmacological aspects.* J Nanobiotechnology, 2022. **20**(1): p. 276.
12. Zhang, C., et al., *Modification of Lipid-Based Nanoparticles: An Efficient Delivery System for Nucleic Acid-Based Immunotherapy.* Molecules, 2022. **27**(6).
13. Hassett, K.J., et al., *Impact of lipid nanoparticle size on mRNA vaccine immunogenicity.* J Control Release, 2021. **335**: p. 237-246.
14. Cullis, P.R. and P.L. Felgner, *The 60-year evolution of lipid nanoparticles for nucleic acid delivery.* Nat Rev Drug Discov, 2024. **23**(9): p. 709-722.
15. Hou, X., et al., *Lipid nanoparticles for mRNA delivery.* Nat Rev Mater, 2021. **6**(12): p. 1078-1094.
16. Zwolsman, R., et al., *Engineering Lipid Nanoparticles for mRNA Immunotherapy.* Wiley Interdiscip Rev Nanomed Nanobiotechnol, 2025. **17**(2): p. e70007.
17. Li, Y., et al., *Lipid-mRNA nanoparticles landscape for cancer therapy.* Front Bioeng Biotechnol, 2022. **10**: p. 1053197.
18. Chou-Yi, H., et al., *An overview of nanoparticles in drug delivery: Properties and applications.* South African Journal of Chemical Engineering, 2023. **46**: p. 233-270.
19. Ranim, S., R. Géza, and S. Tamás, *Pharmacokinetics and toxicity of inorganic nanoparticles and the physicochemical properties/factors affecting them.* Journal of Drug Delivery Science and Technology, 2024. **99**: p. 105979.
20. Li, X., et al., *Viral Vector-Based Gene Therapy.* Int J Mol Sci, 2023. **24**(9).
21. Thomas, C.E., A. Ehrhardt, and M.A. Kay, *Progress and problems with the use of viral vectors for gene therapy.* Nat Rev Genet, 2003. **4**(5): p. 346-58.

22. Rui, Y., D.R. Wilson, and J.J. Green, *Non-Viral Delivery To Enable Genome Editing.* Trends Biotechnol, 2019. **37**(3): p. 281-293.
23. Beach, M.A., et al., *Polymeric Nanoparticles for Drug Delivery.* Chem Rev, 2024. **124**(9): p. 5505-5616.
24. Alshammari, B.H., et al., *Organic and inorganic nanomaterials: fabrication, properties and applications.* RSC Adv, 2023. **13**(20): p. 13735-13785.
25. Tonga, G.Y., et al., *Inorganic Nanoparticles for Therapeutic Delivery: Trials, Tribulations and Promise.* Curr Opin Colloid Interface Sci, 2014. **19**(2): p. 49-55.
26. Bhatti, R., et al., *Inorganic Nanoparticles: Toxic Effects, Mechanisms of Cytotoxicity and Phytochemical Interactions.* Adv Pharm Bull, 2022. **12**(4): p. 757-762.
27. Kamikubo, Y. and H. Sakairi, *Silica nanoparticle toxicity: cellular mechanisms, neurotoxicological concerns, and environmental perspectives.* Frontiers in Nanotechnology, 2025. **Volume 7 - 2025**.
28. Di Bella, M.A., *Overview and Update on Extracellular Vesicles: Considerations on Exosomes and Their Application in Modern Medicine.* Biology (Basel), 2022. **11**(6).
29. Kumar, M.A., et al., *Extracellular vesicles as tools and targets in therapy for diseases.* Signal Transduction and Targeted Therapy, 2024. **9**(1): p. 27.
30. Zheng, X., et al., *Small extracellular vesicles purification and scale-up.* Front Immunol, 2024. **15**: p. 1344681.
31. Yoneda, S., et al., *Enhancement of cerebroprotective effects of lipid nanoparticles encapsulating FK506 on cerebral ischemia/reperfusion injury by particle size regulation.* Biochem Biophys Res Commun, 2022. **611**: p. 53-59.
32. Fan, Y., M. Marioli, and K. Zhang, *Analytical characterization of liposomes and other lipid nanoparticles for drug delivery.* J Pharm Biomed Anal, 2021. **192**: p. 113642.
33. Naseri, N., H. Valizadeh, and P. Zakeri-Milani, *Solid Lipid Nanoparticles and Nanostructured Lipid Carriers: Structure, Preparation and Application.* Adv Pharm Bull, 2015. **5**(3): p. 305-13.
34. Assali, M. and A.N. Zaid, *Features, applications, and sustainability of lipid nanoparticles in cosmeceuticals.* Saudi Pharm J, 2022. **30**(1): p. 53-65.
35. Gao, Y., et al., *Looking back, moving forward: protein corona of lipid nanoparticles.* J Mater Chem B, 2024. **12**(23): p. 5573-5588.
36. Webb, C., et al., *Current Status and Future Perspectives on MRNA Drug Manufacturing.* Mol Pharm, 2022. **19**(4): p. 1047-1058.
37. Anderluzzi, G., et al., *Investigating the Impact of Delivery System Design on the Efficacy of Self-Amplifying RNA Vaccines.* Vaccines (Basel), 2020. **8**(2).
38. Roces, C.B., et al., *Manufacturing Considerations for the Development of Lipid Nanoparticles Using Microfluidics.* Pharmaceutics, 2020. **12**(11).
39. Hussain, M., et al., *Production of mRNA lipid nanoparticles using advanced crossflow micromixing.* J Pharm Pharmacol, 2024. **76**(12): p. 1572-1583.
40. Lindsay, S., et al., *Exploring the Challenges of Lipid Nanoparticle Development: The In Vitro–In Vivo Correlation Gap.* Vaccines, 2025. **13**(4): p. 339.
41. Binici, B., et al., *Exploring the impact of commonly used ionizable and pegylated lipids on mRNA-LNPs: A combined in vitro and preclinical perspective.* J Control Release, 2025. **377**: p. 162-173.
42. Forrester, J., et al., *Low-Cost Microfluidic Mixers: Are They up to the Task?* Pharmaceutics, 2025. **17**(5).
43. Carrasco, M.J., et al., *Ionization and structural properties of mRNA lipid nanoparticles influence expression in intramuscular and intravascular administration.* Commun Biol, 2021. **4**(1): p. 956.

44. Schoenmaker, L., et al., *mRNA-lipid nanoparticle COVID-19 vaccines: Structure and stability.* Int J Pharm, 2021. **601**: p. 120586.
45. Yang, L., et al., *Recent Advances in Lipid Nanoparticles for Delivery of mRNA.* Pharmaceutics, 2022. **14**(12).
46. Sharma, P., et al., *The immunostimulatory nature of mRNA lipid nanoparticles.* Adv Drug Deliv Rev, 2024. **205**: p. 115175.
47. Blakney, A.K., S. Ip, and A.J. Geall, *An Update on Self-Amplifying mRNA Vaccine Development.* Vaccines (Basel), 2021. **9**(2).
48. Suzuki, Y. and H. Ishihara, *Difference in the lipid nanoparticle technology employed in three approved siRNA (Patisiran) and mRNA (COVID-19 vaccine) drugs.* Drug Metab Pharmacokinet, 2021. **41**: p. 100424.
49. Bathula, N.V., et al., *Delivery vehicle and route of administration influences self-amplifying RNA biodistribution, expression kinetics, and reactogenicity.* J Control Release, 2024. **374**: p. 28-38.
50. Chatterjee, S., et al., *Endosomal escape: A bottleneck for LNP-mediated therapeutics.* Proc Natl Acad Sci U S A, 2024. **121**(11): p. e2307800120.
51. *Let's talk about lipid nanoparticles.* Nature Reviews Materials, 2021. **6**(2): p. 99-99.
52. Paramasivam, P., et al., *Endosomal escape of delivered mRNA from endosomal recycling tubules visualized at the nanoscale.* J Cell Biol, 2022. **221**(2).
53. Jung, H.N., et al., *Lipid nanoparticles for delivery of RNA therapeutics: Current status and the role of in vivo imaging.* Theranostics, 2022. **12**(17): p. 7509-7531.
54. Gilleron, J., et al., *Image-based analysis of lipid nanoparticle-mediated siRNA delivery, intracellular trafficking and endosomal escape.* Nat Biotechnol, 2013. **31**(7): p. 638-46.
55. Kulkarni, J.A., et al., *On the Formation and Morphology of Lipid Nanoparticles Containing Ionizable Cationic Lipids and siRNA.* ACS Nano, 2018. **12**(5): p. 4787-4795.
56. Wang, X., X. Shi, and R. Wang, *Regulating mRNA endosomal escape through lipid rafts: A review.* Int J Pharm, 2025. **675**: p. 125571.
57. Hald Albertsen, C., et al., *The role of lipid components in lipid nanoparticles for vaccines and gene therapy.* Adv Drug Deliv Rev, 2022. **188**: p. 114416.
58. Patel, S., et al., *Naturally-occurring cholesterol analogues in lipid nanoparticles induce polymorphic shape and enhance intracellular delivery of mRNA.* Nat Commun, 2020. **11**(1): p. 983.
59. Eygeris, Y., et al., *Deconvoluting Lipid Nanoparticle Structure for Messenger RNA Delivery.* Nano Letters, 2020. **20**(6): p. 4543-4549.
60. Borah, A., et al., *From in vitro to in vivo: The Dominant role of PEG-Lipids in LNP performance.* Eur J Pharm Biopharm, 2025. **212**: p. 114726.
61. Igyarto, B.Z., S. Jacobsen, and S. Ndeupen, *Future considerations for the mRNA-lipid nanoparticle vaccine platform.* Curr Opin Virol, 2021. **48**: p. 65-72.
62. Heinz, F.X. and K. Stiasny, *Distinguishing features of current COVID-19 vaccines: knowns and unknowns of antigen presentation and modes of action.* NPJ Vaccines, 2021. **6**(1): p. 104.
63. Wayne, C.J. and A.K. Blakney, *Self-amplifying RNA COVID-19 vaccine.* Cell, 2024. **187**(8): p. 1822-1822 e1.
64. Li, S., et al., *Payload distribution and capacity of mRNA lipid nanoparticles.* Nat Commun, 2022. **13**(1): p. 5561.
65. Elliott, T., et al., *Enhanced immune responses following heterologous vaccination with self-amplifying RNA and mRNA COVID-19 vaccines.* PLoS Pathog, 2022. **18**(10): p. e1010885.

66. Cullis, P.R. and M.J. Hope, *Lipid Nanoparticle Systems for Enabling Gene Therapies.* Mol Ther, 2017. **25**(7): p. 1467-1475.
67. Hassett, K.J., et al., *Optimization of Lipid Nanoparticles for Intramuscular Administration of mRNA Vaccines.* Mol Ther Nucleic Acids, 2019. **15**: p. 1-11.
68. Nakamura, K., K. Aihara, and T. Ishida, *Importance of Process Parameters Influencing the Mean Diameters of siRNA-Containing Lipid Nanoparticles (LNPs) on the in Vitro Activity of Prepared LNPs.* Biol Pharm Bull, 2022. **45**(4): p. 497-507.
69. Jallow, M.B., K. Huang, and M. Qiu, *Versatility of LNPs across different administration routes for targeted RNA delivery.* J Mater Chem B, 2025. **13**(26): p. 7637-7652.
70. Thi, T.T.H., et al., *Lipid-Based Nanoparticles in the Clinic and Clinical Trials: From Cancer Nanomedicine to COVID-19 Vaccines.* Vaccines (Basel), 2021. **9**(4).
71. Fulton, M.D. and W. Najahi-Missaoui, *Liposomes in Cancer Therapy: How Did We Start and Where Are We Now.* Int J Mol Sci, 2023. **24**(7).
72. Dolgin, E., *The tangled history of mRNA vaccines.* Nature, 2021. **597**(7876): p. 318-324.
73. Cheng, Z., et al., *Applications of liposomes and lipid nanoparticles in cancer therapy: current advances and prospects.* Exp Hematol Oncol, 2025. **14**(1): p. 11.
74. Allen, T.M. and P.R. Cullis, *Liposomal drug delivery systems: from concept to clinical applications.* Adv Drug Deliv Rev, 2013. **65**(1): p. 36-48.
75. Hamilton, A.G., K.L. Swingle, and M.J. Mitchell, *Biotechnology: Overcoming biological barriers to nucleic acid delivery using lipid nanoparticles.* PLoS Biol, 2023. **21**(4): p. e3002105.
76. Johansson, J.M., et al., *Cellular and biophysical barriers to lipid nanoparticle mediated delivery of RNA to the cytosol.* Nat Commun, 2025. **16**(1): p. 5354.
77. Kim, Y., et al., *Physiological Barriers to Nucleic Acid Therapeutics and Engineering Strategies for Lipid Nanoparticle Design, Optimization, and Clinical Translation.* Pharmaceutics, 2025. **17**(10).
78. Voke, E., et al., *Protein corona formed on lipid nanoparticles compromises delivery efficiency of mRNA cargo.* Nat Commun, 2025. **16**(1): p. 8699.
79. Godbout, K. and J.P. Tremblay, *Delivery of RNAs to Specific Organs by Lipid Nanoparticles for Gene Therapy.* Pharmaceutics, 2022. **14**(10).
80. Samaridou, E., J. Heyes, and P. Lutwyche, *Lipid nanoparticles for nucleic acid delivery: Current perspectives.* Adv Drug Deliv Rev, 2020. **154-155**: p. 37-63.
81. Wherry, E.J., et al., *How Did We Get a COVID-19 Vaccine in Less Than 1 Year?* Clin Cancer Res, 2021. **27**(8): p. 2136-2138.
82. NCBI. *Lipid+nanoparticle - search results - pubmed*. 2026 5 February 2026]; Available from: https://pubmed.ncbi.nlm.nih.gov/?term=lipid%2Bnanoparticle.
83. Xu, S., et al., *Lipid nanoparticles: Composition, formulation, and application.* Mol Ther Methods Clin Dev, 2025. **33**(2): p. 101463.
84. O'Brien Laramy, M.N., et al., *Process Robustness in Lipid Nanoparticle Production: A Comparison of Microfluidic and Turbulent Jet Mixing.* Mol Pharm, 2023. **20**(8): p. 4285-4296.
85. Maeki, M., et al., *Microfluidic technologies and devices for lipid nanoparticle-based RNA delivery.* J Control Release, 2022. **344**: p. 80-96.
86. Guevara, M.L., F. Persano, and S. Persano, *Advances in Lipid Nanoparticles for mRNA-Based Cancer Immunotherapy.* Front Chem, 2020. **8**: p. 589959.
87. Lopes, C., et al., *Microfluidic production of mRNA-loaded lipid nanoparticles for vaccine applications.* Expert Opin Drug Deliv, 2022. **19**(10): p. 1381-1395.
88. Shah, V.M., et al., *Liposomes produced by microfluidics and extrusion: A comparison for scale-up purposes.* Nanomedicine, 2019. **18**: p. 146-156.

89. Dimov, N., et al., *Formation and purification of tailored liposomes for drug delivery using a module-based micro continuous-flow system.* Sci Rep, 2017. **7**(1): p. 12045.
90. Anderluzzi, G., et al., *Scalable Manufacturing Processes for Solid Lipid Nanoparticles.* Pharm Nanotechnol, 2019. **7**(6): p. 444-459.
91. Paridhi, A., et al., *A Review of Tangential Flow Filtration: Process Development and Applications in the Pharmaceutical Industry.* Organic Process Research & Development, 2023. **27**(4): p. 571-591.
92. Geng, C., et al., *A preparation method for mRNA-LNPs with improved properties.* J Control Release, 2023. **364**: p. 632-643.
93. Kulkarni, J.A., et al., *On the role of helper lipids in lipid nanoparticle formulations of siRNA.* Nanoscale, 2019. **11**(45): p. 21733-21739.
94. Belliveau, N.M., et al., *Microfluidic Synthesis of Highly Potent Limit-size Lipid Nanoparticles for In Vivo Delivery of siRNA.* Mol Ther Nucleic Acids, 2012. **1**(8): p. e37.
95. Crommelin, D.J.A., et al., *Addressing the Cold Reality of mRNA Vaccine Stability.* J Pharm Sci, 2021. **110**(3): p. 997-1001.
96. Pardi, N., et al., *mRNA vaccines - a new era in vaccinology.* Nat Rev Drug Discov, 2018. **17**(4): p. 261-279.
97. Mitchell, M.J., et al., *Engineering precision nanoparticles for drug delivery.* Nat Rev Drug Discov, 2021. **20**(2): p. 101-124.
98. Maier, M.A., et al., *Biodegradable lipids enabling rapidly eliminated lipid nanoparticles for systemic delivery of RNAi therapeutics.* Mol Ther, 2013. **21**(8): p. 1570-8.
99. Verbeke, R., et al., *Three decades of messenger RNA vaccine development.* Nano Today, 2019. **28**: p. 100766.
100. Ly, H.H., et al., *Optimization of Lipid Nanoparticles for saRNA Expression and Cellular Activation Using a Design-of-Experiment Approach.* Mol Pharm, 2022. **19**(6): p. 1892-1905.
101. Eygeris, Y., et al., *Chemistry of Lipid Nanoparticles for RNA Delivery.* Acc Chem Res, 2022. **55**(1): p. 2-12.
102. Monopoli, M.P., et al., *Biomolecular coronas provide the biological identity of nanosized materials.* Nat Nanotechnol, 2012. **7**(12): p. 779-86.
103. Paunovska, K., et al., *A Direct Comparison of in Vitro and in Vivo Nucleic Acid Delivery Mediated by Hundreds of Nanoparticles Reveals a Weak Correlation.* Nano Lett, 2018. **18**(3): p. 2148-2157.
104. Buschmann, M.D., et al., *Nanomaterial Delivery Systems for mRNA Vaccines.* Vaccines (Basel), 2021. **9**(1).
105. Roces, C.B., et al., *Rapid scale-up and production of active-loaded PEGylated liposomes.* Int J Pharm, 2020. **586**: p. 119566.
106. Kastner, E., et al., *Microfluidic-controlled manufacture of liposomes for the solubilisation of a poorly water soluble drug.* Int J Pharm, 2015. **485**(1-2): p. 122-30.
107. Shepherd, S.J., et al., *Scalable mRNA and siRNA Lipid Nanoparticle Production Using a Parallelized Microfluidic Device.* Nano Lett, 2021. **21**(13): p. 5671-5680.
108. Webb, C., et al., *The Impact of Solvent Selection: Strategies to Guide the Manufacturing of Liposomes Using Microfluidics.* Pharmaceutics, 2019. **11**(12).
109. Hallan, S.S., et al., *Challenges in the Physical Characterization of Lipid Nanoparticles.* Pharmaceutics, 2021. **13**(4).
110. Wang, W., et al., *Prediction of lipid nanoparticles for mRNA vaccines by the machine learning algorithm.* Acta Pharm Sin B, 2022. **12**(6): p. 2950-2962.

111. Forbes, N., et al., *Rapid and scale-independent microfluidic manufacture of liposomes entrapping protein incorporating in-line purification and at-line size monitoring.* Int J Pharm, 2019. **556**: p. 68-81.
112. Kumar, V., et al., *Shielding of Lipid Nanoparticles for siRNA Delivery: Impact on Physicochemical Properties, Cytokine Induction, and Efficacy.* Mol Ther Nucleic Acids, 2014. **3**(11): p. e210.
113. Prakash, G., et al., *Microfluidic fabrication of lipid nanoparticles for the delivery of nucleic acids.* Adv Drug Deliv Rev, 2022. **184**: p. 114197.
114. Javid-Naderi, M.J. and S.A. Mousavi Shaegh, *Advanced microfluidic techniques for the preparation of solid lipid nanoparticles: Innovations and biomedical applications.* Int J Pharm X, 2025. **10**: p. 100399.
115. Hardianto, A., et al., *The Effect of Ethanol on Lipid Nanoparticle Stabilization from a Molecular Dynamics Simulation Perspective.* Molecules, 2023. **28**(12).
116. Fairlamb, M., et al., *Developability assessments with four mRNA-LNP vaccine formulations comparing mouse immunogenicity, structural attributes, and stability profiles.* J Pharm Sci, 2026. **115**(4): p. 104199.
117. Shepherd, S.J., et al., *Throughput-scalable manufacturing of SARS-CoV-2 mRNA lipid nanoparticle vaccines.* Proc Natl Acad Sci U S A, 2023. **120**(33): p. e2303567120.
118. Shkodra, B., et al., *Boosting LNP Performance: Higher Concentrations of Lipid Mixtures Improve In Vivo Gene Expression and Storage Stability.* Pharmaceutics, 2025. **18**(1).
119. Dietrich, A., N. Beckert, and J. Hubbuch, *Time-dependent particle size increase during lipid nanoparticle purification by cross-flow filtration.* J Colloid Interface Sci, 2025. **694**: p. 137663.
120. Terada, T., et al., *Characterization of Lipid Nanoparticles Containing Ionizable Cationic Lipids Using Design-of-Experiments Approach.* Langmuir, 2021. **37**(3): p. 1120-1128.
121. Agrawal, S., A.L. Stokes, and C.E. Nelson, *Standardizing a Protocol for Streamlined Synthesis and Characterization of Lipid Nanoparticles to Enable Preclinical Research and Education.* bioRxiv, 2025.
122. Maeki, M., et al., *Advances in microfluidics for lipid nanoparticles and extracellular vesicles and applications in drug delivery systems.* Adv Drug Deliv Rev, 2018. **128**: p. 84-100.
123. Di, J., et al., *Biodistribution and Non-linear Gene Expression of mRNA LNPs Affected by Delivery Route and Particle Size.* Pharm Res, 2022. **39**(1): p. 105-114.
124. Hunter, M.R., et al., *Understanding Intracellular Biology to Improve mRNA Delivery by Lipid Nanoparticles.* Small Methods, 2023: p. e2201695.
125. Lou, G., et al., *A novel microfluidic-based approach to formulate size-tuneable large unilamellar cationic liposomes: Formulation, cellular uptake and biodistribution investigations.* Eur J Pharm Biopharm, 2019. **143**: p. 51-60.
126. Cui, L., et al., *Efficient Delivery of DNA Using Lipid Nanoparticles.* Pharmaceutics, 2022. **14**(8).
127. Renzi, S., et al., *Structuring lipid nanoparticles, DNA, and protein corona into stealth bionanoarchitectures for in vivo gene delivery.* Nature Communications, 2024. **15**(1): p. 9119.
128. Bailey, J.D., et al., *Isolation and culture of murine bone marrow-derived macrophages for nitric oxide and redox biology.* Nitric Oxide, 2020. **100-101**: p. 17-29.
129. Chen, S., et al., *Macrophages in immunoregulation and therapeutics.* Signal Transduct Target Ther, 2023. **8**(1): p. 207.

130. Zhang, Q., et al., *A Preliminary Study in Immune Response of BALB/c and C57BL/6 Mice with a Locally Allergic Rhinitis Model.* Am J Rhinol Allergy, 2023. **37**(4): p. 410-418.
131. Tanaka, H., et al., *Delivery of Oligonucleotides Using a Self-Degradable Lipid-Like Material.* Pharmaceutics, 2021. **13**(4).
132. Maeki, M., et al., *Understanding the formation mechanism of lipid nanoparticles in microfluidic devices with chaotic micromixers.* PLoS One, 2017. **12**(11): p. e0187962.
133. Zhigaltsev, I.V., et al., *Bottom-up design and synthesis of limit size lipid nanoparticle systems with aqueous and triglyceride cores using millisecond microfluidic mixing.* Langmuir, 2012. **28**(7): p. 3633-40.
134. Patel, P., N.M. Ibrahim, and K. Cheng, *The Importance of Apparent pKa in the Development of Nanoparticles Encapsulating siRNA and mRNA.* Trends Pharmacol Sci, 2021. **42**(6): p. 448-460.
135. Cheng, M.H.Y., et al., *Induction of Bleb Structures in Lipid Nanoparticle Formulations of mRNA Leads to Improved Transfection Potency.* Adv Mater, 2023. **35**(31): p. e2303370.
136. Sciolino, N., et al., *Messenger RNA in lipid nanoparticles rescues HEK 293 cells from lipid-induced mitochondrial dysfunction as studied by real time pulse chase NMR, RTPC-NMR, spectroscopy.* Scientific Reports, 2022. **12**(1).
137. Cui, L., et al., *Efficient Delivery of DNA Using Lipid Nanoparticles.* Pharmaceutics, 2022. **14**(8): p. 1698.
138. Long, J., et al., *Novel Ionizable Lipid Nanoparticles for SARS-CoV-2 Omicron mRNA Delivery.* Advanced Healthcare Materials, 2023. **12**(13): p. 2202590.
139. Cheng, X. and R.J. Lee, *The role of helper lipids in lipid nanoparticles (LNPs) designed for oligonucleotide delivery.* Adv Drug Deliv Rev, 2016. **99**(Pt A): p. 129-137.
140. Meyer, R.A., Neshat, S. Y., Green, J. J., Santos, J. L., & Tuesca, A. D. , *Targeting strategies for mRNA delivery.* Materials Today Advances, 2022. **14**(100240).
141. Jain, P., et al., *In-vitro in-vivo correlation (IVIVC) in nanomedicine: Is protein corona the missing link?* Biotechnol Adv, 2017. **35**(7): p. 889-904.
142. Francia, V., et al., *The Biomolecular Corona of Lipid Nanoparticles for Gene Therapy.* Bioconjug Chem, 2020. **31**(9): p. 2046-2059.
143. Lee, Y., et al., *Immunogenicity of lipid nanoparticles and its impact on the efficacy of mRNA vaccines and therapeutics.* Exp Mol Med, 2023. **55**(10): p. 2085-2096.
144. Zhang, L., et al., *Effect of mRNA-LNP components of two globally-marketed COVID-19 vaccines on efficacy and stability.* NPJ Vaccines, 2023. **8**(1): p. 156.
145. Jorgensen, A.M., R. Wibel, and A. Bernkop-Schnurch, *Biodegradable Cationic and Ionizable Cationic Lipids: A Roadmap for Safer Pharmaceutical Excipients.* Small, 2023. **19**(17): p. e2206968.
146. Sun, D. and Z.R. Lu, *Structure and Function of Cationic and Ionizable Lipids for Nucleic Acid Delivery.* Pharm Res, 2023. **40**(1): p. 27-46.
147. Zhang, Y., et al., *Lipids and Lipid Derivatives for RNA Delivery.* Chem Rev, 2021. **121**(20): p. 12181-12277.
148. Han, X., et al., *An ionizable lipid toolbox for RNA delivery.* Nat Commun, 2021. **12**(1): p. 7233.
149. Herrera, M., et al., *Illuminating endosomal escape of polymorphic lipid nanoparticles that boost mRNA delivery.* Biomaterials Science, 2021. **9**(12): p. 4289-4300.
150. Douka, S., et al., *Lipid nanoparticle-mediated messenger RNA delivery for ex vivo engineering of natural killer cells.* J Control Release, 2023. **361**: p. 455-469.
151. Kim, J., et al., *Engineering Lipid Nanoparticles for Enhanced Intracellular Delivery of mRNA through Inhalation.* ACS Nano, 2022. **16**(9): p. 14792-14806.

152. Medjmedj, A., et al., *In Cellulo and In Vivo Comparison of Cholesterol, Beta-Sitosterol and Dioleylphosphatidylethanolamine for Lipid Nanoparticle Formulation of mRNA.* Nanomaterials (Basel), 2022. **12**(14).
153. McMillan, C., et al., *Tailoring lipid nanoparticle dimensions through manufacturing processes.* RSC Pharmaceutics, 2024. **1**(4): p. 841-853.
154. Ni, H., et al., *Piperazine-derived lipid nanoparticles deliver mRNA to immune cells in vivo.* Nat Commun, 2022. **13**(1): p. 4766.
155. Hashiba, K., et al., *Overcoming thermostability challenges in mRNA-lipid nanoparticle systems with piperidine-based ionizable lipids.* Commun Biol, 2024. **7**(1): p. 556.
156. Chen, Z., et al., *Modular Design of Biodegradable Ionizable Lipids for Improved mRNA Delivery and Precise Cancer Metastasis Delineation In Vivo.* J Am Chem Soc, 2023. **145**(44): p. 24302-24314.
157. Wang, C., et al., *Biomimetic noncationic lipid nanoparticles for mRNA delivery.* Proc Natl Acad Sci U S A, 2023. **120**(51): p. e2311276120.
158. Cornebise, M., et al., *Discovery of a Novel Amino Lipid That Improves Lipid Nanoparticle Performance through Specific Interactions with mRNA.* Advanced Functional Materials, 2022. **32**(8): p. 2106727.
159. Krasnovskaya, O.O., et al., *Thiourea Modified Doxorubicin: A Perspective pH-Sensitive Prodrug.* Bioconjug Chem, 2019. **30**(3): p. 741-750.
160. Palanki, R., et al., *Optimized microfluidic formulation and organic excipients for improved lipid nanoparticle mediated genome editing.* Lab Chip, 2024. **24**(16): p. 3790-3801.
161. Liu, H., et al., *Beyond the Endosomal Bottleneck: Understanding the Efficiency of mRNA/LNP Delivery.* Advanced Functional Materials, 2024. **34**(39): p. 2404510.
162. Herrera-Barrera, M., et al., *Lipid Nanoparticle-Enabled Intracellular Delivery of Prime Editors.* AAPS J, 2023. **25**(4): p. 65.
163. Zeng, Y., et al., *Lipid nanoparticle-based mRNA candidates elicit potent T cell responses.* Biomater Sci, 2023. **11**(3): p. 964-974.
164. Danaei, M., et al., *Impact of Particle Size and Polydispersity Index on the Clinical Applications of Lipidic Nanocarrier Systems.* Pharmaceutics, 2018. **10**(2).
165. Dobrovolskaia, M.A. and S.E. McNeil, *Understanding the correlation between in vitro and in vivo immunotoxicity tests for nanomedicines.* J Control Release, 2013. **172**(2): p. 456-66.
166. Dabbagh Moghaddam, F., et al., *Advances in engineering immune-tumor microenvironments on-a-chip: integrative microfluidic platforms for immunotherapy and drug discovery.* Mol Cancer, 2025. **24**(1): p. 271.
167. Liu, S., et al., *Spleen-targeted mRNA delivery via long-chain PEGylated lipids at low molar ratio enhances antitumor immunity against melanoma.* Mol Ther Nucleic Acids, 2026. **37**(1): p. 102803.
168. Escalona-Rayo, O., et al., *In vitro and in vivo evaluation of clinically-approved ionizable cationic lipids shows divergent results between mRNA transfection and vaccine efficacy.* Biomed Pharmacother, 2023. **165**: p. 115065.
169. Davidson, C.G., et al., *The use of orthogonal analytical approaches to profile lipid nanoparticle physicochemical attributes.* Nano Futures, 2024. **8**(3): p. 035001.
170. Lin, G., et al., *Enhancing protective immunity against SARS-CoV-2 with a self-amplifying RNA lipid nanoparticle vaccine.* J Control Release, 2025. **378**: p. 250-265.
171. Wang, Y., et al., *Impact of B18R-Encoding Messenger Ribonucleic Acid Co-Delivery on Neutralizing Antibody Production in Self-Amplifying Messenger Ribonucleic Acid Vaccines.* Vaccines (Basel), 2025. **13**(5).

172. Xue, Y., et al., *LNP-RNA-mediated antigen presentation leverages SARS-CoV-2-specific immunity for cancer treatment.* Nat Commun, 2025. **16**(1): p. 2198.
173. Kulkarni, J.A., et al., *Design of lipid nanoparticles for in vitro and in vivo delivery of plasmid DNA.* Nanomedicine, 2017. **13**(4): p. 1377-1387.
174. Herweijer, H., et al., *Time course of gene expression after plasmid DNA gene transfer to the liver.* J Gene Med, 2001. **3**(3): p. 280-91.
175. Patel, M.N., et al., *Safer non-viral DNA delivery using lipid nanoparticles loaded with endogenous anti-inflammatory lipids.* Nat Biotechnol, 2026. **44**(1): p. 79-89.
176. Barthelemy, J., G. Bogard, and I. Wolowczuk, *Beyond energy balance regulation: The underestimated role of adipose tissues in host defense against pathogens.* Front Immunol, 2023. **14**: p. 1083191.
177. Zhang, F., et al., *An Adipose Tissue Atlas: An Image-Guided Identification of Human-like BAT and Beige Depots in Rodents.* Cell Metab, 2018. **27**(1): p. 252-262 e3.
178. Vogel, A.B., et al., *Self-Amplifying RNA Vaccines Give Equivalent Protection against Influenza to mRNA Vaccines but at Much Lower Doses.* Mol Ther, 2018. **26**(2): p. 446-455.
179. Blakney, A.K., et al., *Innate Inhibiting Proteins Enhance Expression and Immunogenicity of Self-Amplifying RNA.* Mol Ther, 2021. **29**(3): p. 1174-1185.
180. Davidson, C.G., et al., *The Use of Enhanced Analytical Pipelines for the Characterization of Poly(A) and Poly(A)-LNP Formulation Critical Quality Attributes.* Mol Pharm, 2025. **22**(12): p. 7383-7399.
181. Hourdel, L., et al., *Overview on LNP-mRNA encapsulation unit operation: Mixing technologies, scalability, and influence of formulation & process parameters on physico-chemical characteristics.* Int J Pharm, 2025. **672**: p. 125297.
182. McMillan, C., et al., *Influence of ionisable lipid and sterol variations on lipid nanoparticle properties and performance.* J Control Release, 2025. **386**: p. 114056.

APPENDIX A: SUPPLEMENTARY FIGURES FOR CHAPTER 3

Table S11: NTA data particle trajectories (tracks).

Aqueous: organic phase ratio	Tracks per capture number					Total tracks	Valid tracks (total particle count)
	1	2	3	4	5		
1.3:1	2773	1676	1493	1515	1731	9188	**2774**
1.5:1	1906	1779	1809	1533	1495	8522	**3623**
2:1	6770	3570	4048	6766	2493	23647	**4976**
3:1	3207	3984	6882	3131	2926	20130	**5056**

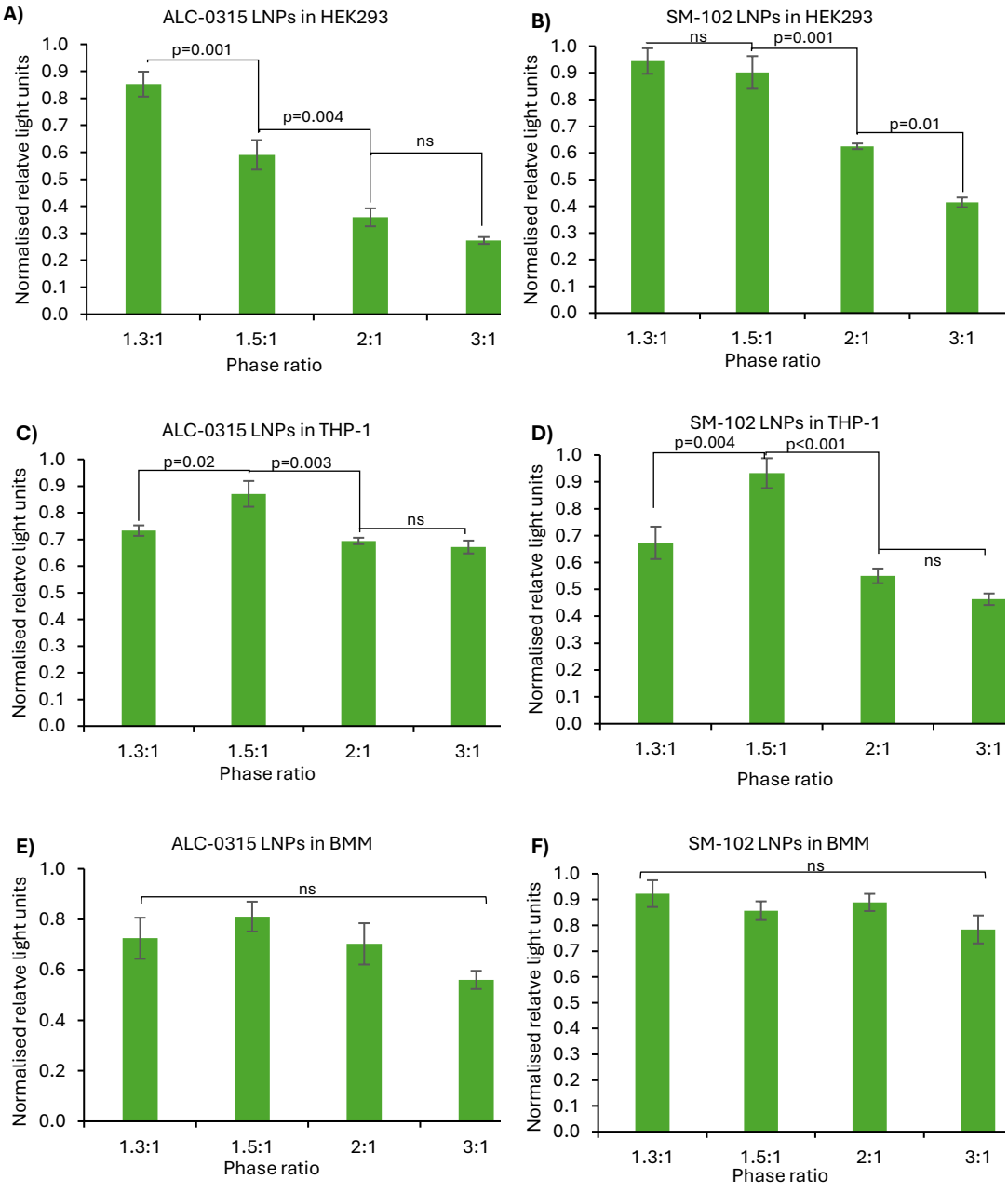

Figure S1: GFP fluorescence quantification from mGreenLantern-loaded LNPs. Comparing the different aqueous:lipid phase ratios in HEK-293 (A-B), THP-1 (C-D) and BMM (E-F) cells for LNPs manufactured with ALC-0315 (A, C, E) and SM-102 (B, D, F) as the ionisable lipid. Values quantified

using ImageJ, as an average of 5 images from each sample. Significance values shown calculated from one-way ANOVA.

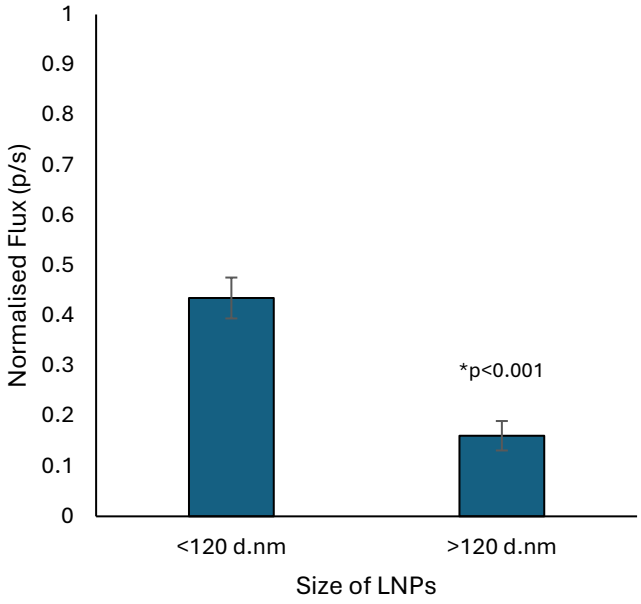

Figure S2: In vivo size versus mRNA expression of LNPs. Comparing LNPs manufactured at sizes smaller than 120d.nm (left) and larger than 120d.nm (right). Error bars shown as ±S.E.M. Statistically analysed using a two-sample unpaired T-test.

APPENDIX B: SUPPLEMENTARY FIGURES FOR CHAPTER 4

Table S12: The structures and molecular weights of the proprietary ionisable/cationic lipids tested. Lipids marked with a (*) are permanently cationic.

Lipid chemical name	Mol. weight (g/mol)	Structure	Structural components (head, linker, tail regions)
ALC-0315	766.3	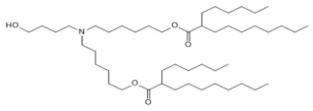	Head: Tertiary amine (+ hydroxybutyl) Linker: 2 esters Tail: (4) branched saturated tails
18:1-18:1-12:0 Thiocarbamate DMA	874.5	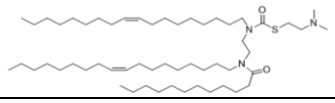	Head: Tertiary amine Linker: thiocarbamate, amide Tail: (3), 2 unsaturated, 1 saturated
18:1-18:1-12:0 ethanolamine	787.4	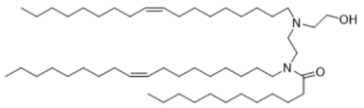	Head: Tertiary amine (ethanolamine) Linker: amide Tail: (3), 2 unsaturated, 1 saturated
18:1-18:1-12:0 thiourea ethanolamine	832.5	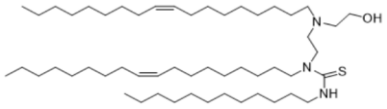	Head: Tertiary amine (ethanolamine) Linker: thiourea Tail: (3), 2 unsaturated, 1 saturated
10:0 N-decanyl PE	681.0	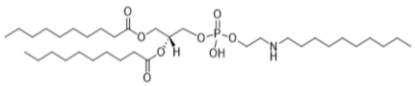	Head: secondary amine (+decanyl) Linker: 1 phosphate, 2 esters Tail: (2) saturated
10:0 N, N-didecanyl PE	821.2	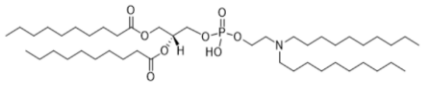	Head: tertiary amine (+ 2 decanyl) Linker: 1 phosphate, 2 esters Tail: (2) saturated
10:0 N-methyl, N-decanyl PE (ammonium salt)	695.0	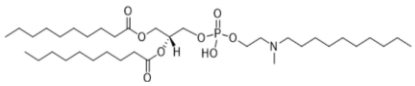	Head: tertiary amine (+ decanyl) Linker: 1 phosphate, 2 esters Tail: (2) saturated
9:1 HPPPG	694.9	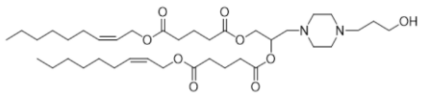	Head: piperazine (hydroxypropyl) Linker: 4 esters Tail: (2) unsaturated
APL-143	Not available	Not available	Not available
APL-718*	938.8	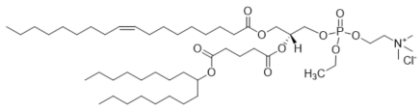	Head: Quaternary amine (cationic) Linker: phosphate (ethyl), 3 esters Tail: (3) 2 branched saturated, 1 unsaturated
APL-719*	1026.9	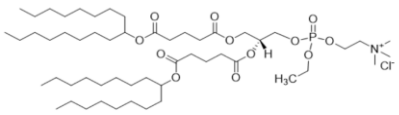	Head: Quaternary amine (cationic) Linker: phosphate (ethyl), 4 esters Tail: (4) branched saturated
16:0 HDA PE	692.0	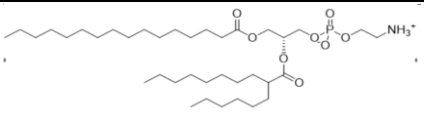	Head: Quaternary amine (cationic) Linker: phosphate (anionic), 2 esters Tail: (3) branched and single saturated

Table S13: The structures and molecular weights of the sterols tested.

Sterol (origin)	Mol. weight (g/mol)	Structure	Key differences from cholesterol
Cholesterol (animals)	386.7	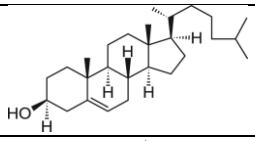	N/A
β-sitosterol (plants)	414.7	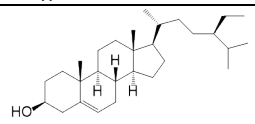	Ethyl group at C24
Campesterol (plants)	400.7	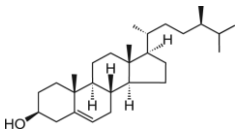	Methyl group at C24
Lanosterol (animals, fungi)	426.7	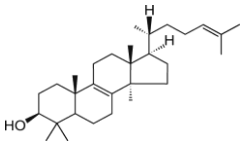	2 methyl groups at C4, methyl at C-14, double bond at C8-C9 instead of C5-C6. Double bond at C24-C25.
Stigmasterol (plants)	412.7	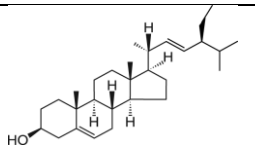	Double bond C22-C23. Ethyl group at C24
Delta 5-avenasterol (plants)	412.7	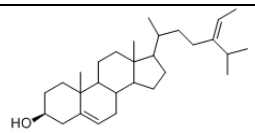	Ethylidene group at C22

Table S14: Comparing LNPs manufactured with DMG-PEG and ALC-0159 peg lipids. Physicochemical attributes of mRNA LNPs manufactured with the proprietary lipid and different peg lipids. The LNPs were manufactured with an N/P ratio of 6 from 5 mg/mL lipid stocks and purified by dialysis in pH 7.4 PBS. Each measurement represents the mean of three independent batches, with ±SD.

	Size		PDI		Zeta Potential (mV)		mRNA encapsulation (%)	
Peg lipid / Ionisable lipid	DMG-PEG	ALC-0159	DMG-PEG	ALC-0159	DMG-PEG	ALC-0159	DMG-PEG	ALC-0159
ALC-0315	78 ± 10	77 ± 7	0.16 ± 0.04	0.09 ± 0.03	-0.22 ± 0.04	-0.24 ± 0.04	93 ± 3	96 ± 2
18:1-18:1-12:0 Thiocarbamate DMA	71 ± 6	72 ± 1	0.18 ± 0.04	0.20 ± 0.01	-1.20 ± 1.38	-0.59 ± 0.19	90 ± 4	95 ± 1.6
18:1-18:1-12:0 ethanolamine	81 ± 13	69 ± 1	0.23 ± 0.04	0.21 ± 0.02	-1.5 ± 2.59	-1.03 ± 0.62	90 ± 4	96 ± 2
18:1-18:1-12:0 thiourea ethanolamine	82 ± 12	97 ± 2	0.23 ± 0.03	0.20 ± 0.01	-0.28 ± 1.42	0.42 ± 0.98	84 ± 3	89 ± 2
10:0 N-decanyl PE	60 ± 7	51 ± 10	0.24 ± 0.04	0.27 ± 0.14	-3.09 ± 1.57	-3.47 ± 1.97	43 ± 28	11 ± 15
10:0 N, N-didecanyl PE	52 ± 11	48 ± 4	0.25 ± 0.02	0.19 ± 0.07	-0.77 ± 0.57	-0.45 ± 0.49	48 ± 24	14 ± 1
10:0 N-methyl, N-decanyl PE	65 ± 4	69 ± 5	0.12 ± 0.01	0.05 ± 0.02	-1.70 ± 2.15	-3.52 ± 2.54	47 ± 28	28 ± 14
9:1 HPPPG	147 ± 14	154 ± 2	0.11 ± 0.02	0.11 ± 0.02	1.32 ± 0.72	2.88 ± 0.35	88 ± 11	81 ± 15
APL-143	77 ± 12	89 ± 13	0.18 ± 0.07	0.12 ± 0.05	0.27 ± 1.12	0.88 ± 0.88	92 ± 12	98 ± 2
APL-718	89 ± 10	97 ± 5	0.29 ± 0.04	0.27 ± 0.06	2.27 ± 2.02	2.62 ± 0.90	87 ± 17	99 ± 1
APL-719	91 ± 10	90 ± 9	0.29 ± 0.08	0.17 ± 0.05	0.16 ± 0.58	0.39 ± 0.58	91 ± 12	99 ± 1
16:0 HDA PE	61 ± 12	45 ± 3	0.30 ± 0.07	0.18 ± 0.04	-1.64 ± 3.12	-1.17 ± 0.90	47 ± 4	14 ± 1

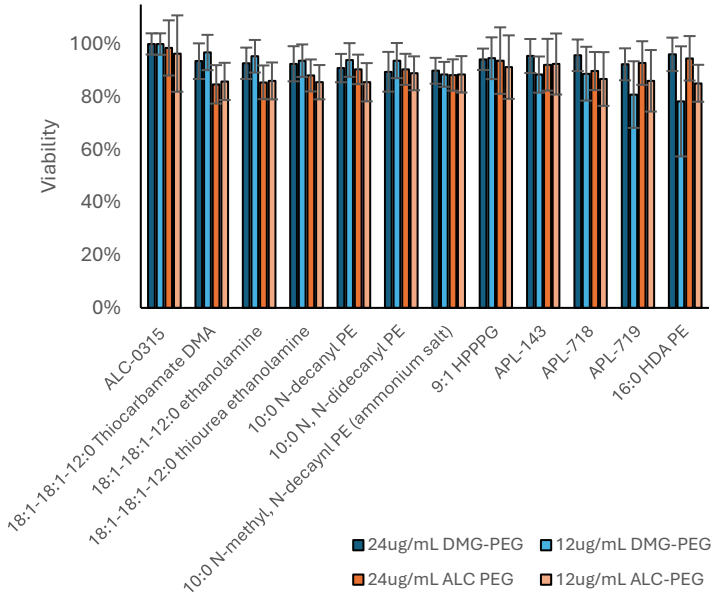

Figure S1: Viability of the proprietary ionisable lipid formulations. Viability of the LNPs in cells after incubation for 24 hours, measured 6 hours after the addition of resazurin. The LNPs were manufactured with an N/P of 6 from 5mg/mL lipid stocks and purified by dialysis in pH 7.4 PBS. Each measurement represents the mean of three independent batches, with error bars indicating ±SD.

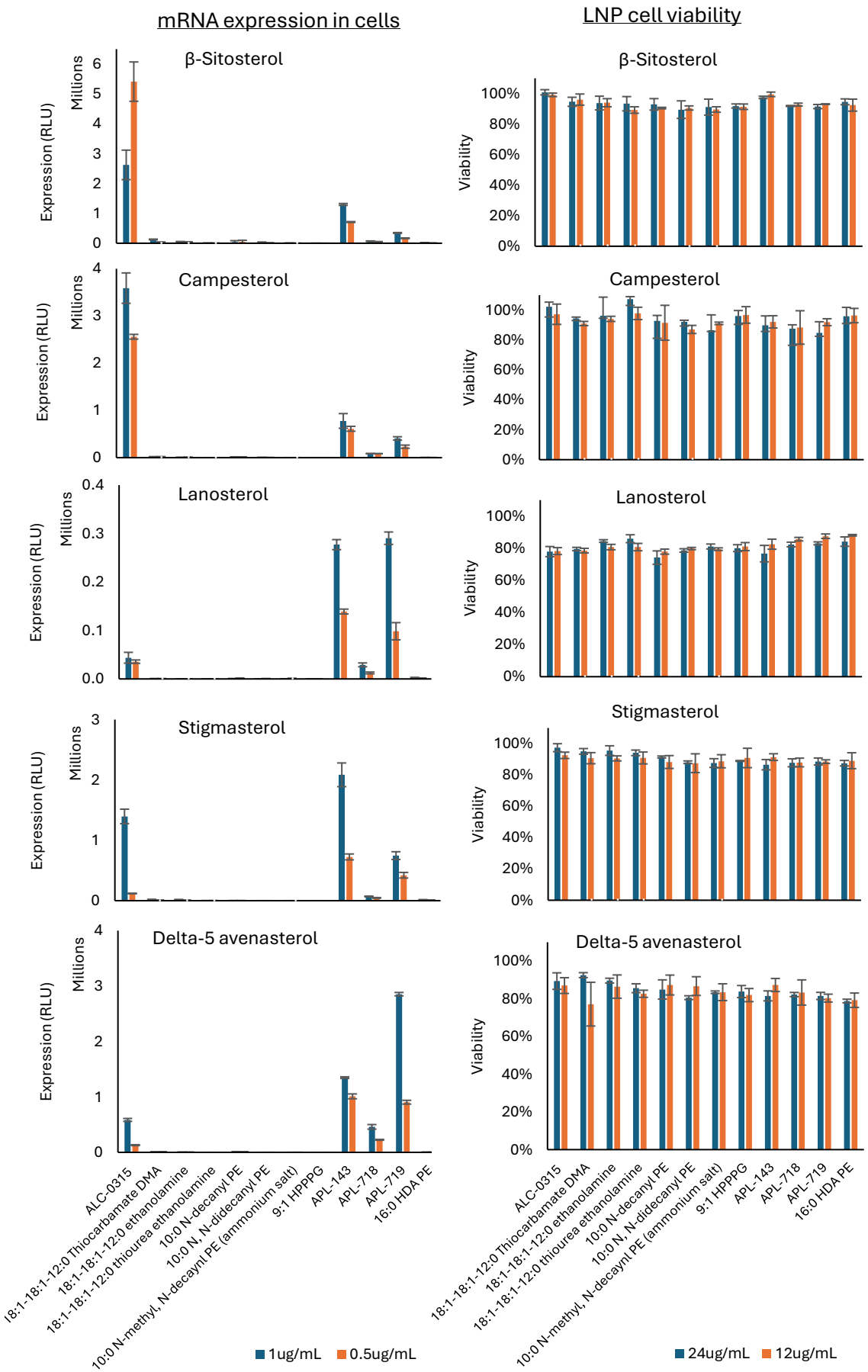

Figure S2: Expression and viability of proprietary ionisable lipid LNPs manufactured with cholesterol alternatives in HeLa cells. Viability of the LNPs in cells after incubation for 24 hours, measured 6 hours after addition of resazurin. The LNPs were manufactured with an N/P of 6 from 5mg/mL lipid stocks and purified by dialysis in pH 7.4 PBS. Each datapoint is a mean of three measurements of one sample with error bars showing ±SD.

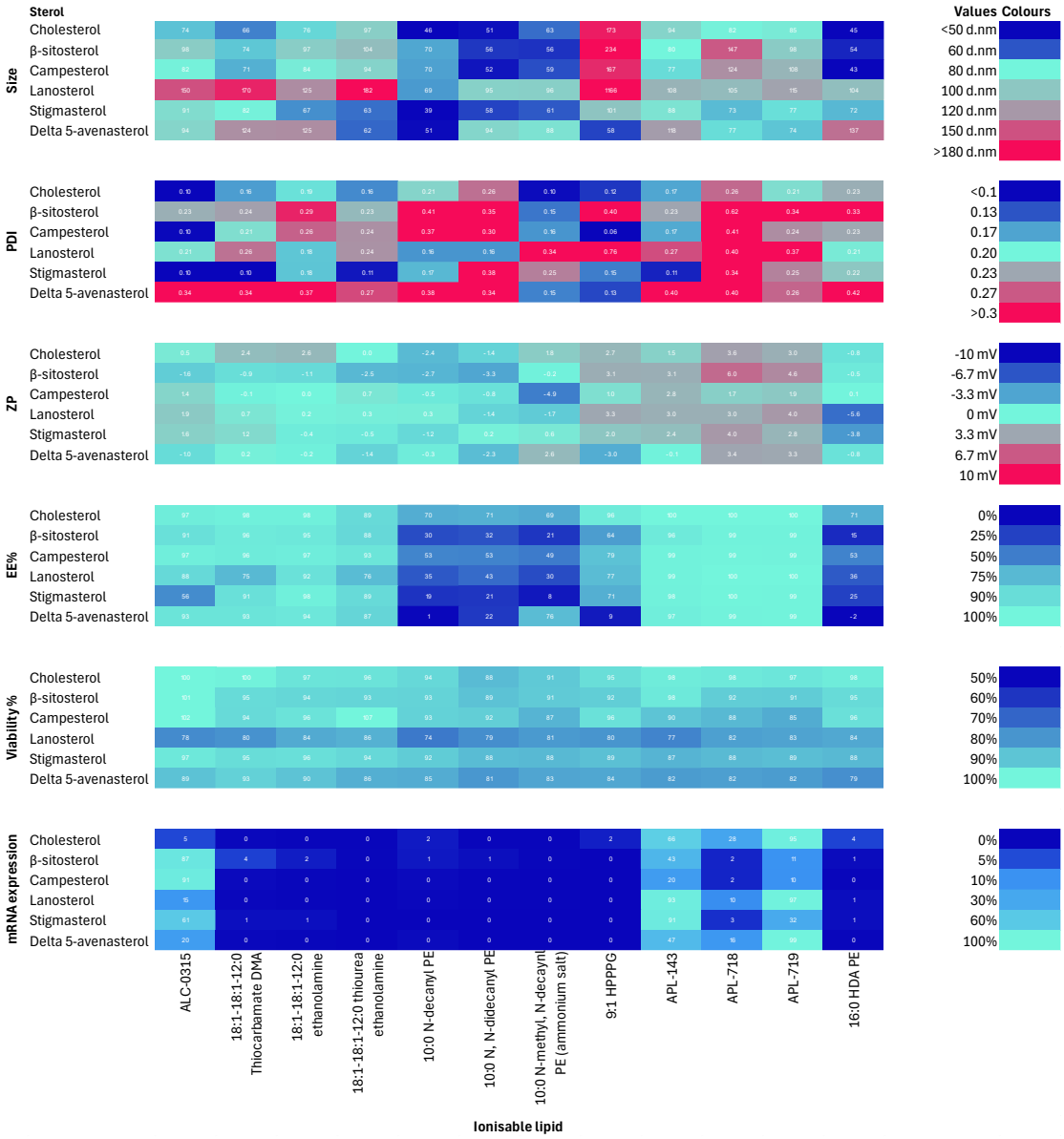

Figure S3: Heatmaps of LNP attributes of LNPs manufactured with different ionisable lipids and sterols. The LNPs were manufactured with an N/P ratio of 6 from 5 mg/mL lipid stocks and purified by dialysis in pH 7.4 PBS. N=1 for each combination. PDI = polydispersity index, ZP zeta potential, EE% encapsulation efficiency.

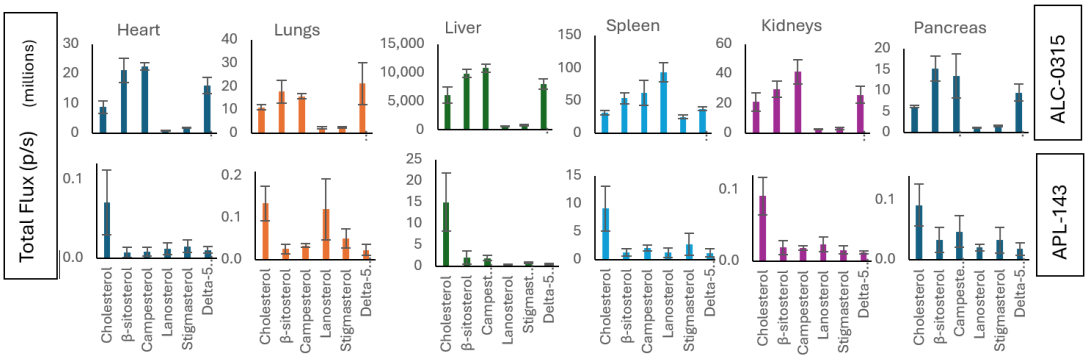

Figure S4: Fluc mRNA expression in each organ 6 hours after intravenous administration of LNPs formulated with the ionisable lipids ALC-0315 or proprietary APL-143 with 6 different sterols.

APPENDIX C: SUPPLEMENTARY FIGURES FOR CHAPTER 5

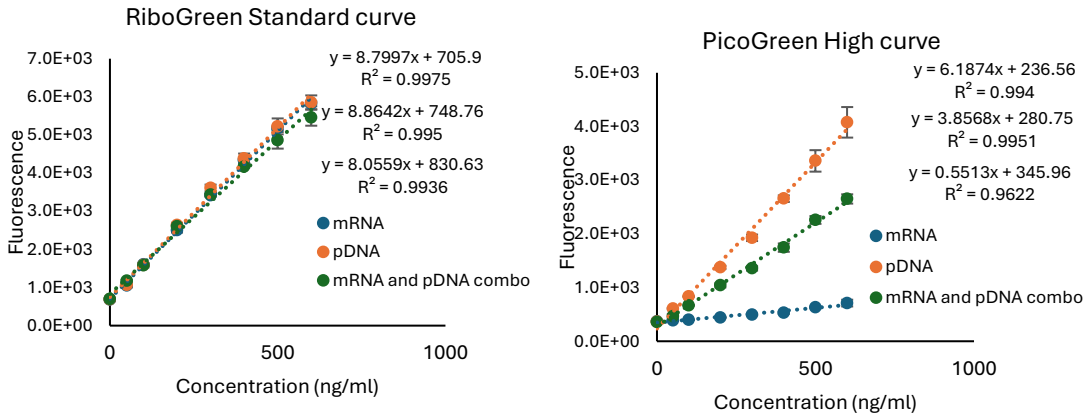

Figure S1: Standard curves generated using RiboGreen™ and PicoGreen™ assays for quantification of naked mRNA, naked plasmid DNA (pDNA), and a 1:1 mixture of these payloads.

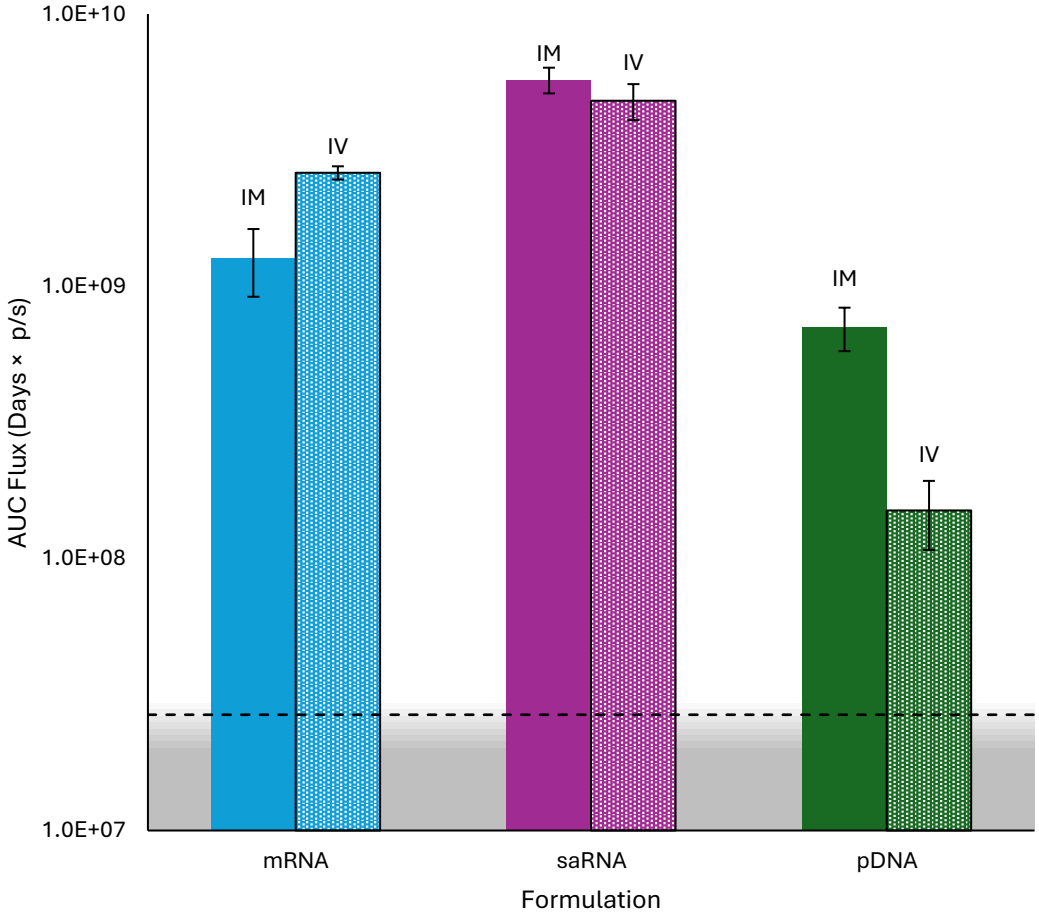

Figure S2: Comparison of cumulative expression profiles (AUC) for mRNA-, saRNA-, and pDNA-LNPs following intramuscular (IM) and intravenous (IV) administration over 18 weeks. AUC values were calculated from bioluminescence expression data to compare total expression across administration routes.

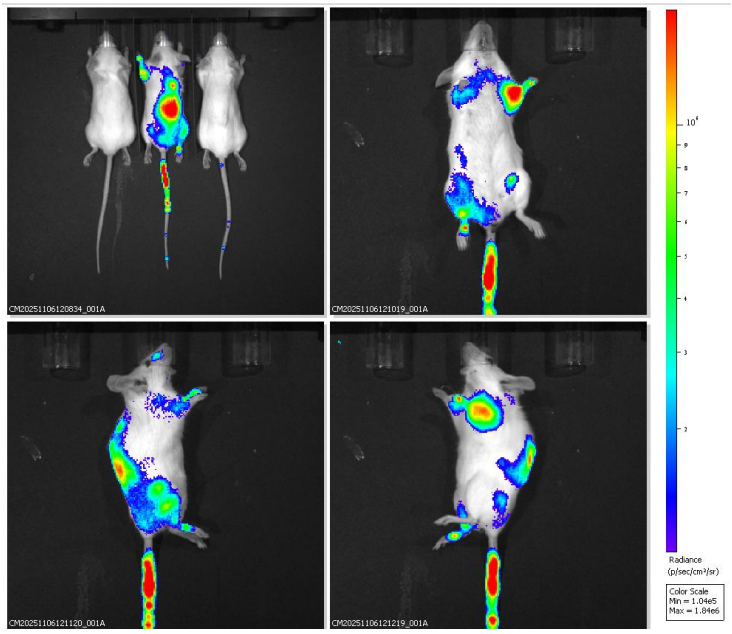

Figure S3: Prone, lateral, and supine IVIS images of a BALB/c mouse at 5 weeks post-intravenous administration of saRNA-loaded lipid nanoparticles, illustrating multi-dimensional distribution of firefly luciferase expression through bioluminescence.

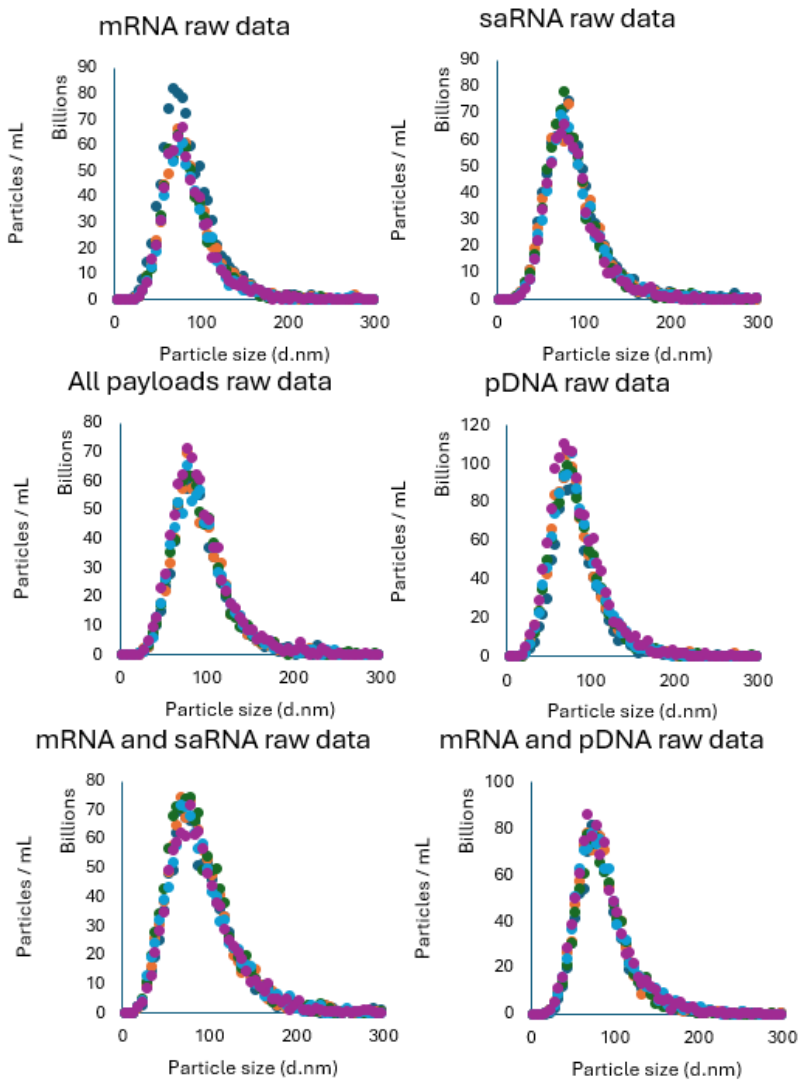

Figure S4: Raw data points from nanoparticle tracking analysis (NTA) used to generate size distribution curves. Each curve shows the data from five video captures per payload formulation.

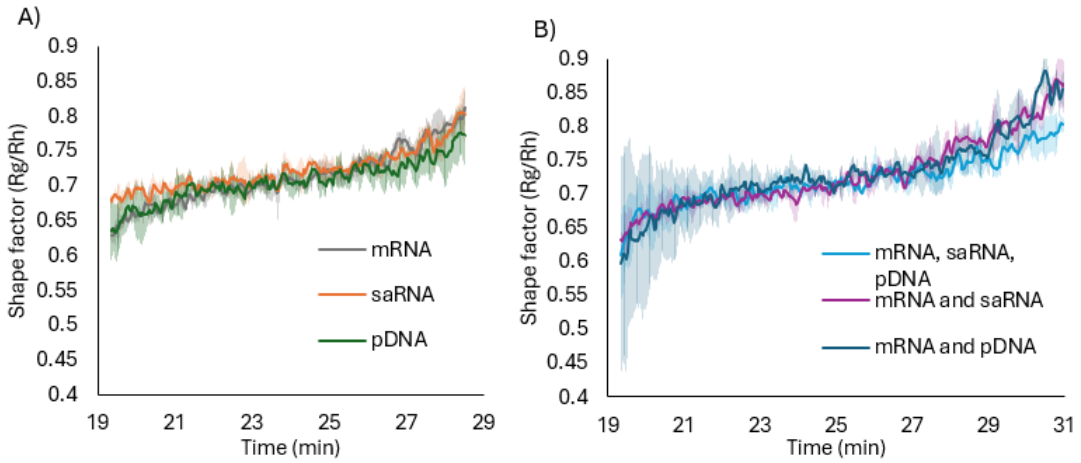

Figure S5: Asymmetric Flow Field-Flow Fractionation (AF4)–derived shape factor profiles for (A) single-payload lipid nanoparticles (LNPs) and (B) combined-payload LNPs. Shape factor values were calculated from the ratio of radius of gyration (Rg) obtained from the MALS detector to hydrodynamic

radius (Rh) obtained from the on-line DLS detector. Data represent the mean of three independent measurements ± standard deviation.

Table S1: AF4 recovery profiles for lipid nanoparticle (LNP) formulations containing single or combined nucleic acid payloads. Values represent the mean recovery percentage ± standard deviation from three independent measurements.

Sample no.	LNP payloads		% recovery
1	single payloads	mRNA	89 ± 16
2		saRNA	84 ± 2
3		pDNA	91 ± 5
4	combined payloads	mRNA, saRNA and pDNA	91 ± 11
5		mRNA and saRNA	85 ± 5
6		mRNA and pDNA	80 ± 7